

MTR00W0000052

MITRE TECHNICAL REPORT

Practical Quantum Cryptography: A Comprehensive Analysis (Part One)

G. Gilbert
M. Hamrick

September 2000

Sponsor: The MITRE Corporation
Dept. No.: W072

Contract No.: DAAB07-00-C-C201
Project No.: 51MSR837

The views, opinions and/or findings contained in this report are those of The MITRE Corporation and should not be construed as an official Government position, policy, or decision, unless designated by other documentation.

Approved for public release;
distribution unlimited.

©2000 The MITRE Corporation

MITRE
Washington C³ Center
McLean, Virginia

Practical Quantum Cryptography: A Comprehensive Analysis (Part One)*

Gerald Gilbert[†] and Michael Hamrick[‡]

The MITRE Corporation
McLean, Virginia 22102

Abstract

We perform a comprehensive analysis of practical quantum cryptography (QC) systems implemented in actual physical environments *via* either free-space or fiber-optic cable quantum channels for ground-ground, ground-satellite, air-satellite and satellite-satellite links.

(1) We obtain the complete universal expressions for the effective secrecy capacity and rate for QC systems taking all direct and ancillary processes into account. The analysis in Part One treats the most general individual quantum bit attacks, including generic admixtures of indirect attacks, direct attacks and previously unconsidered simultaneous combinations of the two types. In all these cases we obtain for the first time *necessary and sufficient* exact closed form expressions for privacy amplification. Our analysis also includes for the first time the explicit calculation in detail of the total cost in bits of *continuous* authentication, thereby obtaining new results for actual ciphers of finite length, as well as previously obtained limits for idealized ciphers of infinite length.

(2) We perform for the first time a detailed, explicit analysis of all systems losses due to and errors and noises, including turbulent and static atmospheric propagation losses, optics package losses, intrinsic channel losses, *etc.*, as appropriate to both optical fiber cable- and satellite communications-based implementations of QC.

(3) We calculate for the first time all system load costs associated to classical communication and computational constraints that are ancillary to, but essential for carrying out, the pure QC protocol itself, including the full classical communications bandwidth requirements and the full computer machine instruction requirements needed to support actual QC implementations.

(4) We introduce an extended family of generalizations of the Bennett-Brassard (BB84) QC protocol that equally provide unconditional secrecy but allow for the possibility of optimizing throughput rates against specific cryptanalytic attacks.

(5) We obtain universal predictions for maximal rates that can be achieved with practical system designs under realistic environmental conditions, taking into account our results for total system losses and loads.

* This research was supported by MITRE under MITRE Sponsored Research Grant 51MSR837.

† ggilbert@mitre.org

‡ mhamrick@mitre.org

(6) We propose a specific QC system design that includes the use of a novel method of high-speed photon detection that may be able to achieve very high throughput rates for actual implementations in realistic environments.

(7) We deduce the dependence of the effective throughput on processing block size for actual ciphers of finite length and derive thereby an upper bound on practical processing block sizes dictated by current available computing machinery. We use this to show how a system employing an array of parallel transmitter and receiver devices can be multiplexed to substantially increase the throughput of shared secret cipher.

PACS: 03.67.Dd, 42.50.Dv, 42.79.Sz, 42.68.Ay, 42.68.Bz, 42.81.Dp, 89.80.+h

PRACTICAL QUANTUM CRYPTOGRAPHY: A COMPREHENSIVE ANALYSIS

PART ONE - Quantum Cryptography without Entangled States (this volume)

PART TWO - Quantum Cryptography with Entangled States (to appear)

Contents

1 Prologue	10
2 Introduction	11
2.1 Overview	11
2.2 Summary of Results	12
2.3 Organization of the Paper	13
2.4 Brief Description of Quantum Key Distribution Protocol	13
2.5 Secrecy and Security in Communications	14
2.5.1 Definitions	14
2.5.2 Technically Sound Quantum Cryptosystem Design and Practice . . .	15
3 Theoretical Analysis of Effective Secrecy Capacity	18
3.1 Derivation of Effective Secrecy Capacity	19
3.1.1 The Sifted Key and the Transmitted Errors	19
3.1.2 Privacy Amplification: General Remarks	30
3.1.3 Privacy Amplification: Error Correction	31
3.1.4 Privacy Amplification: Single Photon Pulses	32
3.1.5 Privacy Amplification: Multiple Photon Pulses	35
3.1.6 Continuous Authentication	82
3.1.7 The Complete Expressions for the Effective Secrecy Capacity and Rate	84
3.2 An Extended Family of Four-State Quantum Key Distribution Protocols . .	88
3.3 Secrecy in the Presence of Weak Coherent Pulses	89
4 Comprehensive Analysis of System Losses and Loads	91
4.1 System Losses: The Line Attenuation - Free Space	92
4.1.1 Diffraction Vacuum Beam Spreading Losses	92

4.1.2	Static Atmospheric Losses	92
4.1.3	Turbulent Atmospheric Losses	94
4.1.4	Optics Package Losses	102
4.1.5	Complete Line Attenuation Losses - Free Space	102
4.2	System Losses: The Line Attenuation - Optical Fiber	106
4.3	The Intrinsic Channel Error	106
4.3.1	Free Space Quantum Channel	106
4.3.2	Optical Fiber Quantum Channel	107
4.4	System Loads	109
4.4.1	The Cost of Continuous Authentication	110
4.4.2	System Load: Total Communications Requirements	127
4.4.3	System Load: Total Computational Requirements	128
5	High-Speed Quantum Cryptography	137
5.1	Methods to Achieve High-Speed Quantum Cryptography	137
5.2	System Components and Constraints	138
5.2.1	Fast Photon Detectors: Hot-Electron Photo-Effect	141
5.2.2	High Pulse-Repetition-Frequency Lasers	142
5.2.3	High Speed Opto-electronics Components	143
5.2.4	Synchronization Constraints	143
5.2.5	Data Recording De-multiplexing Constraints	143
5.2.6	Multiple Transmitter-Receiver Multiplexing Analysis	145
5.2.7	High Speed Random Number Generation	148
5.3	Universal Maximal Rate Predictions	149
5.3.1	Necessary Condition for Unconditional Secrecy	149
5.3.2	Systems with Single Transmitter-Receiver Arrangement	149

5.3.3	Systems with Multiple Transmitter-Receiver Arrangement	162
5.3.4	Rate Improvement with Additional Emerging and Possible Future Technology	162
6	Discussion	164
7	Acknowledgements	164
8	Appendices	165
A	Derivation of the Relation between Intrinsic Channel Error and Polarizer Misalignment	165
B	Packetization Approximation	169
C	Statistical Results for Error Correction	170
D	Assembly Code Segments	180
D.1	Code to compute block parity	180
D.2	Code to extract substring for hash function	181
D.3	Code to compute Carter-Wegman affine hash function for double-word integers	182
D.4	Code to compute multi-word hash function for privacy amplification	184
References		187

List of Figures

1	Comparison of $\eta\psi_{\geq 1}(\mu)\alpha$ with $\psi_{\geq 1}(\eta\mu\alpha)$	29
2	Flow Chart of Analysis of Multi-Photon Pulse Privacy Amplification	36
3	Flow Chart for Analysis of Direct Attacks	40
4	Flow Chart for Analysis of Indirect Attacks	53
5	Flow Chart for Analysis of Combined Direct and Indirect Attacks	60
6	Flow Chart for Analysis of Comparison of Attack Strengths	65
7	Comparison of Strengths of Purely Direct and Purely Indirect Attacks	71
8	Comparison of Strengths of Combined, Purely Direct and Purely Indirect Attacks: Region One	74
9	Comparison of Strengths of Combined, Purely Direct and Purely Indirect Attacks: Region Two	75
10	Flow Chart for Analysis of Complete Expressions for Multi-Photon Pulse Privacy Amplification	76
11	Sample FASCODE Results for Static Atmospheric Attenuation	94
12	The Hufnagel-Valley 5/7 Model for Atmospheric Turbulence	95
13	Pulse Distortion and/or Broadening Graph	101
14	Optics Package Loss Comparison Table	103
15	Line Attenuation for $\lambda = 1550$ nm	104
16	Line Attenuation for $\lambda = 770$ nm	105
17	Information Leaked During Error Correction	123
18	Ratio of Information Leaked to Shannon Limit <i>versus</i> Error Fraction	124
19	Ratio of Information Leaked to Shannon Limit <i>versus</i> ϱ	125
20	Communication Load from Bob to Alice, Fixed m , Variable n	129
21	Communication Load from Bob to Alice, Fixed n/m , Variable m	130
22	Communication Load from Alice to Bob, Fixed m , Variable n	131

23	Communication Load from Alice to Bob, Fixed n/m , Variable m	132
24	Block Diagram for Alice System	139
25	Block Diagram for Bob System	140
26	Block Diagram for Data Recording System	145
27	Effective Rate Graph for Aircraft-to-Satellite (LEO) Link: $\alpha = -10$ dB (“Bob” - 58 cm telescope at 35000’ ; “Alice” - 30 cm telescope on LEO satellite)	150
28	Effective Secrecy Capacity Graph for Aircraft-to-LEO Link: $\eta = 50\%$; $r_c = 0.005$ $\alpha = -10$ dB (58 cm telescope at 35000’ - LEO satellite)	151
29	Effective Rate Graph for Earth-to-Satellite (LEO) Link: $\alpha = -20$ dB (“Bob” - 50 cm telescope at mean sea level ; “Alice” - 30 cm telescope on LEO satellite; clear weather)	153
30	Effective Rate Graph for Earth-to-Satellite (LEO) Link: $\alpha = -10$ dB (“Bob” - 1.6 m telescope at mean sea level ; “Alice” - 30 cm telescope on LEO satellite; clear weather)	154
31	Effective Rate Graph for Earth-to-Satellite (LEO) Link: $\alpha = -60$ dB (“Bob” - 43 cm telescope at mean sea level ; “Alice” - 30 cm telescope on LEO satellite; light rain)	155
32	Effective Rate Graph for Earth-to-Satellite (LEO) Link: $\alpha = -50$ dB (“Bob” - 1.4 m telescope at mean sea level ; “Alice” - 30 cm telescope on LEO satellite; light rain)	157
33	Effective Rate Graph for Earth-to-Satellite (GEO) Link: $\alpha = -26.4$ dB (“Bob” - 10 m telescope at 13500’ ; “Alice” - 30 cm telescope on GEO satellite) .	159
34	Effective Rate Graph for Fiber-Optic Cable Link without Surreptitious Cable Replacement	161
35	Effective Rate Graph for Fiber-Optic Cable Link with Surreptitious Cable Replacement	162
36	Effective Rate Graph for Aircraft-to-Satellite (LEO) Link: $\alpha = -10$ dB (“Bob” - 58 cm telescope at 35000’ ; “Alice” - 30 cm telescope on LEO satellite; commercial (1 MHz) photon detector)	163

List of Tables

1	Set of Distinct Purely Direct, Purely Indirect and Combined Attacks for $l = 5$.	62
2	Set of Distinct Purely Direct, Purely Indirect and Combined Attacks for $l = 8$.	63

1 Prologue

What is the reason for the excitement about quantum cryptography? Quantum cryptography is special because it provides a means for encrypting information that no amount of analysis can break. This is referred to as “unconditional secrecy.” The Great Thing is that this property of quantum cryptography is not a consequence of some “hard” mathematics problem that might be solved one day, nor of some devilishly clever algorithm or fiendishly intricate hardware design that might be reverse-engineered one day, but instead is due to what are believed to be inviolable principles of physical law: the physics of Quantum Mechanics. If our understanding of quantum mechanics is correct, and after three-quarters of a century of research we know of no reason to believe it to be incorrect, quantum cryptography is and *always will be* unconditionally secret, irrespective of whatever advances are made in mathematics or computer science, and probably in any other sphere of human activity. If the question is “What is the strongest *cryptographic* protection possible, as constrained directly by physical law?” the answer is “Quantum Cryptography.”

Quantum cryptography specifically provides a method of distributing the secret keys required to provide unconditionally secret communications - these are the famous “one-time pads” - and its use is guaranteed to reveal the presence of an enemy attempting to compromise the transfer. All quantum communications, such as quantum cryptography, requires the use of a quantum channel, which is a means of transporting physical objects called quantum bits (or “qubits”) in such a way that the quantum mechanical states of the qubits remain preserved from one end of the channel to the other. Two forms of quantum channel for quantum cryptography have thus far been shown to provide viable options, namely optical fiber cable, and (perhaps surprisingly) the atmosphere around us. The demonstrations conducted thus far have proved that it is possible to carry out quantum cryptography at low throughput rates, thus far not exceeding a few thousand bits per second. Our interest is in analyzing the possibilities for increasing the effective throughput rate for practical quantum cryptography systems to a range that is high enough to allow for the real-time encryption of useful volumes of data.

Recent progress in high-speed photon detection, high-speed laser optoelectronics, wavelength and time division multiplexing and lasercomm terminal miniaturization has occurred which makes it for the first time possible to contemplate the design of high-speed quantum cryptography systems. In addition to determining how to optimize quantum cryptography systems built out of currently available technology (and ensure that such systems will be perfectly secret in the presence of system imperfections), our analysis identifies the problems, provides corresponding solutions and demarcates the various constraints that will govern the development of high-speed quantum cryptography as new technology appears. The actual implementation of high-speed quantum cryptography systems would be invaluable, allowing for the first time the the practical possibility of one-time-pad-encrypted, undecipherable high-speed communications in bulk. If this can be achieved it will offer an essentially new degree of security in future high-bandwidth communications.

2 Introduction

2.1 Overview

Quantum key distribution (QKD) is a promising approach to the ancient problem of protecting sensitive communications from the enemy.¹ QKD is not in itself a method of enciphering information: it is instead a means of arranging that separated parties may share a completely secret, random sequence of symbols to be used as a *key* for the purpose of enciphering a message. Our objective is to elevate the use of quantum key distribution to the status of supporting full end-to-end real-time Vernam encryption [1, 2]. The Vernam cipher system (or systems based on it) provides the only known cryptographic method of achieving unconditionally secret communications.² We thus envisage an end-to-end cryptosystem that includes an initial phase of quantum key distribution and a subsequent phase of encryption with the method of the Vernam cipher, continuously and at useful, high data throughput rates. There have been a number of experimental demonstrations of QKD reported recently [3, 4, 5, 6, 7, 8, 9, 10, 11] that have been important in indicating the viability of the concept and in suggesting that it might be possible to incorporate QKD in practical systems applications. The initial demonstrations of QKD have been at low data throughput rates, none exceeding a few kilobits per second. However, the application of quantum key distribution at low data throughput rates does not support unconditionally secret Vernam encryption of modern communications data volumes, although implementation of quantum key distribution at low rates can indeed be useful as a means of distributing the *cryptovariables* that are used in traditional, classical symmetrical cryptography.³ For this purpose QKD systems operating at low data throughput rates of order a few thousand bits per second are perhaps adequate to play a supporting role for classical enciphering systems. However, classical cryptography (symmetrical or not) is not *unconditionally* secret, with the sole exception being the Vernam system (or systems directly based on it). There are situations and circumstances for which it is desirable, and in some cases absolutely essential, to increase the secrecy to the level possible only with the use of the Vernam cipher method. However, since the Vernam method requires a shared cipher at least as long, bit for bit, as the plaintext message to be enciphered, and moreover may under no circumstances be used more than one time, it is clear that slow data rates for key distribution⁴ will not work. Only a high speed QKD system can suffice to distribute, and distribute again and again as required, sufficiently large amounts of cipher material to support real-time Vernam encryption. We propose to reserve

¹ We will sometimes employ the word “enemy,” following the usage of Shannon [1], to denote anyone who may intercept an enciphered message.

² In the Vernam cipher system the message is referred, via the “exclusive or” (XOR) logic operation, to a random string of symbols, the Vernam cipher (one-time pad), resulting in another random string of symbols comprising the ciphertext. As a truly random string, the ciphertext is literally informationless, and cannot be decrypted by anyone not in possession of the random string used for the encryption. This is true irrespective of how much computing power they possess or which algorithms they utilize.

³ For a review of classical cryptography, see [12, 13].

⁴ We will use the words *key* and *cipher* to mean the same thing, since we always have in mind the Vernam system in particular, for which the two are synonymous.

the phrase *quantum key distribution* solely to describe the distribution of cipher material, and suggest that the phrase *quantum cryptography* be used to denote the combination in one complete end-to-end protocol of both QKD *and* subsequent Vernam encryption. Since, as discussed above, practical use in modern communications of the Vernam method requires high speed data throughput rates, quantum cryptography defined in this way for such an application is implicitly *high speed* quantum cryptography. In this sense practical quantum cryptography offers something never before technologically possible: the use of the Vernam cipher for those applications when unconditional secrecy is required or desirable, and indeed the fact that this can be done may lead to the suggestion of its use in circumstances for which it has previously only been thought of as an abstract idealization.

2.2 Summary of Results

The principal new contributions of this paper are as follows. We obtain:

- (1) A universal expression for the effective secrecy capacity that is valid in the general case of an actual cipher of finite length, that can be specialized to the case of an abstract cipher of infinite length, in eqs.(162) and (164). In the course of the derivation we obtain three categories of new results: (a) exact, closed form expressions for the *necessary and sufficient* amount of privacy amplification required to ensure a secret shared key associated with *direct*, *indirect* and newly identified *combined* cryptanalytic attacks on the transmission (eqs.(138) through (140)), (b) a practical, universal bound on the complete privacy amplification function that provides for useful data throughput values, while accounting for all possible individual attacks on the transmission,⁵ that is *always* at least as large as the minimum number of required subtraction bits required to ensure a secret shared key, in eqs.(142) through (151), and (c) a complete closed-form expression for the necessary and sufficient number of bits required to effect continuous authentication, in eqs.(152) through (158).
- (2) Complete characterizations of the total line attenuation losses, for free-space quantum channels, in eqs.(179), (183), (185), (186), (196), (199), (203) and (204).
- (3) A closed form relationship between intrinsic fractional quantum channel error and satellite-ground platform (or satellite-airborne platform or satellite-satellite) misalignment, in eqs.(206) and (332).
- (4) A closed-form expression relating the necessary amount of classical communications throughput to the parameters of the system, in the transmitter-receiver direction as well as in the receiver-transmitter direction (the two are not the same), and we obtain practical working values for particular systems, in eqs.(269), (270), (272) and (273).
- (5) A closed-form expression relating the computational burden, measured in units of neces-

⁵ In Part One of this work we will consider those attacks that the enemy can conduct using classical computing machines. In Part Two we will extend the analysis to include the potential attacks that could be performed in the future if and when quantum computing machines are available.

sary machine instructions, to the system parameters, and we obtain practical working point values, in and below eq.(286).

(6) Universal maximal rate predictions, for a variety of quantum cryptography scenarios, including Earth-to-LEO satellite in clear weather, Earth-to-LEO satellite in poor weather, aircraft-to-LEO satellite, Earth-to-GEO satellite, GEO-to-GEO satellite and fiber-optic cable links, in Sections 5.3.1 and 5.3.2.

2.3 Organization of the Paper

The paper is organized as follows. In Section 3 we carry out a complete formal derivation of the effective secrecy capacity and rate for practical quantum cryptography systems. We obtain exact, closed-form results for the entire system dynamics, including the calculation of exact necessary and sufficient results, as well as useful practical results for the required privacy amplification to ensure the unconditional secrecy of the shared cipher. Our exact results allow us to explicitly determine the requirements for high speed quantum cryptography in practical implementations. In Section 4 we perform a comprehensive analysis of all system losses and loads, for both free-space-based and optical fiber cable-based quantum cryptography systems, including in particular the full classical communications bandwidth requirements and the full computer machine instruction requirements needed to support actual quantum cryptography implementations. In Section 5 we analyze precise requirements for and detailed methods to achieve successful practical high speed quantum cryptography implementations in realistic environments. Our conclusions and a discussion are contained in Section 6, and Sections 7 and 8 contain acknowledgements and several appendices.

2.4 Brief Description of Quantum Key Distribution Protocol

Here we provide a very brief description of the basic elements of quantum key distribution. We will illustrate this with the original four-state QKD protocol developed by Bennett and Brassard in 1984 known as the “BB84” protocol [14]. For definiteness in this illustration we will assume that individual photons serve as the quantum bits for the protocol, or more precisely, the polarization states of individual photons. To carry out the protocol one of the parties transmits a sequence of photons to the other party. The parties publicly agree to make use of two distinct polarization bases which are chosen to be maximally non-orthogonal. In a completely random order, a sequence of photons are prepared in states of definite polarization in one or the other of the two chosen bases and transmitted by one of the parties to the other through a channel that preserves the polarization. The photons are measured by the receiver in one or the other of the agreed upon bases, again chosen in a completely random order. The choices of basis made by the transmitter and receiver thus comprise two independent random sequences. Since they are independent random sequences of binary numbers, about half of the basis choices will be the same and are called the “compatible”

bases, and the other half will be different and are called the “incompatible” bases. The two parties compare publicly, making use for this purpose of a classical communications channel, the two independent random sets of polarization *bases* that were used, without revealing the polarization *states* that they observed. The bit values of those polarization states measured in the compatible bases furnish the “sifted key.” Note that, if the two parties used classical signals to send the key, an eavesdropper could simply measure the signals to obtain complete knowledge of the key. If, on the other hand, the two parties use single photons to transmit the key, the Heisenberg Indeterminacy Principle guarantees that an eavesdropper cannot measure the polarizations without being detected. The sifted keys possessed by each of the parties will in general be slightly different from each other due to errors caused by the use of imperfect equipment. A classical error correction procedure, carried out through the classical communication channel, is executed in order to produce identical, error-free keys at both ends. It is possible that an enemy may have obtained some information about the key during the publicly-discussed error correction phase of the protocol. In addition, it is also possible for the enemy to have obtained information due to the presence in the sequence of quantum bits of multiple photon states. The process of “privacy amplification” is therefore applied to the sifted, error-free key, which has the effect of reducing the information available to the enemy to less than one bit, with extremely high probability.

These basic elements of quantum key distribution are discussed and analyzed in detail in this paper.

2.5 Secrecy and Security in Communications

It is important to be clear about the “security” advantage that does, and does not, derive from the use of quantum key distribution, quantum cryptography and the method of the Vernam cipher in secret communications. For this purpose we introduce standard definitions and discuss issues of context and application.

2.5.1 Definitions

“Secrecy” and “security” do not have the same meaning: the former is included within the latter. Stated differently, all secure communications systems provide secrecy, but not all secret communications systems provide security. In this paper we reserve the word *secrecy*, to mean what Shannon meant by the phrase “perfect secrecy” in his seminal work on the subject: *Communication Theory of Secrecy Systems* (*cf* [1]). The basic requirement for secrecy is that, in comparing the situation *before* the enemy has intercepted the transmission with the situation *after* any such interception (and analysis) has occurred, the *a posteriori* and *a priori* probabilities for the enemy to know the content of the transmission must be

identical.⁶ In an operational sense, we specifically intend the word “secrecy” to characterize, and apply solely to, the protection provided *strictly* by the cryptographic protocol alone. This operational meaning is best explained by placing secrecy in proper perspective in the larger framework of “security,” or more precisely, communications security [15]. Communications *security*, (so called “COMSEC”), may be naturally split into four separate categories (there are other ways of organizing these concepts – here we invoke the standard scheme advocated by the U.S. National Security Agency in [16]):

- (1) cryptosecurity - [The] component of communications security that results from the provision of *technically sound cryptosystems* (emphasis added) and their proper use.
- (2) emission security - Protection resulting from all measures taken to deny unauthorized persons information of value which might be derived from intercept and analysis of compromising emanations from crypto-equipment, computer and telecommunications systems.
- (3) physical security - The component of communications security that results from all physical measures necessary to safeguard classified equipment, material, and documents from access thereto or observation thereof by unauthorized persons.
- (4) transmission security - [The] component of communications security that results from the application of measures designed to protect transmissions from interception and exploitation by means other than cryptanalysis.

The word *secrecy* throughout this paper means no more and no less than *cryptosecurity*, in the sense of definition (1) above. This is the secrecy protection afforded purely *by the cryptographic protocol against purely cryptanalytic attacks* only. *Unconditional secrecy* refers to secrecy that remains intact when the cryptosystem is subjected to attacks by an enemy equipped with unlimited time and - within the constraints dictated by the laws of physics - unlimited computing machinery.

2.5.2 Technically Sound Quantum Cryptosystem Design and Practice

What *security* protection should unconditional *secrecy* provide? Should the purview of cryptosecurity, the protection afforded specifically by the cryptosystem *per sé*, be extended to include protection normally provided by the other three elements of COMSEC? The answer to this question is “no.” Stated more precisely, if a so-called “technically sound cryptosystem” is properly operated, with the consequent balance between the four elements of COMSEC that this implies, there should be no *need* for such an extension of purview. It is not the

⁶ Of course, if the *a posteriori* and *a priori* probabilities are indeed identical, but happen to be identically equal to, say, unity, then we clearly don’t have a secret system. In the case of a string to be used as a Vernam cipher we obviously *also* need that the probability for the enemy to know any specific bit is equal to 50%, independently of the ordering of the bits. Then perfect secrecy in Shannon’s sense means that the probability for the enemy to know the entire string approaches zero exponentially quickly with the number of bits.

purpose of this paper to provide a detailed analysis of proper cryptosystem *praxis*, but two observations should suffice to illustrate the main point.

As one example, we may imagine that a perfect cryptographic system that provides unconditional secrecy has been set up and is in use. If the actual method of use by the secret communicators, however, includes “leaving the door(s) open” at one (or both) of their facilities, so that an eavesdropper can actually *gain access* to their system in some way, the system *security* is obviously entirely lost, in spite of the unconditional *secrecy* of the underlying cryptosystem. Is it reasonable to insist that the cryptosystem, *per sé*, provide protection against such technically unsound cryptographic practice? The answer is “no.” Before commenting on the technical implications of this, let us consider a different situation.

As another example, one might try to argue (erroneously) that free-space *classical* key distribution between a satellite and a ground station is “obviously” perfectly secure without the need for making use of quantum bits, or even any cryptography at all. If the transmission consists of classical bits, encoded in optical pulses generated by a laser and propagated along a highly collimated beam, wouldn’t it be *very difficult* for an enemy to actually physically intercept the beam at all? Wouldn’t it be *almost impossible* for the enemy to somehow grab such a signal out of a highly collimated, thin beam? Of course, the beam becomes broader as it propagates, and moreover, it is possible for the enemy to exploit the scattering of such a beam but nevertheless, the answer to this question is “yes, it is difficult” but that is irrelevant.

What these two examples illustrate are two extremes in regard to what protection the cryptosystem should, and should not provide. We agree strongly with the philosophy that cryptosecurity should be viewed as *only one part* of an overall system for ensuring communications security (*cf*[17]). Technically sound quantum cryptosystem *design*, for instance, dictates that if it is possible to trivially prevent the enemy from modifying photon wavelengths in multiple photon pulses and thereby prevent the “remote” adjustment of the quantum efficiency of the photon detector in a quantum cryptography system by simply placing a narrow bandpass filter at the front of the receiving apparatus, then such a technique, which falls *outside the purview* of pure cryptography and is instead an element of transmission security, must be implemented.⁷ The point is that the fact that this is being implemented can be fully disclosed, without any loss of security whatsoever, to the enemy, as there is nothing that can be done about it. Similarly, technically sound quantum cryptosystem *practice* dictates that the communicating parties must obtain an accurate measurement of the ambient noise along the quantum channel prior to the use of the system. On the other hand, potential attacks on the secret communication cryptosecurity, as such, must be protected against, *solely* on the basis of whatever features the cryptosystem itself provides. It is not a valid argument that a particular attack is “difficult,” since the technological capabilities of the enemy may improve, and moreover, these should never be underestimated. The consequences of the preceding qualitative statements all translate into concrete mathematical implications for

⁷ This particular issue is in fact of considerable importance and is discussed in much more detail later in the paper.

the detailed analysis of the necessary and sufficient amount of privacy amplification (this is introduced in the next section) required in a practical quantum cryptography system, so we codify the meaning of this below.

Quantum Cryptographic Conservative Catechism

We propose the following “doctrine of reasonableness” for analyzing practical quantum cryptography systems: the *Quantum Cryptographic Conservative Catechism* (QC_{CC}), according to which (1) it is presumed that both the physical hardware design *and* the actual operation of any QC system will together furnish a technically sound cryptosystem as determined both by the precedents already established through the history of cryptology and new features specific to quantum communications, and (2) any proper theoretical analysis of the performance characteristics of a practical QC system must incorporate the underlying assumption that the enemy is limited solely by the laws of physics, relaxed *only* to the extent that it is reasonable to take condition (1) into account. This is the approach followed in our study.

3 Theoretical Analysis of Effective Secrecy Capacity

In this chapter we will perform a careful derivation of the functions that provide a full account of the operating characteristics of a general QKD system. Our analysis is specifically constructed to characterize the Bennett-Brassard Four-State (BB84) QKD protocol [14], or more precisely, a set of generalizations that include the original BB84 protocol as a special case.⁸ The figure-of-merit for the operating characteristics and secrecy of a QKD system is provided by the effective secrecy capacity, \mathcal{S} , in terms of which we may define the effective secrecy *rate* for the system, \mathcal{R} .⁹ These quantities provide a full characterization of the operating characteristics of the cryptographic communications system set up between the legitimate communicating parties, traditionally referred to as “Alice” and “Bob.” The effective secrecy capacity is defined as the ratio of the *final length* in bits, of the secret shared cipher, to the number of bits initially transmitted by Alice to Bob in order to establish the final cipher. The “final length” is the length of the string after the full execution of the protocol, including all of the required error correction, privacy amplification and continuous authentication¹⁰ has been applied to the original, “raw” string, *i.e.*, the transmitted string that has not yet been subjected to any processing at all. We denote the number of “raw” pulses¹¹ sent by Alice to Bob as m , the number of bits in the compatible polarization basis that actually reach Bob as n , the number of *those* bits which are in error as e_T , the total number of bits that must be subtracted¹² from the string in order to effect privacy amplification as s , the privacy amplification security parameter as g_{pa} , and the number of bits required to be subtracted in order to carry out continuous authentication as a . Then the

⁸ In fact, the use of a source of data bits that produces an admixture of single- and multiple-particle states means that the system does *not* implement the original, pure BB84 protocol, which by definition requires pure, idealized qubits represented by single particle states. However, our analysis is sufficiently general to include all such implementations. In addition, although our analysis does not focus specifically on quantum cryptography with entangled states, such as the Ekert protocol [18] or the recently demonstrated entangled state *variant* of the original BB84 protocol [19], our results can be modified to apply to it as well. Work is in progress on the latter topic, which will appear as Part Two of the current work [20].

⁹ In our calculation we shall adopt, and considerably expand, the notational scheme introduced by Slutsky, *et. al.* in [21] of the various system characteristics and capacities. Our analysis is more complete than previous treatments in accounting for *all* relevant system processes, and our use of previously established notation will in particular make it easy to identify the ways in which our analysis extends previously obtained results in this area.

¹⁰ It is essential in any complete analysis of the characteristics of a QKD system to fully account for what we refer to as “continuous authentication.” (The authors thank a contact at the U.S. National Security Agency for suggesting to us the phrase “continuous authentication.”) Authentication is intended to ensure that only legitimate parties may communicate via a cryptographic system. We require the minimum amount of authentication, but no less than that, in order to preserve the integrity of the QKD protocol. *Continuous* authentication, for every single transmission between Alice and Bob, is absolutely required, but has not been thoroughly studied before. It is not sufficient to “authenticate” once, as repeated attempts at system intrusion may be made by the enemy. In this paper we carry out a full analysis of this process, along with all other relevant system processes.

¹¹ This number includes the “empty” pulses – those for which the filtering applied to the output of the laser has resulted in the statistical extinction of the photon content.

¹² The privacy amplification subtraction function, s , is defined here so as *not* to include the privacy amplification security parameter g_{pa} .

effective secrecy capacity is defined as¹³

$$\mathcal{S} \equiv \frac{n - e_T - s - g_{pa} - a}{m}. \quad (1)$$

The effective secrecy rate corresponding to the effective secrecy capacity measures the effective throughput of secure Vernam cipher in bits per second and is given by

$$\mathcal{R} = \tau^{-1} \mathcal{S}, \quad (2)$$

where τ is the bit cell period, the period of time that is required for the system hardware to transmit one signal from Alice to Bob, “reset” itself and become ready to transmit the next signal.

3.1 Derivation of Effective Secrecy Capacity

We want to determine the conditions under which a fully realistic, practical system implementation of the BB84 protocol for quantum key distribution can produce unconditionally secret, shared key material between Alice and Bob. Moreover, we want to discover those conditions under which we may obtain the highest possible data throughput rate so that we can use the shared key as a real-time Vernam cipher and thus legitimately speak of end-to-end quantum cryptography, *i.e.*, an unconditionally secret communications system capable of supporting large volumes of data. For this purpose we need to obtain an explicit, closed form expression for the effective secrecy capacity that directly expresses \mathcal{S} in terms of the actual operating parameters for a realistic system implementation of quantum cryptography.

3.1.1 The Sifted Key and the Transmitted Errors

We will deduce explicit expressions for the various quantities that appear in the expression for the effective secrecy capacity, starting with the length of the sifted key and the length of the transmitted error part. We will assume that the “Alice” system instrumentation principally includes a pulsed laser which generates pulses of light in the form of coherent states. This assumption can be made without loss of generality since, as will be evident below, our formulation will include as a special case the situation in which Alice instead utilizes a device that, through whatever means, produces only single-photon states. The state function for a fiducial coherent state produced by the laser is given by¹⁴

$$|\phi\rangle = \sum_{l=0}^{\infty} \sqrt{e^{-\mu} \frac{\mu^l}{l!}} e^{il\phi} |l\rangle \quad (3)$$

¹³ We choose a definition of the effective secrecy capacity appropriate for the QKD protocol in which error correction is effected by identifying and *discarding*, rather than identifying, correcting and *retaining*, the error bits. Our analysis can be easily adapted to the case where error bits are identified, corrected and retained. This is consistent with the conservative approach adopted throughout our analysis and means that the various rate predictions we will make in fact constitute *lower bounds* on achievable throughput values.

¹⁴ The enemy, in general, will not detect potential *intercepted* states precisely as coherent states, but will instead (due to lack of a phase reference) detect a mixture of Fock space states that are characterized by

where ϕ is the quantum mechanical phase and μ is defined as the expectation value of the number operator, and in practice is the mean photon number per pulse. The number of photons produced is thus characterized by a Poisson distribution. We denote by $\hat{\chi}(\mu, l)$ the probability that a laser pulse (in a stream of pulses characterized by μ) will contain exactly l photons and thus

$$\hat{\chi}(\mu, l) = e^{-\mu} \frac{\mu^l}{l!}. \quad (4)$$

We will sometimes find it convenient to use the notation

$$\psi_1(\mu) \equiv \hat{\chi}(\mu, 1) = \mu e^{-\mu} \quad (5)$$

and

$$\psi_2(\mu) \equiv \hat{\chi}(\mu, 2) = \frac{\mu^2}{2} e^{-\mu} \quad (6)$$

for the probabilities that exactly one and two photons, respectively, are in a pulse.

In the same manner we deduce that the probability, $\psi_{\geq 1}$, that a laser pulse will contain one or more photons is given by

$$\psi_{\geq 1}(\mu) = \sum_{l=1}^{\infty} e^{-\mu} \frac{\mu^l}{l!} = 1 - e^{-\mu}, \quad (7)$$

and that the probability, $\psi_{\geq 2}$, that a laser pulse will contain two or more photons is given by

$$\psi_{\geq 2}(\mu) = \sum_{l=2}^{\infty} e^{-\mu} \frac{\mu^l}{l!} = 1 - e^{-\mu} - \mu e^{-\mu}. \quad (8)$$

In our analysis of quantum key distribution¹⁵ we assume that Alice prepares and launches in the direction of Bob a number, m , of laser pulses, referred to as the *raw bits*. The time required to prepare, launch and ready the system to prepare another pulse is the *bit cell period*, τ . The overall QKD event thus lasts for a duration of $m\tau$. Out of the full set of m bit cells sent by Alice, a certain fraction only will survive to become potential bits in the secret key. In deducing the expression for the effective secrecy capacity we must take into account the amount of attenuation, α , that characterizes the propagation loss conditions of the trajectory connecting, and including, the Alice and Bob systems. We also need to take account of the imperfect intrinsic quantum efficiency, η , that characterizes Bob's detector, as well as the intrinsic dark count probability, r_d . Alice and Bob follow the standard protocol, whereby the polarization *bases* (but not the polarization *states*) of the bits collected by Bob are publicly discussed and compared between Alice and Bob. The

a Poisson distribution and described by an appropriate density matrix [22]. This fact has no bearing on the calculation of the number of *sifted* bits shared between Alice and Bob, as they *do* possess the necessary phase reference, and thus the use of explicit coherent states is appropriate.

¹⁵In strict accuracy one should refer to the QKD protocol as quantum key *expansion*, rather than distribution, since the success of the entire process requires that Alice and Bob be in possession of a suitable initial authentication string, which must be secret. This topic of authentication is discussed in much greater detail below.

bases for which Alice and Bob find themselves in agreement are referred to as *compatible* bases, and the remainder are referred to as the *incompatible* bases. The random orientations of the polarizing and polarization-discriminating apparatuses at Alice and Bob are assumed to comprise two completely uncorrelated sequences, so that for about half of the bit cells about which Alice and Bob conduct their discussion they will have noted compatible bases, and for the other half the bases will be incompatible. After taking into account the various other effects that cause the bits shared between Alice and Bob to be diminished in number, we can establish the number, n , of *sifted* bits for the QKD problem.

In order to be as general as possible in our analysis we will formulate the expression for the number of sifted bits from first principles in terms of the various underlying probabilities associated to the different processes that take place. Denoting the various relevant probabilities by \mathcal{P} with appropriate arguments, we have

$$\mathcal{P}(l \text{ photons leave Alice}) = e^{-\mu} \frac{\mu^l}{l!} \equiv \hat{\chi}(\mu, l), \quad (9)$$

$$\mathcal{P}(l' \text{ photons reach Bob} \mid l \text{ photons leave Alice}) = \binom{l}{l'} \alpha^{l'} (1 - \alpha)^{l-l'}, \quad (10)$$

$$\mathcal{P}(l'' \text{ photons detected} \mid l' \text{ photons reach Bob}) = \binom{l'}{l''} \eta^{l''} (1 - \eta)^{l'-l''} (1 - \delta_{0,l''}), \quad (11)$$

$$\mathcal{P}(\text{no dark count event}) = 1 - r_d, \quad (12)$$

and

$$\mathcal{P}(\text{basis compatibility}) = \frac{1}{2}. \quad (13)$$

In writing the expressions in eqs.(10) and (11) we are incorporating assumptions on the statistical nature of the responses of both the qubit detector and the environmental processes responsible for the line attenuation. With the chosen form for the rhs of eq.(10) we are assuming that all attenuation processes act incoherently on a l -photon pulse, and that there is no enhancement or suppression when l photons try to get through together. Similar assumptions apply in the case of eq.(11), in addition to which the factor of $1 - \delta_{0,l}$ enforces the condition that the detector apparatus may not fire when zero photons are incident upon it (modulo dark count events, which are described in a separate term as seen below).

These assumptions are quite reasonable, and they have evidently been implicitly adopted in all previous work on this subject (*e.g.*, [21, 23]), but we here for the first time make them explicitly clear. In fact, the final explicit form for n obtained in eq.(15) below presumably *only* follows upon making these two specific assumptions.¹⁶

¹⁶ Analysis of any specific forms for the number of sifted bits, n , that may arise upon making *different* specific assumptions about the processes that underlie eqs.(10) and (11) appears to have never been carried out. This is a worthwhile area for future research.

We may now deduce the expression for the number of sifted bits by assembling the appropriate probabilities, to yield

$$\begin{aligned}
n &= m \left\{ \left[\sum_{l,l',l''} \mathcal{P} (l \text{ photons leave Alice}) \right. \right. \\
&\quad \times \mathcal{P} (l' \text{ photons reach Bob} \mid l \text{ photons leave Alice}) \\
&\quad \times \mathcal{P} (l'' \text{ photons detected} \mid l' \text{ photons reach Bob}) \\
&\quad \times \mathcal{P} (\text{no dark count event}) \mathcal{P} (\text{basis compatibility}) \Big] \\
&\quad \left. + \mathcal{P} (\text{dark count event}) \mathcal{P} (\text{basis compatibility}) \right\} \\
&= m \left\{ \sum_{l,l',l''} \left[e^{-\mu} \frac{\mu^l}{l!} \binom{l}{l'} \alpha^{l'} (1-\alpha)^{l-l'} \binom{l'}{l''} \eta^{l''} (1-\eta)^{l'-l''} (1-\delta_{0,l''}) (1-r_d) \cdot \frac{1}{2} \right. \right. \\
&\quad \left. \left. + r_d \cdot \frac{1}{2} \right] \right\} \\
&= \frac{m}{2} \left\{ (1-r_d) \sum_{l,l',l''} \left[e^{-\mu} \frac{\mu^l}{l!} \binom{l}{l'} \alpha^{l'} (1-\alpha)^{l-l'} \binom{l'}{l''} \eta^{l''} (1-\eta)^{l'-l''} (1-\delta_{0,l''}) \right] + r_d \right\} \\
&= \frac{m}{2} \left\{ (1-r_d) \sum_{l=0}^{\infty} e^{-\mu} \frac{\mu^l}{l!} \sum_{l'=0}^l \binom{l}{l'} \alpha^{l'} (1-\alpha)^{l-l'} \sum_{l''=0}^{l'} \binom{l'}{l''} \eta^{l''} (1-\eta)^{l'-l''} (1-\delta_{0,l''}) + r_d \right\} \\
&= \frac{m}{2} \left\{ (1-r_d) \sum_{l=0}^{\infty} e^{-\mu} \frac{\mu^l}{l!} \left[1 - \sum_{l'=0}^l \binom{l}{l'} \alpha^{l'} (1-\alpha)^{l-l'} \binom{l'}{0} (1-\eta)^{l'} \right] + r_d \right\} \\
&= \frac{m}{2} \left\{ (1-r_d) \sum_{l=0}^{\infty} e^{-\mu} \frac{\mu^l}{l!} \left[1 - (1-\eta\alpha)^l \right] + r_d \right\} \\
&= \frac{m}{2} \left[(1-r_d) \left\{ 1 - e^{-\mu} \sum_{l=0}^{\infty} \frac{[\mu(1-\eta\alpha)]^l}{l!} \right\} + r_d \right] \\
&= \frac{m}{2} \left[(1-r_d) \left(1 - e^{-\eta\mu\alpha} \right) + r_d \right] \\
&= \frac{m}{2} \left[(1-r_d) \psi_{\geq 1}(\eta\mu\alpha) + r_d \right] \\
&\simeq \frac{m}{2} \left[\psi_{\geq 1}(\eta\mu\alpha) + r_d \right]. \tag{14}
\end{aligned}$$

where $\psi_{\geq 1}$, the probability of encountering one or more than one photon in a pulse, is defined in eq.(7). In the last step above we have neglected r_d in comparison to unity, which means that we are ignoring the *dark count coincidence* events, for which a dark count occurred in precisely the same bit cell as an authentic photon detection event (this is a valid approximation for a good QKD system equipped with a detector apparatus characterized by a small dark count rate).

As discussed below eq.(13), the form that we have derived for the number of sifted bits depends on those assumptions that underlie eqs.(10) and (11). In addition to these assumptions, the result obtained in eq.(15) above requires making the *further* assumption on the intrinsic properties of the quantum channel that the Poisson distribution of photon number that characterizes the output of the source laser at the Alice end *also* describes the state received at the Bob end of the quantum channel.

Let us consider the meaning of the terms in the square bracket in eq.(15) above. The first term, $\psi_{\geq 1}(\eta\mu\alpha)$, is the contribution to the number of sifted bits due to the bit cells comprised of single-photon and multiple-photon pulses characterized by an *effective* mean photon number per pulse of $\eta \times \mu \times \alpha$, reflecting the fact that the stream is subjected to the effects of both line attenuation and imperfect detection by Bob's apparatus. The remaining term is simply the contribution to the number of sifted bits due to those dark counts occurring in Bob's apparatus that do not occur in a bit cell for which an authentic photon detection event takes place.

We also need to deduce the number of sifted bits that are in error, e_T . The calculation is similar to that for n , where we now take into account as well the *intrinsic* quantum channel error rate, r_c . In our parametrization of the QKD problem, r_c measures only the tendency of the system arrangement at Alice and Bob, along with the intrinsic properties of the quantum channel itself, to cause polarization misalignment and dispersion of photon arrival times between the instruments at Alice and Bob, as we are assigning to other quantities (η , r_d and most significantly, α) the role of measuring other system imperfections. In the case of a free-space QKD system in which Alice and/or Bob are located on a moving platform, such as a satellite, r_c may be a measure of the actual physical misalignment of the apparatuses at the two ends. In the case of a fiber-optic cable QKD system, r_c may be a measure of certain dispersion effects intrinsic to the cable. In calculating e_T we also take account of the fact that the dark counts produced by Bob's detector instrument will, by coincidence, be “wrong” half of the time, so that the factor of r_d that appears in the expression for n must be replaced by $r_d/2$.

Following the same approach used to deduce eq.(15) we may assemble the necessary probability functions and carry out the required calculation to obtain the expression for the number of transmitted error bits, e_T , which is found to be given by

$$e_T = \frac{m}{2} \left[\left(1 - \frac{r_d}{2}\right) r_c \psi_{\geq 1}(\eta\mu\alpha) + \frac{r_d}{2} \right] \quad (16)$$

$$\simeq \frac{m}{2} \left[r_c \psi_{\geq 1}(\eta\mu\alpha) + \frac{r_d}{2} \right], \quad (17)$$

where in the second line above we have made the same approximation utilized in deriving eq.(15) and neglected r_d in comparison to (in this case, twice) unity.

Monitoring the Statistics of the Detection Events

It may be advantageous for Alice and Bob to specifically exclude from the sifting process those bit cells which are manifestly associated with multiple photon pulses, since these bit cells provide an opportunity for the enemy to obtain information on the final, shared key. For this analysis, we envisage a generic, purely passive Bob apparatus suitable for use in the BB84 protocol consisting of four photon detectors,¹⁷ for which there is a calculable probability that, given a multi-photon pulse with l photons incident on the apparatus, one and only one of the four detectors will click (we use the word “click” to refer to the registration by the detector of an incident photon). We will express this as the *confounding probability* that Bob will not be able to distinguish a multi-photon pulse from a single-photon pulse, and denote this probability by $\hat{z}(\eta, l)$, where in general there is a dependence on both the photon number l and the detector efficiency η . Thus, Bob and Alice can agree to discard those multi-photon pulses that manifestly produce more than a single click at Bob’s detector (leaving only those multi-photon pulses that happen to produce a single click), and we can incorporate this condition quantitatively in the expression for the effective secrecy capacity. This will result in a shortened length for the sifted string, apparently thus *reducing* the possible value of the effective secrecy capacity. However, this procedure will *also* reduce the size in bits of the associated privacy amplification subtraction amount, thus potentially *increasing* the effective secrecy capacity, and so the two effects compete with each other. Because of the complicated dependence on the various parameters that characterize the QKD problem, such as the line attenuation, the mean photon number per pulse, the detector efficiency and others (as derived in detail below), it is not clear *a priori* which term will dominate. Such a scheme is a variant of implementations of BB84 employing weak coherent pulses in which no distinction at all is made between single- and multiple-photon pulses, and it is designed to explore the extent to which we can optimize the throughput rate as well as guarantee unconditional secrecy identical to that achievable if only pure single photon states are used.¹⁸

To proceed, we return to the expression for the number of sifted bits derived above. To emphasize the contributions to n due separately to the single-photon and multi-photon pulses we can rewrite eq.(15) as (cf eqs.(5), (7) and (8))

$$n = \frac{m}{2} \left[\psi_1(\eta\mu\alpha) + \psi_{\geq 2}(\eta\mu\alpha) + r_d \right]. \quad (18)$$

Inspection of the above expression would seem to indicate that to incorporate monitoring of the click statistics it should be necessary to modify only the second term in the square brackets, since, modulo dark count coincidence events, multiple clicks can obviously never be produced when single-photon pulses (represented by the first term in the square brackets) arrive at Bob’s apparatus. However, it turns out that the first term, *in addition to* the second term, must be appropriately modified, as we show.

¹⁷ The receiver design is discussed in detail in Section 5.2 below.

¹⁸ This extension of the BB84 protocol in fact may be further generalized to include a *family* of generic extensions, distinguished from each other by precisely how Bob monitors the statistics of the distribution of multiple clicks at his detector. In Section 3.2 below we discuss this in more detail.

To understand this, we need to suitably modify the list of probabilities included in eqs.(9) to (13), to allow for the characterization of the single-click detection events. For this purpose we replace

$$\mathcal{P} (l'' \text{ photons detected} \mid l' \text{ photons reach Bob}) = \binom{l'}{l''} \eta^{l''} (1 - \eta)^{l' - l''} (1 - \delta_{0,l''}) \quad (19)$$

with

$$\mathcal{P} (\text{single click event} \mid l' \text{ photons reach Bob}) \equiv \hat{z}_B(\eta, l') , \quad (20)$$

where, as mentioned above, in general there is a dependence in \hat{z}_B on both the number of received photons and the detector efficiency.

The explicit form of $\hat{z}_B(\eta, l)$, the confounding probability for Bob that, given a laser pulse incident upon his apparatus with l photons in it, one and only one of Bob's four detectors will click, will depend on (1) a model that specifies the details of the detector apparatus, *as well as on* (2) the particular click-monitoring scheme that is adopted. In the following we will take as a standard example a model of a purely passive setup with four photon detectors placed behind a pair of polarizing beamsplitters, which in turn are placed behind a purely passive 50/50 beamsplitter (*cf* Figure 25). Having thus picked the detector model, we are still free to specify the click-monitoring scheme. For instance, in one such scheme we could require that Bob discard all bit cells in which any arrangement of simultaneous clicks occurs, while in another scheme we could require that only bit cells in which simultaneous clicks between, say, two detectors occur, but not between three detectors, *etc.*¹⁹ To make the analysis as general as possible we will make no specific assumption on this point. This still allows us to provide explicit expressions for the cases of zero and one photons, so that we have

$$\hat{z}_B(\eta, 0) = 0 , \quad (21)$$

$$\hat{z}_B(\eta, 1) = \eta , \quad (22)$$

which indicates that there is a 100% chance that a detector will fire if a single photon impinges on the receiving apparatus, assuming a perfect detector (this may be easily verified to follow from the assumption of a purely passive Bob apparatus, as described above), and we define

$$\hat{z}_B(\eta, l') \Big|_{l' \geq 2} \equiv \hat{z}_{B,\geq 2}(\eta, l') , \quad (23)$$

where $\hat{z}_{B,\geq 2}$ is a kernel to be operated on by a suitable probability distribution that characterizes the distribution of the l' photons that have in some manner propagated to the input of Bob's detector apparatus (the use of a general expression for values of $l' \geq 2$ allows a general treatment without specifying a particular click-monitoring scheme).

We may now deduce the modified expression for the number of sifted bits, n_{mcs} (the subscript stands for “monitor click statistics”) obtained with explicit monitoring of the statistics of the

¹⁹ Another possibility is that *all four* detectors simultaneously fire. This can only occur if at least one of the four firings is due to a dark count event.

detection clicks, by assembling the appropriate probabilities, now supplemented by eq.(20), to yield (note that we now sum over two rather than three indices)

$$\begin{aligned}
n_{mcs} &= m \left\{ \left[\sum_{l,l'} \mathcal{P} (l \text{ photons leave Alice}) \right. \right. \\
&\quad \times \mathcal{P} (l' \text{ photons reach Bob} \mid l \text{ photons leave Alice}) \\
&\quad \times \mathcal{P} (\text{single click event} \mid l' \text{ photons reach Bob}) \\
&\quad \left. \times \mathcal{P} (\text{no dark count event}) \mathcal{P} (\text{basis compatibility}) \right] \\
&\quad \left. + \mathcal{P} (\text{dark count event}) \mathcal{P} (\text{basis compatibility}) \right\} \\
&= m \left\{ \sum_{l,l'} \left[e^{-\mu} \frac{\mu^l}{l!} \binom{l}{l'} \alpha^{l'} (1-\alpha)^{l-l'} \hat{z}_B(\eta, l') (1-r_d) \cdot \frac{1}{2} \right] + r_d \cdot \frac{1}{2} \right\} \\
&= \frac{m}{2} \left\{ (1-r_d) \sum_{l,l'} \left[e^{-\mu} \frac{\mu^l}{l!} \binom{l}{l'} \alpha^{l'} (1-\alpha)^{l-l'} \hat{z}_B(\eta, l') \right] + r_d \right\} \\
&= \frac{m}{2} \left\{ (1-r_d) \left[\sum_{l=0}^{\infty} e^{-\mu} \frac{\mu^l}{l!} \sum_{l'=0}^l \binom{l}{l'} \alpha^{l'} (1-\alpha)^{l-l'} \hat{z}_B(\eta, l') \right] + r_d \right\} \\
&= \frac{m}{2} \left\{ (1-r_d) \sum_{l=0}^{\infty} e^{-\mu} \frac{\mu^l}{l!} \left[l \alpha (1-\alpha)^{l-1} \eta + \sum_{l'=2}^l \binom{l}{l'} \alpha^{l'} (1-\alpha)^{l-l'} \hat{z}_B(\eta, l') \right] + r_d \right\} \\
&= \frac{m}{2} \left[(1-r_d) \left\{ \eta \mu \alpha e^{-\mu} \sum_{l=0}^{\infty} \left[\frac{\mu^{l-1} (1-\alpha)^{l-1}}{(l-1)!} \right] + \langle \hat{\chi}(\mu, l) \hat{\mathcal{Z}}_{\geq 2}(\eta, \alpha, l) \rangle \right\} + r_d \right] \\
&= \frac{m}{2} \left\{ (1-r_d) \left[\eta \mu \alpha e^{-\mu \alpha} + \langle \hat{\chi}(\mu, l) \hat{\mathcal{Z}}_{\geq 2}(\eta, \alpha, l) \rangle \right] + r_d \right\} \\
&= \frac{m}{2} \left\{ (1-r_d) \left[\eta \psi_1(\mu \alpha) + \langle \hat{\chi}(\mu, l) \hat{\mathcal{Z}}_{\geq 2}(\eta, \alpha, l) \rangle \right] + r_d \right\} \quad (24) \\
&\simeq \frac{m}{2} \left[\eta \psi_1(\mu \alpha) + \langle \hat{\chi}(\mu, l) \hat{\mathcal{Z}}_{\geq 2}(\eta, \alpha, l) \rangle + r_d \right], \quad (25)
\end{aligned}$$

where ψ_1 , the probability of encountering exactly one photon in a pulse, is defined in eq.(5), and we have defined as well

$$\begin{aligned}
\langle \hat{\chi}(\mu, l) \hat{\mathcal{Z}}_{\geq 2}(\eta, \alpha, l) \rangle &\equiv \sum_{l=0}^{\infty} \hat{\chi}(\mu, l) \hat{\mathcal{Z}}_{\geq 2}(\eta, \alpha, l) \\
&= \sum_{l=0}^{\infty} e^{-\mu} \frac{\mu^l}{l!} \hat{\mathcal{Z}}_{\geq 2}(\eta, \alpha, l) ,
\end{aligned} \quad (26)$$

and

$$\hat{\mathcal{Z}}_{\geq 2}(\eta, \alpha, l) \equiv \sum_{l'=2}^l \binom{l}{l'} \alpha^{l'} (1-\alpha)^{l-l'} \hat{z}_{B,\geq 2}(\eta, l') , \quad (27)$$

and in eq.(25) we have once again ignored r_d in comparison to unity.²⁰ ²¹

Let us consider the meaning of the three terms in the square bracket in the first equation on the rhs of eq.(25). The first term, $\eta\psi_1(\mu\alpha)$ (to be compared with the first term in the square brackets in eq.(18) which is $\psi_1(\eta\mu\alpha)$): note the migration of the factor of η out of the argument of ψ_1), is the contribution to the number of sifted bits due to the bit cells comprised of single-photon pulses taken from a stream of pulses characterized by a mean photon number per pulse of $\mu \times \alpha$ and further modified by the detector efficiency, reflecting the fact that the stream is subjected to the effects of both line attenuation and imperfect detection by Bob's apparatus, and incorporating the effects of the click-monitoring procedure. The second term, $\langle \hat{\chi}(\mu, l) \hat{\mathcal{Z}}_{\geq 2}(\eta, \alpha, l) \rangle$, is the contribution to the number of sifted bits due to those multi-photon bit cells that cause only a single click to occur amongst the four detectors in Bob's apparatus. (Those multi-photon pulses which cause multiple clicks in Bob's device are watched for and discarded.) The remaining term is simply the contribution to the number of sifted bits due to those dark counts occurring in Bob's apparatus that do not occur in a bit cell for which an authentic photon detection event takes place.

Eq.(14) can in fact be recovered as a special case of eq.(24). It is easy to see this by rewriting n_{mcs} instead as a sum to manifestly include single photon pulses, so that we have

$$\begin{aligned} n_{mcs} &= \frac{m}{2} \left[(1 - r_d) \langle \hat{\chi}(\mu, l) \hat{\mathcal{Z}}_{\geq 1}(\eta, \alpha, l) \rangle + r_d \right] \\ &\simeq \frac{m}{2} \left[\langle \hat{\chi}(\mu, l) \hat{\mathcal{Z}}_{\geq 1}(\eta, \alpha, l) \rangle + r_d \right], \end{aligned} \quad (28)$$

where

$$\begin{aligned} \langle \hat{\chi}(\mu, l) \hat{\mathcal{Z}}_{\geq 1}(\eta, \alpha, l) \rangle &\equiv \sum_{l=0}^{\infty} \hat{\chi}(\mu, l) \hat{\mathcal{Z}}_{\geq 1}(\eta, \alpha, l) \\ &= \sum_{l=0}^{\infty} e^{-\mu} \frac{\mu^l}{l!} \hat{\mathcal{Z}}_{\geq 1}(\eta, \alpha, l) \end{aligned} \quad (29)$$

and

$$\hat{\mathcal{Z}}_{\geq 1}(\eta, \alpha, l) \equiv \sum_{l'=1}^l \binom{l}{l'} \alpha^{l'} (1 - \alpha)^{l-l'} \hat{z}_B(\eta, l') . \quad (30)$$

The sum over l' in the above expression could just as well be allowed to range from zero to infinity since $\hat{z}_B(\eta, 0)$ vanishes identically. We have here marked the sum as beginning at $l' = 1$ merely to emphasize specific value of the one-photon contribution in the result.

²⁰ We employ a non-standard notation for averages, explicitly including inside the brackets the specific distribution function with respect to which the average is defined, and in particular including the argument of the distribution. This is done to make clear which discrete variable is being summed over in every case.

²¹ In deriving the results in eqs.(24) and eq.(25) we have also made use of the fact that, for *integer* values of l , one has $\Gamma(-l) \rightarrow \infty \Rightarrow 1/\Gamma(-l) = 0 \forall l \geq 1$.

Clearly, making the replacement

$$\sum_{l'=0}^l \binom{l}{l'} \alpha^{l'} (1-\alpha)^{l-l'} \hat{z}_B(\eta, l') \Rightarrow \sum_{l'=0}^l \binom{l}{l'} \alpha^{l'} (1-\alpha)^{l-l'} \sum_{l''=0}^{l'} \binom{l'}{l''} \eta^{l'} (1-\eta)^{l'-l''} (1-\delta_{0,l''}) \quad (31)$$

in eq.(29) and carrying out the sums results in a specialization from $n_{mcs} \Rightarrow n$, corresponding to our previous analysis in which Bob makes no attempt whatsoever to distinguish single photon pulses from multiple photon pulses.

We also need to deduce the modification of the number of transmitted errors necessary to account for the click statistics monitoring prescription by proceeding as in the derivation of eq.(25), from which we obtain

$$e_{T,mcs} = \frac{m}{2} \left\{ \left(1 - \frac{r_d}{2}\right) r_c \left[\eta \psi_1(\mu \alpha) + \langle \hat{\chi}(\mu, l) \hat{\mathcal{Z}}_{\geq 2}(\eta, \alpha, l) \rangle \right] + \frac{r_d}{2} \right\} \quad (32)$$

$$\simeq \frac{m}{2} \left\{ r_c \left[\eta \psi_1(\mu \alpha) + \langle \hat{\chi}(\mu, l) \hat{\mathcal{Z}}_{\geq 2}(\eta, \alpha, l) \rangle \right] + \frac{r_d}{2} \right\}. \quad (33)$$

The functions n_{mcs} and $e_{T,mcs}$ given in eqs.(25) and (33) are quite general expressions that are valid for any multi-click monitoring scheme provided one uses a detector model such that there is unit probability (modified by η) that one detector will click given that a single photon impinges on Bob's apparatus (*cf* eq.(22)).

A Digression on an Incorrect Approach to Calculating \mathcal{S}

At first it might appear that a straightforward derivation of the effective secrecy capacity \mathcal{S} , starting from the definition provided in eq.(1), would consist in a different development than that which was presented in the derivation of eq.(15). The issue here is how to calculate the expression for the number of sifted bits, n (and, directly following on that, the number of transmitted error bits e_T). One might think that the derivation of n should consist in the following argument. One would first note that the probability that a bit cell produced by a pulsed laser (generating a flux of μ) will contain one or more photons is given by $\psi_{\geq 1}(\mu)$ (*cf* eq.(7)). Since we are interested in considering the fate of precisely those bit cells that contain one or more photons, it might then seem that the construction of n should consist merely in multiplying $\psi_{\geq 1}(\mu)$ by the quantum efficiency η of Bob's detector apparatus to account for the probability that the pulse will actually be detected, and by the line attenuation α to account for the signal loss incurred in the passage from Alice to Bob, adding to this product the dark count r_d , and finally multiplying the entire expression by $m/2$ to account for the 50% loss expected from incompatible basis orientations. In this manner one would derive the quantity

$$"n" = \frac{m}{2} [\eta \psi_{\geq 1}(\mu) \alpha + r_d] \quad (34)$$

for the number of sifted bits, where we use the notation “ n ” to distinguish this incorrect expression from the correct expression for the number of sifted bits given by n in eq.(15) above.

Upon comparing eqs.(34) and (15) we see that the difference between the two expressions is in the factors $\psi_{\geq 1}(\eta\mu\alpha)$ versus $\eta\psi_{\geq 1}(\mu)\alpha$. It is clear, however, that the quantity given in eq.(34) certainly cannot be correct in general.

To see this, suppose that some number of sifted bits are established by using a particular QKD setup. Now imagine that the intrinsic quantum efficiency, η , of the detector apparatus is somehow doubled in value to 2η . For instance, suppose that the original value of η is 45%, and we can double its value to 90%. If the *mean* number of photons per pulse, μ , is sufficiently small, say much less than unity, we would expect that the corresponding number of detection clicks at the detector should double. However, if instead μ was a very large number, say $\mu \approx 1000$, we would expect that each bit cell that reached the detector would cause it to click anyway when we had $\eta = 45\%$, so that doubling η to 90% should *not* cause the number of arriving bit cells that cause a click to become larger.

In fact it can easily be seen that the quantity $\eta\psi_{\geq 1}(\mu)\alpha$ furnishes a lower bound to the quantity $\psi_{\geq 1}(\eta\mu\alpha)$. This is illustrated numerically in the figure below. Noting that the product $\eta \times \alpha$ satisfies the inequality $0 \leq \eta \times \alpha \leq 1$ since both $0 \leq \eta \leq 1$ and $0 \leq \alpha \leq 1$, we plot curves that compare the values of $\eta\psi_{\geq 1}(\mu)\alpha$ with $\psi_{\geq 1}(\eta\mu\alpha)$ for four different values of μ .

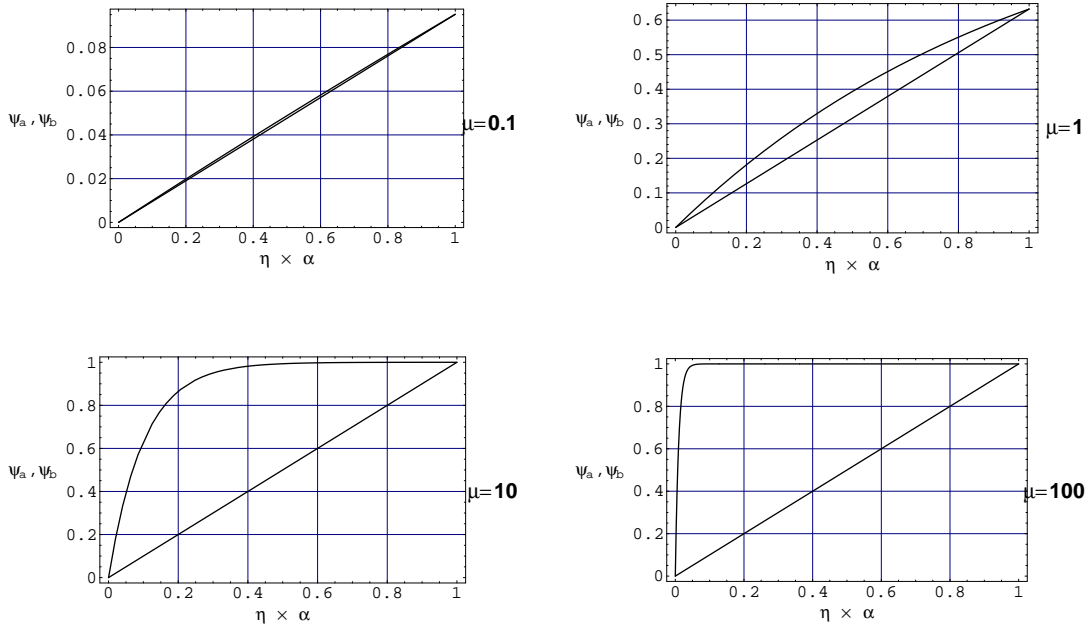


Figure 1: Comparison of $\eta\psi_{\geq 1}(\mu)\alpha$ with $\psi_{\geq 1}(\eta\mu\alpha)$

In each of the four graphs, the upper curve is the function $\psi_{\geq 1}(\eta\mu\alpha)$ and the lower curve the function $\eta\psi_{\geq 1}(\mu)\alpha$. It might *still* appear that it would be sufficient to make use of the latter function in the expression for the the number of sifted bits, n , since, as a lower bound on the

correct expression, one would at worst be underestimating the effective secrecy capacity \mathcal{S} . After all, if $\eta\psi_{\geq 1}(\mu)\alpha$, provides a lower bound to $\psi_{\geq 1}(\eta\mu\alpha)$ then we have “ n ” $\leq n$ as well, so one might think that the effective secrecy capacity \mathcal{S} is lower-bounded in this way as well. However, that is not in general guaranteed to be true. In fact *each term* in the numerator of \mathcal{S} in eq.(1), with the exception of g_{pa} , is a function of μ . (We will be developing the explicit μ -dependence of the quantities contained in the term s in \mathcal{S} , as well as that of a , in the sections below.) Each of these functions is, moreover, a function as well of other quantities such as α , η , *etc.*, which give rise to a complicated parametric behavior.

3.1.2 Privacy Amplification: General Remarks

In the defining expression for the effective secrecy capacity, \mathcal{S} , given in eq.(1), s is the number of bits of the sifted, error-corrected key that must be discarded to implement privacy amplification. This number should be no less (and, ideally, no more) than the number of bits that are “at risk,” in the sense that the eavesdropper may have been able to obtain information as to their values. We refer to s as the privacy amplification subtraction function. According to the *privacy amplification theorem* [24], assuming the use of a representative of the appropriate class of hash function, if s bits are removed from the shared key and upon removing an additional g_{pa} bits,²² it is guaranteed that the probability, P , that the eavesdropper can know one, or more than one bit of the remaining key is given by²³

$$P \leq \frac{2^{-g_{pa}}}{\ln 2} . \quad (35)$$

There are three possible ways in which the eavesdropper might gain partial information about the shared key: (1) The execution of any particular error correction protocol requires that Alice and Bob exchange information via the public channel. Although this channel is assumed to be secured against *spoofing* by the eavesdropper through the use of a suitable authentication protocol (discussed fully in Section 4.4.1), the channel is nevertheless assumed to be completely open to eavesdropping and monitoring, and leakage of information is accordingly possible. (2) The “pure” BB84 protocol, by which we mean the original idealized protocol in which *only* authentic qubits, *i.e.*, single-particle states are transmitted, is provably perfectly secret in the sense defined by Shannon [25, 26, 27, 28]. However, unless the quantum channel is perfect and completely free of any noise whatsoever, it is possible for the eavesdropper to obtain some information from the single particle transmitted states by exploiting the presence of the noise in the channel. Thus, in any *practical* system implementation it is necessary to account for the possibility of information leakage due to measurements performed even on the single particle states. (3) Much attention has been devoted to the use of weak coherent pulses generated by pulsed lasers in implementing QKD. In this case, and indeed in *any* case in which any sort of imperfect source at all²⁴ is employed, it is in fact possible in principle

²² The symbol g_{pa} , which will be discussed in more detail in Section 4.4.1, is referred to as the *privacy amplification security parameter*.

²³ Privacy amplification is described in much greater detail in Sections 3.1.2, 3.1.3, 3.1.4 and 3.1.5 below.

²⁴ This applies both to attenuated lasers and nonlinear crystals.

for the eavesdropper to obtain information from suitable attacks on the multi-photon pulses in the stream, and this potential information leakage must be accounted for in deducing the amount of required privacy amplification subtraction that should be carried out.

The quantity s is thus given by

$$s \equiv q + t + \nu, \quad (36)$$

where q is the Renyi information (in bits) leaked via error correction, t is the Renyi information leaked via measurements on the single-photon pulses, and ν is the corresponding quantity associated to attacks performed on the multiple-photon pulses.²⁵

3.1.3 Privacy Amplification: Error Correction

Since q should provide a bound on possible information leakage caused by eavesdropping on the process of error correction, it is natural to define q so that it is measured in units of error bits. We therefore write

$$q = Q \cdot e_T, \quad (37)$$

so that we must deduce the appropriate form for the bounding function Q , which in all generality should satisfy the equation of state given by

$$Q = Q(x, n, e_T), \quad (38)$$

where, in addition to the dependence on n and e_T we also introduce and define a parameter $x \geq 1$ to measure the degree to which Alice and Bob approach the Shannon bound for perfect error correction in whatever error correction protocol that they utilize. We will refer to x as the *Shannon deficit parameter*, where $x = 1$ corresponds to perfect error correction. It is clear that the bounding function Q should depend on n and e_T through the ratio e_T/n , the error fraction, so that the equation of state becomes

$$Q = Q\left(x, \frac{e_T}{n}\right). \quad (39)$$

Note that in the limit of vanishing dark count, $r_d = 0$, the ratio e_T/n reduces to the intrinsic channel loss, so that we have

$$\left. \frac{e_T}{n} \right|_{r_d=0} = r_c. \quad (40)$$

To deduce the explicit forms for Q and q , we need to determine the entropy associated with the information potentially leaked due to eavesdropping on error correction. This is provided by the Shannon entropy function for binary information states, which is given by

$$h(\zeta) \equiv -\zeta \log_2 \zeta - (1 - \zeta) \log_2 (1 - \zeta) \quad (41)$$

²⁵ We restrict attention to privacy amplification carried out with classical computing machines. So-called “quantum privacy amplification” [29] implemented with quantum computing machines will be considered in Part Two of this paper.

where ζ is the transmitted bit error fraction. Since the bit error fraction associated to the n -bit sifted string is given by e_T/n , the *minimum* amount of information that will be leaked will be for the case of perfect error correction in which the Shannon limit is attained, corresponding to $x = 1$, and is given by

$$q_{min} = nh \left(\frac{e_T}{n} \right). \quad (42)$$

In practice, perfect error correction cannot be attained, so an additional fractional amount of information measured by the Shannon deficit parameter will be leaked. Thus, the total information leakage, q , due to error correction is given by

$$q = xnh \left(\frac{e_T}{n} \right). \quad (43)$$

Comparing (43) with (37) we deduce

$$Q(x, \zeta) \equiv \frac{xh(\zeta)}{\zeta}. \quad (44)$$

Since Q depends on n and e_T only through the ratio of the two, we see that the m -dependence (*i.e.*, the dependence on the number of raw bits) drops out entirely (*cf* eqs.(15) and (17)). This will be a useful fact in determining important characteristics of the behavior of QKD systems. In particular, the form of Q is such that the expression is identically exact in the limit of an arbitrarily long cipher *and* a cipher of finite length.

3.1.4 Privacy Amplification: Single Photon Pulses

Although in the idealized case of a noiseless channel the quantum mechanical properties of the single-photon states guarantee the perfect secrecy of the transmission against any and all attacks by “Eve” (the conventional name used to denote the enemy), the fact that there is noise in a practical quantum channel provides an opportunity to nevertheless carry out measurements which may provide some information to the eavesdropper. The eavesdropper can generally attempt to be clever and simply not measure *too much*, hoping thereby to not generate too much noise, by “flying under the radar” of the noise present in the quantum channel.²⁶ Following the nomenclature of [30], we refer to the function that counts the number of required privacy amplification subtraction bits associated to this possibility as the *defense frontier function*, as it maps out the safe “frontier” for a sufficient amount of privacy amplification. The specific form of this function that is appropriate to the special, limiting case of the distribution of a cipher of infinite length was first obtained by Lütkenhaus in [31]. The generalized form appropriate to actual ciphers of finite length (which includes the previously obtained version applicable to infinite length ciphers as a special case) was later obtained by Slutsky, *et.al.* in [30].

²⁶ Terminology aside, this is in fact a rather apt analogy, since in flying under the radar a pilot tries to mask the radar signature of his aircraft in the radar clutter that is copiously present near the surface of the earth.

In the approach adopted in [30], a defense frontier function was constructed so as to ensure that a “successful” attack against the sifted, error-corrected bits could not be carried out with a probability any larger than a selectable infinitesimal quantity, ϵ .²⁷ The detailed calculation produced a quantity that provides sufficient, but not necessary and sufficient, privacy amplification subtraction to guarantee the desired result. In our application of the defense frontier function, unlike in the original derivation given in [30], we explicitly restrict the arguments of the defense frontier function, t , to the *single photon parts only* of the numbers of sifted and error bits, which we define, respectively, as (cf eqs.(15) and (17))

$$\begin{aligned} n_1 &= n_1(\eta, \mu, \alpha, r_d) \\ &\equiv \frac{m}{2} \left[\psi_1(\eta\mu\alpha) + r_d \right], \end{aligned} \quad (45)$$

and

$$\begin{aligned} e_{T,1} &= e_{T,1}(\eta, \mu, \alpha, r_c, r_d) \\ &\equiv \frac{m}{2} \left[r_c \psi_1(\eta\mu\alpha) + \frac{r_d}{2} \right]. \end{aligned} \quad (46)$$

The reason for this restriction, discussed more fully in Section 3.1.5 below, is that in our analysis we additively split into completely separate terms the privacy amplification subtraction functions associated to the single- and multiple-photon pulses.

With the proviso that we restrict the functional arguments as indicated above, we may adapt the derivation of [30] to obtain as the explicit expression for the defense frontier function

$$t(n_1, e_{T,1}, \epsilon) = (n_1 - e_{T,1}) \bar{I}_{max}^R \left(\frac{e_{T,1}}{n_1} + \xi(n_1, \epsilon) \right) + \xi(n_1, \epsilon) [n_1(n_1 - e_{T,1})]^{1/2}, \quad (47)$$

where \bar{I}_{max}^R is the maximum average amount of Renyi information leaked to the eavesdropper, with \bar{I}_{max}^R calculated to be

$$\bar{I}_{max}^R(\zeta) \equiv 1 + \log_2 \left[1 - \frac{1}{2} \left(\frac{1-3\zeta}{1-\zeta} \right)^2 \right], \quad (48)$$

and ξ is defined by

$$\xi(n_1, \epsilon) \equiv \frac{1}{\sqrt{2n_1}} \text{erf}^{-1}(1-\epsilon). \quad (49)$$

²⁷ Quoting the analysis provided in [30], we define a *successful* attack as one which introduces some number of errors e_T into an n -bit sifted data string resulting from an m -bit transmission, while yielding the enemy an amount of Renyi information $I > t(n, e_T, \epsilon)$, where $t(n, e_T, \epsilon)$ is the defense frontier function displayed below. As we discuss below, our treatment departs somewhat from the analysis given in [30] in explicitly restricting consideration here solely to the *single-photon pulse part* of the entire transmission. This point was left unclear in the original treatment.

We note here that the expression for \bar{I}_{max}^R given above is in fact precisely the same as an associated expression derived by Lütkenhaus in [31, 32], although it doesn't look like at it first sight.²⁸

Recall that in the previous section we chose a form for the quantity $q = Qe_T$ (the bound on the amount of Renyi information that may be leaked to the eavesdropper) that is measured in units of error bits. This is natural in view of the fact that this information leakage is associated with eavesdropping on the error correction process. In the same way, we express the defense frontier function in the form $t = Te_T$, introducing thereby an explicit dependence on both e_T and $e_{T,1}$, since the result of *any* measurements on the single photon pulses is to *necessarily* generate some number of errors in the transmitted string. Here we have introduced the new function T which plays a role similar to that of Q , in that it is a bounding function on the privacy amplification subtraction amount. Upon writing this out explicitly we find

$$t(n_1, e_T, e_{T,1}, \epsilon) = T(n_1, e_T, e_{T,1}, \epsilon) \cdot e_T, \quad (50)$$

where²⁹

$$\begin{aligned} T(n_1, e_T, e_{T,1}, \epsilon) &= \left(\frac{n_1}{e_T} - \frac{e_{T,1}}{e_T} \right) \bar{I}_{max}^R \left(\frac{e_{T,1}}{n_1} + \xi(n_1, \epsilon) \right) + \xi(n_1, \epsilon) \frac{n_1}{e_T} \left(1 - \frac{e_{T,1}}{n_1} \right)^{1/2} \\ &\simeq \left(\frac{n_1}{e_{T,1}} - 1 \right) \bar{I}_{max}^R \left(\frac{e_{T,1}}{n_1} + \xi(n_1, \epsilon) \right) + \xi(n_1, \epsilon) \frac{n_1}{e_{T,1}} \left(1 - \frac{e_{T,1}}{n_1} \right)^{1/2}. \end{aligned} \quad (51)$$

Unlike Q , T does not depend on n and e_T (restricted here, of course, solely to the single-photon pulse parts) *only* through terms that are functions of the ratio of the two, for which the m -dependence identically drops out entirely. In addition, due to the presence of ξ , T includes a dependence on m that does not intrinsically cancel out. Thus, the infinite-cipher limit and finite-length cipher version of T are not identical. A straightforward calculation reveals that

$$\lim_{m \rightarrow \infty} \xi(n_1, \epsilon) = 0 \quad (52)$$

and

$$\lim_{m \rightarrow \infty} \left\{ \xi(n_1, \epsilon) \frac{n_1}{e_{T,1}} \left(1 - \frac{e_{T,1}}{n_1} \right)^{1/2} \right\} = 0, \quad (53)$$

so that we have

$$\begin{aligned} \lim_{m \rightarrow \infty} T(n_1, e_T, e_{T,1}, \epsilon) &= \left(\frac{n_1}{e_{T,1}} - 1 \right) \bar{I}_{max}^R \left(\frac{e_{T,1}}{n_1} \right) \\ &\equiv T_\infty, \end{aligned} \quad (54)$$

which is independent of both m and ϵ . As stated above, this form recovers the expression for ciphers of infinite length first obtained by Lütkenhaus.

²⁸ The two versions of the maximum average Renyi entropy become manifestly equal through the rescaling $\zeta_{\text{rescaled}} \rightarrow \frac{\zeta}{1-\zeta}$, as pointed out in [32].

²⁹ In the approximate form of eq.(51) we are neglecting terms of the first order of smallness as given by $\frac{e_{T,1}}{e_T} \simeq 1 - [r_c \psi_{\geq 2} / (r_c \psi_1 + \frac{r_d}{2})] + \dots$, with a similar expression for $n_1/e_{T,1}$. Recall (cf eqs.(18), (45), etc.) that the argument of both of the functions ψ_1 and $\psi_{\geq 2}$ is $\eta \mu \alpha \ll 1$.

3.1.5 Privacy Amplification: Multiple Photon Pulses

There is reason to be concerned about the effect on the secrecy, and hence the security, of QKD systems when pulsed lasers are used to generate weak coherent pulses in place of ideal, perfect qubits. Indeed, the use of *any* imperfect source, such as excited nonlinear crystals, must be considered to be potentially problematic in this regard. This concern stems from the fact that, unlike the case for single-photon pulses, multi-photon pulses offer the opportunity in principle for an eavesdropper to obtain full information on the bit value encoded in the polarization state. However, this problem can be *completely neutralized* by employing a sufficient amount of privacy amplification in the processing of the shared key. It is essential in the analysis of this problem to use the proper tool, which is the complete, comprehensive form for the effective secrecy capacity of the system. Thus must include *all* the contributing terms, and in particular must include a complete characterization of the full amount of privacy amplification due to all causes (as well as the full amount of shared key material that must be removed to implement continuous authentication). As always in this analysis, it is *required* to determine at least the minimum number of subtraction bits for privacy amplification; it is *acceptable* (although undesirable) to overestimate this number, but it is strictly *unacceptable* to underestimate it.³⁰

The detailed analysis of the privacy amplification associated to multi-photon pulses is rather complicated. As we cannot know in advance precisely how the enemy will choose to attack these pulses, it is necessary to enumerate all possibilities by providing a complete taxonomy of all attacks, after which the various possibilities may be compared against each other to ascertain which are the strongest in various circumstances. It is then possible to deduce the expressions for the requisite amounts of privacy amplification. To provide an overall perspective of the various steps in the logic we illustrate the structure of the analysis with a flow chart in Figure 2.

The “Pyrrhic Victory” Approach to Privacy Amplification

It would of course be possible to guarantee absolutely that none of the information resident in the multi-photon portion of the stream be available to an enemy, by simply carrying out sufficient privacy amplification subtraction to discard *all* of the bit values associated to *all* of the multi-photon pulses. This effectively and completely solves the problem of the vulnerability of the information in the multi-photon pulses, and moreover considerably shortens the analysis! The entire information content of the multi-photon part of the transmission is given by $\psi_{\geq 2}(\mu)$, so that we could denote the total privacy amplification subtraction function by ν_{Pyrrhic} and simply write

$$\nu_{\text{Pyrrhic}} \equiv \psi_{\geq 2}(\mu) \quad (55)$$

and be done with it, confident that the eavesdropper cannot carry out *any* useful attack on

³⁰ Any claim of a QKD system rate based on an underestimated numerical value for the privacy amplification subtraction function is potentially untenable and should be rejected as characterizing a potentially vulnerable communications system.

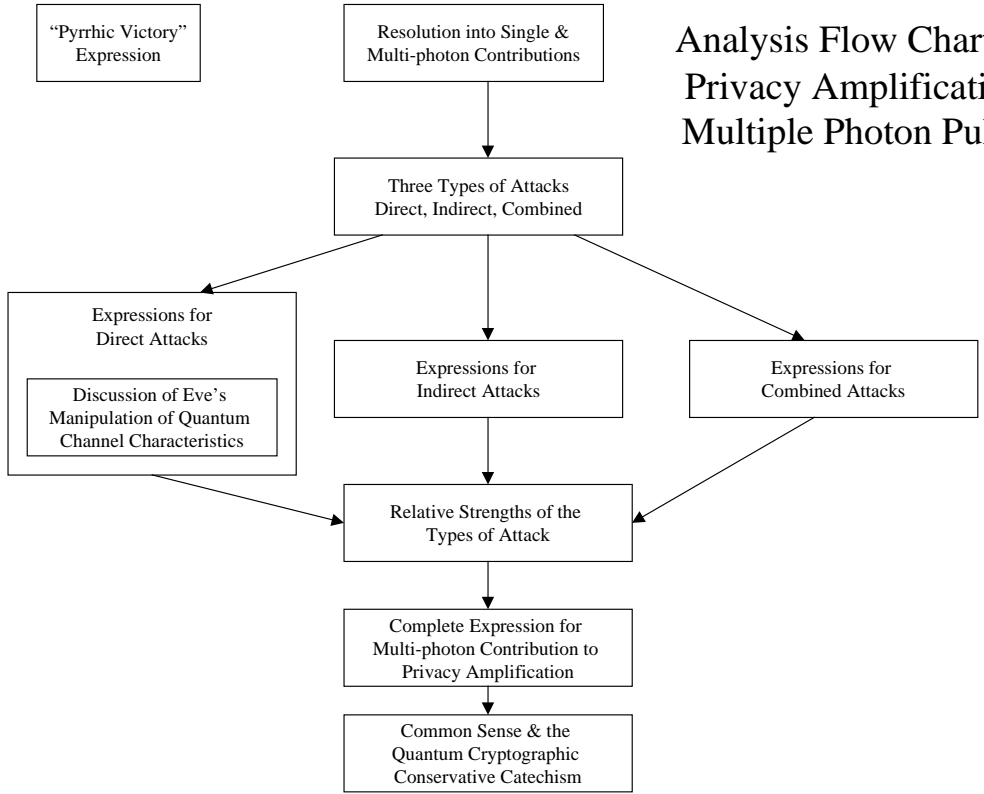


Figure 2: Flow Chart of Analysis of Multi-Photon Pulse Privacy Amplification

the multi-photon pulses: even if she attacks every single multi-photon pulse in any manner whatsoever and is completely successful in every single case, she gains nothing because we will have removed all the associated information. The remaining shared key would be as secret as any key generated by a source of pure single particle states.³¹ However, numerical analysis based on the complete expression for the effective secrecy capacity derived in this paper demonstrates that the achievable throughput rates in this case are unacceptably low. Thus the use of ν_{Pyrrhic} as a privacy amplification amount serves to defeat Alice and Bob as surely as it defeats Eve. We need to try to find a better, not merely sufficient bound that will result in acceptable throughput values.

³¹ That is, such a key will be unconditionally secret in the sense of privacy amplification, assuming as one must, that privacy amplification would be always required for *any practical* system employing even solely single particle states, as they are subject to the effects of machine-induced errors that must be corrected, for which privacy amplification is required to mitigate the effect of possible eavesdropping on the error correction protocol.

In the remainder of this section, as depicted in the flow chart in Figure 2, we therefore construct for the first time the general functions that measure the *necessary and sufficient* amount of privacy amplification subtraction bits required to account for information loss associated to the multiple-photon pulses, in addition to which we also construct an explicit expression that provides a practical, universal bound that is *always* at least as large as the minimum number of required subtraction bits.

Splitting the Privacy Amplification Function into Single- and Multi-Photon Parts

In our analysis we explicitly, *additively* separate into two pieces the privacy amplification associated to single- and multi-photon pulses. The two kinds of cryptanalytic³² attacks on these two kinds of pulses, that necessitate carrying out privacy amplification in the first place, are each of a very different character. Attacks on single-photon pulses *necessarily* generate errors, while attacks on multi-photon pulses, when properly performed by the enemy, generate no detectable errors at all. Thus, as we have emphasized in Section 3.1.4 above, it is natural to mathematically express the privacy amplification subtraction function associated to single-photon pulses in units of error bits, as in eq.(50), while it is clearly not physically correct to do so in the case of the privacy amplification subtraction function associated to multi-photon pulses. Taking this point further, we note that in our view it is neither necessary nor physically meaningful to lump together functionally (as done for instance, in [32]) the privacy amplification subtraction amounts for these two very different kinds of cryptanalytic attacks. Moreover, the form for the privacy amplification subtraction amount associated to single-photon pulses derived in Section 3.1.4 above is appropriate for, and allows us to analyze quantitatively, the dynamics of the transmission of *actual* ciphers of finite length, as opposed to merely idealized ciphers of infinite length. Lumping together the privacy amplification contribution for single- and multi-photon pulses into a functional form which is only applicable to idealized ciphers of infinite length obscures this possibility.

Thus, we advocate cleanly additively splitting into two distinct parts the separate contributions, which serves both to emphasize the different physical characteristics of the two types of attack and allows us to properly analyze the dynamics of ciphers of finite length.

The Three Types of Individual Cryptanalytic Attacks on Multiple Photon Pulses

We first note that there are three (and only three) distinct kinds of attack that can be carried out against the multiple-photon pulses in the stream:³³ (1) *direct* attacks, (2) *indirect* attacks and (3) *combined direct and indirect* attacks.

³² Strictly speaking, we are not referring to cryptanalytic attacks as such, as this is traditionally defined to mean attacks on enciphered *data*, whereas here we are discussing attacks designed to determine the *key*.

³³ As noted above in Section 2.2 we again point out that in Part One of this paper we are only considering so-called “individual attacks,” *i.e.*, those attacks that do not require that the enemy apply unitary transformations to the intercepted state with a quantum computing device. We will address quantum computer-based attacks in Part Two.

We define the *direct* attacks on multi-photon pulses as attacks in which Eve intercepts the stream and attempts to directly determine the polarization of the coherent state by performing a suitable measurement. This attack requires a pulse with three or more photons in it. The direct attack necessarily destroys the state as received by Eve, but, if she is successful in determining the polarization she can attempt to send another state with identical polarization on to Bob.³⁴ We refer to the state prepared by the enemy and sent on to Bob as the *surrogate* pulse. If he receives and detects this state it will have arrived just as if it been sent by Alice and was untouched by Eve, and in this way the information will be known to Eve. There is a quantifiable probability that this attack will be successful, which we discuss below.

We define *indirect* attacks on multi-photon pulses as attacks in which Eve “splits the beam,” as a result of which she “keeps and preserves” one or more of the photons in the pulse, without measuring their state, and allows the remnant pulse to propagate on to Bob. This attack requires a pulse with two or more photons in it. In the indirect attack Eve knows that she must not interfere in any way with the remnant pulse that is allowed to continue on to Bob: it must arrive at Bob’s instrument in the polarization state that it left Alice’s system, only differing from the original multi-photon pulse sent by Alice in that it contains some smaller number of photons than when it left Alice, unbeknownst to Bob. He then measures the state of the pulse, and carries out the public discussion phase of the QKD protocol as per usual. Eve eavesdrops on the public discussion and learns thereby the particular *basis*, but not the *state*, of the pulse. Since she has advanced technology at her disposal and has preserved the photons that she split off in their original state, she merely measures the polarization in the announced basis in order to precisely determine the actual state of polarization. There is a quantifiable probability that this attack will be successful which we discuss below.

Finally, the *combined attack* occurs when a pulse with five or more photons in it (the reason for this requirement on the number of photons is explained below) is intercepted and split up by the enemy, allowing both a direct and indirect attack to be performed. This particular individual attack appears not to have been discussed previously in the literature of this subject.

In any of these cases Eve will have succeeded in determining the state of polarization of the pulse in question, without Alice and Bob noticing that anything has happened: in particular, the enemy will have obtained the information without having induced *any* elevation in the error rate. Without an increase in the error rate to indicate that Eve has compromised the system, there will be no way for Alice and Bob to know that Eve has the same information on those particular bits that they do. Of course, strictly speaking this is not a weakness of *ideal* quantum key distribution, but rather of *practical* quantum key distribution. However, this is a distinction without a difference, as we must concern ourselves with the actual features of a

³⁴ So-called “quantum non-demolition” measurements, which have been experimentally demonstrated to be able to repeatedly count photons without destroying them, play no role here. To profit from the direct attack it is necessary for Eve to determine the state of polarization. In order to measure the state of polarization (more precisely, the eigenvalues of the helicity operator) of the photon, it is necessary to select a particular basis.

realistic implementation in any serious study of this subject. *Ideal* quantum key distribution is actually almost irrelevant here: pure quantum bits propagating along a noiseless quantum channel between perfect Alice and Bob instruments comprise a fiction that has very little to do with anything that can be implemented in practice.

We emphasize again that the potential secrecy weakness of practical systems employing weak coherent pulses produced by a laser is in general *shared* by those systems employing nonlinear crystals and parametric downconversion as a source of raw bits for Alice. As in the case of an attenuated pulsed laser, nonlinear crystals in actual system implementations will also sometimes produce multiple photon pulses, which in principle may be exploited by an enemy equipped with suitable technology.

In our analysis of the requisite privacy amplification function associated to multiple-photon pulses, we will make use of the results we have obtained for the general case in which Bob explicitly monitors for, and eliminates from the sifting process, those bit cells which manifestly contain more than one photon. We also consider the special case in which no such monitoring of click statistics is carried out.

We now consider in more detail the three types of attack that can be carried out on the multi-photon pulses.

Direct Attacks

The logical structure of the analysis carried out in this section is illustrated with the flow chart shown in Figure 3 below.

In the direct attack the enemy intercepts the pulse transmitted by Alice and measures it with her apparatus. It becomes increasingly *more* likely to determine with complete knowledge the polarization state of a multi-photon pulse as the number of photons in the pulse increases. At the same time, owing to the Poisson distribution that governs the output of the pulsed laser used by Alice, and the fact that Alice will in general adjust the flux to be suitably weak through the use of appropriate intensity filters, it becomes increasingly *less* likely to encounter a multi-photon pulse as the number of photons in the pulse increases. Thus, there is a competition between these two effects, and to ensure the secrecy of the shared cipher it is essential to analyze the balance between them to carefully deduce precisely the maximum amount of information that may be obtained by Eve in measuring these states.

An important point, discussed in more detail below, is that the direct attack can only succeed if the pulse received by the enemy apparatus contains three or more photons in it.

To proceed, we note that in [22] it is shown that one may make use of the results of [33] to deduce an explicit expression for the maximum probability to unambiguously determine the polarization of an incident Fock state comprised of l photons distributed according to a Poisson distribution. (Such an incident state includes as a special case in particular a *coherent* state comprised of l photons.) We shall refer to this probability as $\hat{z}_E(l)$, the maximum

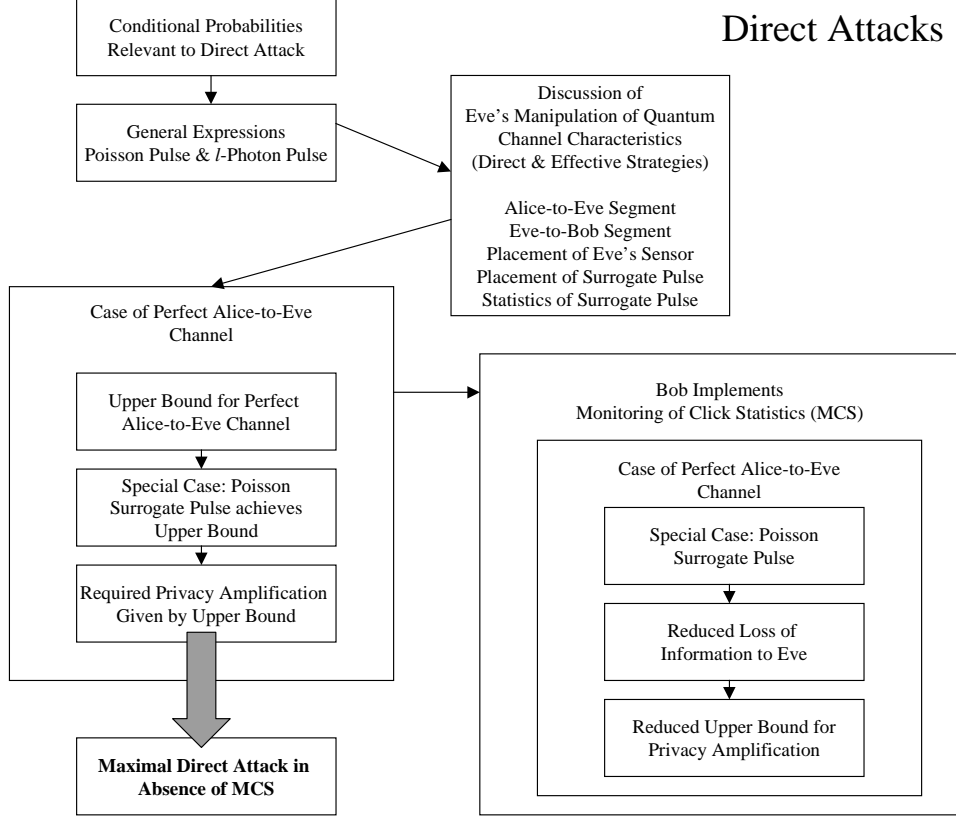


Figure 3: Flow Chart for Analysis of Direct Attacks

probability that Eve may with complete knowledge determine the state of polarization of an incoming l -photon pulse. In [33, 22] this was found to be given by

$$\hat{z}_E(l) = \begin{cases} 0 & l \leq 2 \\ 1 - 2^{1-l/2} & l \text{ even} \\ 1 - 2^{(1-l)/2} & l \text{ odd.} \end{cases} \quad (56)$$

We know that irrespective of the apparatus utilized by Eve, it will be the case that the pulse she intercepts from Alice will be characterized by a Poisson distribution,³⁵ so the appropriate average maximum probability, $z_E(\mu)$, for Eve to be able to determine the polarization state

³⁵ As mentioned above, we *assume* that the intrinsic characteristics of the quantum channel are such that the Poisson number distribution produced by Alice is preserved (of course, as we discuss explicitly below, it is entirely possible that *the enemy* may somehow alter the distribution on its way to being received by Bob).

with complete knowledge is

$$\begin{aligned}
z_E(\mu) &\equiv \sum_{l=0}^{\infty} e^{-\mu} \frac{\mu^l}{l!} \hat{z}_E(l) \\
&\equiv \langle \hat{\chi}(\mu, l) \hat{z}_E(l) \rangle_{l \geq 0} \\
&= \langle \hat{\chi}(\mu, l) \hat{z}_E(l) \rangle_{l \geq 3} \\
&= 1 - e^{-\mu} \left(\sqrt{2} \sinh \frac{\mu}{\sqrt{2}} + 2 \cosh \frac{\mu}{\sqrt{2}} - 1 \right). \tag{57}
\end{aligned}$$

It is obvious that, insofar as determining the polarization *state* with complete knowledge is concerned, a two-photon pulse is no more useful than a single-photon pulse is: with only two photons in the pulse it is not possible to determine the state of polarization, although it is possible to determine the polarization *basis* in this case. However, a direct measurement of the pulse that furnishes the identity of the basis necessarily destroys the polarization of the two photons, making the pulse unsuitable for a further measurement to determine the state. (Moreover, the basis, in any event, would have been publicly revealed to the enemy in the discussion between Alice and Bob.) As expected, and as noted in [22], the leading order behavior of $z_E(\mu)$ varies as the cube of the mean photon number, and is specifically given (*cf* eq.(57)) by $z_E(\mu) = \frac{1}{12}\mu^3 + O(\mu^4)$, reflecting the fact that three or more photons are required in order to unambiguously determine the state of polarization of the pulse. We note that there is no manifest appearance of the efficiency, η_E , of Eve's detector apparatus in the quantities $\hat{z}_E(l)$ or $z_E(\mu)$, as we are implicitly assuming that Eve is equipped with perfect detection equipment, so that we have implicitly set $\eta_E = 1$.

The function $z_E(\mu)$ is “universal,” in the sense that it provides an upper bound for all choices of apparatus on Eve's probability to determine the polarization of an intercepted multi-photon pulse with complete knowledge. With any particular measurement apparatus, Eve may typically in practice realize a *lower* probability of polarization determination: in [34, 35] a particular setup was described which provides Eve with a probability of $\frac{1}{32}\mu^3 + O(\mu^4)$. In our analysis we will employ the maximal value given in eq.(57) above, to allow for the strongest possible enemy attack.

To proceed in as general a manner as possible, we will formulate the expressions for privacy amplification subtraction from first principles in terms of the various underlying probabilities associated to the different processes that take place. This is analogous to our deduction of the numbers of sifted and transmitted error bits previously carried out in Section 3.1.1. There we considered all processes that characterize the propagation of signals in the absence of an eavesdropper. An important difference here is that we must *explicitly* take into account the various types of activities that an eavesdropper may conduct. Denoting as before the various relevant probabilities by \mathcal{P} with appropriate arguments, we have

$$\mathcal{P}(l \text{ photons leave Alice}) = \hat{\chi}(\mu, l) , \tag{58}$$

$$\mathcal{P} (l' \text{ photons reach Eve} \mid l \text{ photons leave Alice}) = \binom{l}{l'} (\alpha_{AE} \rho_{AE})^{l'} (1 - \alpha_{AE} \rho_{AE})^{l-l'} , \quad (59)$$

$$\mathcal{P} (\text{polarization determined with certainty} \mid l' \text{ photons reach Eve}) = \hat{z}_E(l') , \quad (60)$$

$$\mathcal{P} (l_E \text{ photons leave Eve in some distribution } \hat{\Xi}) = \hat{\Xi}(\mu_E, l_E) , \quad (61)$$

$$\mathcal{P} (l'' \text{ photons reach Bob} \mid l_E \text{ photons leave Eve}) = \binom{l_E}{l''} (\alpha_{EB} \rho_{EB})^{l''} (1 - \alpha_{EB} \rho_{EB})^{l_E - l''} \quad (62)$$

and

$$\mathcal{P} (l''' \text{ photons detected} \mid l'' \text{ photons reach Bob}) = \binom{l''}{l'''} \eta^{l'''} (1 - \eta)^{l'' - l'''} (1 - \delta_{0,l''''}) . \quad (63)$$

Note that, as discussed above, $\hat{z}_E(l')$ in eq.(60) embodies the requirement that the pulses vulnerable to the direct attack must contain three or more photons, in effect it includes a factor of the Heaviside function $\theta(l - 3)$ in its definition (*cf* eq.(56)).³⁶

In eqs.(59) and (62) we have introduced the quantities α_{AE} , ρ_{AE} , α_{EB} and ρ_{EB} . The quantities α_{AE} and α_{EB} are, respectively, the line attenuation amounts along the quantum channel for the Alice-Eve and Eve-Bob link segments. Note that the product of the two *partial* line attenuations gives the *total* line attenuation, α , along the entire quantum channel from Alice to Bob (we assume that Eve is between Alice and Bob), so that we have

$$\alpha_{AE} \alpha_{EB} = \alpha . \quad (64)$$

The quantities ρ_{AE} and ρ_{EB} each satisfy the inequalities $0 \leq \rho_{AE} \leq \alpha_{AE}^{-1}$ and $0 \leq \rho_{EB} \leq \alpha_{EB}^{-1}$. These are parameters that measure the degree to which the enemy can somehow “adjust” the transparency of the quantum channel so as to increase the amount of information that can be obtained on the transmitted bits. Thus, a value of $\rho_{AE,EB} = 0 \Rightarrow \alpha_{AE,EB} \rho_{AE,EB} = 0$ corresponds to a totally degraded quantum channel,³⁷ a value of $\rho_{AE,EB} = 1 \Rightarrow \alpha_{AE,EB} \rho_{AE,EB} = \alpha_{AE,EB}$ corresponds to the case when the enemy does not modify the transparency, thus leaving the fiducial amount of line attenuation in the channel, and a value of $\rho_{AE,EB} = \alpha_{AE,EB}^{-1} \Rightarrow \alpha_{AE,EB} \rho_{AE,EB} = 1$ corresponds to the case in which the enemy has made the quantum channel perfectly transparent.

There are different cases for us to consider. In the case of a fiber-optic implementation of QKD, it *may* be reasonable to analyze the case in which the *entire* quantum channel is surreptitiously replaced by the enemy with an “ideal,” lossless cable. In this case, we would

³⁶ Indeed, one way to proceed in evaluating sums over products of $\hat{z}_E(l)$ with generic l -dependent quantities y_l is to write such sums as $\sum_l \hat{z}_E(l) y_l = \sum_{k=1} (1 - 2^{1-k}) y_{2k} + \sum_{k=1} (1 - 2^{-k}) y_{2k+1}$. The implicit factor of $\theta(l - 3)$ in $\hat{z}_E(l)$ ensures that the indicated ranges of summation over k , in each case beginning with $k = 1$, are in fact correct as written for both the even and odd terms in the two sums.

³⁷ This case constitutes denial of service, since no signals of any kind can propagate through the channel when $\rho_{AE,EB} = 0$, and therefore falls outside the purview of an analysis of eavesdropping attacks.

have $\rho_{AE} = \alpha_{AE}^{-1}$ and $\rho_{EB} = \alpha_{EB}^{-1}$ after the cable replacement, resulting in the elimination of the line attenuation along the cable. In the case of a free space implementation, it is *unreasonable* to imagine that the enemy can replace the channel with one of perfect, or even improved, transparency. This is entirely well-motivated physically: in this case a replacement of the quantum channel with one of better transmission characteristics amounts to imagining that Eve can replace the atmosphere with one that *she* prefers. Even if this were possible, it would presumably not go unnoticed by Alice, Bob and the rest of the population of the planet. Note that this effect *cannot* be mimiced by adjusting the frequency of the photons in the reconstructed pulses, as proper “technically sound cryptosystem” operating procedure dictates the use of a narrow bandpass wavelength filter in the front of Bob’s receiver which will physically exclude any such wavelength-modified incoming photons.

However, in the case of a free space QKD implementation it may nevertheless be possible for the enemy to anyhow effect a partial, and sometimes even a complete, *effective* improvement of the transparency of the channel. For instance, we may imagine that the interception apparatus of the enemy is secretly located immediately adjacent to the Alice site (we ascribe to the enemy superb powers of camouflage and technical skill),³⁸ thereby effectively producing the value $\rho_{AE} = \alpha_{AE}^{-1} \Rightarrow \rho_{AE} \alpha_{AE} = 1$. (Strictly speaking we would presumably actually have the condition $\rho_{AE} \simeq \alpha_{AE}^{-1}$ rather than $\rho_{AE} = \alpha_{AE}^{-1}$ in this case, since Eve is presumed *adjacent to*, but not *physically coincident with*, Alice.) In the case of the direct attack, in which a surrogate pulse is sent on to Bob, we may *further* imagine that the physical location of the site from which the surrogate pulse is launched is likewise placed immediately adjacent to (and somehow undetected by) Bob. This allows the two enemy collaborators to entirely circumvent the attenuation of the free space quantum channel by simply communicating instructions to each other classically, which has the effect of causing $\rho_{EB} = \alpha_{EB}^{-1} \Rightarrow \rho_{EB} \alpha_{EB} = 1$. Note that, in the case of the *indirect* attack (to be discussed in great detail below), the same options are not *simultaneously* available to the enemy in the case of the free space quantum channel. This is because, unlike in the direct attack, it is necessary that the pulse that is allowed to travel on to Bob not be modified, and its polarization state remains unknown to the enemy. Hence, no “conspirator” can participate in the transmission of the pulse. Thus, Eve can be located either immediately adjacent to Alice, in which case we have $\rho_{AE} = \alpha_{AE}^{-1} \Rightarrow \rho_{AE} \alpha_{AE} = 1$, or Eve can be located immediately adjacent to Bob, in which case we have $\rho_{EB} = \alpha_{EB}^{-1} \Rightarrow \rho_{EB} \alpha_{EB} = 1$, (or somewhere in between) but both endpoint conditions cannot simultaneously be realized: there cannot be a “second Eve” located at the other end.³⁹

³⁸ As discussed below in Sections 4 and 5, we envisage for the free space case an implementation in which Alice is located on an orbiting satellite and Bob is located on an aircraft or the ground, so that the undetected placement of an eavesdropping interception device immediately adjacent to Alice is almost impossible to imagine for any actual, practical situation unless Eve can literally make herself invisible. Again, we are assuming that the entire praxis of *communications security*, in addition to the narrower requirement of *cryptosecrecy*, is properly implemented, so that physical access of the enemy to the Alice and Bob devices is (1) assumed to be prevented, and (2) in any event is not reasonably within the purview of the QKD protocol *per se*.

³⁹ We emphasize that all detailed discussion of entanglement in quantum cryptography, including analysis of entanglement-assisted attacks, is performed in Part Two of this paper. We here merely point out that

Whether for a free space or fiber optic cable implementation, after imposing the condition $\rho_{AE} = \alpha_{AE}^{-1}$ the expression for the privacy amplification that results will still retain a dependence on α_{EB} . In the case of a free space implementation only, one may without loss of generality always interpret this residual α_{EB} -dependence in fact as dependence on the *entire* line attenuation, α , of the quantum channel, since in this case the value of α_{EB} is due to the conditions along the entire propagation path from Eve (who is adjacent to Alice) to Bob. However, in the case of a fiber-optic cable system, for which it might be possible for Eve to achieve the condition $\rho_{AE} = \alpha_{AE}^{-1}$ by directly replacing the channel between Alice and herself *without* necessarily having to place an interception device immediately adjacent to Alice (although this might also be done), it obviously need not be true in general that the residual α_{EB} -dependence corresponds to the entire line attenuation α .

Note that we do *not* introduce a parameter analogous to ρ_{AE} or ρ_{EB} to describe the degree to which the enemy can remotely “control” or adjust the quantum efficiency, η , of Bob’s detector device. We are assuming, in accord with the discussion in Section 2.4.2, that proper cryptographic procedure and design is followed in the system implementation, so that the enemy *cannot* enforce the condition $\eta \rightarrow 1$, nor even cause any non-negligible change in the value of η at all. The only physically reasonable method whereby such remote “control” could succeed is through the modification of the wavelength of those photons that propagate successfully to Bob’s detector. Clearly this cannot work in the case of the indirect attack, as its success *requires* that Eve not prepare the state allowed to continue on to Bob in any way. Moreover, even for the direct attack such wavelength modification can, as mentioned above, be trivially neutralized in any event by placing a narrow bandpass filter in front of Bob’s detector apparatus, thereby preventing (with high probability) any photons of modified wavelength from entering the device.

After successfully determining the polarization state of the intercepted pulse, the enemy may prepare an identically polarized state in any way that is deemed to be advantageous and send the surrogate pulse on to Bob. Although the enemy may send *any* (properly polarized) pure state or mixture to Bob, these states may practically be regarded as mixtures of number states⁴⁰ owing to the facts that (1) Bob is employing a photon number detector, and (2) anything *else* will provide a signature that the eavesdropper has tampered with the signal, alerting Alice and Bob who will then discard the bit cell. Therefore, although the distribution function $\hat{\Xi}$ in eq.(61) is not necessarily identical to the Poisson distribution, we can without loss of generality *always* take it to be some *discrete* distribution, $\hat{\Xi} = \hat{\Xi}(\mu_E, l_E)$, that is characterized for each bit cell by both a mean, μ_E , and a particular number, l_E , of photons. Of course, there need be no particular *a priori* relation between the number of photons, l' , in the pulse that Eve intercepted and measured in order to determine the polarization state,

inclusion of entanglement-assisted attacks against *individual* quantum bits in particular, which would allow a second Eve adjacent to Bob to effectively eliminate the line attenuation even for the indirect attack (if prior entanglement is shared between her and the first Eve located adjacent to Alice), does *not* change the functional form of the final expressions for multi-photon privacy amplification obtained in eqs.(141) through (151) below. The only change is that the distinction between optical-fiber and free-space implementations is eliminated, with a consequent modification of the associated throughput rates [20].

⁴⁰ This has been noted as well in [22].

and the number of photons, l_E , that is sent on by Eve to Bob.

We may now deduce the explicit expression for the privacy amplification subtraction function associated to individual direct attacks, which we denote by ν_d , by assembling the appropriate probabilities from eqs.(58) through (63). We find

$$\begin{aligned}
\nu_d &= \frac{m}{2} \sum_{l, l', l'', l''', l_E} \mathcal{P}(l \text{ photons leave Alice}) \\
&\quad \times \mathcal{P}(l' \text{ photons reach Eve} \mid l \text{ photons leave Alice}) \\
&\quad \times \mathcal{P}(\text{polarization determined with certainty} \mid l' \text{ photons reach Eve}) \\
&\quad \times \mathcal{P}(l_E \text{ photons leave Eve in some distribution } \hat{\Xi}) \\
&\quad \times \mathcal{P}(l'' \text{ photons reach Bob} \mid l_E \text{ photons leave Eve}) \\
&\quad \times \mathcal{P}(l''' \text{ photons detected} \mid l'' \text{ photons reach Bob}) \\
&= \frac{m}{2} \sum_{l=0}^{\infty} \hat{\chi}(\mu, l) \sum_{l'=0}^l \binom{l}{l'} (\alpha_{AE} \rho_{AE})^{l'} (1 - \alpha_{AE} \rho_{AE}) \hat{z}_E(l') \\
&\quad \sum_{l_E=0}^{\infty} \hat{\Xi}(\mu_E, l_E) \sum_{l''=0}^{l_E} \binom{l_E}{l''} (\alpha_{EB} \rho_{EB})^{l''} (1 - \alpha_{EB} \rho_{EB})^{l_E - l''} \\
&\quad \sum_{l'''=0}^{l''} \binom{l''}{l'''} \eta^{l'''} (1 - \eta)^{l'' - l'''} (1 - \delta_{0, l''''}) \\
&= \frac{m}{2} \sum_{l=0}^{\infty} \hat{\chi}(\mu, l) \sum_{l'=0}^l \binom{l}{l'} (\alpha_{AE} \rho_{AE})^{l'} (1 - \alpha_{AE} \rho_{AE})^{l-l'} \hat{z}_E(l') \\
&\quad \sum_{l_E=0}^{\infty} \hat{\Xi}(\mu_E, l_E) \sum_{l''=0}^{l_E} \binom{l_E}{l''} (\alpha_{EB} \rho_{EB})^{l''} (1 - \alpha_{EB} \rho_{EB})^{l_E - l''} [1 - (1 - \eta)^{l''}] \\
&= \frac{m}{2} \sum_{l=0}^{\infty} \hat{\chi}(\mu, l) \sum_{l'=0}^l \binom{l}{l'} (\alpha_{AE} \rho_{AE})^{l'} (1 - \alpha_{AE} \rho_{AE})^{l-l'} \hat{z}_E(l') \\
&\quad \sum_{l_E=0}^{\infty} \hat{\Xi}(\mu_E, l_E) [1 - (1 - \eta \alpha_{EB} \rho_{EB})^{l_E}] . \tag{65}
\end{aligned}$$

The general form of this quantity is simple to explain in physical terms: it is the probability that the enemy can with certainty determine the polarization of a multi-photon pulse given that it has been intercepted, multiplied by the probability that a surrogate pulse in the same state of polarization can arrive at and be detected by Bob, measured in a distribution $\hat{\Xi}$ chosen solely by the eavesdropper.⁴¹

This expression provides the amount of privacy amplification subtraction required in order to compensate for direct attacks on *all* of the multi-photon pulses that contain three or more

⁴¹ We note in passing that the sum $\sum_{l'=0}^l \binom{l}{l'} (\alpha_{AE} \rho_{AE})^{l'} (1 - \alpha_{AE} \rho_{AE})^{l-l'} \hat{z}_E(l')$ can be explicitly evaluated to a closed form, but as it is not particularly illuminating we have not displayed the result here.

photons. It is clearly not the most general expression for the total amount of privacy amplification subtraction required in order to ensure unconditional secrecy, as such a uniform attack on all multi-photon pulses with three or more photons is only one possible cryptanalytic strategy that may be employed by the enemy. In general, we also need the expression for the amount of privacy amplification required in order to protect against a direct attack on any *particular* multi-photon pulse with l photons in it, which we denote by $\nu_{d,l}$. We may obtain the relevant quantity by direct inspection of eq.(65), to find

$$\begin{aligned} \nu_{d,l} &= \frac{m}{2} \hat{\chi}(\mu, l) \sum_{l'=0}^l \binom{l}{l'} (\alpha_{AE} \rho_{AE})^{l'} (1 - \alpha_{AE} \rho_{AE})^{l-l'} \hat{z}_E(l') \\ &\quad \sum_{l_E=0}^{\infty} \hat{\Xi}(\mu_E, l_E) \left[1 - (1 - \eta \alpha_{EB} \rho_{EB})^{l_E} \right] \\ &= \frac{m}{2} \psi_l(\mu) \sum_{l'=0}^l \binom{l}{l'} (\alpha_{AE} \rho_{AE})^{l'} (1 - \alpha_{AE} \rho_{AE})^{l-l'} \hat{z}_E(l') \\ &\quad \sum_{l_E=0}^{\infty} \hat{\Xi}(\mu_E, l_E) \left[1 - (1 - \eta \alpha_{EB} \rho_{EB})^{l_E} \right], \end{aligned} \quad (66)$$

where we have introduced the notation $\psi_l(\mu) \equiv \hat{\chi}(\mu, l)$. Inspection of the above expression reveals the fact that, irrespective of the particular form of $\hat{\Xi}$, the magnitude of the privacy amplification function associated to direct attacks *increases* as the quantum efficiency of Bob's photon detector increases (recall that the product $\eta \alpha_{EB} \rho_{EB}$ satisfies the inequality $\eta \alpha_{EB} \rho_{EB} \leq 1$). Thus, we have the seemingly paradoxical situation that, due to the special nature of the direct attack, *more* information is potentially at risk to compromise by Eve when Bob's detector apparatus is characterized by a better detector efficiency than when characterized by a poorer efficiency.

Now we note that, if $\rho_{AE} = \alpha_{AE}^{-1}$, which means either that in some way the enemy has arranged that the quantum channel between Alice and herself is free of any attenuation (in the case of a fiber-optic cable system), or effectively done the same thing by situating the interception apparatus immediately adjacent to Alice (in either a cable- or free space-based implementation), the cofactor of \hat{z}_E in the summand of the sum over l' becomes a Kronecker delta⁴² enforcing $l' \rightarrow l$, so that we have (note that the sums over l' and l_E are completely functionally independent of each other)

$$\begin{aligned} \nu_d \Big|_{\rho_{AE} = \alpha_{AE}^{-1}} &= \frac{m}{2} \sum_{l=0}^{\infty} \hat{\chi}(\mu, l) \hat{z}_E(l) \sum_{l_E=0}^{\infty} \hat{\Xi}(\mu_E, l_E) \left[1 - (1 - \eta \alpha_{EB} \rho_{EB})^{l_E} \right] \\ &= \frac{m}{2} z_E(\mu) \sum_{l_E=0}^{\infty} \hat{\Xi}(\mu_E, l_E) \left[1 - (1 - \eta \alpha_{EB} \rho_{EB})^{l_E} \right], \end{aligned} \quad (67)$$

⁴² Upon specifically setting $\rho_{AE} = \alpha_{AE}^{-1}$ in the general sum $\sum_{l'=0}^l \binom{l}{l'} (\alpha_{AE} \rho_{AE})^{l'} (1 - \alpha_{AE} \rho_{AE})^{l-l'} y_{l'}$ we obtain $\sum_{l'=0}^l \binom{l}{l'} (1)^{l'} (1 - 1)^{l-l'} y_{l'} = \sum_{l'=0}^l \binom{l}{l'} \delta_{l,l'} y_{l'} = y_l$ for any l' -dependent quantity $y_{l'}$.

in the case that the enemy has performed a direct attack on *all* the multi-photon pulses with three or more photons (where $z_E(\mu)$ is given in eq.(57)), and

$$\nu_{d,l} \Big|_{\rho_{AE} = \alpha_{AE}^{-1}} = \frac{m}{2} \psi_l(\mu) \hat{z}_E(l) \sum_{l_E=0}^{\infty} \hat{\Xi}(\mu_E, l_E) \left[1 - \left(1 - \eta \alpha_{EB} \rho_{EB} \right)^{l_E} \right], \quad (68)$$

in the case of a direct attack on any *particular* pulse with l photons in it.

We now confront an important fact about the direct attack. Alice and Bob may *never* be able to learn the detailed functional form of $\hat{\Xi}(\mu_E, l_E)$, and certainly will not if we simply (conservatively) assume that the enemy is *always* capable of withholding this information from them. Without knowing the explicit form of $\hat{\Xi}(\mu_E, l_E)$ chosen by the enemy for the preparation of the surrogate pulse to be sent on to Bob, we are to a certain extent limited as to what we can predict about the effect of this function on the operating characteristics of a practical QKD system. However, we may note that the sum over l_E is a probability function, and thus its value is constrained to range between 0 and 1 only. Thus from the point of view of Alice and Bob, the *worst case*, or maximum values possible for either ν_d or ν_{dl} are

$$\nu_d \Big|_{\rho_{AE} = \alpha_{AE}^{-1}}^{max} = \frac{m}{2} z_E(\mu) \quad (69)$$

and

$$\nu_{d,l} \Big|_{\rho_{AE} = \alpha_{AE}^{-1}}^{max} = \frac{m}{2} \psi_l(\mu) \hat{z}_E(l), \quad (70)$$

respectively. We note that these worst case results, which have been defined to be independent of α_{AE} , are clearly also independent of both η and α_{EB} (and therefore also independent of $\alpha_{AE} \alpha_{EB} = \alpha$). Thus, if the enemy can choose a suitable distribution function $\hat{\Xi}$ in which to prepare the surrogate pulses such that sum over l_E in eq.(65) (or eq.(66)) becomes

$$\sum_{l_E=0}^{\infty} \hat{\Xi}(\mu_E, l_E) \left[1 - \left(1 - \eta \alpha_{EB} \rho_{EB} \right)^{l_E} \right] = 1, \quad (71)$$

the enemy can gain full effective control over both the total line attenuation *and* the quantum efficiency of Bob's detector without having to physically tamper with either the quantum channel or the detector! In order for her to achieve this, though, it is essential that Bob *not* monitor the click statistics of his detector. If he does monitor click statistics, as we discuss below, he can partly prevent Eve from gaining such control: he can prevent her from controlling his detector efficiency, but cannot prevent her from gaining control over the line attenuation.

We can do more if we assume a particular form for $\hat{\Xi}(\mu_E, l_E)$. If as before, we take $\rho_{AE} = \alpha_{AE}^{-1}$ and we *further* assume that the enemy in particular prepares the surrogate photon states in a Poisson distribution, so that we have $\hat{\Xi} = \hat{\chi}$, we find

$$\nu_d \Big|_{\substack{\rho_{AE} = \alpha_{AE}^{-1} \\ \hat{\Xi} = \hat{\chi}}} = \frac{m}{2} z_E(\mu) \sum_{l_E=0}^{\infty} \hat{\chi}(\mu_E, l_E) \left[1 - \left(\eta \alpha_{EB} \rho_{EB} \right)^{l_E} \right]$$

$$\begin{aligned}
&= \frac{m}{2} z_E(\mu) \left\{ 1 - e^{-\mu_E} \sum_{l_E=0}^{\infty} \frac{[\mu_E (1 - \eta \alpha_{EB} \rho_{EB})]^{l_E}}{l_E!} \right\} \\
&= \frac{m}{2} z_E(\mu) \left[1 - e^{-\mu_E} e^{\mu_E (1 - \eta \alpha_{EB} \rho_{EB})} \right] \\
&= \frac{m}{2} z_E(\mu) \left(1 - e^{-\eta \mu_E \alpha_{EB} \rho_{EB}} \right) \\
&= \frac{m}{2} z_E(\mu) \psi_{\geq 1}(\eta \mu_E \alpha_{EB} \rho_{EB}) ,
\end{aligned} \tag{72}$$

in the case of a direct attack on all of the multi-photon pulses containing three or more photons, and

$$\nu_{d,l} \Big|_{\substack{\rho_{AE} = \alpha_{AE}^{-1} \\ \hat{\Xi} = \hat{\chi}}} = \frac{m}{2} \psi_l(\mu) \hat{z}_E(l) \psi_{\geq 1}(\eta \mu_E \alpha_{EB} \rho_{EB}) , \tag{73}$$

in the case of a direct attack on any *particular* pulse with l photons in it. This result is easily interpreted as the probability that Alice sends a pulse with l photons in it, multiplied by the probability that Eve can with complete knowledge determine the state of polarization of that pulse, multiplied by the probability that Bob will observe a pulse with one or more photons in it, taken from a stream sent by Eve characterized by an effective mean photon number per pulse of $\eta \mu_E \alpha_{EB} \rho_{EB}$.

We now see, quite explicitly in the case of the direct attack based on the use by Eve of a Poisson distribution for the surrogate pulses allowed to go on to Bob, that the value of the fact that Eve cannot “remotely” control the value of the quantum efficiency, η , of Bob’s detector⁴³ is *completely taken away*. In other words, it doesn’t matter that Eve can’t directly control the quantum efficiency of Bob’s detector: as long as Bob chooses *not* to monitor the click statistics of his detector (to be discussed below), Eve can effectively mimic control over η . An appropriate tuning by the enemy of the value of the statistical mean flux μ_E such that the product $\eta \mu_E \alpha_{EB} \rho_{EB}$ is as large as required to produce a value of $\psi_{\geq 1}(\eta \mu_E \alpha_{EB} \rho_{EB})$ that is arbitrarily close to unity, can evidently have the effect of achieving the same result of maximizing the amount of compromised bit information.⁴⁴ By the same token we see that Eve does not have to arrange for a collaborator to be located next to Bob: the tuning of μ_E also results in the effective replacement of α_{EB} by unity.

⁴³ As discussed previously, this is due to the presumed use by Bob of a narrow bandpass wavelength filter in front of his apparatus.

⁴⁴ Note that Eve does not need to know in advance the value of η to achieve this (in general Eve won’t know the value of η if Alice and Bob follow proper technically sound cryptosystem practice and withhold this from her). If Eve doesn’t know the value of η in advance she can infer the value as follows: During a period of the transmission in which she does not carry out any attacks as such, she may perform quantum non-demolition photon number measurements from which she can determine the value of the mean photon number μ characterizing Alice’s source. She can also determine the fraction n/m by listening to the public discussion pertaining to this portion of the transmission. Using the relationship $n/m = \frac{1}{2} [\psi_{\geq 1}(\eta \mu \alpha) + r_d] \simeq \frac{1}{2} \psi_{\geq 1}(\eta \mu \alpha) \approx \eta \mu \alpha$ (cf eqs.(7) and (15)) she can then deduce the approximate value of the product $\eta \alpha$, from which she can then infer the value of η . Alternatively she can simply reasonably assume that Bob is using a detector for which the value of η is not too small to be useful and adjust μ_E accordingly.

Thus, to sum up, *in the absence of explicit monitoring of click statistics by Bob*, whether a free space *or* optical fiber quantum channel is used is immaterial: in either case, with or without an enemy collaborator located at another position along the quantum channel, and with or without any capability to physically adjust the transparency of the quantum channel in any way, and without ascribing to Eve the physically nonsensical ability to “remotely control” the quantum efficiency of Bob’s detector, in carrying out the direct attack the enemy can anyhow entirely “tune away” the values of both α and η to the values that allow for maximal vulnerability of the transmitted multi-photon pulses. This has explicitly been proved to be true (*cf* eq.(72)) in the case that the enemy prepares the surrogate pulse in a Poisson distribution, and is probably true for many other distributions that might be chosen as well. However, the fact that we have found at least one distribution for which this is clearly possible dictates that we must assume that Eve can always choose to achieve this maximal, worst-case possibility. Thus, we can replace the expression given in eq.(69) with a universal maximal privacy amplification amount for the direct attack, for which we no longer impose *only* the condition $\rho_{AE} = \alpha_{AE}^{-1}$, but also $\rho_{EB} = \alpha_{EB}^{-1}$ (which amounts to allowing that Eve has completely eliminated the attenuation by effecting the replacement $\alpha \rightarrow 1$):

$$\begin{aligned} \nu_d \bigg|_{\substack{\rho_{AE} = \alpha_{AE}^{-1} \\ \rho_{EB} = \alpha_{EB}^{-1}}}^{max} &= \frac{m}{2} z_E(\mu) \\ &\equiv \nu_d^{max} \end{aligned} \quad (74)$$

and

$$\begin{aligned} \nu_{d,l} \bigg|_{\substack{\rho_{AE} = \alpha_{AE}^{-1} \\ \rho_{EB} = \alpha_{EB}^{-1}}}^{max} &= \frac{m}{2} \psi_l(\mu) \hat{z}_E(l) \\ &\equiv \nu_{d,l}^{max}. \end{aligned} \quad (75)$$

However, we have assumed thus far that Bob adamantly does *not* monitor the statistics of his detector clicks in the above analysis. As we shall now show, the very strong capabilities of the enemy reflected by the above two equations are somewhat reduced if Bob explicitly *does* monitor click statistics.

Now we examine the more general case in which Bob explicitly monitors the click statistics and discards those bit cells which manifestly contain more than one photon by having produced simultaneous clicks. We do this by following the procedure used in making the replacement of eq.(15) by eq.(25), in which case we find (as before, the subscript *mcs* stands for “monitor click statistics”)

$$\nu_{d,mcs} = \frac{m}{2} \sum_{l=0}^{\infty} \hat{\chi}(\mu, l) \sum_{l'=0}^l \binom{l}{l'} (\alpha_{AE} \rho_{AE})^{l'} (1 - \alpha_{AE} \rho_{AE}) \hat{z}_E(l')$$

$$\begin{aligned}
& \sum_{l_E=0}^{\infty} \hat{\Xi}(\mu_E, l_E) \sum_{l''=0}^{l_E} \binom{l_E}{l''} \left(\alpha_{EB} \rho_{EB} \right)^{l''} \left(1 - \alpha_{EB} \rho_{EB} \right)^{l_E-l''} \hat{z}_B(\eta, l'') \\
&= \frac{m}{2} \sum_{l=0}^{\infty} \hat{\chi}(\mu, l) \sum_{l'=0}^l \binom{l}{l'} \left(\alpha_{AE} \rho_{AE} \right)^{l'} \left(1 - \alpha_{AE} \rho_{AE} \right)^{l-l'} \hat{z}_E(l') \\
& \quad \sum_{l_E=0}^{\infty} \hat{\Xi}(\mu_E, l_E) \left[l_E \eta \alpha_{EB} \rho_{EB} \left(1 - \alpha_{EB} \rho_{EB} \right)^{l_E-1} \right. \\
& \quad \left. + \sum_{l''=2}^{l_E} \binom{l_E}{l''} \left(\alpha_{EB} \rho_{EB} \right)^{l''} \left(1 - \alpha_{EB} \rho_{EB} \right)^{l_E-l''} \hat{z}_{B, l'' \geq 2}(\eta, l'') \right], \tag{76}
\end{aligned}$$

in the case that all multi-photon pulses with three or more photons are subjected to a direct attack, and

$$\begin{aligned}
\nu_{d,l,mcs} &= \frac{m}{2} \hat{\chi}(\mu, l) \sum_{l'=0}^l \binom{l}{l'} \left(\alpha_{AE} \rho_{AE} \right)^{l'} \left(1 - \alpha_{AE} \rho_{AE} \right)^{l-l'} \hat{z}_E(l') \\
& \quad \sum_{l_E=0}^{\infty} \hat{\Xi}(\mu_E, l_E) \left[l_E \eta \alpha_{EB} \rho_{EB} \left(1 - \alpha_{EB} \rho_{EB} \right)^{l_E-1} \right. \\
& \quad \left. + \sum_{l''=2}^{l_E} \binom{l_E}{l''} \left(\alpha_{EB} \rho_{EB} \right)^{l''} \left(1 - \alpha_{EB} \rho_{EB} \right)^{l_E-l''} \hat{z}_{B, l'' \geq 2}(\eta, l'') \right] \\
&= \frac{m}{2} \psi_l(\mu) \sum_{l'=0}^l \binom{l}{l'} \left(\alpha_{AE} \rho_{AE} \right)^{l'} \left(1 - \alpha_{AE} \rho_{AE} \right)^{l-l'} \hat{z}_E(l') \\
& \quad \sum_{l_E=0}^{\infty} \hat{\Xi}(\mu_E, l_E) \left[l_E \eta \alpha_{EB} \rho_{EB} \left(1 - \alpha_{EB} \rho_{EB} \right)^{l_E-1} \right. \\
& \quad \left. + \sum_{l''=2}^{l_E} \binom{l_E}{l''} \left(\alpha_{EB} \rho_{EB} \right)^{l''} \left(1 - \alpha_{EB} \rho_{EB} \right)^{l_E-l''} \hat{z}_{B, l'' \geq 2}(\eta, l'') \right], \tag{77}
\end{aligned}$$

in the case of a direct attack on any *particular* pulse with l photons in it.

As in our previous analysis leading to eq.(67), if we again (very conservatively) assume that the enemy has the capability of somehow arranging for the removal of any line attenuation between the location of Alice and the interception site, so that we have $\rho_{AE} = \alpha_{AE}^{-1}$, we find

$$\begin{aligned}
\nu_{d,mcs} \Big|_{\rho_{AE} = \alpha_{AE}^{-1}} &= \frac{m}{2} \sum_{l=0}^{\infty} \hat{\chi}(\mu, l) \hat{z}_E(l) \sum_{l_E=0}^{\infty} \hat{\Xi}(\mu_E, l_E) \left[l_E \eta \alpha_{EB} \rho_{EB} \left(1 - \alpha_{EB} \rho_{EB} \right)^{l_E-1} \right. \\
& \quad \left. + \sum_{l''=2}^{l_E} \binom{l_E}{l''} \left(\alpha_{EB} \rho_{EB} \right)^{l''} \left(1 - \alpha_{EB} \rho_{EB} \right)^{l_E-l''} \hat{z}_{B, l'' \geq 2}(\eta, l'') \right] \\
&= \frac{m}{2} z_E(\mu) \sum_{l_E=0}^{\infty} \hat{\Xi}(\mu_E, l_E) \left[l_E \eta \alpha_{EB} \rho_{EB} \left(1 - \alpha_{EB} \rho_{EB} \right)^{l_E-1} \right.
\end{aligned}$$

$$+ \sum_{l''=2}^{l_E} \binom{l_E}{l''} \left(\alpha_{EB} \rho_{EB} \right)^{l''} \left(1 - \alpha_{EB} \rho_{EB} \right)^{l_E - l''} \hat{z}_{B,l'' \geq 2}(\eta, l'') \Bigg], \quad (78)$$

and

$$\begin{aligned} \nu_{d,l,mcs} \Big|_{\rho_{AE} = \alpha_{AE}^{-1}} &= \frac{m}{2} \psi_l(\mu) \hat{z}_E(l) \sum_{l_E=0}^{\infty} \hat{\Xi}(\mu_E, l_E) \left[l_E \eta \alpha_{EB} \rho_{EB} \left(1 - \alpha_{EB} \rho_{EB} \right)^{l_E - 1} \right. \\ &\quad \left. + \sum_{l''=2}^{l_E} \binom{l_E}{l''} \left(\alpha_{EB} \rho_{EB} \right)^{l''} \left(1 - \alpha_{EB} \rho_{EB} \right)^{l_E - l''} \hat{z}_{B,l'' \geq 2}(\eta, l'') \right]. \end{aligned} \quad (79)$$

If we now also examine the case in which the enemy in particular prepares the surrogate states in a Poisson distribution so that $\hat{\Xi} = \hat{\chi}$, one obtains

$$\begin{aligned} \nu_{d,mcs} \Big|_{\substack{\rho_{AE} = \alpha_{AE}^{-1} \\ \hat{\Xi} = \hat{\chi}}} &= \frac{m}{2} z_E(\mu) \left\{ e^{-\mu_E} \mu_E \eta \alpha_{EB} \rho_{EB} \sum_{l_E=0}^{\infty} \frac{\left[\mu_E \left(1 - \alpha_{EB} \rho_{EB} \right) \right]^{l_E - 1}}{(l_E - 1)!} \right. \\ &\quad \left. + \langle \hat{\chi}(\mu_E, l_E) \mathcal{Z}_{\geq 2}(\eta, \alpha_{EB} \rho_{EB}, l_E) \rangle \right\} \\ &= \frac{m}{2} z_E(\mu) \left[\eta \mu_E \alpha_{EB} \rho_{EB} e^{-\mu_E} e^{\mu_E (1 - \alpha_{EB} \rho_{EB})} + \langle \hat{\chi}(\mu_E, l_E) \mathcal{Z}_{\geq 2}(\eta, \alpha_{EB} \rho_{EB}, l_E) \rangle \right] \\ &= \frac{m}{2} z_E(\mu) \left[\eta \mu_E \alpha_{EB} \rho_{EB} e^{-\mu_E \alpha_{EB} \rho_{EB}} + \langle \hat{\chi}(\mu_E, l_E) \mathcal{Z}_{\geq 2}(\eta, \alpha_{EB} \rho_{EB}, l_E) \rangle \right] \\ &= \frac{m}{2} z_E(\mu) \left[\eta \psi_1(\mu_E \alpha_{EB} \rho_{EB}) + \langle \hat{\chi}(\mu_E, l_E) \mathcal{Z}_{\geq 2}(\eta, \alpha_{EB} \rho_{EB}, l_E) \rangle \right] \end{aligned} \quad (80)$$

and

$$\nu_{d,l,mcs} \Big|_{\substack{\rho_{AE} = \alpha_{AE}^{-1} \\ \hat{\Xi} = \hat{\chi}}} = \frac{m}{2} \psi_l(\mu) \hat{z}_E(l) \left[\eta \psi_1(\mu_E \alpha_{EB} \rho_{EB}) + \langle \hat{\chi}(\mu_E, l_E) \mathcal{Z}_{\geq 2}(\eta, \alpha_{EB} \rho_{EB}, l_E) \rangle \right]. \quad (81)$$

Comparison of eqs.(81) with (73) reveals the benefit of incorporating the monitoring of click statistics into the QKD protocol. First we rewrite eq.(73) as

$$\begin{aligned} \nu_{d,l} \Big|_{\substack{\rho_{AE} = \alpha_{AE}^{-1} \\ \hat{\Xi} = \hat{\chi}}} &= \frac{m}{2} \psi_l(\mu) \hat{z}_E(l) \psi_{\geq 1}(\eta \mu_E \alpha_{EB} \rho_{EB}) \\ &= \frac{m}{2} \psi_l(\mu) \hat{z}_E(l) \left[\psi_1(\eta \mu_E \alpha_{EB} \rho_{EB}) + \psi_{\geq 2}(\eta \mu_E \alpha_{EB} \rho_{EB}) \right] \end{aligned} \quad (82)$$

and compare with eq.(81). Looking first at the *first terms* in each of the square brackets, we see that by tuning the mean flux μ_E appropriately, the products $\mu_E \alpha_{EB} \rho_{EB}$ and $\eta \mu_E \alpha_{EB} \rho_{EB}$ (for the cases of $\nu_{d,l,mcs}$ and $\nu_{d,l}$, respectively) can assume values such that the functions $\psi_1(\eta \mu_E \alpha_{EB} \rho_{EB})$ and $\psi_1(\mu_E \alpha_{EB} \rho_{EB})$ reach their maximal, optimal values (from the perspective of the enemy), thereby maximizing the amount of information obtainable by the enemy. However, we see that, by employing monitoring of the click statistics, Alice and Bob can *force* the reduction of this maximum amount of vulnerable information on bit encodings otherwise available to Eve by an amount η : this is where significance of the fact that Eve cannot “remotely” control the value of η comes into full force. An analogous reduction in the amount of vulnerable information will arise from the remaining terms in the square brackets, which will in general depend on the details of the functional form of $\hat{z}_B(\eta, l)$.

Indirect Attacks

The logical structure of the analysis carried out in this section is illustrated with the flow chart shown in Figure 4 below.

As described above, in the indirect attack the enemy receives a multi-photon pulse, “splits the beam” and retains one or more photons - unmeasured - in an appropriate quantum memory while allowing the remaining photons in the pulse to propagate on to Bob, without disturbing them in any way. As always in our analysis, we ascribe to the enemy superior technological capabilities, and do not delve into the methods whereby the photon or photons retained in quantum memory can actually be so preserved. We also assume as before that the enemy possesses perfect photon detection equipment, so that η_E , the intrinsic quantum efficiency of Eve’s detector apparatus, may be once and for all set equal to unity.

We proceed to deduce the form of the privacy amplification function appropriate to indirect attacks on multi-photon pulses. As before we work from first principles by listing the relevant probabilities for the various processes that make up the dynamics, which are given by

$$\mathcal{P}(l \geq 2 \text{ photons leave Alice}) = \hat{\chi}(\mu, l) \theta(l-2) , \quad (83)$$

$$\mathcal{P}(l' \text{ photons reach Eve} \mid l \geq 2 \text{ photons leave Alice}) = \binom{l}{l'} (\alpha_{AE} \rho_{AE})^{l'} (1 - \alpha_{AE} \rho_{AE})^{l-l'} , \quad (84)$$

$$\mathcal{P}(l'' \text{ photons reach Bob} \mid l' - u \text{ photons pass Eve}) = \binom{l' - u}{l''} (\alpha_{EB} \rho_{EB})^{l''} (1 - \alpha_{EB} \rho_{EB})^{l'-u-l''} \quad (85)$$

and

$$\mathcal{P}(l''' \text{ photons detected} \mid l'' \text{ photons reach Bob}) = \binom{l''}{l'''} \eta^{l'''} (1 - \eta)^{l''-l'''} (1 - \delta_{0,l''''}) . \quad (86)$$

In eq.(83) the θ -function enforces the condition that there must be at least two photons in the pulse received by the enemy in order to carry out the indirect attack. In eq.(85) u is

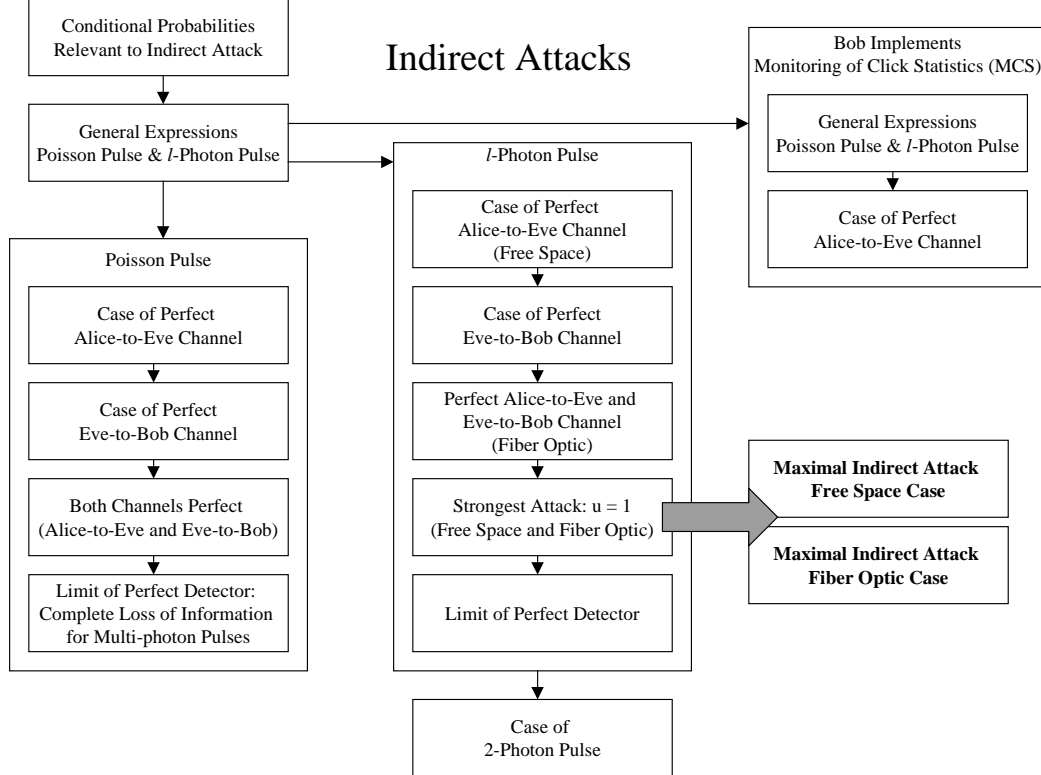


Figure 4: Flow Chart for Analysis of Indirect Attacks

the number of photons split off (and preserved in some suitable quantum memory) by the enemy, and it satisfies the inequality $u \leq u_{max}$, where u_{max} is (one less than) the number of photons that were contained in the pulse as received by Eve. We refer to the part of the pulse that is allowed to propagate on to Bob as the “remnant” pulse. Unlike the case in the direct attack, the remnant pulse must not be amplified or prepared in any way by Eve, lest she give herself away. In the general implementation scenario in which Bob monitors the statistics of the detector clicks, it is not obvious *a priori* which value for u is optimal for the enemy. For instance, if Eve splits off and retains *one* photon, this allows the maximum strength remnant pulse to go on to Bob, which is presumably advantageous in the case of a channel with strong attenuation, but in this case there will be some admixture of multiple clicks observed and discarded by Bob. Alternatively, if Eve splits off and retains *all but one* of the photons in the pulse, then the single photon in the remnant pulse will definitely *not* cause a multiple click to occur in Bob’s detectors, and thus the factor $z_B(\eta, l)$ will not cause Eve to lose some of her advantage, although the received signal will be fully subjected to the

effects of line attenuation and Bob's detector inefficiency. This type of puzzle can be resolved through the use of numerical methods. In the case of the indirect attack on a multi-photon pulse with l photons, there will in general be $l - 1$ distinct possible values for u that may be chosen by the enemy.

We now deduce the explicit expression for the privacy amplification subtraction function associated to indirect attacks, which we denote by $\nu_i^{(u)}$, where the superscript “ (u) ” indicates the number of photons that the enemy chooses to remove from the multi-photon pulse and retain untouched in quantum memory. Upon assembling the appropriate probabilities from eqs.(83) through (86) we find

$$\begin{aligned}
\nu_i^{(u)} &= \frac{m}{2} \sum_{l, l', l'', l'''} \mathcal{P}(l \geq 2 \text{ photons leave Alice}) \\
&\quad \times \mathcal{P}(l' \text{ photons reach Eve} \mid l \geq 2 \text{ photons leave Alice}) \\
&\quad \times \mathcal{P}(l'' \text{ photons reach Bob} \mid l' - u \text{ photons pass Eve}) \\
&\quad \times \mathcal{P}(l''' \text{ photons detected} \mid l'' \text{ photons reach Bob}) \\
&= \frac{m}{2} \sum_{l=0}^{\infty} \hat{\chi}(\mu, l) \theta(l-2) \sum_{l'=0}^l \binom{l}{l'} \left(\alpha_{AE} \rho_{AE} \right)^{l'} \left(1 - \alpha_{AE} \rho_{AE} \right)^{l-l'} \\
&\quad \sum_{l''=0}^{l'-u} \binom{l'-u}{l''} \left(\alpha_{EB} \rho_{EB} \right)^{l''} \left(1 - \alpha_{EB} \rho_{EB} \right)^{l'-u-l''} \\
&\quad \sum_{l'''=0}^{l''} \binom{l''}{l'''} \eta^{l'''} (1-\eta)^{l''-l'''} (1 - \delta_{0,l''''}) \\
&= \frac{m}{2} \sum_{l=0}^{\infty} \hat{\chi}(\mu, l) \theta(l-2) \sum_{l'=0}^l \binom{l}{l'} \left(\alpha_{AE} \rho_{AE} \right)^{l'} \left(1 - \alpha_{AE} \rho_{AE} \right)^{l-l'} \\
&\quad \sum_{l''=0}^{l'-u} \binom{l'-u}{l''} \left(\alpha_{EB} \rho_{EB} \right)^{l''} \left(1 - \alpha_{EB} \rho_{EB} \right)^{l'-u-l''} [1 - (1-\eta)^{l''}] \\
&= \frac{m}{2} \sum_{l=0}^{\infty} \hat{\chi}(\mu, l) \theta(l-2) \sum_{l'=0}^l \binom{l}{l'} \left(\alpha_{AE} \rho_{AE} \right)^{l'} \left(1 - \alpha_{AE} \rho_{AE} \right)^{l-l'} [1 - (1 - \eta \alpha_{EB} \rho_{EB})^{l'-u}] \\
&= \frac{m}{2} \sum_{l=0}^{\infty} \hat{\chi}(\mu, l) \theta(l-2) \left[1 - \sum_{l'=0}^l \binom{l}{l'} \left(\alpha_{AE} \rho_{AE} \right)^{l'} \left(1 - \alpha_{AE} \rho_{AE} \right)^{l-l'} (1 - \eta \alpha_{EB} \rho_{EB})^{l'-u} \right] \\
&= \frac{m}{2} \sum_{l=0}^{\infty} \hat{\chi}(\mu, l) \theta(l-2) \left[1 - (1 - \eta \alpha_{EB} \rho_{EB})^{-u} (1 - \eta \alpha_{AE} \rho_{AE} \alpha_{EB} \rho_{EB})^l \right] \\
&= \frac{m}{2} \sum_{l=2}^{\infty} \hat{\chi}(\mu, l) \left[1 - (1 - \eta \alpha_{EB} \rho_{EB})^{-u} (1 - \eta \alpha_{AE} \rho_{AE} \alpha_{EB} \rho_{EB})^l \right] \\
&= \frac{m}{2} \left[\psi_{\geq 2}(\mu) - (1 - \eta \alpha_{EB} \rho_{EB})^{-u} \sum_{l=2}^{\infty} \hat{\chi}(\mu, l) (1 - \eta \alpha_{AE} \rho_{AE} \alpha_{EB} \rho_{EB})^l \right]
\end{aligned}$$

$$\begin{aligned}
&= \frac{m}{2} \left\{ \psi_{\geq 2}(\mu) - \left(1 - \eta \alpha_{EB} \rho_{EB}\right)^{-u} e^{-\mu} \sum_{l=2}^{\infty} \frac{[\mu(1 - \eta \alpha_{AE} \rho_{AE} \alpha_{EB} \rho_{EB})]^l}{l!} \right\} \\
&= \frac{m}{2} \left\{ \psi_{\geq 2}(\mu) - \left(1 - \eta \alpha_{EB} \rho_{EB}\right)^{-u} e^{-\mu} \left[e^{\mu(1 - \eta \alpha_{AE} \rho_{AE} \alpha_{EB} \rho_{EB})} - 1 - \mu(1 - \eta \alpha_{AE} \rho_{AE} \alpha_{EB} \rho_{EB}) \right] \right\} \\
&= \frac{m}{2} \left[\left[\psi_{\geq 2}(\mu) - \left(1 - \eta \alpha_{EB} \rho_{EB}\right)^{-u} \left\{ e^{-\eta \mu \alpha_{AE} \rho_{AE} \alpha_{EB} \rho_{EB}} - e^{-\mu} \left[1 + \mu(1 - \eta \alpha_{AE} \rho_{AE} \alpha_{EB} \rho_{EB}) \right] \right\} \right] \right] \tag{87}
\end{aligned}$$

The physical description of this result is straightforward. This quantity is the total amount of the information contained in the multi-photon pulses (the first term, $\psi_{\geq 2}$, in the double square brackets), diminished by a complicated expression that takes into account the effects of the imperfect nature of both the quantum channel itself and the quantum efficiency of Bob's detector. This form clearly shows that simply subtracting the *entire* amount of information contained in the multi-photon pulses (as has apparently been done in all previous analyses) in order to protect against eavesdropping attacks is sufficient, but obviously not necessary in the presence of attenuation and/or imperfect detector efficiency in Bob's apparatus.

The above result provides the amount of privacy amplification subtraction required to compensate for indirect attacks on *all* multi-photon pulses. As in the case of the direct attack, we also need the expression for the amount of privacy amplification required in order to protect against an indirect attack on any *particular* multi-photon pulse with l photons in it, which we denote by $\nu_{i,l}^{(u)}$. Reading off the relevant quantity from the above calculation, we have

$$\begin{aligned}
\nu_{i,l}^{(u)} &= \frac{m}{2} \hat{\chi}(\mu, l) \theta(l-2) \left[1 - \left(1 - \eta \alpha_{EB} \rho_{EB}\right)^{-u} \left(1 - \eta \alpha_{AE} \rho_{AE} \alpha_{EB} \rho_{EB}\right)^l \right] \\
&= \frac{m}{2} \psi_l(\mu) \theta(l-2) \left[1 - \left(1 - \eta \alpha_{EB} \rho_{EB}\right)^{-u} \left(1 - \eta \alpha_{AE} \rho_{AE} \alpha_{EB} \rho_{EB}\right)^l \right]. \tag{88}
\end{aligned}$$

These results may be explored in a number of limits. If we specialize the above to the case $\rho_{AE} = \alpha_{AE}^{-1}$, we have

$$\nu_i^{(u)} \Big|_{\rho_{AE} = \alpha_{AE}^{-1}} = \frac{m}{2} \left[\left[\psi_{\geq 2}(\mu) - \left(1 - \eta \alpha_{EB} \rho_{EB}\right)^{-u} \left\{ e^{-\eta \mu \alpha_{EB} \rho_{EB}} - e^{-\mu} \left[1 + \mu(1 - \eta \alpha_{EB} \rho_{EB}) \right] \right\} \right] \right]. \tag{89}$$

In the case that we have $\rho_{EB} = \alpha_{EB}^{-1}$, we find

$$\nu_i^{(u)} \Big|_{\rho_{EB} = \alpha_{EB}^{-1}} = \frac{m}{2} \left[\left[\psi_{\geq 2}(\mu) - (1 - \eta)^{-u} \left\{ e^{-\eta \mu \alpha_{AE} \rho_{AE}} - e^{-\mu} \left[1 + \mu(1 - \eta \alpha_{AE} \rho_{AE}) \right] \right\} \right] \right]. \tag{90}$$

If we consider the case in which both $\rho_{AE} = \alpha_{AE}^{-1}$ and $\rho_{EB} = \alpha_{EB}^{-1}$, corresponding to the situation for a fiber-optic cable implementation⁴⁵ in which the enemy has somehow replaced

⁴⁵ As discussed above, in the case of a free space implementation it is not necessary to analyze the case in

the cable with an ideal “lossless” channel, we have

$$\begin{aligned} \nu_i^{(u)} \Big|_{\rho_{AE} = \alpha_{AE}^{-1}, \rho_{EB} = \alpha_{EB}^{-1}} &= \frac{m}{2} \left[\left[\psi_{\geq 2}(\mu) - (1 - \eta)^{-u} \left\{ e^{-\eta\mu} - e^{-\mu} [1 + \mu(1 - \eta)] \right\} \right] \right] \\ &\equiv \nu_i^{(u),max} . \end{aligned} \quad (91)$$

We note that, unlike the case for the direct attack, in the indirect attack there is no parameter that multiplies η that is under the control of the enemy that can be used by the enemy to “remotely control” or adjust the value of the quantum efficiency of Bob’s detector to a value that is optimal for Eve, so that the above expression is indeed the worst case (from the perspective of Alice and Bob), or maximal value of the amount of privacy amplification subtraction that needs to be carried out to ensure a secret shared cipher.

Note that if we anyway examine the (artificial) limit of perfect detector efficiency, $\eta \rightarrow 1$, the quantity $\nu_i^{(u),max}$ in this “more-than-maximal” case (denoted by the superscript “*max+*”) becomes

$$\begin{aligned} \nu_i^{(u),max+} &\equiv \lim_{\eta \rightarrow 1} \nu_i^{(u),max} \\ &= \lim_{\eta \rightarrow 1} \nu_i^{(u)} \Big|_{\rho_{AE} = \alpha_{AE}^{-1}, \rho_{EB} = \alpha_{EB}^{-1}} \\ &= \frac{m}{2} \left\{ \psi_{\geq 2}(\mu) - \lim_{\eta \rightarrow 1} \frac{e^{-\eta\mu} - e^{-\mu} [1 + \mu(1 - \eta)]}{(1 - \eta)^u} \right\} \\ &= \frac{m}{2} \psi_{\geq 2}(\mu) , \end{aligned} \quad (92)$$

so that, as expected, in the limit of a perfectly lossless channel (so that all of the multi-photon pulses reach Eve and that all of the split-off pieces she lets pass go on to reach Bob), perfect detector efficiency (ensuring that all of the split-off pulses that reach Bob are in fact detected) and complete, indirect attack compromise of *all* of the multi-photon pulses (effected by the sum over all l), there is a corresponding loss to the enemy of *all* of the information contained in those pulses.

The results in eqs.(87) through (92) apply to the case in which all multi-photon pulses are subjected to indirect cryptanalytic attack. In case of an indirect attack on a particular multi-photon pulse with l photons in it, for the situation in which $\rho_{AE} = \alpha_{AE}^{-1}$, we have

$$\nu_{i,l}^{(u)} \Big|_{\rho_{AE} = \alpha_{AE}^{-1}} = \frac{m}{2} \psi_l(\mu) \theta(l-2) \left[1 - \left(1 - \eta \alpha_{EB} \rho_{EB} \right)^{l-u} \right] , \quad (93)$$

and in the case that $\rho_{EB} = \alpha_{EB}^{-1}$ we have

$$\nu_{i,l}^{(u)} \Big|_{\rho_{EB} = \alpha_{EB}^{-1}} = \frac{m}{2} \psi_l(\mu) \theta(l-2) \left[1 - (1 - \eta)^{-u} \left(1 - \eta \alpha_{AE} \rho_{AE} \right)^l \right] . \quad (94)$$

which the transparency of the quantum channel is modified. At most, in this case we can imagine that *either* $\rho_{AE} = \alpha_{AE}^{-1}$ (meaning that Eve is physically next to Alice) *or* $\rho_{EB} = \alpha_{EB}^{-1}$ (meaning that Eve is physically next to Bob), but both conditions together are not possible for Eve to impose.

The situation described by eq.(93) for the case that $\rho_{AE} = \alpha_{AE}^{-1}$, which arises either if Eve is located immediately adjacent to Alice (in the case of a free-space or fiber-optic cable implementation) or if Eve has somehow been able to replace the cable between herself and Alice with a perfect one, is particularly interesting. We will see that it is *always* advantageous, irrespective of the values of ρ_{AE} or ρ_{EB} (and, importantly, in the absence of click statistics monitoring by Bob), for the enemy to choose the value $u = 1$, which means that only *one* photon in the multi-photon pulse is split off and retained in quantum memory, with the other $l - 1$ photons allowed to travel on to Bob in the remnant pulse. For example, there are two possible values for u in the case of a three-photon pulse: $u = 1$ and $u = 2$. We find

$$\nu_{i,l=3}^{(2)} \Big|_{\rho_{AE} = \alpha_{AE}^{-1}} = \frac{m}{2} \psi_3(\mu) \eta \alpha_{EB} \rho_{EB} , \quad (95)$$

and

$$\begin{aligned} \nu_{i,l=3}^{(1)} \Big|_{\rho_{AE} = \alpha_{AE}^{-1}} &= \frac{m}{2} \psi_3(\mu) \left[1 - (1 - \eta \alpha_{EB} \rho_{EB})^2 \right] \\ &= \frac{m}{2} \psi_3(\mu) \left(-\eta^2 \alpha_{EB}^2 \rho_{EB}^2 + 2\eta \alpha_{EB} \rho_{EB} \right) \\ &= \frac{m}{2} \psi_3(\mu) \eta \alpha_{EB} \rho_{EB} (2 - \eta \alpha_{EB} \rho_{EB}) \\ &= \nu_{i,l=3}^{(2)} \Big|_{\rho_{AE} = \alpha_{AE}^{-1}} (2 - \eta \alpha_{EB} \rho_{EB}) \\ &\geq \nu_{i,l=3}^{(2)} \Big|_{\rho_{AE} = \alpha_{AE}^{-1}} , \end{aligned} \quad (96)$$

since $2 - \eta \alpha_{EB} \rho_{EB} \geq 1$ due to the fact that $\eta \alpha_{EB} \rho_{EB} \leq 1$, and using eq.(88) it is easy to show that in general one has

$$\nu_{i,l}^{(1)} \geq \nu_{i,l}^{(u>1)} , \quad (97)$$

and finally we note that this inequality remains true for all allowed values of ρ_{EB} , and in particular for the case $\rho_{EB} = \alpha_{EB}^{-1}$. When *both* $\rho_{AE} = \alpha_{AE}^{-1}$ and $\rho_{EB} = \alpha_{EB}^{-1}$ we have modeled the worst case scenario (from the perspective of Alice and Bob) in which the enemy has completely replaced the quantum channel with one of perfect transparency,⁴⁶ so that

$$\begin{aligned} \nu_{i,l}^{(u)} \Big|_{\substack{\rho_{AE} = \alpha_{AE}^{-1} \\ \rho_{EB} = \alpha_{EB}^{-1}}} &= \frac{m}{2} \psi_l(\mu) \theta(l-2) \left[1 - (1 - \eta)^{l-u} \right] \\ &\equiv \nu_{i,l}^{(u),max} , \end{aligned} \quad (98)$$

and we have

$$\nu_{i,l}^{(1),max} \geq \nu_{i,l}^{(u>1),max} \quad (99)$$

⁴⁶ As noted before, this is perhaps reasonable to discuss in the case of a fiber-optic cable implementation, but is not possible in the case of a free-space implementation. Moreover, since we are now analyzing the indirect rather than the direct attack, it is not possible for the enemy to circumvent the physical line attenuation by employing a collaborator located adjacent to Bob. Accordingly, when predictions derived from the use of $\nu_{i,l}^{(u),max}$, based as it is on the absence of any line attenuation whatsoever, are applied to the case of a free space implementation, any such results can be safely understood to be overly conservative.

in complete generality. Since in the above case we assume that there is no explicit monitoring of multiple click statistics, this result is easily explained. The enemy retains only one photon, maximizing the number of photons in the remnant pulse and thereby increasing the chance that the remnant pulse will be able to propagate through to Bob in spite of the presence of some amount of line attenuation. Of course, if Bob is actively monitoring click statistics, the enemy faces the risk that a larger number of photons in the remnant pulse will cause the bit cell to be identified as carrying a multi-photon pulse and thus be discarded from the sifting process.

As with eq.(92), where we studied for the case of the indirect attack on *all* the multi-photon pulses the artificial (and unenforceable by the enemy) but theoretically interesting limit in which $\eta \rightarrow 1$, we may examine this for the “more-than-maximal” strength indirect attack on a *particular* multi-photon pulse (denoted as before by the superscript “*max+*”). From eq.(98) we have

$$\begin{aligned}
\nu_{i,l}^{(u),\text{max+}} &\equiv \lim_{\eta \rightarrow 1} \nu_{i,l}^{(u),\text{max}} \\
&= \lim_{\eta \rightarrow 1} \nu_{i,l}^{(u)} \Big|_{\substack{\rho_{AE} = \alpha_{AE}^{-1} \\ \rho_{EB} = \alpha_{EB}^{-1}}} \\
&= \frac{m}{2} \lim_{\eta \rightarrow 1} \left\{ \psi_l(\mu) \theta(l-2) \left[1 - (1-\eta)^{l-u} \right] \right\} \\
&= \frac{m}{2} \psi_l(\mu) \theta(l-2) (1 - \delta_{l,u}) . \tag{100}
\end{aligned}$$

This result means that as before, in the limit of a perfectly lossless channel and perfect detector efficiency in Bob’s apparatus, as long as the enemy doesn’t make the mistake of keeping *all* of the intercepted photons (which corresponds to setting $u = l$, in which case none of the information is compromised since Bob doesn’t receive anything, effected by the factor $1 - \delta_{l,l} = 0$), *all* of the information contained in the l -photon pulse is compromised in this artificial and unrealizable more-than-maximal version of the indirect attack.

The case of pulses with precisely two photons is of considerable importance, since *only* indirect attacks are possible for these. In this case the only allowed value for u is $u = 1$, and we find

$$\nu_{i,l=2}^{(1)} = \frac{m}{2} \psi_2(\mu) \left[1 - \left(1 - \eta \alpha_{EB} \rho_{EB} \right)^{-1} \left(1 - \eta \alpha_{AE} \rho_{AE} \alpha_{EB} \rho_{EB} \right)^2 \right] . \tag{101}$$

If we specialize to the case that $\rho_{AE} = \alpha_{AE}^{-1}$ this becomes

$$\begin{aligned}
\nu_{i,l=2}^{(1)} \Big|_{\rho_{AE} = \alpha_{AE}^{-1}} &= \frac{m}{2} \psi_2(\mu) \left[1 - \left(1 - \eta \alpha_{EB} \rho_{EB} \right) \right] \\
&= \frac{m}{2} \psi_2(\mu) \eta \alpha_{EB} \rho_{EB} . \tag{102}
\end{aligned}$$

If we now *also* set $\rho_{EB} = \alpha_{EB}^{-1}$, which as above amounts to assuming that the enemy has completely replaced the quantum channel with one of perfect transparency, we see that the

worst case (again, from the perspective of Alice and Bob), or maximum value of required privacy amplification is

$$\nu_{i,l=2}^{(1),max} = \frac{m}{2} \psi_2(\mu) \eta . \quad (103)$$

Thus, the fact that the enemy cannot remotely control and alter the value of η is very significant, as it implies that the enemy *cannot* obtain the full information content of the two-photon pulses in the transmission. Unlike the case of the direct attack, for which the quantity μ_E provides the enemy with a parameter (that is beyond the control of Alice and Bob) that can “tune” the quantum efficiency of Bob’s detector to that value which is optimal for Eve, in the indirect attack the enemy can *at most* obtain a fraction η of the information content of the two-photon pulses.

We may reconsider the entire analysis of indirect attacks for the case corresponding to explicit monitoring of click statistics. Carrying through the algebra for this yields

$$\begin{aligned} \nu_{i,mcs}^{(u)} = & \frac{m}{2} \sum_{l=0}^{\infty} \hat{\chi}(\mu, l) \theta(l-2) \left\{ \eta \alpha_{EB} \rho_{EB} \frac{(1 - \alpha_{AE} \rho_{AE} \alpha_{EB} \rho_{EB})^l}{(1 - \alpha_{EB} \rho_{EB})^{u+1}} \left[\frac{l \alpha_{AE} \rho_{AE} (1 - \alpha_{EB} \rho_{EB})}{1 - \alpha_{AE} \rho_{AE} \alpha_{EB} \rho_{EB}} - u \right] \right. \\ & + \sum_{l'=0}^l \binom{l}{l'} (\alpha_{AE} \rho_{AE})^{l'} (1 - \alpha_{AE} \rho_{AE})^{l-l'} \\ & \left. \sum_{l''=2}^{l'-u} \binom{l'-u}{l''} (\alpha_{EB} \rho_{EB})^{l''} (1 - \alpha_{EB} \rho_{EB})^{l'-u-l''} \hat{z}_{B,\geq 2}(\eta, l'') \right\}, \end{aligned} \quad (104)$$

for the case that *all* the multi-photon pulses are subjected to the indirect attack in the presence of click statistics monitoring, and

$$\begin{aligned} \nu_{i,l,mcs}^{(u)} = & \frac{m}{2} \hat{\chi}(\mu, l) \theta(l-2) \left\{ \eta \alpha_{EB} \rho_{EB} \frac{(1 - \alpha_{AE} \rho_{AE} \alpha_{EB} \rho_{EB})^l}{(1 - \alpha_{EB} \rho_{EB})^{u+1}} \left[\frac{l \alpha_{AE} \rho_{AE} (1 - \alpha_{EB} \rho_{EB})}{1 - \alpha_{AE} \rho_{AE} \alpha_{EB} \rho_{EB}} - u \right] \right. \\ & + \sum_{l'=0}^l \binom{l}{l'} (\alpha_{AE} \rho_{AE})^{l'} (1 - \alpha_{AE} \rho_{AE})^{l-l'} \\ & \left. \sum_{l''=2}^{l'-u} \binom{l'-u}{l''} (\alpha_{EB} \rho_{EB})^{l''} (1 - \alpha_{EB} \rho_{EB})^{l'-u-l''} \hat{z}_{B,\geq 2}(\eta, l'') \right\}, \end{aligned} \quad (105)$$

for the case that a particular l -photon pulse is attacked.

If we assume that $\rho_{AE} = \alpha_{AE}^{-1}$ we find the considerably simplified forms

$$\begin{aligned} \nu_{i,mcs}^{(u)} \Big|_{\rho_{AE} = \alpha_{AE}^{-1}} = & \frac{m}{2} \sum_{l=0}^{\infty} \hat{\chi}(\mu, l) \theta(l-2) \left[\eta \alpha_{EB} \rho_{EB} (1 - \alpha_{EB} \rho_{EB})^{l-u-1} (l-u) \right. \\ & \left. + \sum_{l''=2}^{l-u} \binom{l-u}{l''} (\alpha_{EB} \rho_{EB})^{l''} (1 - \alpha_{EB} \rho_{EB})^{l-u-l''} \hat{z}_{B,\geq 2}(\eta, l'') \right], \end{aligned} \quad (106)$$

and

$$\begin{aligned} \nu_{i,l,mcs}^{(u)} \Big|_{\rho_{AE} = \alpha_{AE}^{-1}} &= \frac{m}{2} \hat{\chi}(\mu, l) \theta(l-2) \left[\eta \alpha_{EB} \rho_{EB} \left(1 - \alpha_{EB} \rho_{EB}\right)^{l-u-1} (l-u) \right. \\ &\quad \left. + \sum_{l''=2}^{l-u} \binom{l-u}{l''} \left(\alpha_{EB} \rho_{EB}\right)^{l''} \left(1 - \alpha_{EB} \rho_{EB}\right)^{l-u-l''} \hat{z}_{B,\geq 2}(\eta, l'') \right]. \end{aligned} \quad (107)$$

Combined Direct and Indirect Attacks

The logical structure of the analysis carried out in this section is illustrated with the flow chart shown in Figure 5 below.

Combined Attacks

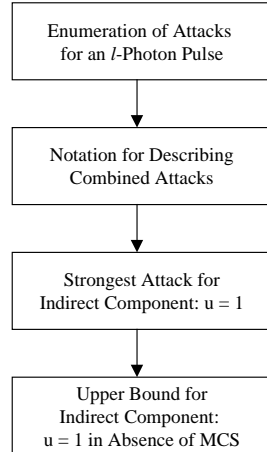


Figure 5: Flow Chart for Analysis of Combined Direct and Indirect Attacks

Until now we have considered the situation in which, having intercepted a multi-photon pulse

containing l photons, the enemy carries out *either* the direct attack *or* the indirect attack, and we have considered this in the cases that the attacks are performed either on a particular pulse or on some number of them (including all of them). However, in addition to carrying out a general admixture of *purely* direct and *purely* indirect attacks, distributed in some way amongst the various multi-photon pulses, it is also possible for the enemy to perform what we shall refer to as a *combined* direct and indirect attack on any given intercepted multi-photon pulse, as long as the pulse contains *five or more* photons. This type of attack appears to have never been previously analyzed. The requirement for five or more photons arises as follows. To carry out the *direct* part of the attack, the enemy requires at least three photons in order to determine the state of polarization with complete knowledge; to carry out the *indirect* part of the attack, the enemy must split the beam and retain at least one (unmeasured) photon in a suitable quantum memory, and allow a remnant pulse of at least one (unmeasured) photon to propagate on to Bob. Of course, any given attack on any given intercepted multi-photon pulse is either successful in providing the enemy the identity of the state or it isn't: the purpose for the enemy in carrying out the combined attack would be to try to increase the likelihood that the information extracted on the pulse can be increased to a higher value than possible with either a purely direct or purely indirect attack. The question is whether or not this occurs. As we will show, in the general case the combined attack is not as strong as either a particular purely direct or purely indirect attack.⁴⁷ The combined attack furnishes, for any given multi-photon pulse, a "continuum region" of success outcomes for the enemy connecting the purely direct and purely indirect attacks. The analysis is complicated by the competing effects of the quantum efficiency of Bob's detector and any residual line attenuation on the quantum channel that the enemy has not managed to in some way eliminate.

There are a variety of ways in which the photon content of a given multi-photon pulse with five or more photons in it can be disassembled by the enemy to carry out the combined attack. The number of distinct types of combined attack grows rapidly with the number of photons in the multi-photon pulses. For example, with a multi-photon pulse that contains $l = 5$ photons, there is only *one* possible combined attack. In this case the enemy can split off three photons from the pulse to carry out the direct attack and subject the remaining two photons to the indirect attack, for which the number of photons in the remnant pulse is necessarily unity so that $u = 1$ photon is retained in quantum memory by the enemy. When there are $l = 6$ photons in the pulse, there are *three* distinct combined attacks possible: (1) the enemy can split off three photons for the direct attack, which leaves three photons for the indirect attack, of which $u = 1$ is retained in quantum memory with two photons in the remnant pulse, or (2) the enemy can split off three photons for the direct attack, which leaves three photons for the indirect attack, of which $u = 2$ are retained in quantum memory with one photon in the remnant pulse, or (3) the enemy can split off four photons for the direct attack, which leaves two photons for the indirect attack, of which $u = 1$ is retained in quantum memory with one photon in the remnant pulse.

The analysis of the various possibilities is governed by the fact that, for any given multi-

⁴⁷ For completeness it is nevertheless of value to understand the combined attack in detail.

$$\begin{aligned}
&(5, (0)) \\
&(4, (1)) \\
&(3, 2)^{1+1} \\
&((2), 3)^{1+2} \\
&((2), 3)^{2+1} \\
&((1), 4)^{1+3} \\
&((1), 4)^{2+2} \\
&((1), 4)^{3+1} \\
&((0), 5)^{1+4} \\
&((0), 5)^{2+3} \\
&((0), 5)^{3+2} \\
&((0), 5)^{4+1}
\end{aligned}$$

Table 1: Set of Distinct Purely Direct, Purely Indirect and Combined Attacks for $l = 5$.

photon pulse, the enemy can choose to perform any of the allowed combined attacks, or any of the allowed purely direct or indirect attacks. To organize the different possibilities, we introduce the following notation to represent the particular way in which a given l -photon pulse has been disassembled by the enemy in order to carry out a chosen attack: for an l -photon pulse, we designate by $(l_d, l_i)^{u+(l_i-u)}$, subject to the constraint $l_d + l_i = l$, the situation in which l_d of the photons in the pulse are subjected to a direct attack and l_i of the photons are subjected to an indirect attack, with u photons being intercepted and stored in quantum memory by the enemy for the indirect part. This *kinematical symbol* notation is completely general and is very useful in describing any possible attack. For example, in the case of a pulse containing $l = 8$ photons, the symbol $(3, 5)^{1+4}$ means that 3 of the photons are subjected to a direct attack, and the remaining 5 photons are subjected to the an indirect attack, with Eve choosing to split off and retain 1 of those 5 photons, letting the remaining 4 photons go on to Bob. In the event that so many of the photons are taken for one kind of attack that there are not enough left to carry out the *other* kind of attack, we place the remaining number inside parentheses: thus, the symbol $((1), 7)^{4+3}$ means that 7 of the 8 photons in the intercepted pulse are taken by the enemy for the indirect attack (here with $u = 4$ of these retained by Eve and 3 allowed to go on to Bob), which only leaves 1 additional photon, which is not enough to carry out a direct attack, and so it is placed inside parentheses.

To illustrate the different types of attack that are possible, in Table 1 we enumerate in full the 12 distinct attacks that are possible to carry out on a multi-photon pulse containing $l = 5$ photons, and in Table 2 we do the same for the 30 distinct attacks that are possible on a multi-photon pulse containing $l = 8$ photons.

The entries in each list comprises a continuum of attacks ranging from purely direct to purely indirect. In the $l = 5$ case, of the 12 possibilities there are two distinct, purely direct attacks (represented by $(5, (0))$ and $(4, (1))$), one combined attack (represented by

$(8, (0))$	$((1), 7)^{1+6}$
$(7, (1))$	$((1), 7)^{2+5}$
$(6, 2)^{1+1}$	$((1), 7)^{3+4}$
$(5, 3)^{1+2}$	$((1), 7)^{4+3}$
$(5, 3)^{2+1}$	$((1), 7)^{5+2}$
$(4, 4)^{1+3}$	$((1), 7)^{6+1}$
$(4, 4)^{2+2}$	$((0), 8)^{1+7}$
$(4, 4)^{3+1}$	$((0), 8)^{2+6}$
$(3, 5)^{1+4}$	$((0), 8)^{3+5}$
$(3, 5)^{2+3}$	$((0), 8)^{4+4}$
$(3, 5)^{3+2}$	$((0), 8)^{5+3}$
$(3, 5)^{4+1}$	$((0), 8)^{6+2}$
$((2), 6)^{1+5}$	$((0), 8)^{7+1}$
$((2), 6)^{2+4}$	
$((2), 6)^{3+3}$	
$((2), 6)^{4+2}$	
$((2), 6)^{5+1}$	

Table 2: Set of Distinct Purely Direct, Purely Indirect and Combined Attacks for $l = 8$.

$(3, 2)^{1+1}$), and a total of 9 purely indirect attacks (represented by the ordered pairs in which the first element is contained within parentheses). Similarly, in the $l = 8$ case, of the 30 possibilities there are two distinct, purely direct attacks (represented by $(8, (0))$ and $(7, (1))$), ten different combined attacks (represented by the various entries for which neither element inside the ordered pair is contained within parentheses), and a total of 18 purely indirect attacks (as before, represented by the ordered pairs in which the first element is contained within parentheses). As always, it is simple to identify an attack that is optimal from the perspective of the enemy. The attack for which the net value of the associated privacy amplification function is maximal is the strongest attack, as it requires the largest number of bits to be subtracted in order to ensure that the remaining bits shared between Alice and Bob will be secret. As we shall see, most of the attacks displayed in the two Tables are *not* optimal from the perspective of the enemy, and are listed here only for completeness.

In the absence of explicit click statistics monitoring by Bob we may continue to assume for the combined attack, just as was shown in eqs.(96) and (97) for the case of the purely indirect attack, that the indirect attack *part* of a given combined attack is optimal for the enemy if the value $u = 1$ is selected, so that only one photon is retained in quantum memory and thus the largest possible number of photons are allowed to go on to Bob in the remnant pulse, thereby increasing the likelihood of overcoming whatever line attenuation may be present in the quantum channel. This assumption, which is only demonstrably valid when *no* click monitoring is in effect, considerably reduces the number of distinct types of combined attack that need to be considered in our analysis: now, if the intercepted multi-photon pulse contains l photons, it is easy to see that there are a total of $l - 4$ possible distinct *combined*

attacks available to the enemy. More generally, if we restrict consideration of indirect attacks to those for which $u = 1$ there are a total altogether of $l - 1$ distinct attacks of *any* kind. Thus, in the case of a multi-photon pulse with $l = 5$ photons, out of the 12 possible attacks, we see from Table 1 that there is $5 - 4 = 1$ combined attack for which $u = 1$ (in this case this is also the *only* combined attack), and we see that there are $5 - 1 = 4$ attacks in general in which the indirect part is characterized by $u = 1$. The reduction in the number of attacks that need to be considered is much more dramatic in the case of $l = 8$: here we see from Table 2 that, of the 30 attacks that are possible in total, only $8 - 4 = 4$ of them are combined attacks for which $u = 1$, and only $8 - 1 = 7$ of them include indirect attacks, combined or not, for which $u = 1$.

It is useful to study this reduced set of attacks for which $u = 1$, since in this case we know (in the absence of click statistics monitoring) that the attack is optimal for the enemy, *both* due to having $u = 1$ *and* due to the absence of click statistics monitoring, since the modifying the former condition can only have the effect of reducing the strength of the enemy's attack, and the same is true if the latter activity is implemented. Thus, the associated amount of privacy amplification subtraction is guaranteed to provide sufficient protection against the strongest possible cryptanalytic attacks, as Bob is needlessly weakening his protection (*i.e.*, Bob is not executing a “technically sound quantum cryptosystem”) against the enemy by not monitoring click statistics.

Having sketched a taxonomy and thus delineated the “kinematics” of the various types of multi-photon attacks we now turn our attention to the “dynamics,” *i.e.* an assessment of the relative strengths of the purely direct, purely indirect and combined attacks by making use of the closed form expressions for the privacy amplification that we have derived.

Comparison of Strengths of Direct, Combined and Indirect Attacks

The logical structure of the analysis carried out in this section is illustrated with the flow chart shown in Figure 6 below.

The enemy can choose to carry out any admixture of purely direct and purely indirect attacks, or to carry out simultaneous combinations of the two types, and we must assume that the relative proportion chosen for each is unknown to Alice and Bob, who must therefore implement sufficient privacy amplification subtraction to protect against the worst case scenario. By an “adixture of purely direct and purely indirect attacks” we mean that, for a given transmission from Alice to Bob that includes some fixed number of multi-photon pulses that contain l photons each, the enemy can choose to carry out the purely indirect attack on a fraction j_l of the l -photon pulses and subject the remaining fraction of $1 - j_l$ of the l -photon pulses in the stream to the purely direct attack (as long as $l \geq 3$, since otherwise the direct attack cannot succeed). There is no reason that the j_l values need to be the same for different values of l , and in general we need to consider the case that they are not, in order to assess what the strongest enemy attack might be. To understand this it is important to compare directly against each other the strengths of the direct and indirect

Comparison of Strengths

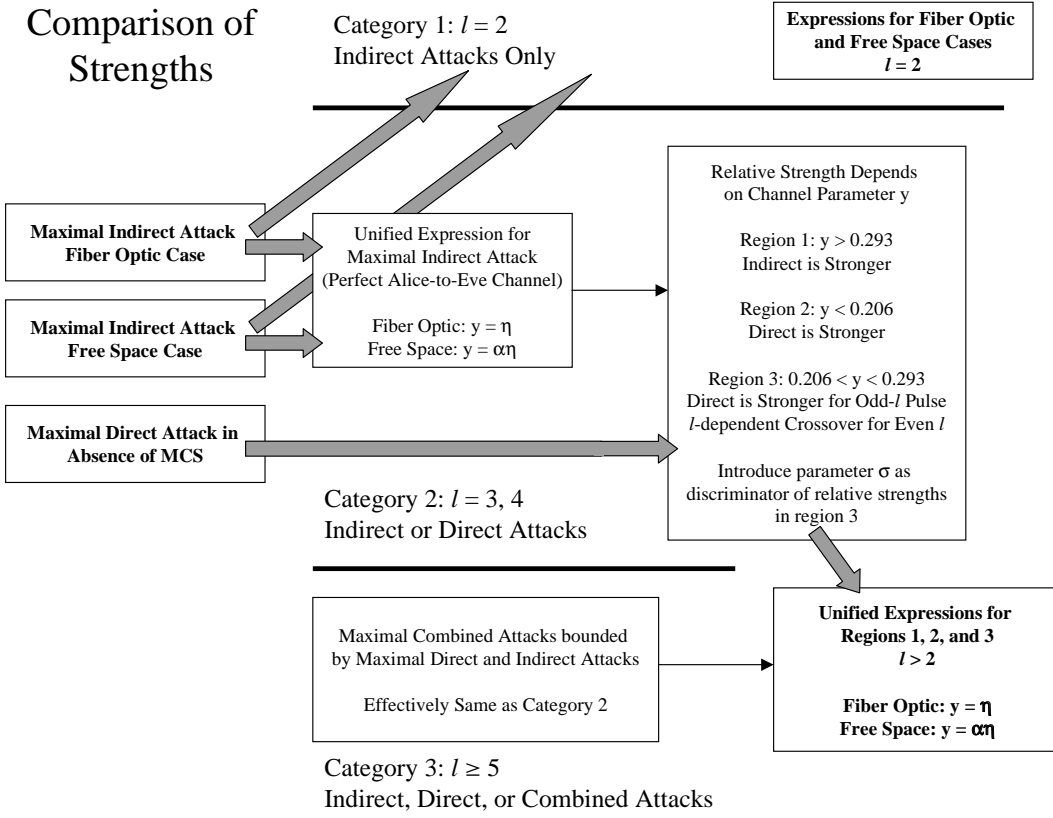


Figure 6: Flow Chart for Analysis of Comparison of Attack Strengths

attacks.

We first note that there are three different categories of multi-photon pulses to consider in this analysis, based on the associated value of l : Category 1: $l = 2$, Category 2: $l = 3$ and $l = 4$ and Category 3: $l \geq 5$. We address each category in turn.

- Category 1, $l = 2$: For two-photon pulses, *only* indirect attacks are possible.

We conservatively assume that *all* two-photon pulses are subjected to indirect attack. Thus no comparison of strengths of different types of attacks is necessary or possible: the only question to address is the appropriate amount of privacy amplification to apply (necessary and sufficient, or sufficient). This is addressed in the following section in which we write down the complete expression for multi-photon pulse privacy amplification.

- Category 2, $l = 3$ and $l = 4$: For three- and four-photon pulses, *either* a direct *or* an indirect attack, but not both, are possible on any given pulse, and thus no combined attack

is possible.

We conservatively assume that *all* three- and four-photon pulses are subjected to one or the other of the two types of attack, denoting the fraction of three-photon pulses subjected to indirect attack by j_3 , and the fraction of three-photon pulses subjected to direct attack by $1 - j_3$ (with similar meanings for j_4 and $1 - j_4$, respectively, for the case of four-photon pulses).

- Category 3, $l \geq 5$: For multi-photon pulses with five or more photons direct, indirect or combined direct and indirect attacks are possible.

In the absence of special intelligence information provided through espionage or other means, Alice and Bob cannot in general expect to know the values that the enemy will choose for the various j_l that will be used against pulses from categories 2 and 3, and they will also not know which combined attacks, if any, may be carried out against pulses from category 3, so that the only way to ensure secrecy is to determine the strength of the worst case attack. For this purpose we explicitly compare the closed form expressions for the privacy amplification functions deduced above.

As written above, no comparison of attack strengths is required for Category 1 pulses since only indirect attacks are possible. We will proceed by first comparing the strengths of the purely direct and purely indirect attacks, which are the *only* kind possible in Category 2, and then show that (as mentioned above) for any given multi-photon pulse it is always the case that the strongest possible attack is *either* a purely direct attack or a purely indirect attack and never a combined attack, so that for *both* Category 2 and Category 3 it suffices to consider direct and indirect attacks only.

In addition to not knowing the values of the j_l , as discussed above Alice and Bob will also not in general know the identity of the distribution function $\hat{\Xi}$ chosen by the enemy for the preparation of the surrogate pulse in the case of the direct attack. However, we found above that if Eve chooses in particular to prepare the surrogate pulse in the Poisson distribution, $\hat{\Xi}(\mu_E, l_E) = \hat{\chi}(\mu_E, l_E)$, she can in principle tune the value of μ_E such that the entire line attenuation and detector inefficiency of Bob's apparatus are effectively eliminated, resulting in the strongest possible direct attack, $\nu_{d,l}^{\max}$, given in eq.(75) as

$$\nu_{d,l}^{\max} = \frac{m}{2} \psi_l(\mu) \hat{z}_E(l) . \quad (108)$$

Since we have explicitly demonstrated that it is *possible* for the enemy to achieve the maximal strength direct attack, we must assume that the maximal strength direct attack *will* be achieved (assuming that the direct attack has been chosen). Of course, as we found in eq.(77), the strength of this attack can be controlled and reduced by Bob through active monitoring of the click statistics, resulting in a leading order diminution (*cf* eq.(81)) of the strength of the attack by a factor of η . We will proceed at first by assuming that Bob does *not* employ click statistics monitoring, which means we will be working with the absolutely worst case scenario from the perspective of Alice and Bob, the strongest possible version of the direct attack, *i.e.*, the form given by eq.(108) above. This form equally applies to the

cases of a free space or fiber optic cable quantum channel since the difference between them, *i.e.*, the fact that it is not possible for the enemy to physically improve the transparency of the atmosphere, is effectively eliminated since the enemy can tune the value of μ_E to achieve the same result.

Similarly, we found in eq.(98) the form of the maximal strength indirect attack that can be carried out on a multi-photon pulse,

$$\nu_{i,l}^{(u),max} = \frac{m}{2} \psi_l(\mu) \theta(l-2) \left[1 - (1-\eta)^{l-u} \right], \quad (109)$$

which is the applicable form if the enemy has somehow managed to surreptitiously replace the quantum channel with another one of perfect transparency, which is only reasonable to suppose is possible (if at all!) in the case of a fiber optic cable implementation. In the case of a free space implementation we should instead use eq.(88),

$$\nu_{i,l}^{(u)} = \frac{m}{2} \psi_l(\mu) \theta(l-2) \left[1 - \left(1 - \eta \alpha_{EB} \rho_{EB} \right)^{-u} \left(1 - \eta \alpha_{AE} \rho_{AE} \alpha_{EB} \rho_{EB} \right)^l \right]. \quad (110)$$

The interception apparatus of the enemy must of course be located *somewhere*, and for this analysis we will take as this location a position immediately adjacent to the Alice site, which has the effect of setting $\rho_{AE} = \alpha_{AE}^{-1}$, and this becomes (*cf* eq.(93))

$$\begin{aligned} \nu_{i,l}^{(u)} \Big|_{\rho_{AE} = \alpha_{AE}^{-1}} &= \frac{m}{2} \psi_l(\mu) \theta(l-2) \left[1 - \left(1 - \eta \alpha_{EB} \rho_{EB} \right)^{l-u} \right] \\ &= \frac{m}{2} \psi_l(\mu) \theta(l-2) \left[1 - (1-\eta\alpha)^{l-u} \right], \end{aligned} \quad (111)$$

where in the second equation above we have simply set $\alpha_{EB} \rho_{EB} = \alpha$, since in the case of the generic free space system that we are discussing, the residual amount α_{EB} of line attenuation appearing in the first equation above is simply the total line attenuation α , and the condition $\rho_{EB} = 1$ is imposed by the physical impossibility of replacing the atmosphere with one of improved transmissivity. The difference between eqs.(109) and (111) for the maximal strength fiber optic cable and free space implementation versions of the indirect attack privacy amplification amount is then just the presence of the factor of α that multiplies η .

Thus, the general, worst case (for Alice and Bob) combination of attacks for multi-photon pulses with $l = 3$ or $l = 4$ photons is given by

$$j_l \nu_{i,l}^{(u),max} + (1 - j_l) \nu_{d,l}^{max} \quad (112)$$

where $\nu_{i,l}^{(u),max}$ is understood to be given by eq.(109) in the case of a fiber-optic cable implementation and by eq.(111) in the case of a free space implementation. Of course, the above expression denotes the most general possible mix between purely direct and purely indirect attacks for *any* value of $l \geq 3$, not just the cases $l = 3$ and $l = 4$, but for the latter two values this form encompasses all possibilities since no combined attacks are allowed. The question

now is: what values of j_l will optimize this for the enemy, thereby prescribing for Alice and Bob the corresponding amount of needed privacy amplification?

We consider the situation in which Bob does not actively monitor the click statistics of his detector. In this case we found in eq.(97) that the maximum strength indirect attack takes place when the enemy selects the value $u = 1$, retaining only one photon from the split beam. To be as conservative as possible we utilize this value of u in the following analysis, thus ensuring that we are considering worst case results. To measure the relative strengths of the two types of maximal attack we examine functions of their differences and ratios. We first note that the quantities $\nu_{i,l}^{(u),max}$ and $\nu_{d,l}^{max}$ are each proportional to the factor $\frac{m}{2}\psi_l(\mu)$. We therefore construct the normalized difference function Δ^{max} between the two maximal privacy amplification amounts as

$$\Delta^{max} \equiv \frac{\nu_{i,l}^{(1),max} - \nu_{d,l}^{max}}{\frac{m}{2}\psi_l(\mu)} . \quad (113)$$

More generally, we note that with the help of eqs.(66) and (88) we can define the universal difference function that is *always* valid (not just for maximal attacks) in the absence of click statistics monitoring as

$$\Delta \equiv \frac{\nu_{i,l}^{(u)} - \nu_{d,l}}{\frac{m}{2}\psi_l(\mu)} , \quad (114)$$

and, if click statistics monitoring is executed, we may write using eqs.(77) and (105)

$$\Delta_{mcs} \equiv \frac{\nu_{i,l,mcs}^{(u)} - \nu_{d,l,mcs}}{\frac{m}{2}\psi_l(\mu)} . \quad (115)$$

Proceeding with the analysis of Δ^{max} , since $\frac{m}{2}\psi_l(\mu) > 0$, we see that when the condition $\Delta^{max} > 0$ is satisfied the maximal *indirect* attack is the stronger of the two for the enemy, and when $\Delta^{max} < 0$ the maximal *direct* attack is superior. Owing to the form of the function $\hat{z}_E(l)$ contained within the quantity $\nu_{d,l}^{max}$, we must write the difference function out separately for multi-photon pulses with even and odd numbers of photons. Upon defining $y \equiv \eta\alpha$ (satisfying $0 \leq y \leq 1$) in order to consider both the fiber-optic cable and free space implementation cases with the same notation, we have for the even integer case, when $l = 2k$ with $k \geq 2$ (due to the chosen range for k we have not needed to manifestly include either the explicit θ -function $\theta(l-2)$ contained in $\nu_{i,l}^{(1),max}$ or the implicit θ -function $\theta(l-3)$ contained in $\nu_{d,l}^{max}$ as they are both equal to unity)

$$\begin{aligned} \Delta_e^{max} &= \Delta_e^{max}(k, y) \\ &= 1 - (1-y)^{2k-1} - (1-2^{1-k}) \\ &= 2^{1-k} - (1-y)^{2k-1} , \end{aligned} \quad (116)$$

and for the odd integer case, when $l = 2k+1$ with $k \geq 1$ we have (for the same reason as above we have not needed to write out the θ -functions)

$$\Delta_o^{max} = \Delta_o^{max}(k, y)$$

$$\begin{aligned}
&= 1 - (1 - y)^{2k} - (1 - 2^{-k}) \\
&= 2^{-k} - (1 - y)^{2k}.
\end{aligned} \tag{117}$$

To determine the boundary separating the regions for which $\Delta^{max} > 0$ and $\Delta^{max} < 0$ we can solve the equations

$$0 = \Delta_e^{max} (k, y) \Big|_{y=y_e} \tag{118}$$

and

$$0 = \Delta_o^{max} (k, y) \Big|_{y=y_o} \tag{119}$$

for k and invert the solutions to obtain

$$\begin{aligned}
y_e &= y_e(k) \\
&= 1 - 2^{-\frac{1-k}{1-2k}} \quad \forall k \geq 2
\end{aligned} \tag{120}$$

for the even photon number case with $l = 2k$, and

$$\begin{aligned}
y_o &= 1 - \frac{1}{\sqrt[3]{2}} \quad \forall k \geq 1 \\
&\simeq 0.292893
\end{aligned} \tag{121}$$

for the odd photon number case with $l = 2k + 1$. In solving the equations to obtain y_e and y_o all other solutions than the two that are listed here were discarded since they either do not yield real values for $y_{e,o}$ or do not satisfy the unitarity constraints $0 \leq y_{e,o} \leq 1$. We also note in particular that y_o is manifestly independent of any specific value of k .

We note that the solution y_e is a monotonic function⁴⁸ of k , with its smallest value given by

$$y_e(2) = 1 - \frac{1}{\sqrt[3]{2}}, \tag{122}$$

and we find that it asymptotically achieves its maximum in the limit

$$\lim_{k \rightarrow \infty} y_e(k) \uparrow 1 - \frac{1}{\sqrt[3]{2}}. \tag{123}$$

We have thus found the answer to the question: “Which is stronger for a given multi-photon pulse, the maximal purely direct attack or the maximal purely indirect attack?” The answer is completely determined, in all generality, by the value of the quantity $\eta\alpha$ in the case of a free space implementation of quantum cryptography, or by the value of the quantity η in the case of a fiber optic cable implementation (if we wish to be conservative and allow for the possibility that the enemy might surreptitiously replace the cable with a “lossless” one). Rather than writing expressions first with $\eta\alpha$ and then again with η , we will continue to employ the symbol y with the appropriate substitution understood for free space or fiber optic cable systems. The relative strength of maximal purely direct and maximal purely indirect attacks is determined by locating y in one of the following regions:

⁴⁸ The function y_e is of course strictly only defined at discrete, integer values of its argument k .

- Region 1 - when the condition

$$y > 1 - \frac{1}{\sqrt{2}} \simeq 0.293 \quad (124)$$

is satisfied, it is *always true that the indirect attack is stronger than the direct attack for multi-photon pulses with any number of photons*,

- Region 2 - when the condition

$$y < 1 - \frac{1}{\sqrt[3]{2}} \simeq 0.206 \quad (125)$$

is satisfied, it is *always true that the direct attack is stronger than the indirect attack for multi-photon pulses with any number of photons*,

- Region 3 - when the condition

$$1 - \frac{1}{\sqrt[3]{2}} < y < 1 - \frac{1}{\sqrt{2}} \quad (126)$$

i.e.,

$$0.206 \lesssim y \lesssim 0.293 \quad (127)$$

is satisfied, for multi-photons pulses with an odd number $l = 2k + 1$ of photons it is always true that the direct attack is stronger than than the indirect attack, and for multi-photon pulses with an even number $l = 2k$ of photons the particular value of y which separates the two cases is determined for a particular value of k by the expression given on the rhs in eq.(120).⁴⁹

We are able to unambiguously deduce these results since we are directly comparing the *maximal* values of the explicit privacy amplification functions for the two types of attack. Recall in particular that, from eq.(66), the largest possible value of $\nu_{d,l}$ occurs when, for a given value of μ , the coefficient in $\nu_{d,l}$ of $\frac{m}{2}\psi_l(\mu) \sum_{l'=0}^l \binom{l}{l'} (\alpha_{AE}\rho_{AE})^{l'} (1 - \alpha_{AE}\rho_{AE})^{l-l'} \hat{z}_E(l')$ is as large as it can be, which is unity since that coefficient is itself a probability function. The critical value and region $\eta\alpha \gtrsim 0.293$ determine the condition for which the *strongest*

⁴⁹ Note that the special value $\eta\alpha \simeq 0.293$ was also noted in [22], but there the full significance of this number was not inferred (nor was the critical value $\eta\alpha \simeq 0.206$ discovered at all). There it was concluded that as long as the condition $\eta\alpha \gtrsim 0.293$ is satisfied it is not always possible for the direct attack to succeed. This result is contained in our result. We have inferred the universal conclusion that if $\eta\alpha \gtrsim 0.293$ it is *always* the case that some purely indirect attack is stronger than any purely direct attack for any given multi-photon pulse where both attacks are possible (*i.e.*, for $l \geq 3$).

possible purely direct attack is not as strong as *some* purely indirect attack, and the critical value and region $\eta\alpha \lesssim 0.206$ determine the condition for which the *strongest possible* purely indirect attack is not as strong as *some* purely direct attack.

These analytical results are illustrated numerically in Figure 7 where we display a graph of curves of the maximal difference function Δ^{max} , resolved into the even and odd parts Δ_e^{max} and Δ_o^{max} . This is done for Region 1 and Region 2, represented by y values of $y = 0.5$ and $y = 0.1$, respectively.

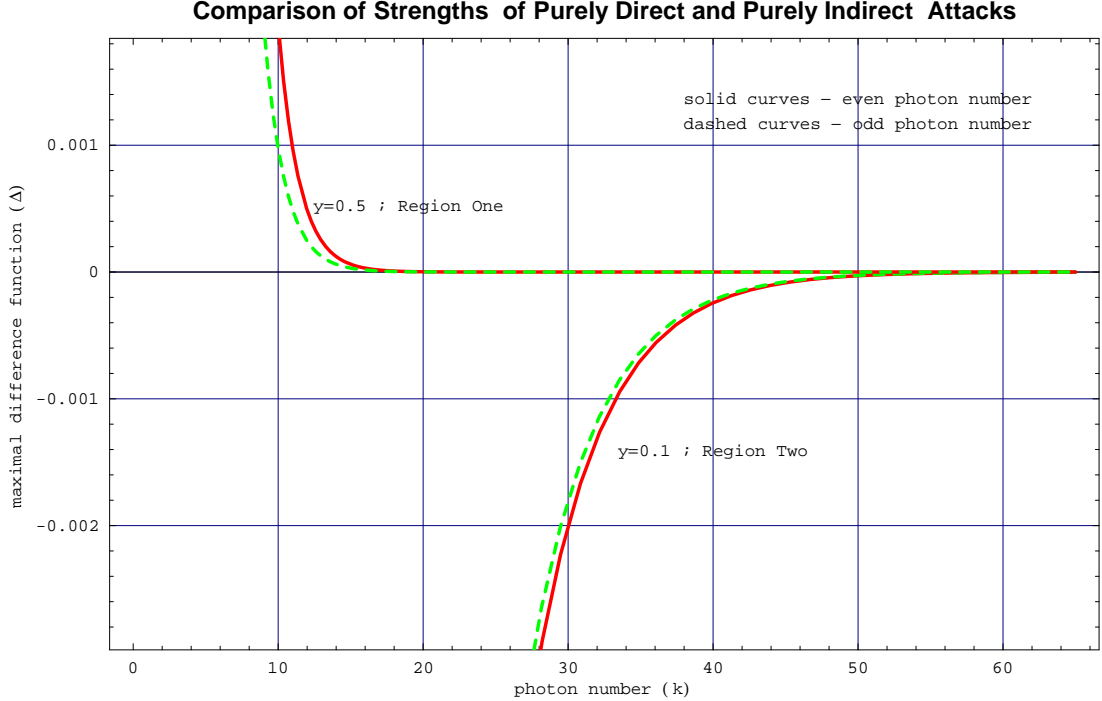


Figure 7: Comparison of Strengths of Purely Direct and Purely Indirect Attacks

The preceding analysis was carried out in order to establish whether, for a given value of l , the maximal purely direct or maximal purely indirect is stronger. We have answered this in all generality for all multi-photon pulses in Regions 1 and 2, as well as for pulses with an odd number of photons in Region 3. To complete the analysis and determine this for the case of even values of l in Region 3 where $1 - 1/\sqrt[3]{2} \leq y \leq 1 - 1/\sqrt{2}$ we need to introduce the quantity

$$\sigma_e^{max} \equiv \frac{\nu_{i,l}^{(1),max}}{\nu_{d,l}^{max}} \quad (128)$$

which measures the relative strength of the two types of attacks. Although we will only need this function for the case of even values of l , for completeness we can as above separately consider both the cases when l is an even integer and when l is an odd integer (and as before we do not display the θ -functions due to the chosen ranges for k):

$$\sigma_e^{max} = \sigma_e(k, y)$$

$$= \frac{1 - (1 - y)^{2k-1}}{1 - 2^{1-k}} , \quad (129)$$

and

$$\begin{aligned} \sigma_o^{max} &= \sigma_o(k, y) \\ &= \frac{1 - (1 - y)^{2k}}{1 - 2^{-k}} . \end{aligned} \quad (130)$$

We will use σ_e^{max} in the next section where we assemble the complete expression for multi-photon pulse privacy amplification.

Having performed a direct comparison of the strengths of direct *versus* indirect attacks, which are the only possible attacks for pulses with $l = 3$ and $l = 4$ photons, we now consider pulses with five or more photons. In this case the full set of attacks include the combined as well as purely direct and purely indirect attacks. Inspection of the kinematical symbol entries in Tables 1 and 2 reveals that the full set of allowed attacks for any given multi-photon pulse fills out a continuum of attack strengths. To see this explicitly, we consider as an example the entry for $l = 8$ displayed in Table 2, and restrict our analysis to the case that $u = 1$ for all indirect attacks (both for purely indirect attacks and the indirect *parts* of the allowed combined attacks), and as before assume that the enemy carries out the *maximal* attack always. To analyze the privacy amplification function for a generic combined attack, we need to introduce the additional notation $\nu_{c(d),l,l_d}$ and $\nu_{c(i),l,l_i}^{(u)}$. The first symbol denotes the privacy amplification function associated to the *direct part* of a combined attack (this is indicated by the “*c(d)*” in the subscript) on a multi-photon pulse with a total of l photons out of which l_d photons have been taken by the enemy for the direct attack part. Similarly, the second symbol denotes the privacy amplification function associated to the *indirect part* of a combined attack on a multi-photon pulse with a total of l photons out of which l_i photons have been taken by the enemy for the indirect attack part.

Note that in the cases that $l_d = l$ and $l_i = l$ the quantities $\nu_{c(d),l,l_d}$ and $\nu_{c(i),l,l_i}^{(u)}$ should reduce, respectively, to the expressions for $\nu_{d,l}$ and $\nu_{i,l}^{(u)}$, so that we have

$$\nu_{c(d),l,l} = \nu_{d,l} \quad (131)$$

and

$$\nu_{c(i),l,l}^{(u)} = \nu_{i,l}^{(u)} . \quad (132)$$

The important point to observe is that the constraint $l = l_d + l_i$ must always be satisfied in the combined attack, and this means in particular that the photon number arguments of different factors that appear in the associated privacy amplification functions will always be different from each other in the case of any combined attack, only becoming equal to each other in the limit that either $l_d = l$ or $l_i = l$, in which case the combined attack reduces to a purely direct or purely indirect attack. For example, in the case of the direct attack part of a generic combined attack on a pulse with l photons, we have (for this example we are assuming that the direct attack part of this combined attack is maximal)

$$\nu_{c(d),l,l_d}^{max} = \frac{m}{2} \psi_l(\mu) \hat{z}_E(l_d) , \quad (133)$$

where the subscript for ψ_l is indeed different than the argument for \hat{z}_E , with an analogous splitting amongst the appropriate arguments between l and l_i in the case of the privacy amplification function for the indirect part.

In the above expression the constraint $l_d \leq l$ must always be satisfied. With equality between l_d and l we now see explicitly that the above expression goes over to the privacy amplification function for the purely direct attack on *all* the photons in a multi-photon pulse with l photons:

$$\begin{aligned}\nu_{c(d),l,l}^{\max} &= \frac{m}{2} \psi_l(\mu) \hat{z}_E(l) \\ &= \nu_{d,l}^{\max}.\end{aligned}\quad (134)$$

Thus, to compare the strengths of any of the direct attack parts of a combined attack on a multi-photon pulse with l photons, it suffices to compare the magnitudes of $\hat{z}_E(l_d)$ and $\hat{z}_E(l)$ for all l_d satisfying $l_d < l$. Inspection of eq.(56) for $\hat{z}_E(l)$ reveals that one has

$$\hat{z}_E(l_d) < \hat{z}_E(l) \quad \forall l_d < l \quad (135)$$

and therefore

$$\nu_{c(d),l,l_d}^{\max} < \nu_{d,l}^{\max} \quad \forall l_d < l. \quad (136)$$

Thus, for a given value of l , there is no direct attack part of any combined attack that is stronger than the purely direct attack carried out on the full set of l photons contained in the pulse. A similar argument can easily be made to show the analogous result in the case of the relation between the indirect part of any combined attack and the associated purely indirect attack. Not surprisingly, as a result it turns out that for any fixed value of l , the various allowed combined attacks *always* are characterized by maximal privacy amplification function values (*i.e.*, worst case attack strengths) that are less than those for the maximal purely direct and maximal purely indirect attacks, the “endpoint” symbols in lists such as in Tables 1 and 2. We can also motivate this result numerically as follows. Going down the list of entries in Table 2 from first to last, let us examine four representative attacks denoted by the kinematical symbols $(8, (0))$, $(6, 2)^{1+1}$, $(3, 5)^{1+4}$ and $((0), 8)^{1+7}$. We see that:

$(8, (0))$ corresponds to the single privacy amplification function $\nu_{d,8}^{\max}$,

$(6, 2)^{1+1}$ corresponds to the *two* privacy amplification functions $\nu_{c(d),8,6}^{\max}$ and $\nu_{c(i),8,2}^{(1),\max}$,

$(3, 5)^{1+4}$ corresponds to the two privacy amplification functions $\nu_{c(d),8,3}^{\max}$ and $\nu_{c(i),8,5}^{(1),\max}$,

$((0), 8)^{1+7}$ corresponds to the single privacy amplification function $\nu_{i,8}^{(1),\max}$.

In Figures 8 and 9 we have plotted for Regions 1 and 2, respectively, the six privacy amplification functions corresponding to the different attacks identified by the four kinematical symbols listed above. The two solid curves in each graph are the privacy amplification functions for the purely direct and purely indirect attacks, and the four dashed curves in each graph correspond to the various combined attacks. Inspection of the curves in the graphs reveals that, depending on the value of $y = \eta\alpha$ in precisely the way determined by y_e and y_o given in eqs.(120) and (121), the purely direct or purely indirect attacks are *always* stronger than any of the combined attacks. We are led to conclude that we can therefore bound the worst possible effect of any combined attacks on multi-photon pulses with $l \geq 5$ photons by carrying out the privacy amplification analysis as if *only* purely direct or purely indirect attacks were available to the enemy. Putting this together with the previous analysis for the multi-photon pulses with $l = 3$ and $l = 4$ photons, we see that for *all* multi-photon pulses with $l \geq 3$ photons we can determine the strongest combination of direct and indirect attacks in a universal manner by making use of the critical values for $\eta\alpha$, for even or odd photon number, as determined by eqs.(120) and (121). The generic expression for privacy amplification, now for all $l \geq 3$, is therefore given by

$$j_l \nu_{i,l}^{(u)} + (1 - j_l) \nu_{d,l} \quad (137)$$

as in (112) above.

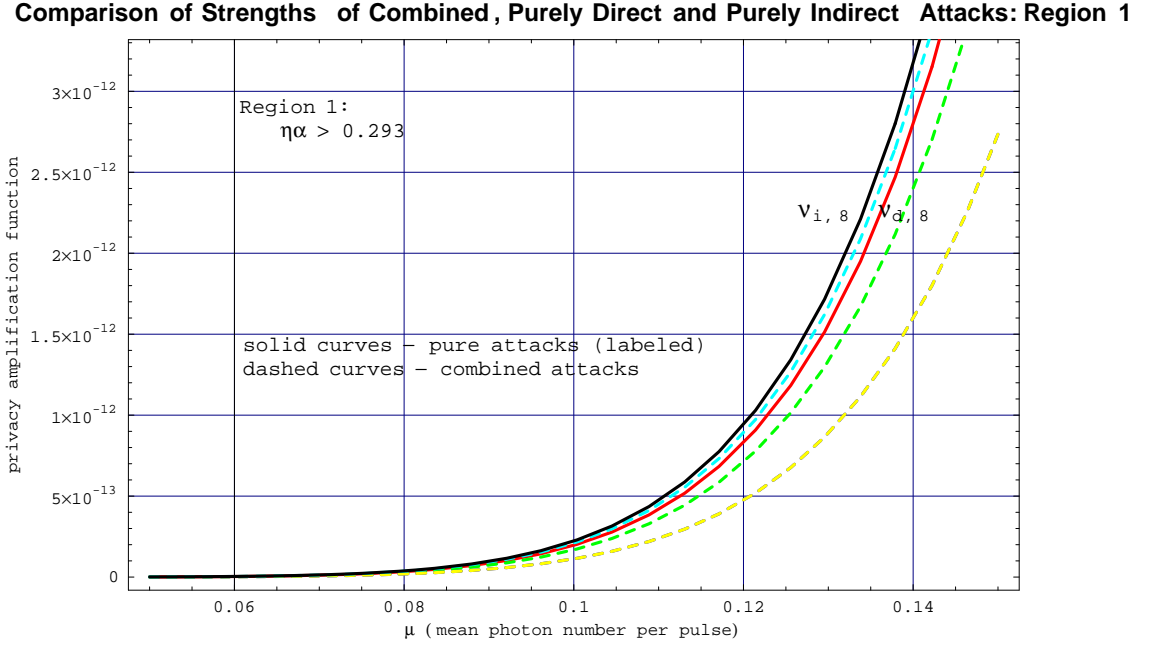


Figure 8: Comparison of Strengths of Combined, Purely Direct and Purely Indirect Attacks: Region One

ification functions corresponding to the different attacks identified by the four kinematical symbols listed above. The two solid curves in each graph are the privacy amplification functions for the purely direct and purely indirect attacks, and the four dashed curves in each graph correspond to the various combined attacks. Inspection of the curves in the graphs reveals that, depending on the value of $y = \eta\alpha$ in precisely the way determined by y_e and y_o given in eqs.(120) and (121), the purely direct or purely indirect attacks are *always* stronger than any of the combined attacks. We are led to conclude that we can therefore bound the worst possible effect of any combined attacks on multi-photon pulses with $l \geq 5$ photons by carrying out the privacy amplification analysis as if *only* purely direct or purely indirect attacks were available to the enemy. Putting this together with the previous analysis for the multi-photon pulses with $l = 3$ and $l = 4$ photons, we see that for *all* multi-photon pulses with $l \geq 3$ photons we can determine the strongest combination of direct and indirect attacks in a universal manner by making use of the critical values for $\eta\alpha$, for even or odd photon number, as determined by eqs.(120) and (121). The generic expression for privacy amplification, now for all $l \geq 3$, is therefore given by

$$j_l \nu_{i,l}^{(u)} + (1 - j_l) \nu_{d,l} \quad (137)$$

Comparison of Strengths of Combined, Purely Direct and Purely Indirect Attacks: Region 2

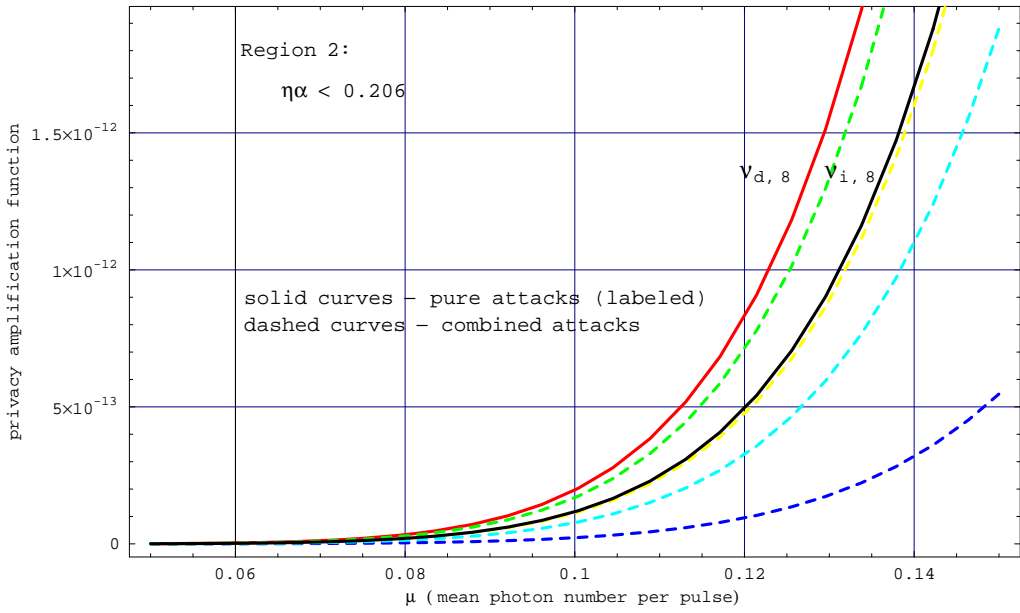


Figure 9: Comparison of Strengths of Combined, Purely Direct and Purely Indirect Attacks: Region Two

The Complete Expression for Multi-Photon Pulse Privacy Amplification

The logical structure of the analysis carried out in this section is illustrated with the flow chart shown in Figure 10 below.

Here we assemble the complete expression that provides both necessary and sufficient privacy amplification to ensure unconditional secrecy (in the sense of the privacy amplification theorem) against attacks on the multi-photon pulse part of the transmission from Alice to Bob. We adopt the very conservative assumption that *all* multi-photon pulses are intercepted and subjected to some form of attack. We at first proceed by considering the possible attacks on a photon number-by-photon number basis.

- For two-photon pulses, *only* indirect attacks are possible.
We assume that all two photon pulses are subjected to the maximal indirect attack.
- For three- and four-photon pulses each, *either* a direct *or* an indirect attack, but not both, are possible.
We assume that all three- and four-photon pulses are subjected to the maximal version of one or the other of the two types of attack, whichever is stronger.
- For pulses with five or more photons, direct, indirect or combined direct and indirect attacks are possible.

Complete Expressions

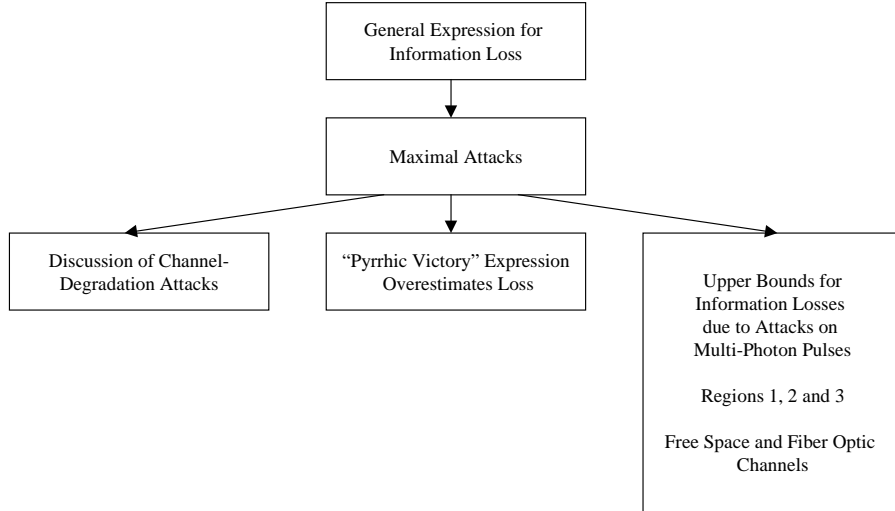


Figure 10: Flow Chart for Analysis of Complete Expressions for Multi-Photon Pulse Privacy Amplification

In the previous section we showed that, for any fixed number of photons in a multi-photon pulse, the strength of the generic combined attack is always less than a particular maximal purely direct or maximal purely indirect attack. We therefore proceed by assuming that all pulses with five or more photons are subjected to one or the other of the two types of pure attack, whichever is stronger, just as for three- and four-photon pulses.

Putting together our various results, the overall expression for the *necessary and sufficient* amount of privacy amplification ν , in all generality, for the entire multi-photon pulse part of the transmission from Alice to Bob is finally given by

$$\nu = \nu_{i,2}^{(u)} + \sum_{l=3}^{\infty} \left[j_l \nu_{i,l}^{(u)} + (1 - j_l) \nu_{d,l} \right], \quad (138)$$

where

$$\nu_{i,l}^{(u)} = \frac{m}{2} \psi_l(\mu) \theta(l-2) \left[1 - \left(1 - \eta \alpha_{EB} \rho_{EB}\right)^{-u} \left(1 - \eta \alpha_{AE} \rho_{AE} \alpha_{EB} \rho_{EB}\right)^l \right] \quad (139)$$

and

$$\begin{aligned} \nu_{d,l} &= \frac{m}{2} \psi_l(\mu) \sum_{l'=0}^l \binom{l}{l'} \left(\alpha_{AE} \rho_{AE} \right)^{l'} \left(1 - \alpha_{AE} \rho_{AE}\right)^{l-l'} \hat{z}_E(l') \\ &\quad \sum_{l_E=0}^{\infty} \hat{\Xi}(\mu_E, l_E) \left[1 - \left(1 - \eta \alpha_{EB} \rho_{EB}\right)^{l_E} \right]. \end{aligned} \quad (140)$$

Although this is indeed the most general, necessary and sufficient expression for the privacy amplification function ν , its use by Alice and Bob in practical application to actual quantum cryptography is problematic at best, and typically this expression cannot in fact be used. It provides the formally necessary and sufficient amount of privacy amplification, presuming that Alice and Bob have somehow ascertained various facts that are in principle, entirely under the control of the enemy, such as the particular distribution $\hat{\Xi}$ chosen by the enemy for the preparation of surrogate pulses, the value of u chosen by the enemy, *etc.*

Since such information will in general not be available, the only alternative is to utilize the maximal versions of the privacy amplification amounts that we have derived above. This has the virtue of ensuring that Alice and Bob will share secret bits irrespective of the attacks carried out by the enemy, while at the same time avoiding the situation of the “Pyrrhic victory” that results when *too many* bits are subtracted, as would occur if eq.(55) were used instead. Thus, we have as the *best practical expression* for the required amount of privacy amplification on multi-photon pulses:

$$\nu^{max} = \nu_{i,2}^{(1),max} + \sum_{l=3}^{\infty} \left[j_l \nu_{i,l}^{(1),max} + (1 - j_l) \nu_{d,l}^{max} \right]. \quad (141)$$

The natural way to organize this practical expression for multi-photon pulse privacy amplification is in terms of location in $\eta\alpha$ -space, rather than in terms of photon numbers, and moreover to do so separately for the cases of free space and optical fiber cable implementations. An issue of importance, over which Alice and Bob have no control, is how much modification, if any, the enemy will impose on the transparency of the quantum channel. For *both* the free space and optical fiber implementations of QC we will ignore the possibility that the enemy might be able to, and will decide to, *degrade* the transmissivity of the channel. Thus we do not consider the situation in which Eve causes a reduction in the value of α from the fiducial value initially measured by Alice and Bob to some lower value. This is because, as our explicit derivations of the various privacy amplification functions show,

such a decrease in the value of α leads to a *decrease* in the number of bits that can be compromised by the enemy, who will presumably not want this outcome to occur, and moreover any degradation of channel transparency constitutes an attempt at denial of service rather than information compromise in any event.⁵⁰

Thus we are left with two possibilities: (1) In the case of a free space implementation we can assume that the value of the product $\eta\alpha$ is given once and for all by the fiducial value initially measured by Alice and Bob.⁵¹ They will thus adjust their privacy amplification appropriately according to the $\eta\alpha$ regions mapped out below. (2) In the case of an optical fiber cable implementation, Alice and Bob cannot be confident that the fiducial value of α that they believe characterizes the cable will not be increased by the enemy. They must therefore compare the value of $\eta\alpha$, based on the fiducial value of α , with the value of η . If both endpoints of this set of values lie within one and only one of the three regions mapped out below, then they should simply *set* $\alpha = 1$ in the appropriate privacy amplification function. Otherwise, the supremum of the privacy amplification functions between the different regions, calculated for the two endpoint values, should be used in a practical system implementation. In the following list, we will assume for simplicity in the case of the optical fiber cable implementations that both endpoints (η and $\eta\alpha$) lie within one and only one of the designated regions. We then have the following requirements for appropriate privacy amplification processing associated to the multi-photon pulses:

$$\text{Region 1: } \eta\alpha > 1 - \frac{1}{\sqrt{2}} \quad (\text{i.e., } \eta\alpha \gtrsim 0.293) \Rightarrow j_l = 1$$

- Free space implementation of quantum cryptography

$$\begin{aligned} \nu^{max} &= \nu_{i,2}^{(1),max} + \sum_{l=3}^{\infty} \left[j_l \nu_{i,l}^{(1),max} + (1 - j_l) \nu_{d,l}^{max} \right] \\ &= \nu_{i,2}^{(1),max} + \sum_{l=3}^{\infty} \nu_{i,l}^{(1),max} \\ &= \sum_{l=2}^{\infty} \nu_{i,l}^{(1),max} \end{aligned}$$

⁵⁰ Strictly speaking, even though a reduction in the value of α reduces the number of bits that may be compromised, one should allow for the possibility that, by reducing the value of α and thus reducing the value of the product $\eta\alpha$, the enemy will drive the attack dynamics from Region 1 to either Region 3 or to Region 2 (or drive the attack dynamics from Region 3 to Region 2). Presumably the enemy will attempt to degrade the quantum channel surreptitiously, so that if Alice and Bob don't notice this they will not know that they should adjust the privacy amplification function accordingly. This might *possibly* be advantageous for the enemy since, in Region 1, the privacy amplification should be optimized for the indirect attack, while in Region 2, say, the privacy amplification should be optimized for the direct attack. The outcome will depend on whether the specific number of fewer bits that may be compromised by the enemy as a result of having reduced the value of α is greater or smaller than the *difference* between the attack strength of the indirect attack evaluated at the *original* value of α and the attack strength of the direct attack evaluated at the *reduced* value of α . This analysis will be performed elsewhere.

⁵¹ As always, we are presuming that proper, “technically sound cryptosystem” technique is being executed by Alice and Bob, and they have thus obtained an accurate initial measurement for the *a priori* value of α , and we also assume that they know very well what the value of η is.

$$= \frac{m}{2} \left[\left[\psi_{\geq 2}(\mu) - (1 - \eta\alpha)^{-1} \left\{ e^{-\eta\mu\alpha} - e^{-\mu} \left[1 + \mu(1 - \eta\alpha) \right] \right\} \right] \right]. \quad (142)$$

- Optical fiber cable implementation of quantum cryptography

$$\nu^{max} = \frac{m}{2} \left[\left[\psi_{\geq 2}(\mu) - (1 - \eta)^{-1} \left\{ e^{-\eta\mu} - e^{-\mu} \left[1 + \mu(1 - \eta) \right] \right\} \right] \right]. \quad (143)$$

Region 2: $\eta\alpha < 1 - \frac{1}{\sqrt[3]{2}}$ (i.e., $\eta\alpha \lesssim 0.206$) $\Rightarrow j_l = 0$

- Free space implementation of quantum cryptography

$$\begin{aligned} \nu^{max} &= \nu_{i,2}^{(1),max} + \sum_{l=3}^{\infty} \left[j_l \nu_{i,l}^{(1),max} + (1 - j_l) \nu_{d,l}^{max} \right] \\ &= \nu_{i,2}^{(1),max} + \sum_{l=3}^{\infty} \nu_{d,l}^{max} \\ &= \frac{m}{2} \psi_2(\mu) \eta\alpha + \frac{m}{2} z_E(\mu) \\ &= \frac{m}{2} \left[\psi_2(\mu) \eta\alpha + 1 - e^{-\mu} \left(\sqrt{2} \sinh \frac{\mu}{\sqrt{2}} + 2 \cosh \frac{\mu}{\sqrt{2}} - 1 \right) \right]. \end{aligned} \quad (144)$$

- Optical fiber cable implementation of quantum cryptography

$$\nu^{max} = \frac{m}{2} \left[\psi_2(\mu) \eta + 1 - e^{-\mu} \left(\sqrt{2} \sinh \frac{\mu}{\sqrt{2}} + 2 \cosh \frac{\mu}{\sqrt{2}} - 1 \right) \right]. \quad (145)$$

Before proceeding to the case of Region 3 we recall that we must now separately consider the cases of multi-photon pulses with even and odd numbers of photons. Eq.(121) above implies that for *all* multi-photon pulses with an odd number of photons the strongest attack is a maximal purely direct attack in Region 3, and thus in this case Alice and Bob should always choose $j_l = 0$. However, in the case of multi-photon pulses with an even number of photons it is necessary to determine which of the two maximal attacks is strongest on the basis of the solution to eq.(120). For this purpose we now make use of the strength ratio function $\sigma_e(k, y)$ introduced in eq.(129) to define the appropriate value of j_l , for even l only, as

$$j_l = \theta(\sigma_e(k, y) - 1) \quad l = 2k, \quad k \geq 2. \quad (146)$$

We observe that this form ensures that the value of j_l correctly identifies in Region 3 (actually, it could also be used in the other two regions, but it is not needed there) the optimal attack for multi-photon pulses with even numbers of photons, yielding $j_l = 1$ when a maximal indirect attack is the strongest, and yielding $j_l = 0$ when a maximal direct attack is the strongest. This expression can be easily computed for any particular value of $k = l/2$, and thus provides a practical method of determining for the multi-photon pulses with an even

number of photons in Region 3 what the correct amount of privacy amplification is. We then have:

$$\text{Region 3: } 1 - \frac{1}{\sqrt{2}} < \eta\alpha < 1 - \frac{1}{\sqrt{2}} \quad (\text{i.e., } 0.206 \lesssim \eta\alpha \lesssim 0.293)$$

- Free space implementation of quantum cryptography

$$\begin{aligned} \nu^{max} &= \nu_{i,2}^{(1),max} + \sum_{l=3}^{\infty} \left[j_l \nu_{i,l}^{(1),max} + (1 - j_l) \nu_{d,l}^{max} \right] \\ &= \nu_{i,2}^{(1),max} + \sum_{\substack{l=3 \\ (l \text{ even})}}^{\infty} \left[j_l \nu_{i,l}^{(1),max} + (1 - j_l) \nu_{d,l}^{max} \right] + \sum_{\substack{l=3 \\ (l \text{ odd})}}^{\infty} \nu_{d,l}^{max} \\ &= \nu_{i,2}^{(1),max} + \sum_e + \sum_o, \end{aligned} \quad (147)$$

where

$$\begin{aligned} \sum_o &\equiv \sum_{\substack{l=3 \\ (l \text{ odd})}}^{\infty} \nu_{d,l}^{max} \\ &= \sum_{\substack{l=3 \\ (l \text{ odd})}}^{\infty} \frac{m}{2} \psi_l(\mu) \hat{z}_E(l) \\ &= \frac{m}{2} e^{-\mu} \sum_{k=1}^{\infty} \frac{\mu^{2k+1}}{(2k+1)!} (1 - 2^{-k}) \\ &= \frac{m}{2} e^{-\mu} \left(\sinh \mu - \sqrt{2} \sinh \frac{\mu}{\sqrt{2}} \right) \end{aligned} \quad (148)$$

and

$$\begin{aligned} \sum_e &\equiv \sum_{\substack{l=3 \\ (l \text{ even})}}^{\infty} \left[j_l \nu_{i,l}^{(1),max} + (1 - j_l) \nu_{d,l}^{max} \right] \\ &= \frac{m}{2} \sum_{k=2}^{\infty} \psi_{2k}(\mu) \left\{ \theta(\sigma_e(k, y) - 1) [1 - (1 - y)^{2k-1}] + [1 - \theta(\sigma_e(k, y) - 1)] (1 - 2^{1-k}) \right\} \\ &\equiv \sum_e(y, \mu), \end{aligned} \quad (149)$$

so that we finally have

$$\begin{aligned} \nu^{max} &= \frac{m}{2} \left[\left[\psi_2(\mu) \eta\alpha + e^{-\mu} \left(\sinh \mu - \sqrt{2} \sinh \frac{\mu}{\sqrt{2}} \right) \right. \right. \\ &\quad \left. \left. + \sum_{k=2}^{\infty} \psi_{2k}(\mu) \left\{ \theta(\sigma_e(k, y) - 1) [1 - (1 - y)^{2k-1}] + [1 - \theta(\sigma_e(k, y) - 1)] (1 - 2^{1-k}) \right\} \right] \right] \Big|_{y=\eta\alpha} \end{aligned} \quad (150)$$

- Optical fiber cable implementation of quantum cryptography

$$\begin{aligned}
\nu^{max} = & \frac{m}{2} \left[\left[\psi_2(\mu) \eta + e^{-\mu} \left(\sinh \mu - \sqrt{2} \sinh \frac{\mu}{\sqrt{2}} \right) \right. \right. \\
& \left. \left. + \sum_{k=2}^{\infty} \psi_{2k}(\mu) \left\{ \theta(\sigma_e(k, y) - 1) [1 - (1 - y)^{2k-1}] + [1 - \theta(\sigma_e(k, y) - 1)] (1 - 2^{1-k}) \right\} \right] \right] \Big|_{y=\eta} \quad (151)
\end{aligned}$$

It should be pointed out that, as will be shown in Section 4, a practical system implementation will typically be characterized by a large amount of line attenuation, corresponding to a small numerical value for α . Moreover the quantum efficiencies of available detectors are usually smaller than one would desire. Thus realistic system values of $\eta\alpha$ will typically lie well within Region 2 as defined above, so that eqs.(144) and (145) will usually be the appropriate values for multi-photon pulse privacy amplification.

Common Sense and the Quantum Cryptographic Conservative Catechism

As presented in the Introduction, the Quantum Cryptographic Conservative Catechism (QCCC) provides a “doctrine of reasonableness” that serves as a guide in analyzing the various cryptanalytic attacks that the enemy may perform. Consistent with this, we have determined in this section the proper amount of privacy amplification subtraction required to ensure that Alice and Bob share bits that are secret, based on the assumption that the enemy is essentially only constrained by the laws of physics (modified, though, by point (1) in the definition of QCCC in Section 2.5.2). Thus, we have *not* presumed that the enemy is limited by currently perceived difficulties of practical engineering that may indeed constrain the possibility of actually *carrying out* the attacks that we study in this paper.

Having said that, however, it ought to at least be mentioned in passing that practical engineering issues are in fact *highly* constraining today. The attacks that can realistically be carried out by the enemy are greatly limited as a result. As one example, in the case of the direct attack, it is necessary that the *time* required for the enemy to perform all physical manipulations to intercept the pulse, measure the state of the pulse, prepare a chosen surrogate pulse *and* have the surrogate pulse propagate through whatever distance is required in order to reach Bob, be *no greater than the bit cell period*. If this time constraint is violated then Alice and Bob will be able to detect a corresponding error. Related constraints also apply in the case of the indirect attack (such as a constraint on the time required to place the retained part of the pulse in an appropriate quantum memory). For a high speed quantum cryptosystem characterized by a small bit cell period this basic constraint may be so difficult to satisfy that the associated attack might as well be forbidden by the laws of physics.

3.1.6 Continuous Authentication

As has been stressed several times above, it is important to ensure that the quantum cryptography system remains protected against possible spoofing for the *entire duration* of the transmission. “Spoofing” occurs when the enemy gains access to the public channel, interposes herself between the legitimate transmitter and receiver and attempts to misrepresent her identity in order to gain information, interfere with the system or both. It must be assumed *on each and every use* of the public channel that the enemy will attempt to carry out a spoofing attack, which explains the need for continuous authentication. The detailed derivations of the explicit functional forms of the complete continuous authentication cost functions are provided in Section 4.4.1 below. Here we anticipate those results and list what the cost functions are so that we may incorporate them into the complete expressions for the effective secrecy capacity and effective secrecy rate of QKD systems. Although the need for *initial* authentication of the public channel in quantum key distribution has been mentioned by many authors, previous analyses have not included explicit derivations of the exact functions that describe the full and precise cost in bits of *continuous* authentication.

The complete analytical expression for the cost function for continuous authentication obtained in Section 4.4.1 is found to be given by

$$a = \tilde{g}_{EC} + \sum_{j=1}^5 w_j(g_j, c_j(\mu)) , \quad (152)$$

where we define the important *Wegman-Carter function*, $w(g, c_i)$, as⁵²

$$w(g_i, c_i) = 4 \left[g_i + \log_2(\log_2 c_i) \right] \log_2 c_i . \quad (153)$$

The authentication cost function a is the sum of six terms: two of the terms in the sum represent the authentication cost associated with the sifting process, and the remaining four terms are the cost associated with the error correction process.

In Sections 4.4.1 and 4.4.2 we explicitly derive the complete distinct costs, in bits, of the various communications exchanges required to support the continuous authentication of the public channel. We list there that

$$c_1 = 2n(1 + \log_2 m) , \quad (154)$$

$$c_2 = 2n , \quad (155)$$

$$c_3 = n , \quad (156)$$

⁵² The full and complete expression for the quantity that we denote by w and refer to as the Wegman-Carter function, which is of crucial importance in practical quantum cryptography, does not appear to have been properly analyzed previously in the context of QC (nor apparently even *named* by any authors). Surprisingly, the closed-form function, as such, doesn’t appear as a numbered equation in [36]. In fact, it must be obtained instead by combining quantities that appear in lines 3 and 17 in the first paragraph of section 3 in [36].

$$c_4 = g_{EC} \quad (157)$$

and

$$c_5 = \tilde{g}_{EC} , \quad (158)$$

and all of the security parameter constants g_i that appear in the summand in eq.(152), which includes the quantities g_{EC} and \tilde{g}_{EC} , are (as explained in Section 4.4.1) taken to be equal to 30.

These quantities characterize the amount of communications required to effect continuous authentication for the sifting and error correction phases of the QC protocol. We note that no communication, and hence no authentication at all, is required to execute the privacy amplification phase of the protocol. This may at first appear surprising and appears not to have been discussed in detail before in the literature.⁵³ The bit values that must be identically shared between Alice and Bob in explicitly carrying out privacy amplification consist of a random set to be used to compute the privacy amplification hash function. This set can be obtained without any communication at all between Alice and Bob, and as indicated above, since there is nothing to be communicated via the public channel, there is obviously no need to authenticate that channel for this purpose. The trick is for Alice and Bob to exploit the *untapped randomness* resident in the processes used to execute the protocol. During the public sifting discussion Alice and Bob keep a record not only of the identities of the compatible bases, but should as well keep a record of the index position within the overall bit cell stream of those compatible basis events. They will be able to generate, in real time, two random strings of bits, each of length $m/2$ (modulated by the system losses), by first simply recording the index positions, respectively, of the compatible and incompatible basis events. Then Alice and Bob may compute the *parities* of these two strings to obtain two completely random bit strings of length $m/2$ each. Either of these two strings (this choice can be made by public agreement between Alice and Bob) can be used to compute the privacy amplification hash function, and *no* information will have been communicated between Alice and Bob for this purpose. Although Eve can *also* perform this exercise, since the particular random sequence generated in this way for use in the privacy amplification hash function doesn't *exist* prior to the sifting discussion, it is of no use at all to Eve in deducing any information about the shared key whatsoever.

As discussed in the next section, we will need to solve an extremization equation in order to deduce the optimal values for both the effective secrecy capacity \mathcal{S} and the effective secrecy rate \mathcal{R} . To solve the optimization equation we need an explicit expression for $2a_{,\mu}/m$, which we find is given by

$$\frac{-2a_{,\mu}}{m} = \frac{-8\psi_{\geq 1,\mu}}{\psi_{\geq 1} + r_d} \cdot \frac{1}{m} \cdot \left\{ 3(g+1) + \log_2 \left[(\log_2 c_1) (\log_2 c_2) (\log_2 c_3) \right] \right\}, \quad (159)$$

where the c_i are the costs listed above, in classical bits, of the various communication links

⁵³ We thank J. Guttman for emphasizing the fact that there need be no communication between Alice and Bob to carry out privacy amplification.

required for continuous authentication. In the next section we will also consider the effective secrecy capacity in the limit of an infinitely long cipher, for which purpose we will need to use the fact that

$$\lim_{m \rightarrow \infty} \frac{a}{m} = 0 , \quad (160)$$

which is straightforward to verify using the expression for a given in eq.(152) above.

3.1.7 The Complete Expressions for the Effective Secrecy Capacity and Rate

We are now in a position to put together the results we have obtained on the numbers of sifted bits, error bits, privacy amplification subtraction bits and continuous authentication bits to obtain the complete expressions for the effective secrecy capacity, \mathcal{S} , and the effective secrecy rate, \mathcal{R} , of general, practical QKD systems implementations. For this purpose we first introduce the useful function, f , which we define as

$$f \equiv 1 + Q + T \quad (161)$$

in the case of a QC system implementation in which Alice and Bob identify and *discard* error bits in the sifted string.⁵⁴ The purpose of the function f is as follows. Of the total amount of information that must be removed from the sifted string in order to achieve a secret shared key, the function f groups together and measures just that portion that is natural to measure directly in units of error bits. (This leaves in distinct terms those portions of the information that is to be removed that are due to multi-photon pulses, continuous authentication and the privacy amplification security parameter.) For instance, in the case of f as defined in eq.(161), appropriate to the error correction procedure in which error bits are discarded, the first term of unity indicates that the entire fiducial set of error bits are indeed subtracted, and the second and third terms of Q and T represent the subtractions for error correction information leakage and single-photon pulse measurements, respectively.

We now collect the results of the above sections for the number of sifted bits, the number of error bits, the total amount of privacy amplification and the cost of continuous authentication and substitute them into eq.(1) to deduce the form of the complete, effective secrecy capacity as

$$\begin{aligned} \mathcal{S} &\equiv \frac{n - e_T - s - g_{pa} - a}{m} \\ &= \frac{n - fe_T - \nu - g_{pa} - a}{m} \\ &= \frac{1}{2} \left[\psi_{\geq 1} + r_d - f \left(r_c \psi_{\geq 1} + \frac{r_d}{2} \right) - \tilde{\nu} \right] - \frac{g_{pa} + a}{m} \end{aligned}$$

⁵⁴ In the case of a QC system implementation in which Alice and Bob identify, correct and *retain* error bits in the sifted string, we would instead have $f \equiv Q + T$. As stated in Section 3.1.1 above, unless explicitly otherwise mentioned, in this paper we will adopt the “error discard” approach, with the consequence that the various rate predictions based on it will furnish universal *lower bounds* on achievable throughput rates.

$$= \frac{1}{2} \left[\psi_{\geq 1} (1 - fr_c) + \left(1 - \frac{f}{2}\right) r_d - \tilde{\nu} \right] - \frac{g_{pa} + a}{m} , \quad (162)$$

where we have defined

$$\tilde{\nu} \equiv 2\nu/m \quad (163)$$

so that the rescaled quantity $\tilde{\nu}$ is independent of the number of raw bits, m . In the above expression for \mathcal{S} the argument of the first term in the square brackets, *i.e.* the argument of the function $\psi_{\geq 1}$, is equal to $\eta\mu\alpha$ as derived and discussed in Section 3.1.1 above.

The m -dependence in \mathcal{S} is important, as it allows us to study the dynamics of actual ciphers of finite length in addition to studying properties of abstract ciphers of infinite length. Note that in addition to the manifest m -dependence that appears in the term $\frac{g_{pa} + a}{m}$, there is also m -dependence contained within the function f through *its* dependence on T (*cf* eqs.(49) and (50)), but not on Q (*cf* eq.(39)).

Making use of eq.(160) from Section 3.1.6, we see that the expression for the effective secrecy capacity in the limit of a cipher of infinite length becomes

$$\begin{aligned} \lim_{m \rightarrow \infty} \mathcal{S} &= \frac{1}{2} \lim_{m \rightarrow \infty} \left[\psi_{\geq 1} (1 - fr_c) + \left(1 - \frac{f}{2}\right) r_d - \tilde{\nu} \right] - \lim_{m \rightarrow \infty} \frac{g_{pa}}{m} - \lim_{m \rightarrow \infty} \frac{a}{m} \\ &= \frac{1}{2} \left[\psi_{\geq 1} (1 - f_{\infty} r_c) + \left(1 - \frac{f_{\infty}}{2}\right) r_d - \tilde{\nu} \right] \\ &\equiv \mathcal{S}_{\infty} , \end{aligned} \quad (164)$$

where

$$f_{\infty} \equiv 1 + Q + T_{\infty} \quad (165)$$

and T_{∞} is given in eq.(54).

The effective secrecy rate is given by

$$\mathcal{R} = \mathcal{S}/\tau , \quad (166)$$

where τ is the bit cell period of the QKD system implementation.

We stress that the various quantities $\psi_{\geq 1}$, f , $\tilde{\nu}$ and a appearing in \mathcal{S} depend in a complicated way on a large number of parameters. Rather than writing this out in full, we display the complete parametric dependence of the effective secrecy capacity and rate with the following equations of state:

$$\mathcal{S} = \mathcal{S}(\eta, \mu, \alpha, r_c, r_d, m, \vec{g}, \epsilon, \vec{\rho}, \vec{j}, x) , \quad (167)$$

and

$$\mathcal{R} = \mathcal{R}(\eta, \mu, \alpha, r_c, r_d, m, \vec{g}, \epsilon, \vec{\rho}, \vec{j}, x, \tau) . \quad (168)$$

The mean photon number per pulse, μ , is the one system parameter that can by assumption always be directly controlled and adjusted by Alice. This is accomplished by adding or removing neutral density filters, as appropriate, to achieve the desired value of emitted intensity. This desired value should optimize the effective secrecy capacity and rate of the system. The optimization equation for determining the optimal value, μ_{opt} , of the mean number of photons per pulse is given by

$$0 = \mathcal{S}_{,\mu} \Big|_{\mu=\mu_{\text{opt}}} , \quad (169)$$

which is explicitly written as

$$0 = \psi_{\geq 1,\mu} (1 - fr_c) - \psi_{\geq 1} f_{,\mu} r_c - \frac{f_{,\mu}}{2} r_d - \tilde{\nu}_{,\mu} - \frac{2a_{,\mu}}{m} \Big|_{\mu=\mu_{\text{opt}}} . \quad (170)$$

The resulting optimal value μ_{opt} satisfies the equation of state

$$\mu_{\text{opt}} = \mu_{\text{opt}} (\eta, \alpha, r_c, r_d, m, \vec{g}, \epsilon, \vec{\rho}, \vec{j}, x) . \quad (171)$$

The optimal value of the effective secrecy capacity, \mathcal{S}_{opt} , is obtained by evaluating \mathcal{S} at μ_{opt} , so that we have

$$\mathcal{S}_{\text{opt}} = \mathcal{S} (\mu_{\text{opt}}) , \quad (172)$$

and the corresponding expression for the optimal effective secrecy rate is given by

$$\mathcal{R}_{\text{opt}} = \mathcal{S}_{\text{opt}} / \tau . \quad (173)$$

The optimal effective secrecy capacity and rate, \mathcal{S}_{opt} and \mathcal{R}_{opt} , are the quantities that should be used in practice to make predictions about and study the performance characteristics of any particular quantum cryptography system.

When the *complete* explicit expressions for the functions $\psi_{\geq 1}$, $\psi_{\geq 1,\mu}$, f , $f_{,\mu}$, $\tilde{\nu}_{,\mu}$ and $a_{,\mu}$ are written out in full and substituted into the optimization equation (eq.(170)), it becomes apparent that numerical methods must be used to obtain an answer for the optimal value of μ . The *general* problem of practical quantum cryptography exhibits such a complicated dependence on the many parameters that are required to provide a complete system characterization that a full mathematical description evidently does not admit closed form analytical solutions for μ_{opt} , except in special limiting cases.

Effective Secrecy Capacity and Rate with Click Statistics Monitoring

In the general case for which Bob monitors the click statistics and discards those bit cells that manifestly contain multiple photon pulses, the expression for the effective secrecy capacity becomes

$$\mathcal{S}_{mcs} \equiv \frac{n - e_T - s - g_{pa} - a}{m} \Big|_{mcs}$$

$$\begin{aligned}
&= \frac{n - fe_T - \nu - g_{pa} - a}{m} \Big|_{mcs} \\
&= \frac{1}{2} \left[\left(\eta \psi_1 + \langle \hat{\chi} \hat{\mathcal{Z}}_{\geq 2} \rangle \right) (1 - f_{mcs} r_c) + \left(1 - \frac{f_{mcs}}{2} \right) r_d - \tilde{\nu}_{mcs} \right] - \frac{g_{pa} + a_{mcs}}{m} .
\end{aligned} \tag{174}$$

In the above expression for \mathcal{S}_{mcs} , the argument of ψ_1 is equal to $\mu\alpha$. The functions f_{mcs} and a_{mcs} are defined in terms of the quantities n_{mcs} and $e_{T,mcs}$ in place of the corresponding quantities n and e_T . For example, f_{mcs} is given explicitly by

$$\begin{aligned}
f_{mcs} &\equiv (1 + Q + T) \Big|_{mcs} \\
&= 1 + Q \left(x, \frac{e_{T,mcs}}{n_{mcs}} \right) + T(n_{mcs}, e_{T,mcs}, \epsilon) ,
\end{aligned} \tag{175}$$

and a_{mcs} is given by

$$a_{mcs} = \tilde{g}_{EC} + \sum_{j=1}^5 w_j(g_j, c_j(\mu)) \Big|_{n=n_{mcs}} . \tag{176}$$

The quantity $\tilde{\nu}_{mcs} \equiv 2\nu_{mcs}/m$ is formed from the appropriate expressions for $\nu_{d,l,mcs}$ and $\nu_{i,l,mcs}^{(u)}$, respectively, given in eqs.(77) and (105).

Effective Secrecy and Capacity and Rate in Special Limits

It is worthwhile to examine this result in the special case that there is no eavesdropping activity but for which there *is* attenuation in the quantum channel and loss at Bob's detector, in which circumstance we may define the associated secrecy capacity, $\mathcal{S}_{\text{no enemy}}$. If there is no eavesdropping activity we have $Q = T = 0$ (since no information is lost in particular due to eavesdropping on either error correction or single-photon pulses), so that we also have $f = 1$. We may set $\tilde{\nu} = 0$, since none of the multi-photon pulses are at risk in this scenario. In the absence of an eavesdropper it should also not be necessary to undertake any authentication, so that we can impose the condition $a = 0$. Moreover, in this case we can safely set the privacy amplification security parameter, g_{pa} , equal to zero, so that we finally have

$$\mathcal{S}_{\text{no enemy}} = \frac{1}{2} \left[\psi_{\geq 1} (1 - r_c) + \frac{1}{2} r_d \right] \tag{177}$$

Inspection of the above expression reveals the basic physical effects that are responsible for the effective bit rate: the factor $(1 - r_c)$ gives the proportion of the bit cells that will reach Bob without being subjected to depolarization or other intrinsic channel errors, the factor $\psi_{\geq 1}$ gives the probability that a particular laser pulse will contain at least one photon, and in the argument of $\psi_{\geq 1}$ the factor α gives the proportion of qubit photons that will reach Bob in spite of attenuation due to atmospheric losses, the factor η gives the fraction of photons that will actually be detected at Bob's receiving instrument in spite of the intrinsic inefficiency of his apparatus, the overall factor of $1/2$ gives the fraction of photons lost as a result of the statistically independent, random choices of polarization basis made between Alice and

Bob, and finally the term $\frac{1}{2}r_d$ gives the contribution to the effective secrecy capacity due to the presence of dark count activity.

Finite Length versus Infinite Length Ciphers

It is crucially important to obtain, as we have done, closed form, analytical expressions for the effective secrecy capacity and rate that are valid for actual ciphers of finite length, as opposed to expressions that are only valid in the abstract limit of infinitely long ciphers. Why is this? One of our principal objectives in this study is to determine how and under what conditions we may achieve high data throughput rates for practical quantum cryptography systems. As we shall discuss in detail in Section 5.2.6, one of the techniques that may be used to achieve this objective is to assemble a collection of transmitters and multiplex their outputs together in a common transmission stream. However, the totality of computing resources (measured by the number of basic computer machine instructions) required to *actually carry out* the QKD protocol furnishes an important practical constraint on any quantum cryptography system. As this has never been analyzed before, we work out the details in full in this paper in Section 4.4.3 below. We find for the first time a closed form expression (eq.(286) below) relating the computing resources required for carrying out the protocol to the processing block size taken from the transmitted bit stream. With the help of this functional relationship, and also making use of the optimal effective secrecy capacity to numerically determine the dependence of the throughput rate on any reduction or increase in the number of transmitted raw bits assigned to each processing block, it is possible to deduce the rate of any proposed multiplexing scheme while satisfying the important constraint that there are sufficient computing resources to achieve it. *This is not possible to do without closed form expressions for the secrecy capacity and rate that are valid for ciphers of finite length.* With such functions at our disposal, however, we will determine in Section 5.3 below what are the highest possible rates than can actually be achieved for practical quantum cryptography.

3.2 An Extended Family of Four-State Quantum Key Distribution Protocols

We saw in the discussion in Section 3.1.1 above that there are a number of choices of schemes that may be adopted by Bob and Alice (and fully disclosed to Eve) to effect the monitoring of click statistics. As described there, to fully define any such scheme it is necessary to both select a particular model that specifies the details of the detector apparatus *and* to select a particular click-monitoring scheme to be used in that model. For each such choice one obtains different numerical values for the higher-order terms⁵⁵ in the explicit expressions for the number of sifted bits, the number of transmitted error bits, the cost of continuous authentication and the various privacy amplification subtraction functions. Each of these

⁵⁵ These are terms (cf eq.(26)) such as $\left\langle \hat{\chi}(\mu, l) \hat{\mathcal{Z}}_{\geq 2}(\eta, \alpha, l) \right\rangle \equiv \sum_{l=0}^{\infty} \hat{\chi}(\mu, l) \hat{\mathcal{Z}}_{\geq 2}(\eta, \alpha, l)$.

choices will generate different specific numerical results for overall system performance, in particular affecting the total integrated cipher throughput rates that can be achieved. Each of these may be thought of as an element in an extended family of BB84-like protocols. In fact, there are a denumerable infinity of different versions of these click monitoring-based schemes, distinguished from each other according to how Bob chooses to distribute any click monitoring he carries out amongst the bit cells. He can choose to monitor click statistics for the entire transmission, for certain fractions of the transmission, for certain fractions of the transmission for different amounts of time *etc.* Although these different variations will in the general case of the strongest possible attack by Eve be suboptimal from the perspective of Alice and Bob compared to simply carrying out the maximum amount of click monitoring, *i.e.*, executing the monitoring all of the time, for the entire transmission, and discarding *all* multiple-click event bit cells, there are situations for which it is preferable for Alice and Bob to choose one of the other options. If Alice and Bob happen to have, through whatever means, access to privileged information regarding the set of attacks that the enemy can or will carry out, it is possible to tailor an appropriate click monitoring scheme specifically against that set of attacks - such a specially “tailored” click statistics monitoring scheme may result in a greater overall throughput of secret bits. A full analysis and discussion of this sensitive topic is beyond the scope of the present paper, and will be treated elsewhere.

3.3 Secrecy in the Presence of Weak Coherent Pulses

The four-state quantum cryptography protocol (the BB84 protocol) in the ideal situation – *i.e.*, in the absence of any system noise and with a source of perfect quantum bits – is unconditionally secret in the presence of any cryptanalytic attacks by Eve. Our purpose here, though, is in considering the case of a *realistic* system for quantum cryptography. Any actual implementation of the BB84 protocol obviously requires the use of actual physical hardware: we know that in *any* actual implementation the real system will be such that the intended communication will be characterized by both transmission losses and errors. It is the inevitable presence of the errors, in particular, that absolutely forces us to effectively redefine the “pure” BB84 protocol (*i.e.*, generation of the sifted key only) to include sufficient error correction and privacy amplification in order to assure that Alice and Bob share a secret Vernam cipher at the end of the communication. The privacy amplification functions calculated in great detail in the previous section serve the purpose of ensuring that any information possibly obtained by Eve through whatever means is removed from the final string shared between Alice and Bob. Of course, if Alice and Bob somehow knew with certainty that Eve did not exist, or that if she did exist was not present, or if present would not eavesdrop now or in the future, it would not be necessary to implement privacy amplification, although it would still be necessary to carry out error correction, due to the presence of system errors. However, in this unrealistic case – the absence of present or future adversaries – it would not be necessary to make use of *any* cryptography, quantum or classical, in the first place. In *real* circumstances we must assume that Eve might be present, either actively attempting to decode our communications, or attempting to intercept, record

and store them for possible future cryptanalysis. In this case, which describes the real world of communications in the presence of adversaries, we *must* implement privacy amplification. In other words, as a *practical* protocol for secret key distribution the “pure” BB84 protocol is not complete: in any actual application the noise inherent to the system hardware dictates that the protocol actually used must be BB84 supplemented by sufficient error correction and privacy amplification. In several extant implementations quantum key distribution has been implemented by generating the signal states with an intensity–filtered pulsed laser. As discussed in great detail in the previous section, the output of the laser in this case is in the form of weak coherent pulses of laser light: some of the pulses contain no more than a single photon, and some of the pulses contain two or more than two photons. The need to carry out privacy amplification, however, applies equally for the formal BB84 protocol implemented solely with proper quantum bits, which would consist solely of single photon states, *or* the weak coherent pulse implementation, which would include both single and multiple photon states. Even if there are no multi-photon pulses *at all* amongst the signals sent from Alice to Bob, the fact that the physical hardware generates errors, combined with the fact that Eve may be present, requires privacy amplification. This means that, even if the pure BB84 protocol involving solely proper single-particle qubits is implemented on a real system, the effect of the required execution of privacy amplification dictates that the probability P that Eve will be able to know more than one bit of the final shared key sequence is given by $P \leq \frac{2^{-g_{pa}}}{\ln 2}$, where g_{pa} is the privacy amplification security parameter (the length in bits of the tag for the hash function utilized in effecting the privacy amplification). *Precisely the same degree of secrecy* is realized if the BB84 protocol is implemented with pulsed lasers generating weak coherent pulses that include amongst them multi-photon states, as long as sufficient additional privacy amplification is performed to account for the maximum amount of Renyi information that may have possibly been obtained by Eve as a result of any physically allowed attacks on such states.

4 Comprehensive Analysis of System Losses and Loads

In order to apply the expressions for the effective secrecy capacity and rate that we have derived to a realistic system it is essential to supply accurate values for the various parameters that characterize the losses and loads which result in a reduction of the throughput of secret key material. This must of course include the various quantities that specify the actual losses suffered by the signal as it propagates from Alice to Bob, but it is also important to include in the analysis those *ancillary* costs associated to the supporting classical communication required to actually carry out the QKD protocol. In addition, it is crucial to estimate and include in the analysis the amount of computing power that is required to carry out the various operations including error correction, computation of authentication and privacy amplification hash functions, real-time data record keeping, *etc.*, that must go on “behind the scenes” in order for a practical system to actually work. Such costs can only be determined for actual ciphers of finite length, as abstract limits for infinitely long ciphers are inapplicable to the practical situation. It is only after complete account is taken of *all* these effects that one can accurately estimate the actual throughput rates and other operating characteristics that describe a real QKD system.

Some Practical System Considerations

In Section 5 of this paper we consider in detail the practical requirements for achieving QKD at a high throughput rate. Looking ahead to that development, in the various sections below of this chapter we will illustrate the general analytical results that we obtain for system losses by making use of certain system parameter values to calculate sample numerical results. In these illustrations we will typically consider a system in which Alice uses a laser that produces light at a wavelength of 1550 nanometers (consistent with many modern telecommunications and laser communications systems). Moreover for the case in which a free space quantum channel is utilized, such as for QKD between a satellite and a ground station, we in general assume a QKD configuration in which *Alice is elevated and Bob is on the ground* (or possibly in an aircraft). As we will see, a consequence of the various system losses for a QKD system operating through the atmosphere is that it is advantageous in optimizing the throughput rate to *increase* the size of Bob’s receiving instrument aperture compared to Alice’s, and it is easier and less expensive to do that by placing the Bob system on the ground (or in an airplane) and the Alice system on the satellite. In these cases we will principally consider numerical examples for two different satellite altitudes: a low earth orbit (LEO) satellite located at 300 kilometers altitude, and a geosynchronous (GEO) satellite located at 35783 kilometers (22236 miles) altitude.

We now turn to an analysis of all of the above issues.

4.1 System Losses: The Line Attenuation - Free Space

The line attenuation, α , is *defined* to include the loss suffered by the signal due to four distinct causes: (1) the diffraction loss, *i.e.*, the geometrical vacuum beam spreading loss, (2) the static atmospheric losses, due to atmospheric scattering and absorption, (3) the turbulent atmospheric losses, due to several causes as enumerated in Section 4.1.3 below, and (4) the “optics package” losses due to the imperfect nature of the various components present in the system. Note that the line attenuation α is *not* the “total” attenuation suffered by the qubit signal. Specifically not included in the definition of the line attenuation are: the loss, η , associated with photon detector efficiency, the intrinsic quantum channel loss, r_c , the basic, 50% sifting loss due to the definition of the BB84 protocol, the dark count loss, r_d , associated to the photon detector, and the loss associated with the use of weak laser pulses, described by the probabilistic distributions $\psi_l(\mu)$, $\psi_{\geq 1}$, *etc.*, in the effective secrecy capacity \mathcal{S} .⁵⁶

4.1.1 Diffraction Vacuum Beam Spreading Losses

The use of finite optics dictates that the beam generated at Alice and transmitted to Bob will become a spread beam due to diffraction. The radius, ρ_d , of the purely diffraction-limited spot size of the beam incident upon a flat receiving plane at the location of Bob’s apparatus is found from a straightforward calculation to be given by

$$\rho_d = \left[\frac{4L^2}{(kD_A)^2} + \left(\frac{D_A}{2} \right)^2 \right]^{1/2}, \quad (178)$$

where L is the path length over which the signal propagates, D_A is the diameter of the aperture of Alice’s transmitting instrument and k is the wavenumber of the photons in the beam. The calculation of loss associated with this spreading of the beam will be deferred to allow for the inclusion of the additional beam spreading loss caused by atmospheric turbulence as deduced in Section 4.1.3 below.

4.1.2 Static Atmospheric Losses

Even in the absence of any turbulent motions at all, the atmosphere will induce a variety of scatterings and absorptions of the pulses in the beam, leading to a reduction in the received signal intensity at Bob. We have made use of the FASCODE (“Fast Atmospheric Signature Code”) [37, 38, 39] computer code developed by the U.S. Air Force Research Laboratory to numerically compute typical examples of such losses in a wide variety of operating environmental conditions. In our analysis many computations were carried out for

⁵⁶ Our line attenuation, α , is defined to be equal (in linear units) to unity when there is no signal loss, and equal to zero when there is complete loss of signal. This is often referred to as the transmittance.

a wide range of boundary conditions. As a representative example some of our computations were done with the following assumptions input to the code: (1) 1550 nanometer wavelength light, using the high-resolution version of FASCODE, (2) 45 degrees slant angle (the slant angle is defined to be equal to 90 degrees at zenith), (3) inputted geographic coordinates for Hanscom Air Force Base, Massachusetts, (4) minor sunspot activity, (5) azimuth angle equal to 0 degrees (*i.e.*, looking northward), (6) clear conditions (this defined as yielding 23 kilometers visibility),⁵⁷ (7) no significant recent weather or volcanic activity, (8) date and time for computer run: 21 March, 2000, noon.

We will denote the losses defined by the output of FASCODE runs by

$$\mathcal{L}_{\text{static atmospheric}} = 10 \cdot \log_{10} (\text{normalized FASCODE signal output}) , \quad (179)$$

and incorporate this in Section 4.1.5 below in a complete account of the total free space line attenuation.

A summary of the physical meaning of these numerical computations follows:

- The typical attenuation obtained for a path length of 300 kilometers, representing the distance from mean sea level (MSL) to a low-earth-orbit (LEO) satellite, in the direction of propagation from satellite to ground against clear weather conditions for 1550 nanometer laser light indicates a static atmospheric attenuation of order -1 dB.⁵⁸
- The static atmospheric attenuation effectively disappears when the two ends of the link are located at elevations of 10 kilometers and 300 kilometers, respectively.
- Rain, and even light drizzle, will severely attenuate the beam to the extent that in many cases useful signal cannot be transmitted at all.

The results of typical FASCODE computer runs are illustrated in Figure 11 with a set of numerical curves that depict characteristic static atmospheric losses. For the computations in this example we have assumed that clear weather conditions obtain, defined as above to yield 23 kilometers visibility. In this graph we display curves of the atmospheric transmission as a function of the declination angle with respect to zenith, with 0 degrees corresponding to the zenith position. Inspection of the curves reveals the expected functional dependence, with the static atmospheric transmission loss increasing as the declination angle increases from 0 degrees to 50 degrees.

(The computer analysis was specifically carried out using the Air Force Research Laboratory's PLEXUS system [40], which provides an interface to FASCODE.)

⁵⁷ This is only representative, as FASCODE computations were carried out for a variety of less favorable weather conditions, as reflected in the analysis presented in Section 5.3.2 of this paper.

⁵⁸ In this paper we adopt the convention of denoting attenuation values (when measured in decibels) as negative quantities.

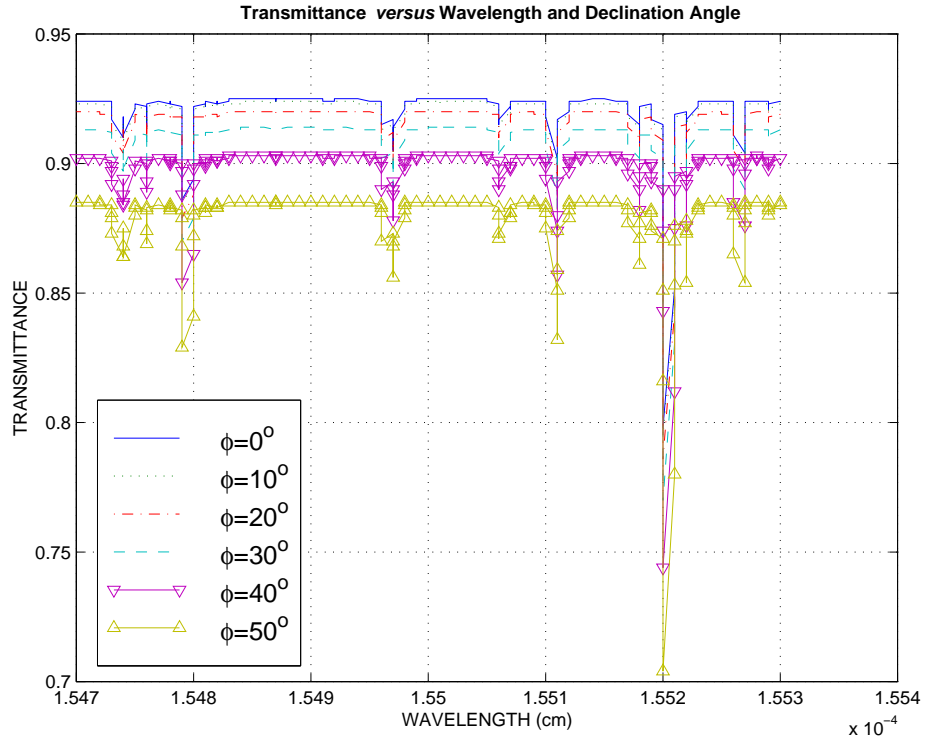


Figure 11: Sample FASCODE Results for Static Atmospheric Attenuation

4.1.3 Turbulent Atmospheric Losses

Atmospheric turbulence will potentially induce a variety of signal losses in the propagating beam. These are: (1) turbulence-induced beam spreading (this is beam spreading *in addition to* that beam spreading due to purely geometrical diffraction effects), (2) turbulence-induced beam wander, (3) turbulence-induced coherence loss, (4) turbulence-induced scintillation, and (5) turbulence-induced pulse distortion and/or broadening. (Another well-known type of turbulence-related loss, *thermal blooming*, is not relevant here as the filled bit cells in the beam comprise principally a sequence of single photons which can only heat the atmosphere to a negligible degree.)

In analyzing turbulence-induced losses, it is necessary to adopt a particular model for the refractive index structure function C_n^2 in order to characterize the turbulent motions in the atmosphere. In our analysis we have made use of two standard models of atmospheric turbulence, the Hufnagel-Valley 5/7 model [41, 42, 43] and the CLEAR I model [44, 45, 46]. The dependence on altitude of C_n^2 in the former model is illustrated in Figure 12.

We now consider in turn each of the five types of turbulence-associated losses enumerated above.

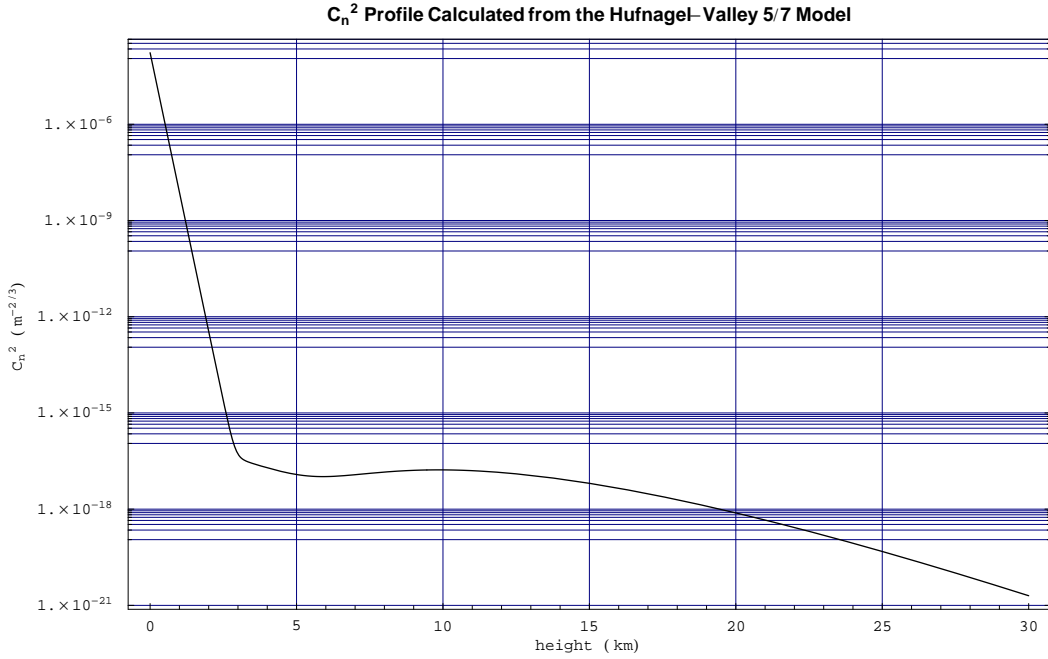


Figure 12: The Hufnagel-Valley 5/7 Model for Atmospheric Turbulence

Turbulence-Induced Beam Spreading

From standard results in turbulence theory [47, 48] the transverse coherence length is given by

$$\rho_0 = \left[1.46k^2 \sec \varphi \int_0^L d\eta C_n^2(\eta) \left(1 - \frac{\eta}{L}\right)^{5/3} \right]^{-3/5}, \quad (180)$$

where k is the wavenumber, L is the path length over which the signal propagates, φ is the declination angle with respect to the zenith direction and C_n^2 is the refractive index structure function. The (mean squared value of the) “short-time beam spread radius” due to *both* turbulence and vacuum geometrical effects is given by

$$\langle \rho_s^2 \rangle = \rho_d^2 + \frac{4L^2}{(k\rho_0)^2} \left[1 - 0.62 \left(\frac{\rho_0}{D_A} \right)^{1/3} \right]^{6/5}, \quad (181)$$

where D_A is the diameter of the aperture of Alice’s transmitting instrument and

$$\rho_d = \left[\frac{4L^2}{(kD_A)^2} + \left(\frac{D_A}{2} \right)^2 \right]^{1/2} \quad (182)$$

is the vacuum beam spread radius presented in Section 4.1.1 above.⁵⁹ Then the associated

⁵⁹ The expressions used in eq.(181) for $\langle \rho_s^2 \rangle$ and in eq.(184) below for $\langle \rho_c^2 \rangle$ are valid [47] in the region of the system parameter space characterized by the inequalities $\rho_0 \ll D_A < L_o$ and $L \lesssim kX^2$, where L_o furnishes a measure of the largest distances over which fluctuations in the index of refraction are correlated (typically $L_o \approx 100$ m), X is the smaller of D_A and ρ_0 , and L is the signal path length. In the cases considered here it is straightforward to show numerically that both inequalities are satisfied.

loss, *i.e.* the *total* beam spread loss due to both turbulence and vacuum geometrical effects, is given by

$$\mathcal{L}_{\text{beam spread}} = \mathcal{L}_{\text{beam spread}}(k, \varphi, L, D_A, D_B) = 10 \cdot \log_{10} \left(\frac{D_B^2}{4\langle \rho_s^2 \rangle} \right), \quad (183)$$

where D_B is the diameter of Bob's receiving instrument. The above expression is defined to give a negative value (*i.e.*, indicate a loss) when the area of Bob's receiving instrument is less than the effective area of the turbulence- and diffraction-limited spot of the fully spread laser beam. (In this approach it is assumed that there is uniform illumination across the turbulence- and diffraction-limited received spot. This is acceptable because a different situation in which, say, there is a Gaussian pattern, will generate *less* loss, so that we are at worst *overestimating* the loss in this case.)

As a particular example, we assume that the diameter of the aperture of Alice's transmitting instrument is $D_A = 30$ cm for laser light at 1550 nanometers wavelength. The largest amount of diffraction- and turbulence-induced beam spread loss will be realized in systems with receiving apertures that are too small. We consider two cases: (1) Alice is on a LEO satellite orbiting at 300 kilometers altitude above Bob who is at mean sea level. If the diameter of Bob's receiving instrument is $D_B = 30$ cm, the total beam spread loss is -17.3237 dB with Alice located at zenith above Bob, and increases to -19.0205 dB with Alice at a slant angle of 45 degrees. If the diameter of Bob's receiving instrument is increased to $D_B = 1$ m, these losses are reduced to -6.86612 dB and -8.56288 dB, respectively. (2) Alice is on a GEO satellite orbiting at 22236 miles altitude and Bob is assumed to be located either on a mountain at high altitude, or on an aircraft, in either case such that most of the turbulent effects are effectively very small. In this case the signal loss due to beam spreading can be determined from the effects of diffraction: if $D_B = 1$ m and Bob is on a mountain at an altitude of 13500 feet (such as at the Mauna Kea Observatory location) the loss is -41.4144 dB; if Bob is on an airplane at 35000 feet altitude the loss is -41.4128 dB. If $D_B = 10$ m, which is the size of the effective aperture of the Keck Telescope on Mauna Kea, these losses decrease to -21.4144 dB and -21.4128 dB, respectively.

Turbulence-Induced Beam Wander

The presence of atmospheric turbulence will cause the beam to appear to “wander” around a bit on its passage through the space between Alice and Bob. The mean squared value of the radius of this beam wander region is given by turbulence theory [47, 48] as

$$\langle \rho_c^2 \rangle = \frac{2.97L^2}{k^2 \rho_0^{5/3} D_A^{1/3}}. \quad (184)$$

Existing engineered devices that apply active closed-loop feedback control between Alice and Bob are available to generate in excess of 30 dB rejection of turbulence-induced beam wander [49]. These systems employ fast steering mirrors that scan the incoming tracking beam to correct for lower frequency wander (≤ 100 Hz).

The explicit loss in signal associated specifically with turbulence-induced beam wander is given by

$$\mathcal{L}_{\text{beam wander}} = \mathcal{L}_{\text{beam wander}}(k, \varphi, L, D_A, D_B) = 10 \cdot \log_{10} \left(\frac{D_B^2}{4\langle \rho_c^2 \rangle} \right). \quad (185)$$

As a particular example, we again assume that the diameter of the aperture of Alice's transmitting instrument is $D_A = 30$ cm for laser light at 1550 nanometers wavelength. As with the loss due to beam spreading, the largest amount of turbulence-induced beam wander loss will be realized in systems with receiving apertures that are too small. We again consider two cases: (1) Alice is on a LEO satellite orbiting at 300 kilometers altitude. Even if the diameter of Bob's receiving instrument is as small as $D_B = 30$ cm, the same size as for Alice, the beam wander loss is -16.4917 dB with Alice located at zenith above Bob, and increases to -17.9969 dB with Alice at a slant angle of 45 degrees. (2) Alice is on a GEO satellite orbiting at 22236 miles altitude. As long as $D_B \geq 2.11$ meter the beam wander loss is no worse than -30 dB if the slant angle is not taken into account: this is appropriate in the case of the earth-GEO satellite link, as it is assumed that the receiving platform will be located either on an aircraft or a mountain (such as the Mauna Kea Observatory location) in order to minimize atmospheric effects in general.

Thus, we can arrange that the total signal loss associated with turbulence-induced beam wander can be suppressed to a level less than a magnitude of 30 dB in the cases of interest, for which purpose there are engineering solutions available to completely mitigate this loss.

Therefore, it is possible to construct a QKD system in which beam wander loss is effectively eliminated for both LEO and GEO satellite links.

Turbulence-Induced Coherence Loss

In this section we consider two types of coherence loss that will affect the state of the pulse as it arrives at Bob's detector. In principle, these coherence losses could affect the probability that photons arriving at the Bob's apparatus will be detected, thus reducing the rate at which secret bits can be produced. We will show that, if the effective cross section of the detector is sufficiently large, these effects do not reduce the count rate of Bob's apparatus.

The first effect is due to the loss of spatial coherence. Consider first what happens when a classical optical signal impinges on a telescope [50]. If the lateral coherence length of the signal is less than the diameter of the receiving optics, the intensity pattern at the focus becomes spread out over a larger area. This is due to a diffraction effect in which the effective aperture is given by the coherence length of the signal rather than the diameter of the telescope objective. In applying this to the case of a weak pulse containing small numbers of photons, we note that the classical intensity corresponds to the probability of measuring a photon in a given region. As long as the detector is designed to capture any signal that appears in the diffraction disk, it can be expected to collect individual photons that propagate through the same optical device. Provided this condition is met, there is no

loss of photon counts due to loss of spatial coherence in the incoming pulse, and we then have

$$\mathcal{L}_{\text{spatial coherence}} = 0 . \quad (186)$$

The second effect is the decoherence of the quantum mechanical phases associated with the initial coherent state sent by Alice. The initial state is described by a coherent superposition of photon number states:

$$|\phi\rangle = \sum_{k=0}^{\infty} \sqrt{\frac{e^{-\mu} \mu^k}{k!}} e^{ik\phi} |k\rangle , \quad (187)$$

where ϕ is the semi-classical phase of the coherent state. Note that we idealized the pulse as a pure monochromatic state, and that we have suppressed polarization and wavevector indices. The actual physical pulse will be a superposition of such states summed over a region of wavevectors to produce a wave packet that is localized in space and time. This linear superposition is irrelevant to our argument, as we will only be concerned with the relative phases of the terms appearing in the monochromatic coherent state. The density matrix corresponding to this state is

$$\rho^{(coh)} = \sum_{k,l=0}^{\infty} e^{-\mu} \sqrt{\frac{\mu^{k+l}}{k!l!}} e^{i\phi_{kl}} |k\rangle\langle l| , \quad (188)$$

where we define the phase factor

$$\phi_{kl} \equiv (k - l) \phi . \quad (189)$$

Since the phases for the on-diagonal elements are identically zero, this can be rewritten as

$$\begin{aligned} \rho^{(coh)} &= \sum_{k=0}^{\infty} e^{-\mu} \frac{\mu^k}{k!} |k\rangle\langle k| \\ &+ \sum_{k \neq l}^{\infty} e^{-\mu} \sqrt{\frac{\mu^{(k+l)}}{k!l!}} e^{i\phi_{kl}} |k\rangle\langle l| . \end{aligned} \quad (190)$$

The density matrix for the incoherent state is obtained by averaging over the phases ϕ_{kl} . The resulting density matrix is

$$\begin{aligned} \rho^{(incoh)} &= \sum_{k=0}^{\infty} e^{-\mu} \frac{\mu^k}{k!} |k\rangle\langle k| \\ &+ \sum_{k \neq l}^{\infty} e^{-\mu} \sqrt{\frac{\mu^{(k+l)}}{k!l!}} \langle e^{i\phi_{kl}} \rangle |k\rangle\langle l| . \end{aligned} \quad (191)$$

We now use these expressions to find the response of the detector in the coherent and incoherent cases. An idealized detector is a device which produces a count if it measures in state $|k\rangle$ for $k \geq 1$. This measurement corresponds to the projection operator

$$\begin{aligned} \mathcal{M} &= \sum_{k=1}^{\infty} |k\rangle\langle k| \\ &= \mathbf{1} - |0\rangle\langle 0| , \end{aligned} \quad (192)$$

so that the expectation value of the measurement on a mixed state characterized by the density matrix ρ is

$$\begin{aligned}\langle \mathcal{M} \rangle &= \text{Tr}(\rho \mathcal{M}) \\ &= 1 - \rho_{00}.\end{aligned}\quad (193)$$

But from equations (190) and (191), we see that

$$\rho_{00}^{(coh)} = \rho_{00}^{(incoh)}, \quad (194)$$

and

$$\langle \mathcal{M} \rangle_{(coh)} = \langle \mathcal{M} \rangle_{(incoh)}, \quad (195)$$

so that the result of the measurement is independent of whether or not the quantum mechanical phases have lost coherence on their way from Alice to Bob, and we thus have

$$\mathcal{L}_{\text{quantum coherence}} = 0. \quad (196)$$

It is clear from the discussion that this insensitivity to the coherence properties of the received signal is due to two factors. First, the loss of quantum coherence only affects the off-diagonal terms in the density matrix, and, second, the response of the detector is dependent only on the diagonal terms. This property of the detector is due to the fact that it is essentially a photon counting device, which performs measurements that projects the measured states onto a set of states described in terms of the photon number basis. Our conclusions apply to any detector that can be so described, including the imperfect ($\eta < 1$) detectors of a real implementation.

Turbulence-Induced Scintillation

Atmospheric turbulence will cause the received value of the signal intensity I to fluctuate about its average value. This will manifest itself as a distinct scintillation of the laser beam. We will calculate the magnitude of the scintillation in the weak turbulence regime, for which the Rytov approximation holds. (There is little point in QKD applications in considering the regime of stronger turbulence as we would not expect sufficient signal to survive the transit to even a LEO satellite in this case.)

The magnitude of the normalized variance of the signal intensity that is responsible for the intensity scintillations is given by [47, 48]

$$\sigma_I^2 = \frac{\langle (I - \langle I \rangle)^2 \rangle}{\langle I \rangle^2} \simeq 4\sigma_\chi^2, \quad (197)$$

where

$$\sigma_\chi^2 = 0.56k^{7/6} \int_0^L dz C_n^2(z) z^{5/6}, \quad (198)$$

so that we have for the associated loss

$$\mathcal{L}_{\text{scintillation}} = \mathcal{L}_{\text{scintillation}}(k, L) = 10 \cdot \log_{10} \left(1 - \sqrt{\sigma_I^2} \right). \quad (199)$$

The Rytov approximation appropriate for the regime of weak turbulence is specified by the inequality

$$\sigma_I^2 \leq 0.3. \quad (200)$$

As a numerical example, if we assume that Alice transmits laser pulses at a wavelength of 1550 nanometers and we employ the Hufnagel-Valley 5/7 model for the refractive index structure function we obtain $\sigma_x^2 = 0.0158$, corresponding to $\sigma_I^2 \approx 0.06305$, which indicates that we are well within the regime of validity for the Rytov theory. This implies a signal loss due to intensity scintillations of -1.26 dB. Note that, due to the rapid decay with increasing altitude of the Hufnagel-Valley 5/7 model, this result holds almost identically for the cases of Alice located on a LEO satellite *and* on a GEO satellite.

Turbulence-Induced Pulse Distortion and/or Broadening

For pulses of sufficiently short duration the consequences of atmospheric turbulence can include inducing distortion and/or broadening of the shape of the pulses through the generation of dispersion. In order to mitigate this problem we would like to find the conditions that ensure that the spectrum of a short pulse *in* a turbulent medium be equal to that of the same pulse when it was *incident upon* and entered the medium. These conditions have been worked out by Fante and consist of the two inequalities (eq.(106) and eq.(107) in [47]):

$$\frac{0.91\Omega C_n^2 L^2}{cl_o^{1/3}} \ll 1 \quad (201)$$

and

$$\frac{0.39\Omega^2 C_n^2 L_o^{5/3} L}{c^2} \ll 1. \quad (202)$$

Here c is the speed of light, Ω is the bandwidth of the pulse, L is the path length and L_o and l_o are, respectively, the outer and inner scale sizes of typical turbulent eddies: L_o (as mentioned in footnote 59 above) furnishes a measure of the largest distances over which fluctuations in the index of refraction are correlated, and l_o is a measure of the smallest correlation distances.

The above inequalities can be numerically solved and inspection of the plotted results allows one to identify parameter regions where pulse distortion and/or broadening do occur and where they do not. We have plotted in Figure 13 below a numerical solution for the case when the laser pulses are at a frequency of 1550 nanometers, and we have taken typical values [47] of $L_o = 100$ m and $l_o = 0.001$ m, making use of the Hufnagel-Valley 5/7 model for the refractive index structure function. We see that when Alice is orbiting on a LEO satellite at 300 kilometers altitude, in order to avoid incurring any pulse distortion and/or broadening loss, the width of the pulse must be greater than 19.8 picoseconds, corresponding to a laser pulse repetition frequency (PRF) of no greater than about 50 GHz.⁶⁰ This means

⁶⁰ Note that the bit cell period, τ , which is by definition equal to the reciprocal of the PRF of the laser, is in general larger than the width of the pulse. The calculation of a lower bound on the pulse width thus enables us to deduce an upper bound on the value of the PRF.

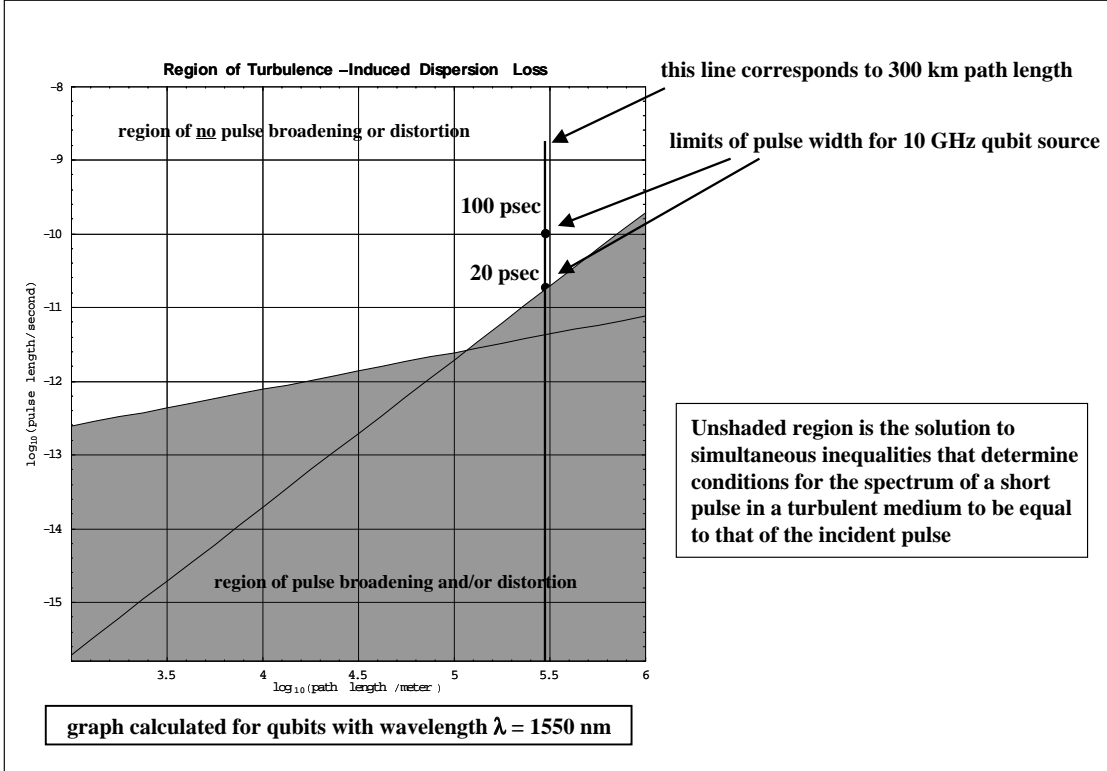


Figure 13: Pulse Distortion and/or Broadening Graph

that, ignoring for the moment all other concerns regarding operating a QKD system at a basic clock rate of 50 GHz (such as photon detection, real-time data recording, *etc.*), it is preferable to utilize lasers with PRFs of less than 50 GHz for an Earth-LEO satellite link, and even slower laser pulse rates for links to higher altitude satellites. When these conditions are met we have for the associated loss

$$\mathcal{L}_{\text{pulse distortion/broadening}} = 0. \quad (203)$$

These are not necessarily rigid constraints on system design, however. In the case of an Earth-LEO satellite link, for example, the use of a laser with a larger PRF than 50 GHz *might* be acceptable: the effect of the addition to the line attenuation, and the corresponding decrease in system throughput caused by the resulting noise would need to be balanced against the increase in throughput caused by the shorter bit cell period. Such an analysis would be a fruitful area for future numerical research.

In Section 5 below we will discuss the design of a practical high speed QKD system in

which a laser with a PRF of 10 GHz is employed, corresponding to a bit cell period of 100 picoseconds. In Figure 13 we have indicated the two limits on the pulse width provided by the 100 picosecond and 19.8 picosecond points, respectively.

4.1.4 Optics Package Losses

The optics package losses can be estimated by comparing a proposed system design for the Alice and Bob apparatuses with demonstrated optical communications systems of comparable complexity. This complexity is assessed in terms of approximately equal numbers of system components of corresponding quality and characteristics appropriate for a QKD system setup. In Figure 14 below we compare the demonstrated losses for a variety of laser communications terminals as reported in the literature.⁶¹

Based on this analysis of extant systems of comparable complexity, it is reasonable to take a value of -5 dB for the expected optics package loss associated to the QC system proposed in Section 5 below. We will employ this value of loss for the optics package in computing the total line attenuation for a free space implementation.

“Behind-the-Telescope Loss”

We briefly mention here the loss that may arise between the “back” of Bob’s telescope and front of his detector apparatus, deferring to Section 5.2.1 below a more detailed discussion. We have already calculated and discussed the beam spreading loss associated to the passage of the laser beam from Alice to Bob. The consequence of this effect is that the laser “spot” that is incident upon the front of Bob’s telescope is larger than we would like it to be - this is a problem of received beam size. There is *another* beam size problem that can develop behind Bob’s telescope, if the received beam incident upon the surface of Bob’s photon detection apparatus is too large. We propose in Section 5.2.1 below a method of mitigating such loss for the novel type of fast photon detector that is a central and unique feature of the high-speed QKD system we describe. It is important, in general, to take careful account of this source of loss, as it can be a very important contribution to the overall optics package loss unless successfully mitigated.

4.1.5 Complete Line Attenuation Losses - Free Space

We collect here the results of the above sections to display the total line attenuation-associated losses on the strength of the signal in the case of free-space propagation. This analysis allows us to understand the operating characteristics of an actual quantum cryptography implementation set up as a free space communications system. The various losses that contribute to the complete free space line attenuation α can be assembled into a single

⁶¹ We thank C.P. McClay for assembling this information.

References for Receiver Optics Losses

System	Atmospheric Attenuation (dB)	Optics Package Loss (dB)	MISSION	Wavelength (nm)	Reference	Notes
JPL-OCD		-1.9	lab demo	840	SPIE vol. 3266 pp. 33-41	measured
AF Airborne ACT	-4.8	-3	air-to-air	810	SPIE vol. 3266 pp. 178-197	design; 500 km airborne demo at 40,000 ft alt.
JPL-OCD	-5		terrestrial point-to-point	780	SPIE vol. 3615 pp. 43-53	measured
JPL-OCD	-6		terrestrial point-to-point	840	SPIE vol. 3615 pp. 43-53	measured
JPL-DSO	-3.65	-3.36	deep space to ground	800	SPIE vol. 3615 pp. 154-169	design
JPL-OCDHRLF	-2		earth orbit to ground	1550	SPIE vol. 3615 pp. 185-191	design
JPL-X2000		-4	deep space to ground	550-1000	SPIE vol. 3615 pp. 206-211	design
JPL-GOLD	-3.14	-8.24	ground to GEO	514.5	SPIE vol. 2990 pp. 70-81	measured
JPL-GOLD	-2.19	-1.94	GEO to ground	830	SPIE vol. 2990 pp. 70-81	measured
CRL	-3	-6.5	GEO to ground	1550	SPIE vol. 2990 pp. 142-151	design
CRL ETS-VI	-3	-8.2	ground to GEO	514.5	SPIE vol. 2990 pp. 264-275	measured
CRL ETS-VI	-2	-4.4	GEO to ground	830	SPIE vol. 2990 pp. 264-275	measured
CRL LCE	-2	-7.2	GEO to ground	830	SPIE vol. 2990 pp. 264-275	estimated

Figure 14: Optics Package Loss Comparison Table

function that can be numerically plotted. Putting together the expressions from eqs.(179), (183), (185), (186), (196), (199), and (203), we form the complete line attenuation function $\alpha_{free\ space}$ as the sum of all losses:

$$\begin{aligned}
 \alpha_{free\ space} &= \alpha_{free\ space}(k, \varphi, L, D_A, D_B) \\
 &= \sum \mathcal{L} \\
 &= \mathcal{L}_{\text{static atmospheric}} + \mathcal{L}_{\text{beam spread}} + \mathcal{L}_{\text{beam wander}} + \mathcal{L}_{\text{spatial coherence}} \\
 &\quad + \mathcal{L}_{\text{quantum coherence}} + \mathcal{L}_{\text{scintillation}} + \mathcal{L}_{\text{pulse distortion/broadening}} + \mathcal{L}_{\text{optics package}} ,
 \end{aligned} \tag{204}$$

where the equation of state in the first line above displays only some of the various functional dependences that characterize the total line attenuation. As only one example of several

additional ones that could be discussed, the dependence on fog conditions that is implicit in the term $\mathcal{L}_{\text{static atmospheric}}$ is not *explicitly* indicated as part of the functional dependence, although it certainly needs to be specified in order to obtain a concrete numerical result (and in practice this is done by providing fog data in an appropriate input file for the FASCODE runs discussed in Section 4.1.2 above).

In Figures 15 and 16 below we plot the dependence of this loss on the diameter of the

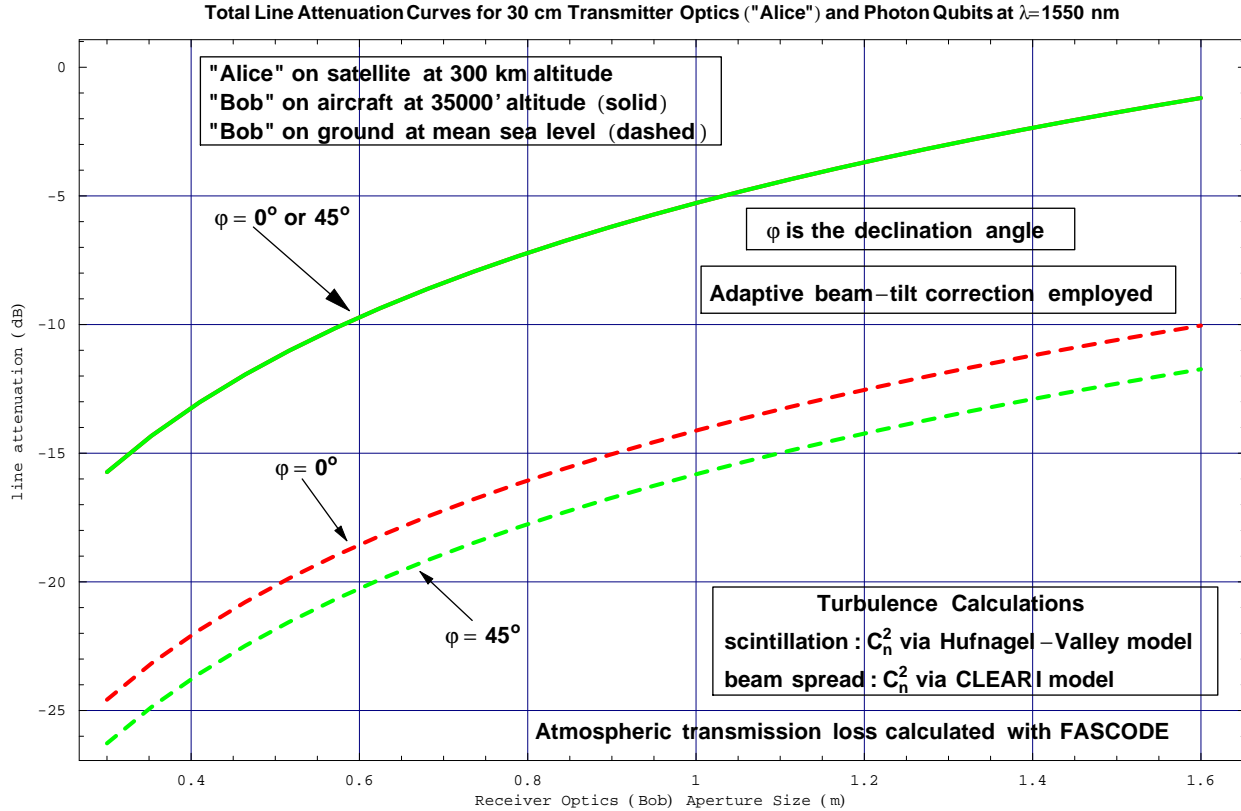


Figure 15: Line Attenuation for $\lambda = 1550$ nm

aperture of Bob's receiving instrument, D_B , assuming that the transmitting instrument used by Alice has a diameter of $D_A = 30$ cm. These curves are computed for the cases of light at wavelengths of $\lambda = 1550$ nanometers and $\lambda = 770$ nanometers, respectively. As discussed in Section 4.1.3 above, the use of sufficient adaptive beam tilt correction to have effectively mitigated the effects of beam wander has been assumed. The static atmospheric transmission losses have been computed using the FASCODE computer program as described in Section 4.1.2 above. The scintillation and beam spread losses were calculated using the Hufnagel-Valley 5/7 and CLEAR I atmospheric turbulence models, respectively. For all the curves it has been assumed that Alice is located on a LEO satellite at 300 kilometers altitude. The solid curves are for Bob located at an altitude of 35000' for arbitrary slant angle, and the dashed curves are for Bob located at mean sea level for different slant angles of 0 degrees

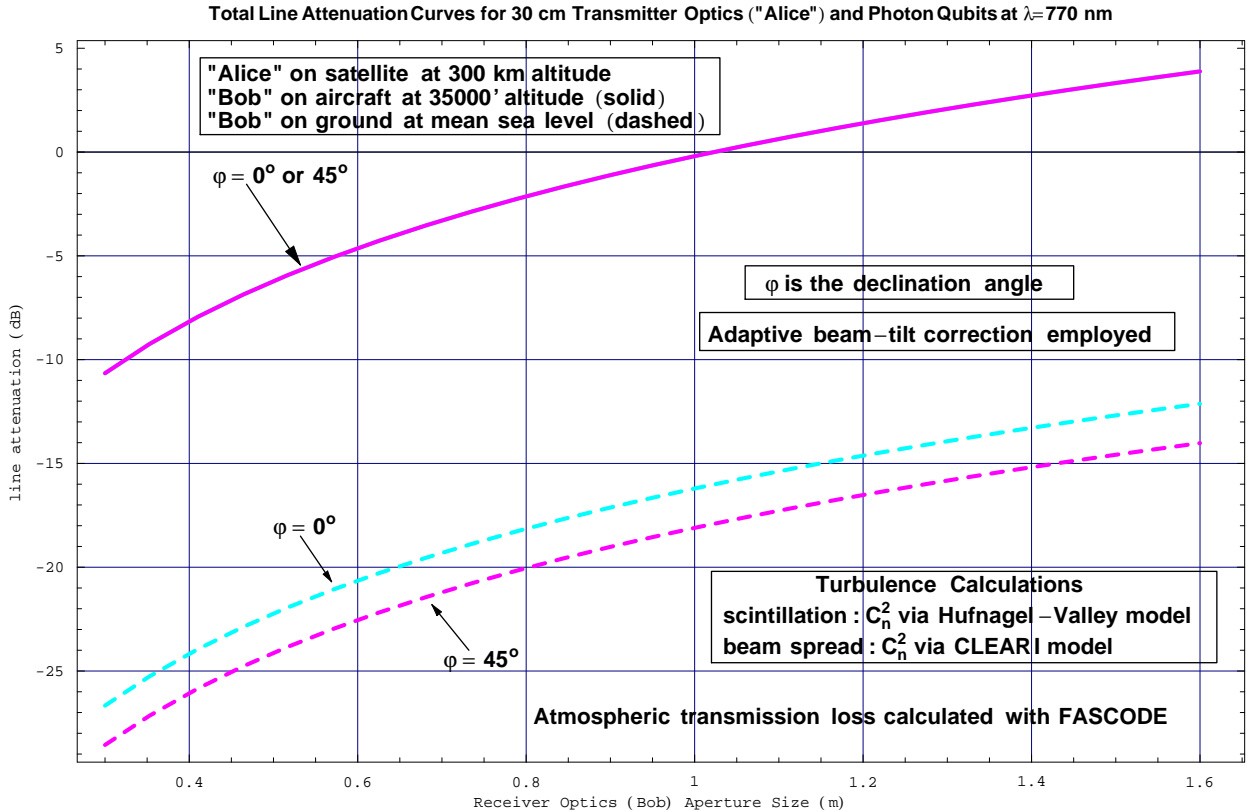


Figure 16: Line Attenuation for $\lambda = 770$ nm

and 45 degrees. We have assumed that clear weather conditions apply for the curves in both Figure 15 and Figure 16.⁶²

As an example, inspection of Figure 15 reveals that, at $\lambda = 1550$ nanometers for a value of $D_A = 30$ cm and with Bob on an airborne platform at 35000 feet, in order to achieve a line attenuation amount of -10 dB it is necessary for Bob to use a receiving instrument with an aperture of 58 cm. If we switch to a wavelength of 770 nanometers, inspection of Figure 16 reveals that roughly the same size of aperture for Bob will produce a line attenuation value of -5 dB.⁶³

⁶² As mentioned in Section 4.1.2 above “clear weather” conditions are defined as yielding 23 kilometers visibility.

⁶³ An analysis is given in [51] of the Ground/Orbiter Lasercomm Demonstration (GOLD) free-space optical communications experiment carried out between Table Mountain Facility near the Jet Propulsion Laboratory in Pasadena, California and the (geosynchronous) Japanese ETS-VI satellite. Both the predicted values and the measured values given there for the losses are larger than the values predicted in our analysis. This is due to the fact that the authors of [51] have defined and calculated system losses by making use of the generic radar equation, in particular modelling optical elements as antennas. When the appropriate antenna gain quantities are taken into account, the predicted and measured values given in [51] become consistent with the predicted values for the line attenuation given here, after substituting LEO for GEO.

4.2 System Losses: The Line Attenuation - Optical Fiber

The line attenuation for a QKD system with optical fiber as the quantum channel is expressed in a different way from that for a free space quantum channel. The general expression is given in this case as

$$\begin{aligned}\alpha_{fiber} &= \alpha_{fiber}(L_{fiber}, A, \kappa) \\ &= 10^{-\frac{AL_{fiber}+\kappa}{10}},\end{aligned}\quad (205)$$

where L_{fiber} is the length of the fiber cable connecting Alice and Bob. In this expression A is a parameter that measures the intrinsic loss characteristic, per unit length, of the fiber (this is a quantity essentially “built in” at the factory where the cable is manufactured) and κ is the “bulk loss” constant associated with the fiber that includes, for example, splicing losses due to the presence of spliced links of fiber. At the present time it is possible to obtain optical fiber cable of high quality for the transmission of 1550 nanometer wavelength light that has an intrinsic attenuation constant of $A = 0.2$ dB/kilometer. In addition to the attenuation, *per sé*, along the fiber, one must also take into account the intrinsic channel error, r_c , which is caused by the phenomenon of dispersion of photon arrival times as the pulse propagates from the Alice to Bob sites. As we will discuss below, this problem can be mitigated by including appropriate segments of so-called “compensating” fiber in the channel. Each such inserted link, however, introduces a contribution to the value of the bulk loss constant κ , thereby affecting the net value of α_{fiber} . Thus, in the case of an optical fiber implementation of quantum cryptography, the intrinsic channel error r_c and the line attenuation α_{fiber} are “connected” to each other in a way that is not the case for a free space implementation, as we discuss below.

4.3 The Intrinsic Channel Error

The effective secrecy capacity \mathcal{S} exhibits a sensitive dependence on the intrinsic quantum channel error parameter r_c . Relatively small changes in the value of the intrinsic channel error can have a significant effect on the magnitude of the effective secrecy capacity and total throughput rate of a practical quantum cryptography system, even if all other sources of system loss have been mitigated. In this section we analyze the characteristics and causes of this source of error.

4.3.1 Free Space Quantum Channel

The intrinsic channel error, r_c , is the parameter that measures the tendency of the free space QKD system characteristics to cause the states transmitted by Alice to suffer polarization misalignment by the time they are detected by Bob. For a free-space quantum channel the depolarization rate will be determined principally by the actual angular mismatch between

the Alice and Bob instruments as the platforms supporting one or the other or both of them move. This will occur, for instance, if Alice is on a satellite and Bob is located at a ground station, or perhaps on another moving platform.

In Appendix A it is demonstrated that, if the relative angular mismatch between the Alice and Bob instruments is denoted by δ , the fractional error rate due to polarizer misalignment is given by

$$r_c = \sin^2(\delta) . \quad (206)$$

Thus, even if δ is as large as 1/10 radian (5.7 degrees) the probability of error is less than 1%. Since δ is *relative* angular mismatch between Alice and Bob, the solid angle cone within which relative motion is allowed (for a given value of r_c) is 2δ . Thus if the platforms on which Alice and Bob are located can be subjected to attitude control such that corrections can be applied that allow motion through a cone of solid angle of no more than 11.5 degrees, the intrinsic channel error can be made to satisfy $r_c \leq 0.01$. This constraint on the necessary real-time control of the attitude of a satellite on which the Alice device could be placed and on telescope adjustment requirements is well within the currently achievable state-of-the-art [52, 53], and it is therefore reasonable for us to employ a value of $r_c = 0.01$ in the effective secrecy capacity in computing the operating characteristics of a free space implementation of quantum cryptography.

4.3.2 Optical Fiber Quantum Channel

In the case of a fiber-optic quantum channel, the dispersion characteristics of the fiber will generate an intrinsic error rate. Dispersion causes the shape of the transmitted pulse to spread as it travels along the fiber. We envisage an optical fiber cable-based QKD system built using single mode telecom fiber, used to transmit signals at a wavelength of 1550 nanometers. In this situation we are primarily concerned with two types of dispersion that appear in available optical fiber cables: (1) chromatic pulse dispersion (CD), and (2) polarization-mode pulse dispersion (PMD). Because we neither advocate nor analyze a QKD system built from multi-mode fiber we will not be concerned with other types of dispersion effects that can arise, such as modal dispersion.

If the effects of dispersion along the cable are not mitigated this will specifically appear as a certain amount of dispersion of the photon arrival time of the transmitted signal as received by Bob. The figure-of-merit in assessing this is provided by comparing the dispersion delay time with the appropriate characteristic *critical time*, which is given by the bit cell period τ (the reciprocal of the pulse repetition frequency) of the data source laser at Alice. In the special case of an interferometry-based quantum cryptography system as described in [54, 55], one should compare the dispersion delay time with *two* generally different characteristic critical times, the bit cell period τ as before, and the coherence time, τ_{coh} associated with the data source laser.

Chromatic Pulse Dispersion

Chromatic pulse dispersion stems from the dependence of the index of refraction on the wavelength. In more detail, chromatic dispersion in a fiber is partly due to “material dispersion,” the dependence of the fiber core index of refraction on the wavelength, and to “waveguide dispersion,” the dependence of the constant propagation mode on the wavelength. For single mode fibers that transmit light at 1550 nanometers wavelength, the amount of chromatic dispersion, d_{CD} , is given by

$$d_{CD} \approx 4 \frac{\text{picoseconds}}{\text{nanometer} \cdot \text{kilometer}} , \quad (207)$$

which corresponds to a chromatic dispersion pulse delay time, τ_{CD} , of

$$\begin{aligned} \tau_{CD} &= d_{CD} \cdot L \cdot \Delta\lambda \\ &\approx 160 \text{ picoseconds} \end{aligned} \quad (208)$$

for a cable link of $L = 50$ kilometers, assuming a laser source with a linewidth of $\Delta\lambda = 0.8$ nanometer. To compare this with the two characteristic times we assume that the source laser has a coherence time τ_{coh} of at least 1 nanosecond, or $\tau_{coh} = 1000$ picosecond. We therefore have

$$\tau_{CD} < \tau_{coh} , \quad (209)$$

and no mitigation of chromatic pulse dispersion is required on this basis. However we see that the requirement

$$\tau_{CD} < \tau \quad (210)$$

means that we must mitigate chromatic pulse dispersion if we use a fast data source laser with a bit cell period shorter than 160 picoseconds, corresponding to a pulse repetition frequency greater than 6.25 GHz. As we discuss below, we envisage the use of high speed lasers with pulse repetition frequencies of 10 GHz. We conclude that chromatic pulse dispersion needs to be mitigated if we utilize a high speed laser with a pulse repetition frequency of 10 GHz (corresponding to a bit cell period of 100 picoseconds). Mitigation of this problem can be accomplished by making use of appropriate lengths of dispersion compensation fiber spliced into the line to reduce the photon arrival time dispersion to less than approximately 50 picoseconds. (As discussed in Section 4.2 above, each additional inserted cable link will increase the line attenuation by increasing the splicing loss.)

Polarization-Mode Pulse Dispersion

Polarization-mode dispersion due to intrinsic and induced birefringence will cause the pulses to broaden as they propagate along the fiber [56]. In currently available good quality single mode fiber operating at a wavelength of 1550 nanometers, the amount of polarization-mode dispersion, d_{PMD} , is typically given by⁶⁴

$$d_{PMD} \approx 0.1 \frac{\text{picoseconds}}{\sqrt{\text{kilometer}}} . \quad (211)$$

⁶⁴ In this example we have used representative sample numerical values appropriate for Lucent TrueWaveTM fiber.

The corresponding polarization-mode dispersion pulse delay time, τ_{PMD} , is given for a cable link of $L = 50$ kilometers by

$$\begin{aligned}\tau_{PMD} &= d_{PMD} \cdot \sqrt{L} \\ &\approx 0.7 \text{ picoseconds}.\end{aligned}\quad (212)$$

We see that, again assuming a laser coherence time of 1 nanosecond, this polarization arrival time dispersion strongly satisfies the requirement

$$\tau_{PMD} < \tau_{coh}.\quad (213)$$

Furthermore we see that the requirement

$$\tau_{PMD} < \tau\quad (214)$$

is satisfied unless the pulse repetition frequency of the laser is greater than $\tau_{PMD}^{-1} = 1.43$ THz. The current state-of-the-art in photon detection and data correlation is such that this value does not furnish a constraint. Thus, polarization-mode dispersion will not be a practical problem.

4.4 System Loads

In the previous section we analyzed the various *losses* that together reduce the effective throughput of a QKD system. In this section we consider the complete set of system *loads* that together must be taken into account as well to establish a bound on the achievable data rate. Our analysis includes careful calculations of the cost in bits of maintaining *continuous* authentication of the QKD protocol, the throughput requirements on the classical communications channel, and the computational requirements measured in machine instructions that must be satisfied in order to carry out real-time processing of the key.

Although these processes are crucial to the implementation of any QKD system, there has been essentially no explicit, quantitative analysis of any of them presented heretofore in the literature on the subject. In the case of the authentication cost this seems to stem from the erroneous notion that an initially supplied, “short” authentication string shared between Alice and Bob will suffice to protect the protocol from spoofing. This is mistaken: (1) either the initially supplied, shared authentication string is indeed “short,” in which case in due course it will be used up and must be replaced by removing bits from the key generated by the QKD protocol itself, or (2) the initially supplied, shared authentication string is in fact “long,” in which case a primary justification for the use of quantum key distribution in the first place is severely weakened. In the case of the communications throughput load, the potential use of QKD on satellite systems in particular, clearly requires a detailed analysis of the constraints that must be satisfied by the specialized satcom equipment that will be used, and similar importance attaches to the computational burden, again with special consideration for the satellite problem, owing to obvious space constraints on the computing hardware that can in practice be installed on a spaceborne platform.

4.4.1 The Cost of Continuous Authentication

General Remarks

Prior to the error correction phase, the BB84 protocol furnishes Alice and Bob with a block of n bits, of which Eve has managed to obtain an amount of information equivalent to at most $t + \nu$ bits by making undetected measurements of single photon pulses and by using some combination of direct and indirect attacks on the multiple photon pulses. The blocks obtained by Alice and Bob are not identical due to the errors introduced by imperfections in the physical apparatus. By listening to the public transmissions by which Alice and Bob eliminate the errors from their blocks, Eve is able to obtain additional information about Alice and Bobs bits, giving her a total of at most $q+t+\nu$ bits of information about the error-corrected block. As the last step of the process, Alice and Bob use a privacy amplification technique as described in [24] to arrive at a block of bits that is shared identically between them and about which Eve is expected to have no information to a high degree of confidence. This section describes the details of a specific implementation of the error correction and privacy amplification process. It is assumed throughout that Eve has complete knowledge of the protocols, as well as unrestricted access to all communications between Alice and Bob that occur during this period.

Our description of these protocols is intended to achieve two goals. The first is to determine the authentication cost of the protocols. This authentication cost is the number of shared secret bits that need to be sacrificed in order to guarantee that the protocols perform correctly, that is, that execution of the protocols results in some predictable amount of secret key material that is shared identically between Alice and Bob but about which Eve has no information with a high degree of confidence. Since the authentication cost represents a sacrifice of previously existing key material in order to guarantee the generation of a new block of key material, this cost has a direct impact on the rate at which keys can be generated.

The second goal is to estimate the burdens these protocols place on computational and communications resources. Unlike the authentication cost, these costs have no direct effect on the rate of key generation, but they do provide an estimate of the computational and communications resources required to support key generation, resulting in constraints on the rate of key generation for given set of resources. In addition, the fact that the computational complexity is quadratic in the block size of the key material results in a practical upper bound on the block size, again for a given set of computational resources.

We begin by giving a brief overview of the protocol. The first phase is the production of a sifted string of bits shared, except for some errors, by Alice and Bob. This is achieved by applying the BB84 protocol previously described. If the equipment were perfect and there were no possibility of errors, the sifted strings would be identical and any attempt by Eve to obtain more than a few bits would be revealed by the presence of errors in the sifted string. Since this is not the case for a practical implementation, it is essential to include mechanisms to correct the errors and to eliminate information leaked to Eve in the process.

The second phase is thus error correction. Alice and Bob agree on a systematic scheme of computing and comparing parities for subsets of the sifted string in order to identify and correct the errors. Since Eve can eavesdrop on this discussion, an additional amount of data is leaked. The third phase is privacy amplification, during which Alice and Bob apply a hash transformation to the error-corrected string which results in a shorter string about which Eve's expected information is vanishingly small. At various points during these three phases, Alice and Bob must authenticate their communications to ensure that Eve is not making a man-in-the-middle attack.

Sifting Phase

The first phase of the key distribution protocol is the generation of an initial sifted string that is shared between Alice and Bob, but which may contain errors and about which Eve may have partial information. We describe a specific implementation of the BB84 protocol. Alice generates two blocks of m random bits. The first block is the raw key material, and the second block determines the choice of basis she uses to transmit the bits over the quantum channel. Bob generates a single block of m bits that reflect his choice of basis in measuring the incoming qubits. Bob must now identify to Alice those pulses for which he detected a qubit and inform her of his choice of basis for those pulses. Bob has several choices available in deciding how he wants to encode this information. The simplest approach is to send two bits corresponding to each of Alice's pulses. The first bit tells whether a photon was detected, the second describes the choice of basis. This means that Bob must send $2m$ bits to Alice for each block of key material. A more efficient version of this scheme is to send the second bit only when the first bit indicates that a photon was detected. In this case, Bob only sends $m + 2n$ bits on average. (The factor of 2 in $2n$ comes from the fact that Bob's choice of basis agrees with Alice's on average half of the time, so that there are twice as many detected photons as there are bits in the sifted key.) Since we always have $2n \leq m$ this alternative is no less efficient than the first, and usually it is more efficient. A third alternative is to send two pieces of information for each detected photon, the first indicating for which of the m bit cells the photon was detected, and the second giving Bob's choice of basis. This requires that Bob send $2n(1 + \log_2 m)$ bits for each block of key material. This alternative is more efficient than the others when

$$2n \log_2 m < m \tag{215}$$

Since we are primarily concerned with situations in which $m \gg n$, this is normally the most efficient of the three alternatives thus far discussed. More efficient encodings are certainly possible. For instance one might imagine sending differences between successive indices instead of the entire index. For purposes of obtaining reasonable estimates of the communications cost without overcomplicating the analysis, the third alternative is a reasonable choice, and we will proceed by restricting the protocol to this case in subsequent discussions.

Once Alice has received Bob's information, she compares Bob's basis choices with her own and informs Bob of the results. Alice can accomplish this by sending Bob a single bit corresponding to each of the photons Bob detected, giving a total of $2n$ bits.

We now augment the protocol with provisions that will prevent Eve from making the so called man-in-the-middle attack. In this attack, Eve interposes herself between Alice and Bob, measuring Alice's pulses on the quantum channel as though she were Bob, and generating a distinct set of pulses to send to Bob as though she were Alice. In all her subsequent correspondence with Alice over the classical channel, she responds just as Bob would, and in all correspondence with Bob she plays the role of Eve. After the first phase of the protocol, Eve has two blocks of sifted keys, one of which she shares with Alice and the other with Bob. Assuming she can continue this attack through the error correction and privacy amplification phases, she will have completely compromised Alice and Bob's ability to use the keys to transmit secret information. In fact, Eve will be able to decipher any encrypted information sent between Alice and Bob, always passing the ciphertext to the intended recipient so that neither Alice nor Bob is any the wiser.

In order to prevent this state of affairs, it is necessary to provide an authentication mechanism to guarantee that the transmissions received by Bob were sent by Alice, not Eve, and that the transmissions received by Alice were sent by Bob. Wegman and Carter [36] describe an authentication technique that is well suited to this problem. The authentication works as follows. Alice and Bob first agree upon a suitable space of hash functions to be used for authentication. All details of their agreement may be revealed to Eve without compromising the authentication. For each message that is to be authenticated, Alice picks a hash function from the space that is known to Bob, but not to Eve. She does this by using a string of secret bits that is known only to herself and Bob as an index to select the hash function. She then applies the hash function to the block of raw data to produce an authentication key. This authentication key is transmitted to Bob along with the message. Bob uses the same string of secret bits to pick the same hash function, applies it to the message, and compares the result with the authentication key sent by Alice. If they match, Bob concludes that Alice, and not Eve was the sender of the message. Wegman and Carter describe a class of hash functions such that the probability that Eve can generate the correct authentication key without knowing the index used is vanishingly small. Let \mathcal{M}_1 denote the precondition that Eve has obtained a copy of the message to be authenticated and $\mathcal{T}_1^{(E)}$ denote the set of outcomes in which Eve guesses the tag for the message. The probability of such an outcome is

$$\mathcal{P}(\mathcal{T}_1^{(E)} | \mathcal{M}_1) = 2^{-g_{auth}}, \quad (216)$$

where g_{auth} depends on the space of hash functions Alice and Bob have chosen to use for the protocol. It can be made as large as desired by making the space sufficiently large. Alice and Bob do pay a price for increased confidence. A larger space of functions requires a larger set of indices, and thus a longer string of secret bits must be sacrificed to perform the authentication. The other restriction on the protocol is that a new hash function, and thus a new index, must be used for each message to be authenticated if we desire to maintain this upper bound on Eve's ability to spoof the authentication process. If we allow Eve to obtain one prior message and tag, denoted as $\mathcal{M}_1 \mathcal{T}_1$, and then allow her to obtain the next message, denoted as \mathcal{M}_2 , as well as the information that Alice and Bob intend to use the

same hash function for both, her chances of guessing the second tag improve only slightly to

$$\mathcal{P}(\mathcal{T}_2^{(E)} | \mathcal{M}_1 \mathcal{T}_1 \mathcal{M}_2) = 2^{1-g_{auth}}. \quad (217)$$

If we allow additional messages to be authenticated using the same hash function, Wegman and Carter's analysis provides no upper bound on Eve's ability to produce a correct authentication tag. Although it would be more efficient to allow the same hash function to be applied exactly twice, we will consider the simpler case in which a new hash function is picked for each message.

We now consider which transmissions need to be authenticated. We will not attempt to authenticate the communications on the quantum channel. Any man-in-the-middle attack by Eve on the quantum channel will become evident when the error correction process reveals that there is no correlation between the Alice and Bob's sifted strings. Eve also gains no advantage from a selective attack on a subset of the pulses sent by Alice. Suppose Alice and Bob predict an expected number of errors $\langle e_T \rangle$ based on the known physical properties of the channel and their equipment. They then select a maximum threshold value $e_T^{max} > \langle e_T \rangle$ so that, if the measured error rate is greater than the threshold, that is, if

$$e_T^{meas} > e_T^{max} \quad (218)$$

then they will conclude that Eve has interfered with the quantum channel, perhaps by making a man-in-the-middle attack, and will terminate processing for that block of data. There is still the possibility that $e_T^{meas} < e_T^{max}$, but that Eve has nevertheless corrupted the quantum channel. In this case, the protocol proceeds as usual, the additional errors are identified and corrected, and the information leaked to Eve is removed during privacy amplification. This type of attack falls under the category of an attack on secrecy that has no effect other than to reduce the overall generation rate of key material.

Authentication is required for the classical discussion of Alice and Bob's choice of bases and the identification of the pulses received by Bob. If there is no authentication of this step, Eve can successfully mount the man-in-the-middle attack which results in two sets of keys, one shared between Alice and herself, the other between Bob and herself. Authentication guarantees Alice and Bob that they are working with the same subset of the pulses sent by Alice and that any remaining errors are due to physical imperfections of the equipment or attempts by Eve to measure, and therefore disturb, the pulses sent by Alice.

The authentication of the classical discussion results in a cost to the overall rate of quantum key generation, since some of the secret bits produced by previous iterations of the protocol must be sacrificed to generate an authentication tag that Alice or Bob can validate but that Eve cannot forge. Wegman and Carter [36] show that the size of the secret index required to select a hashing function is

$$w(g, c) = 4(g + \log_2 \log_2 c) \log_2 c \quad (219)$$

where c is the length in bits of the message to be authenticated and g is the length in bits of the authentication tag. Note that g determines the degree of confidence in the authentication

according to eq. (216), in which g is denoted g_{auth} . We define the parameter g_{auth} as the length of the authentication tags used in this protocol. The first message to be authenticated is Bob's transmission of the indices of the detected pulses and his choice of basis for each. The length of the message is

$$c_1 = 2n(1 + \log_2 m) , \quad (220)$$

giving an authentication cost of

$$w_1 = 4 \left\{ g_{auth} + \log_2 \log_2 [2n(1 + \log_2 m)] \right\} \log_2 [2n(1 + \log_2 m)] . \quad (221)$$

The second message is Alice's transmission of her choice of basis for the pulses that Bob detected. The length of the message is

$$c_2 = 2n , \quad (222)$$

and the corresponding authentication cost is

$$w_2 = 4 \left[g_{auth} + \log_2 \log_2 (2n) \right] \log_2 (2n) . \quad (223)$$

We consider next the load this phase imposes on the classical communication channel. We assume that the communication protocol employs some form of error-correction coding that increases the length of the message by a factor χ_{EC} [57]. The protocol then breaks the message into packets of length m_p and adds an amount of frame overhead f_o to each packet. Finally, the authentication tag is sent as a single packet, on the assumption that the tag size after encoding for error correction is less than m_p :

$$\chi_{EC} g_{auth} \leq m_p \quad (224)$$

This is a reasonable assumption, as we generally will take $g_{auth} < 50$, $\chi_{EC} \approx 2$, so that we only require $m_p > 100$, which is easily achieved for typical optical ground-to-satellite links or terrestrial fiber optic channels. The number of packets sent from Bob to Alice is then

$$\mathcal{N}_{B \rightarrow A}^{sift} = \left\lceil \frac{\chi_{EC} 2n (1 + \log_2 m)}{m_p} \right\rceil + 1 , \quad (225)$$

and the load in bits carried by the channel is, approximately,

$$\begin{aligned} \mathcal{C}_{B \rightarrow A}^{sift} \simeq & \left(1 + \frac{f_o}{m_p} \right) \left[\chi_{EC} 2n (1 + \log_2 m) \right] \\ & + (\chi_{EC} g_{auth} + f_o) , \end{aligned} \quad (226)$$

where we have used the packetization approximation described in Appendix B. The communication from Alice to Bob required for sifting is given similarly by

$$\begin{aligned} \mathcal{C}_{A \rightarrow B}^{sift} \simeq & \left(1 + \frac{f_o}{m_p} \right) (\chi_{EC} 2n) \\ & + (\chi_{EC} g_{auth} + f_o) . \end{aligned} \quad (227)$$

Error Correction Phase

At this point Bob and Alice move on to the error correction phase. We will estimate the authentication, communication, and computational costs for a modified version of the error correction protocol described by Bennett *et. al.*, [34]. More efficient techniques have been developed, for example the “Shell” and “Cascade” protocols described in [58], but the method described here is more suitable for our purposes since it is simpler to analyze and can be expected to provide a practical upper bound for the communications cost.

At the beginning of the error correction phase, Alice and Bob each have a string of n bits. The strings are expected to be nearly identical, but they will also contain errors for which Alice and Bob disagree on the value of the bit. It is the goal of error correction to identify and remove all of these errors, so that Alice and Bob can proceed with a high degree of certainty that the strings are identical. Error correction consists of three steps. The first step is the error detection and correction step, which eliminates all or almost all of the errors. The validation step which follows eliminates any residual errors and iteratively tests randomly chosen subsets of the string to generate a high degree of confidence that the strings are identical. The final step is authentication, which protects against a man-in-the-middle attack by Eve during the error correction process.

At the beginning of the error detection and correction step, Alice and Bob each shuffle the bits in their string using a random shuffle upon which they have previously agreed. The purpose of this shuffle is to separate bursts of errors so that the errors in the shuffled string are uniformly distributed. Alice and Bob may use the same shuffle each time they process a new string of sifted bits, and security is not compromised if Eve has complete prior knowledge of the shuffling algorithm, even including any random numbers used as parameters.

The error detection and correction step is an iterative process. Alice and Bob begin each iteration i by breaking their strings into shorter blocks. The block length is chosen so that the expected number of errors in each block is given by a parameter ϱ . The number of blocks in the string is then

$$J^{(i)} = \left\lceil \frac{e_T^{(i-1)}}{\varrho} \right\rceil. \quad (228)$$

and the average number of bits per block is

$$k^{(i)} = \frac{n}{J^{(i)}}, \quad (229)$$

where $e_T^{(i)}$ is the expected number of errors remaining after the i th, or at the beginning of the $i+1$ st, iteration. In principle the parameter ϱ could change from iteration to iteration. We assume that it is a constant to simplify the analysis. Alice and Bob compute the parity of each of the blocks and exchange their results. Blocks for which the parities match necessarily contain at least one error. For each of the blocks in which Alice and Bob have detected an error, they isolate the erroneous bit by a bisective search, which proceeds as follows. Alice

and Bob bisect one of the blocks containing an error, that is, they divide it as evenly as possible into 2 smaller blocks. Alice and Bob each compute the parity of one of the blocks, say the one that lies closer to the beginning of the shuffled string, and exchange the results. If the parities do not match, the error is in the lower block. If they match, the error is in the upper block. Alice and Bob then bisect the block that contains the error and proceed recursively until they find an erroneous bit. Bob then inverts that bit in his string, and in so doing the error is removed.

We have described the bisective search as though the search were completed for any block containing a detected error before beginning the bisection on the next block. In fact, it is more efficient from a communications standpoint to apply each bisection to all the blocks with detected errors at the same time, exchange parities for all of the sub-blocks, and then to proceed recursively to the next bisection. This results in fewer, but larger, packets of data for each exchange between Bob and Alice, thus reducing the overall frame overhead.

When the bisective search is completed for all blocks in which an error is detected, a new blocksize is computed based on the expected number of errors remaining, the string is broken up into a new set of larger blocks, parity checks are compared for the blocks, and bisective searches are made in those blocks containing detected errors. This process is repeated until there would be only one or two blocks in the string for the next iteration, that is, until

$$J^{(N_1+1)} \leq 2 , \quad (230)$$

where N_1 is the number of iterations in the error correction and detection step. An equivalent stopping criterion is that the blocksize for the subsequent iteration is more than half the length of the string, that is

$$k^{(N_1+1)} \geq \frac{n}{2} , \quad (231)$$

and the expected number of errors remaining after the final iteration satisfies

$$e_T^{(r)} \equiv e_T^{(N_1)} \leq 2\varrho . \quad (232)$$

We summarize here some important results that are needed for an analytical description of the communications required to support this part of the error correction phase. As shown in the appendix “Statistical Results for Error Correction,” the expected number of errors remaining after the i th iteration is

$$e_T^{(i)} \simeq \beta^i e_T^{(0)} , \quad (233)$$

and the expected number of errors found and corrected in the i th iteration is

$$e_f^{(i)} \simeq (1 - \beta) \beta^{i-1} e_T^{(0)} , \quad (234)$$

where β is defined by the expression

$$\beta \equiv \frac{2\varrho - 1 + e^{-2\varrho}}{2\varrho} . \quad (235)$$

We obtain the number of iterations in the error detection and correction step by setting $J^{(N_1+1)} \leq 2$, which gives

$$N_1 = \left\lceil \frac{\log_2 \frac{2\varrho}{e_T^{(0)}}}{\log_2 \beta} \right\rceil , \quad (236)$$

and the expected number of remaining errors becomes

$$e_T^{(r)} \simeq \beta^{N_1} e_T^{(0)} \simeq 2\varrho . \quad (237)$$

The second step in the error correction phase, validation, is also iterative. During each iteration, Alice and Bob select the same random subset of their blocks. They compute the parities and exchange them. If the parities do not match, Alice and Bob execute a bisective search to find and eliminate the error. Iterations continue until N_2 consecutive matching parities are found. At this point, Alice and Bob conclude that their strings are error free. As shown in the appendix “Statistical Results for Error Correction,” the probability of one or more errors remaining is

$$\mathcal{P}(\text{errors after validation}) \leq e^{2\varrho} \left(\frac{1}{2}\right)^{N_2} \quad (238)$$

the expected number of iterations in which no error is found is given, to a good approximation, by

$$N_2^{(n)} \simeq N_2 + e_T^{(r)} \simeq N_2 + 2\varrho , \quad (239)$$

and the expected number of iterations in which an error is found is

$$N_2^{(f)} \simeq e_T^{(r)} \simeq 2\varrho . \quad (240)$$

The selection of the same random subsets for validation can be accomplished by using a deterministic random number generator [59] and resetting the random seed to a predetermined value at the beginning of the validation phase. We will assume that Eve has complete knowledge of the algorithm and the random seed as well. Note that it is to Alice and Bob’s

advantage to keep the algorithm and seed secret, since Eve can make use of this information to interpret the parities she intercepts on the public channel, but it is not essential to the secrecy of the overall result, since we eliminate all the information Eve can have obtained in privacy amplification.

The last step in the error correction phase is authentication. Up until now, Alice and Bob have made no attempt to authenticate their exchange of parity information on the classical channel. Eve could mount a man-in-the-middle attack during the error correction phase that would fool Alice and Bob into correcting the wrong set of bits. This would not give Eve any additional information about the secret string, but it could result in Alice and Bob believing that their strings are identical when in fact they are not. Even if one bit is different, the privacy amplification phase will produce strings that are completely uncorrelated, and Alice and Bob will still believe that their strings are identical. The solution to this problem is for Alice and Bob to verify that their strings are the same at the end of the error correction phase. This effectively authenticates their prior communications, since any successful attempt by Eve to steer the error correction process will be immediately apparent.

This approach presupposes that Alice and Bob can verify that their strings are the same without leaking too much additional information to Eve. This can be accomplished if Alice and Bob apply the same hash function to their strings and compare the resulting tag. This does not provide an absolute guarantee that the strings are the same, but if the hash function is chosen as described in [36], the probability that two different strings will yield the same tag is

$$\mathcal{P}(\text{same tag, two strings}) = 2^{-g_{EC}} , \quad (241)$$

where g_{EC} is the length of the tag. This gives a high degree of confidence that the strings are identical even for relatively short ($g_{EC} \sim 30$) tags. The price Alice and Bob have to pay for this is that they must use a portion of the secret bits obtained from previous iterations of the protocol to select the hash function, indicate whether the keys match, and authenticate their transmissions.

We introduce a specific protocol for Alice and Bob to carry out the authentication step for purposes of estimating the costs associated with this step. Alice and Bob agree to set aside a portion of the secret bits derived from each block of the quantum transmission for use in processing subsequent blocks. Some of these bits are used for authentication during the sifting phase as previously discussed. Some additional bits are required to use as a key to select the hash function for the equivalence check. The size of this key is given by eq. (219), where

$$c_3 = n , \quad (242)$$

is the length of the string to be hashed and g_{EC} is the length of the tag, so that the

authentication cost for equivalence checking is

$$w_3 = 4(g_{EC} + \log_2 \log_2 n) \log_2 n . \quad (243)$$

Alice and Bob both compute an equivalence tag using this hash function, and Bob sends his to Alice. Bob must also authenticate his message, since otherwise Eve can mount a man-in-the-middle attack in which she simply sends an arbitrary tag to Alice, convincing her that her string doesn't match Bob's string when, in fact, it does. Although this is only a denial-of-service attack, Alice and Bob will not detect the attack unless Bob authenticates his message. Since Bob's message to Alice is of length

$$c_4 = g_{EC} , \quad (244)$$

and the authentication tag is of length g_{auth} , the authentication cost for the transmission is

$$w_4 = 4(g_{auth} + \log_2 \log_2 g_{EC}) \log_2 g_{EC} . \quad (245)$$

If Alice determines that her equivalence tag matches the one Bob sent to her, and if the authentication tag agrees as well, she indicates that the authentication was successful by sending \tilde{g}_{EC} secret bits to Bob. The authentication cost for this step is

$$w_5 = \tilde{g}_{EC} . \quad (246)$$

bits to signal her agreement to Bob. Alice must also authenticate this message to protect against a man-in-the-middle attack by Eve. The length of the message to be authenticated is:

$$c_6 = \tilde{g}_{EC} \quad (247)$$

and the authentication tag is of length g_{auth} so that the authentication cost is

$$w_6 = 4(g_{auth} + \log_2 \log_2 \tilde{g}_{EC}) \log_2 \tilde{g}_{EC} . \quad (248)$$

Classical communications between Alice and Bob are required in each step of the error correction phase. During each iteration of the error detection and correction step, Bob sends to Alice a single transmission containing the parities computed for each of the $J^{(i)}$ blocks. Alice sends a similar transmission to Bob containing her parities. For each such iteration, the communication load in bits in each direction is approximately

$$\left(1 + \frac{f_o}{m_p}\right) \chi_{EC} J^{(i)} , \quad (249)$$

where we have used the packetization approximation described in the appendix. Then, for each block containing a detected error, Alice and Bob bisect the block and exchange the parities of the bisected blocks. This requires a communication in each direction of

$$\left(1 + \frac{f_o}{m_p}\right) \chi_{EC} e_f^{(i)} \quad (250)$$

bits. The bisective search repeats for a total of $\lceil \log_2 k^{(i)} \rceil$ iterations. The total communications load in bits for this step is thus

$$\Delta \mathcal{C}_{B \rightarrow A}^{EC,1} = \Delta \mathcal{C}_{A \rightarrow B}^{EC,1} = \sum_{i=1}^{N_1} \left[\left(1 + \frac{f_o}{m_p}\right) \chi_{EC} J^{(i)} + \lceil \log_2 k^{(i)} \rceil \left(1 + \frac{f_o}{m_p}\right) \chi_{EC} e_f^{(i)} \right] . \quad (251)$$

For the next step, Alice and Bob each compute the parity for a random subset of their strings and exchange the results. One bit of parity information is sent in each direction, so that the communication load is $\chi_{EC} + f_o$ bits in each direction. If the parities are different, Alice and Bob carry out a bisective search for the error, resulting in $\lceil 1 + \log_2 \frac{n}{2} \rceil$ transmissions of $\chi_{EC} + f_o$ bits in each direction. This is repeated until N_2 successive parities match. The communications load for this step is then

$$\Delta \mathcal{C}_{B \rightarrow A}^{EC,2} = \Delta \mathcal{C}_{A \rightarrow B}^{EC,2} = N_2^{(n)} (\chi_{EC} + f_o) + N_2^{(f)} \left\lceil 1 + \log_2 \frac{n}{2} \right\rceil (\chi_{EC} + f_o) , \quad (252)$$

where $N_2^{(n)}$ is the number of iterations which do not find an error and $N_2^{(f)}$ is the number of iterations which do find an error.

In the third step, authentication, Bob sends to Alice an equivalence tag of length g_{EC} and an authentication tag of length g_{auth} giving a communication load of

$$\Delta \mathcal{C}_{B \rightarrow A}^{EC,3} = \chi_{EC} (g_{EC} + g_{auth}) + f_o \quad (253)$$

bits. Alice sends a confirmation string of length \tilde{g}_{EC} and an authentication tag of length g_{auth} for a communications load of

$$\Delta \mathcal{C}_{A \rightarrow B}^{EC,3} = \chi_{EC} (\tilde{g}_{EC} + g_{auth}) + f_o \quad (254)$$

bits. Note that we have implicitly assumed that the tags are short enough to send in a single packet. Since the tags are typically less than 50 bits, this amounts to a requirement that the packet size m_p exceed 200 bits so as to accomodate two tags plus error correction codes. This is a modest constraint on the optical communications system.

Collecting all of the contributions to the communications load, we obtain the following expressions for the load during the error correction phase:

$$\begin{aligned}\mathcal{C}_{B \rightarrow A}^{EC} = & \sum_{i=1}^{N_1} \left[\left(1 + \frac{f_o}{m_p}\right) \chi_{EC} J^{(i)} + \left\lceil \log_2 k^{(i)} \right\rceil \left(1 + \frac{f_o}{m_p}\right) \chi_{EC} e_f^{(i)} \right] \\ & + N_2^{(n)} (\chi_{EC} + f_o) + N_2^{(f)} \left\lceil 1 + \log_2 \frac{n}{2} \right\rceil (\chi_{EC} + f_o) \\ & + \chi_{EC} (g_{EC} + g_{auth}) + f_o ,\end{aligned}\quad (255)$$

and

$$\begin{aligned}\mathcal{C}_{A \rightarrow B}^{EC} = & \sum_{i=1}^{N_1} \left[\left(1 + \frac{f_o}{m_p}\right) \chi_{EC} J^{(i)} + \left\lceil \log_2 k^{(i)} \right\rceil \left(1 + \frac{f_o}{m_p}\right) \chi_{EC} e_f^{(i)} \right] \\ & + N_2^{(n)} (\chi_{EC} + f_o) + N_2^{(f)} \left\lceil 1 + \log_2 \frac{n}{2} \right\rceil (\chi_{EC} + f_o) \\ & + \chi_{EC} (\tilde{g}_{EC} + g_{auth}) + f_o .\end{aligned}\quad (256)$$

The communications load can be expressed in terms of the fundamental quantities $n, e_T^{(0)}$, and ϱ by using eqs. (362), (363), (361), (386), and (390). The necessary summations are elementary:

$$\begin{aligned}\sum_{i=1}^{N_1} J^{(i)} & \simeq \frac{e_T^{(0)}}{\varrho} \sum_{i=1}^{N_1} \beta^{i-1} \\ & \simeq \frac{e_T^{(0)}}{\varrho} \frac{1 - \beta^{N_1}}{1 - \beta} \\ & \simeq \frac{e_T^{(0)}}{\varrho} \frac{1 - \frac{2\varrho}{e_T^{(0)}}}{1 - \frac{2\varrho - 1 + e^{-2\varrho}}{2\varrho}} \\ & \simeq 2 \frac{e_T^{(0)} - 2\varrho}{1 - e^{-2\varrho}} ,\end{aligned}\quad (257)$$

where we have approximated the results by disregarding the rounding up of real quantities to integers, and

$$\begin{aligned}\sum_{i=1}^{N_1} \log_2 k^{(i)} e_f^{(i)} & \simeq \sum_{i=1}^{N_1} \log_2 \left(\frac{\varrho n}{e_T^{(i-1)}} \right) e_f^{(i)} \\ & \simeq \sum_{i=1}^{N_1} \log_2 \left(\frac{\varrho n}{\beta^{i-1} e_T^{(0)}} \right) (1 - \beta) \beta^{(i-1)} e_T^{(0)} \\ & \simeq e_T^{(0)} \left\{ \log_2 \left(\frac{\varrho n}{e_T^{(0)}} \right) (1 - \beta^{N_1}) - \frac{\beta \log_2 \beta}{1 - \beta} [1 - N_1 \beta^{N_1-1} + (N_1 - 1) \beta^{N_1}] \right\} ,\end{aligned}\quad (258)$$

where a similar approximation is made. Inserting these results and eqs.(386) and (390) into eq.(255) gives the following expressions for the communications load:

$$\begin{aligned}
\mathcal{C}_{B \rightarrow A}^{EC} \simeq & 2 \left(1 + \frac{f_o}{m_p} \right) \chi_{EC} \frac{e_T^{(0)} - 2\varrho}{1 - e^{-2\varrho}} \\
& + \left(1 + \frac{f_o}{m_p} \right) \chi_{EC} e_T^{(0)} \\
& \cdot \left\{ \log_2 \left(\frac{\varrho n}{e_T^{(0)}} \right) (1 - \beta^{N_1}) - \frac{\beta \log_2 \beta}{1 - \beta} \left[1 - N_1 \beta^{N_1-1} + (N_1 - 1) \beta^{N_1} \right] \right\} \\
& + (N_2 + 2\varrho) (\chi_{EC} + f_o) \\
& + 2\varrho \left[1 + \log_2 \frac{n}{2} \right] (\chi_{EC} + f_o) \\
& + \chi_{EC} (g_{EC} + g_{auth}) + f_o , \tag{259}
\end{aligned}$$

and

$$\begin{aligned}
\mathcal{C}_{A \rightarrow B}^{EC} \simeq & 2 \left(1 + \frac{f_o}{m_p} \right) \chi_{EC} \frac{e_T^{(0)} - 2\varrho}{1 - e^{-2\varrho}} \\
& + \left(1 + \frac{f_o}{m_p} \right) \chi_{EC} e_T^{(0)} \\
& \cdot \left\{ \log_2 \left(\frac{\varrho n}{e_T^{(0)}} \right) (1 - \beta^{N_1}) - \frac{\beta \log_2 \beta}{1 - \beta} \left[1 - N_1 \beta^{N_1-1} + (N_1 - 1) \beta^{N_1} \right] \right\} \\
& + (N_2 + 2\varrho) (\chi_{EC} + f_o) \\
& + 2\varrho \left[1 + \log_2 \frac{n}{2} \right] (\chi_{EC} + f_o) \\
& + \chi_{EC} (\tilde{g}_{EC} + g_{auth}) + f_o . \tag{260}
\end{aligned}$$

Since parity information is exchanged over a classical channel, and since we assume that all classical communications are intercepted and correctly interpreted by Eve, we must therefore assume that some information about the strings shared by Alice and Bob is leaked to Eve during the error correction phase. The degree to which this protocol leaks such information is an important characteristic of the protocol. As was seen in Section 3.1.3, the theoretical lower bound on this leakage is given by (*cf* eq. (42))

$$q_{\min} = nh \left(\frac{e_T^{(0)}}{n} \right) , \tag{261}$$

where h is the binary entropy function. We estimate the leakage q_p associated with our error correction protocol by counting the parity bits that were exchanged during error correction. During each iteration of the first step, 1 bit of parity is leaked for each of the $J^{(i)}$ blocks, and an additional $\lceil \log_2 k^{(i)} \rceil$ bits is leaked for each block in which an error was detected.

During the second step, one bit is leaked for each iteration that does not reveal an error and $\lceil 1 + \log_2 \frac{n}{2} \rceil$ bits are leaked for each iteration that does reveal an error. The total is thus

$$q_p = \sum_{i=1}^{N_1} \left(J^{(i)} + \log_2 k^{(i)} e_f^{(i)} \right) + N_2^{(n)} + N_2^{(f)} \left\lceil 1 + \log_2 \frac{n}{2} \right\rceil. \quad (262)$$

Using eqs. (257), (258, (386), and (390) , this becomes

$$q_p \simeq 2 \frac{e_T^{(0)} - 2\varrho}{1 - e^{-2\varrho}} + e_T^{(0)} \left\{ \log_2 \left(\frac{\varrho n}{e_T^{(0)}} \right) (1 - \beta^{N_1}) - \frac{\beta \log_2 \beta}{1 - \beta} [1 - N_1 \beta^{N_1-1} + (N_1 - 1) \beta^{N_1}] \right\} + (N_2 + 2\varrho) + 2\varrho \left\lceil 1 + \log_2 \frac{n}{2} \right\rceil. \quad (263)$$

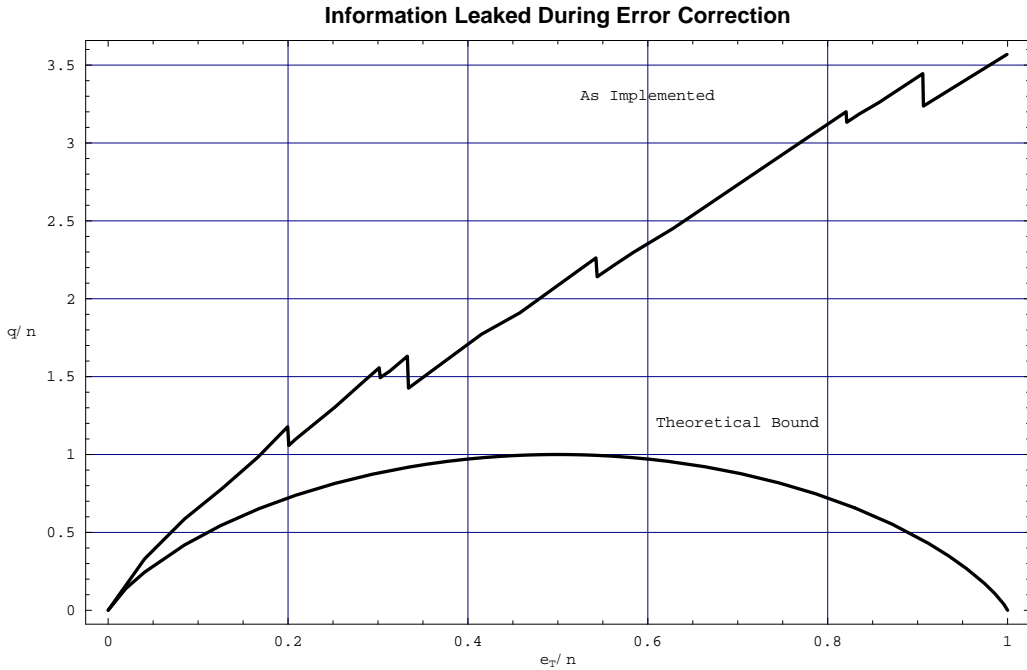


Figure 17: Information Leaked During Error Correction

Figure 17 is a comparison of the information leaked by the protocol to the theoretical minimum for error correction parameters $\varrho = 0.5$ and $N_2 = 30$ and for a sifted string blocksize

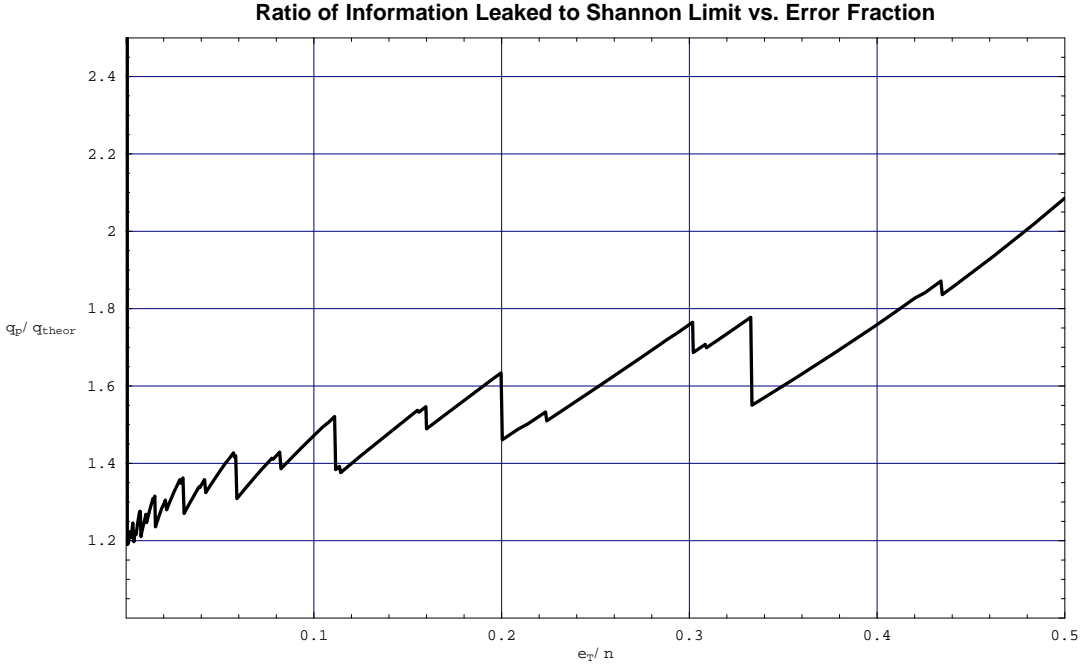


Figure 18: Ratio of Information Leaked to Shannon Limit *versus* Error Fraction

$n = 2 \times 10^5$ bits. The results are plotted as a function of the error fraction $e_T^{(0)}/n$. As expected, the theoretical minimum represents a lower bound for the result predicted for the protocol. The ratio of the predicted leakage to the theoretical minimum, q_p/q_{\min} , is shown in Figure 18. The ratio diverges at very low error rates due to the fact that some parity bits are exchanged even if there are no errors in the string. (This divergence is not apparent on the scale of the figure.) The discontinuities in the curve occur at points where an increase in the error rate causes additional iterations at some point in the protocol. For error fractions between 2% and 10%, the ratio fluctuates between about 1.2 and 1.5, indicating that the actual protocol can be expected to leak up to 50% more information than the theoretical minimum.

Figure 19 shows the ratio q_p/q_{\min} as a function of ϱ for an error fraction $e_T^{(0)}/n$ of 1%. This indicates that a choice of ϱ in the neighborhood of 0.5 results in minimum leakage of information relative to the theoretical minimum for this choice of sifted string size and error fraction.

Privacy Amplification Phase

The general scheme of privacy amplification is described in [24] and [60]. The hash functions map a sifted, error corrected string of length n to a string of length L , where

$$L \equiv n - e_T^{(0)} - q - t - \nu - a - g_{pa} . \quad (264)$$

The resulting string is shorter than the sifted string by the number of bits that Eve may have

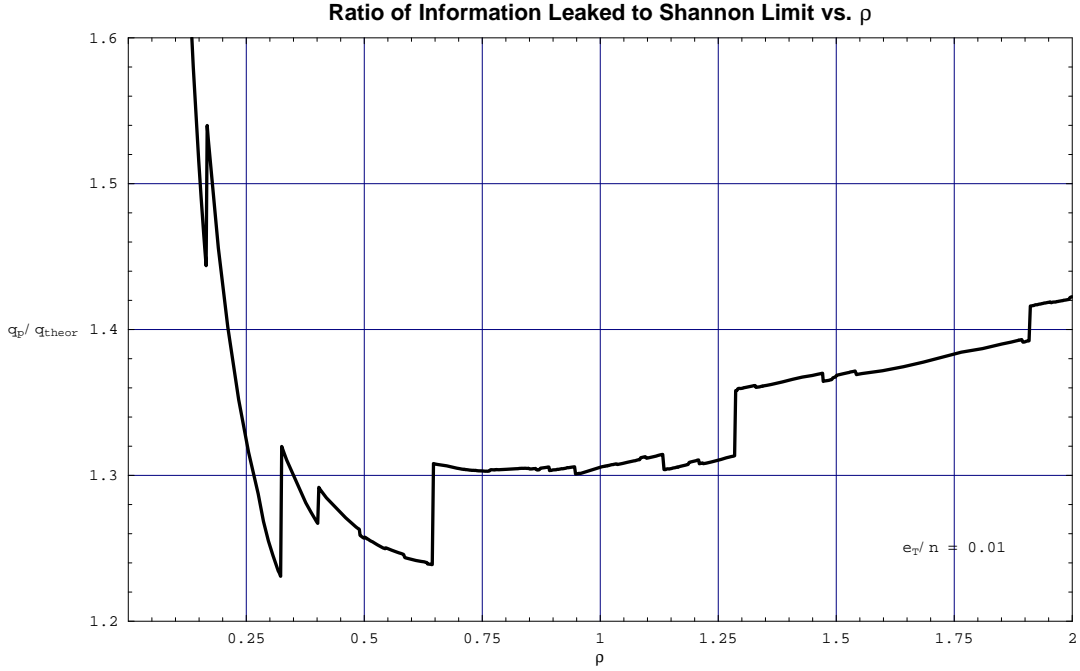


Figure 19: Ratio of Information Leaked to Shannon Limit *versus* ρ

obtained by listening to the classical discussion, plus an additional parameter g_{pa} . In [24] it is shown that the expected information, I , that Eve can retain about the hashed string is bounded by a quantity that can be made very small by a suitable choice of g_{pa} :

$$I \leq \frac{2^{-g_{pa}}}{\ln 2} . \quad (265)$$

Hash functions appropriate for privacy amplification are described by Carter and Wegman [60]. The class of hash functions used for authentication and equivalence checking is not practical for privacy amplification due to the much larger size of the output string. The authentication hash functions are designed to produce output strings that are no more than half as long as the input string. Since we wish to retain as much information as possible, it is clearly advantageous to use hash functions that can produce an output string that is nearly as long as the input string. Furthermore, recall that the length of the index for choosing an authentication hash function is

$$w(g, c) = 4(g + \log_2 \log_2 c) \log_2 c \quad (266)$$

where c and g are the lengths of the input and output strings, respectively. For purposes of authentication and error correction, an output string of length $g \leq 50$ is adequate, and the length of the index is relatively short even for long input strings due to the logarithmic

factors. In privacy amplification, where the output string is nearly as long as the input string, this index is roughly 4 times as long as the string to be hashed. In contrast, the hash functions suitable for privacy amplification are described by two parameters, each as long as the input string, so that the total size of the index is only twice as long as the input string. Since the index represents shared secret bits that must be sacrificed in order to achieve privacy amplification, it is desirable to use the class of hash functions that requires the shorter index. The Carter-Wegman functions described in [60] are a good choice for privacy amplification since they are capable of producing keys nearly as long as the input and since they require shorter indices for their definition given the large size of the output strings.

The error correction phase guarantees that the strings Alice and Bob have obtained are identical to a high probability. Bob and Alice implement privacy amplification by agreeing on an index and applying the hash functions separately to their strings. The resulting strings are identical and secret in the sense of privacy amplification (*cf* eq.(265)). Note that the sifting protocol itself supplies random strings of sufficient length to define the required hash index. Bob's choice of basis for the $2n$ pulses he receives is one such source. Another alternative is to compute the parities of the indices Bob sends to Alice by which he identifies which pulses were detected by his equipment.

The privacy amplification protocol requires no communications between Alice and Bob, as described in Section 3.1.6 above. The security parameter g_{pa} is an additional secrecy cost incurred due to privacy amplification, but privacy amplification entails no additional authentication cost.

Total Continuous Authentication Cost

The total continuous authentication cost is the number of bits from each block of sifted bits that need to be sacrificed during the processing of the subsequent block to provide authentication and equivalence checking as described above. Collecting the contributions from eqs.(220), (221), (222), (223), (242), (243), (244), (245), (246), (247), and (248) the result is the following sum of six terms:

$$\begin{aligned}
a &= a(n, m) \\
&= 4\{g_{auth} + \log_2 \log_2 [2n(1 + \log_2 m)]\} \log_2 [2n(1 + \log_2 m)] \\
&\quad + 4[g_{auth} + \log_2 \log_2 (2n)] \log_2 (2n) \\
&\quad + 4(g_{EC} + \log_2 \log_2 n) \log_2 n \\
&\quad + 4(g_{auth} + \log_2 \log_2 g_{EC}) \log_2 g_{EC} \\
&\quad + \tilde{g}_{EC} \\
&\quad + 4(g_{auth} + \log_2 \log_2 \tilde{g}_{EC}) \log_2 \tilde{g}_{EC} \\
&= \tilde{g}_{EC} + \sum_{j=1}^5 w_j(g_j, c_j(\mu)) ,
\end{aligned} \tag{267}$$

as in eq.(152).

For example, if we take $m = 2 \times 10^8$ bits, and $n = 2 \times 10^5$ bits to be the processing block lengths of the raw and sifted strings, and if we set all security parameters g_i to 30, we obtain a total authentication cost of 9.5×10^3 bits per processing block. For a laser pulse repetition rate of 10 GHz, $\tau = 10^{-10}$ sec, and the rate at which secret bits are consumed is

$$\frac{a}{m\tau} = 4.7 \times 10^5 \text{ bits/second} . \quad (268)$$

4.4.2 System Load: Total Communications Requirements

The total communications load is the number of bits transmitted in either direction over the classical communications channel to support the sifting and error correction protocols for a single block of data. Combining eqs.(226) and (255), the result for the Bob-to-Alice link is

$$\begin{aligned} \mathcal{C}_{B \rightarrow A} \simeq & \left(1 + \frac{f_o}{m_p}\right) [\chi_{EC} 2n (1 + \log_2 m)] \\ & + (\chi_{EC} g_{auth} + f_o) \\ & + \sum_{i=1}^{N_1} \left[\left(1 + \frac{f_o}{m_p}\right) \chi_{EC} J^{(i)} + \lceil \log_2 k^{(i)} \rceil \left(1 + \frac{f_o}{m_p}\right) \chi_{EC} e_f^{(i)} \right] \\ & + N_2^{(n)} (\chi_{EC} + f_o) + N_2^{(f)} \lceil 1 + \log_2 \frac{n}{2} \rceil (\chi_{EC} + f_o) \\ & + \chi_{EC} (g_{EC} + g_{auth}) + f_o , \end{aligned} \quad (269)$$

and the result for the Alice-to-Bob link is

$$\begin{aligned} \mathcal{C}_{A \rightarrow B} \simeq & \left(1 + \frac{f_o}{m_p}\right) (\chi_{EC} 2n) \\ & + (\chi_{EC} g_{auth} + f_o) \\ & + \sum_{i=1}^{N_1} \left[\left(1 + \frac{f_o}{m_p}\right) \chi_{EC} J^{(i)} + \lceil \log_2 k^{(i)} \rceil \left(1 + \frac{f_o}{m_p}\right) \chi_{EC} e_f^{(i)} \right] \\ & + N_2^{(n)} (\chi_{EC} + f_o) + N_2^{(f)} \lceil 1 + \log_2 \frac{n}{2} \rceil (\chi_{EC} + f_o) \\ & + \chi_{EC} (\tilde{g}_{EC} + g_{auth}) + f_o . \end{aligned} \quad (270)$$

For large m and n , the sifting transmission from Bob to Alice is by far the largest term. Eqs. (257), (258), (386), and (390) can be used to express these in terms of N_2 , $e_T^{(0)}$, and ϱ if desired. The throughput requirement \mathcal{R}^{comm} is found by dividing the total load by the transmission time $m\tau$ for a single block on the quantum channel:

$$\mathcal{R}^{comm} = \frac{\mathcal{C}}{m\tau} . \quad (271)$$

Evaluated for reasonable, conservative, values of the parameters ($m = 2 \times 10^8$ bits, $n = 2 \times 10^5$ bits, $e_T^{(0)} = 2 \times 10^3$ bits, $\tau = 10^{-10}$ sec, $m_p = 1000$ bits, $\chi_{EC} = 2$, $f_o = 400$ bits, $\varrho = 0.5$, $g_{EC} = \tilde{g}_{EC} = g_{auth} = N_2 = 30$), we obtain a throughput requirement of

$$\mathcal{R}^{comm} \Big|_{Bob-to-Alice} = 1600 \text{ Mbps} \quad (272)$$

for the Bob-to-Alice link, and

$$\mathcal{R}^{comm} \Big|_{Alice-to-Bob} = 60 \text{ Mbps} \quad (273)$$

for the Alice-to-Bob link.⁶⁵

Figures 20, 21, 22, and 23 show the communication load between Bob and Alice. The dependence on n is roughly linear for fixed m . The dependence on m is relatively weak for large m and for a fixed ratio n/m .

4.4.3 System Load: Total Computational Requirements

In this section we investigate the computational resources that are required to implement the sifting, error correction, and privacy amplification algorithms we have been discussing. In principle, the processing could be done with special purpose hardware that is designed to perform the necessary operations as efficiently as possible. In this analysis, however, we will assume that the operations are to be carried out using a general purpose computer. As the instruction set of a general purpose computer is not particularly well suited to operations such as finding the parities of long bit strings, the results of the analysis should represent a conservative upper bound for the processing requirements as compared to what is achievable with special purpose devices.

We first analyze the algorithms for sifting, error correction, and privacy amplification into processing steps of a size suitable for implementation as assembly language subroutines. The steps for Bob's computation that require iteration on the entire string are:

Pack received polarizations and indices

$$(2n(1 + \log_2 m) \text{ bits})$$

⁶⁵ These values of the required communications bandwidth do not exceed the capabilities of currently available optical classical communications technology. As we will see in Section 5.3.2 below, the specific numerical parameter values chosen in this example correspond to the case of various free space quantum cryptography systems set up between a LEO satellite node and a ground-based (or airplane-based) node. Existing classical optical satcom links operating at 1550 nanometers wavelength providing duplex communications at rates ranging from 51 Megabits per second to 1.244 Gigabits per second between a ground station and GEO satellite have been developed [49]. Thus it is clear that these communications requirements, in particular the 1.6 Gigabits per second requirement, can be satisfied for a LEO satellite link, for which there is much less attenuation than for the GEO satellite link. As discussed below, it turns out that there are in fact *smaller* classical communications bandwidth requirements than those given in eqs.(272) and (273) for a free space quantum cryptography system between a ground station and a GEO satellite, which can easily be accommodated by existing communications systems, and the same is true for fiber-optic cable quantum cryptography systems.

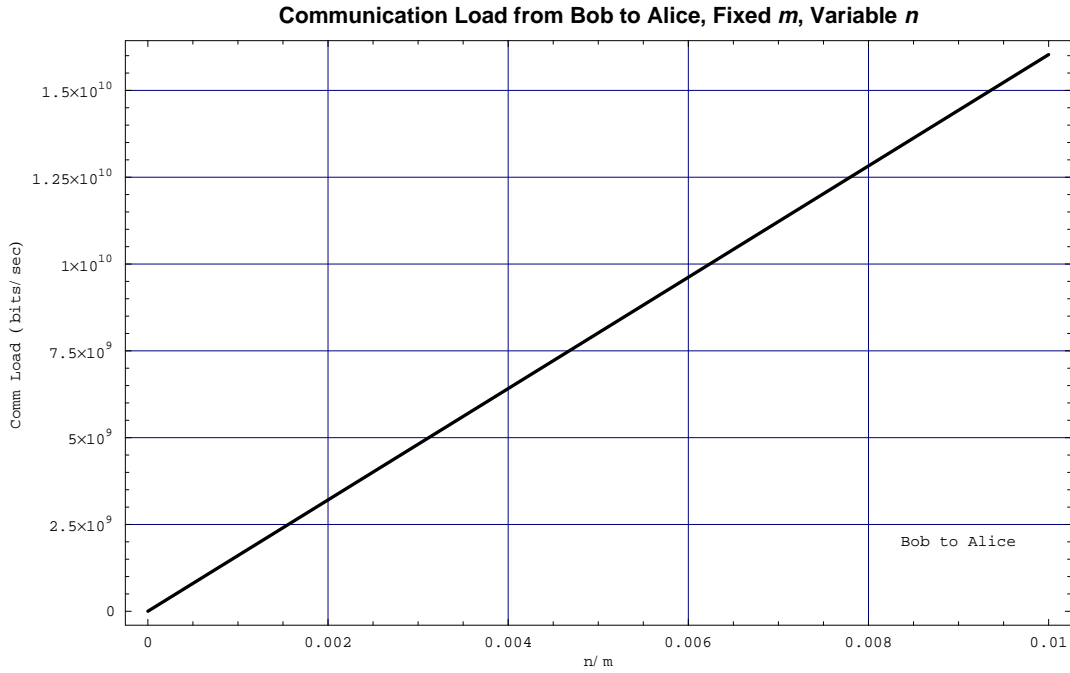


Figure 20: Communication Load from Bob to Alice, Fixed m , Variable n

- Compute authentication tag
($2n(1 + \log_2 m)$ bits in, g_{auth} bits out)
- Unpack Alice's response
($2n$ bits)
- Check authentication tag from Alice
($2n$ bits in, g_{auth} bits out)
- Sift bit string
($2n$ bits in, n bits out)
- Perform random shuffle
(n bits)
- Compute block parities for error detection and correction step
(N_1 iterations, n bits processed)
- Perform bisective search
(N_1 iterations, each performing $e_f^{(i)}$ searches, each search involving $k^{(i)}$ bits)
- Extract blocks for validation step
($N_2^{(n)} + N_2^{(f)}$ iterations, n bits processed)
- Compute block parities for validation
($N_2^{(n)} + N_2^{(f)}$ iterations, $\frac{n}{2}$ bits processed)
- Perform bisective search
($N_2^{(f)} = e_T^{(r)}$ blocks of size $\frac{n}{2}$)
- Pack error corrected string
(n bits)

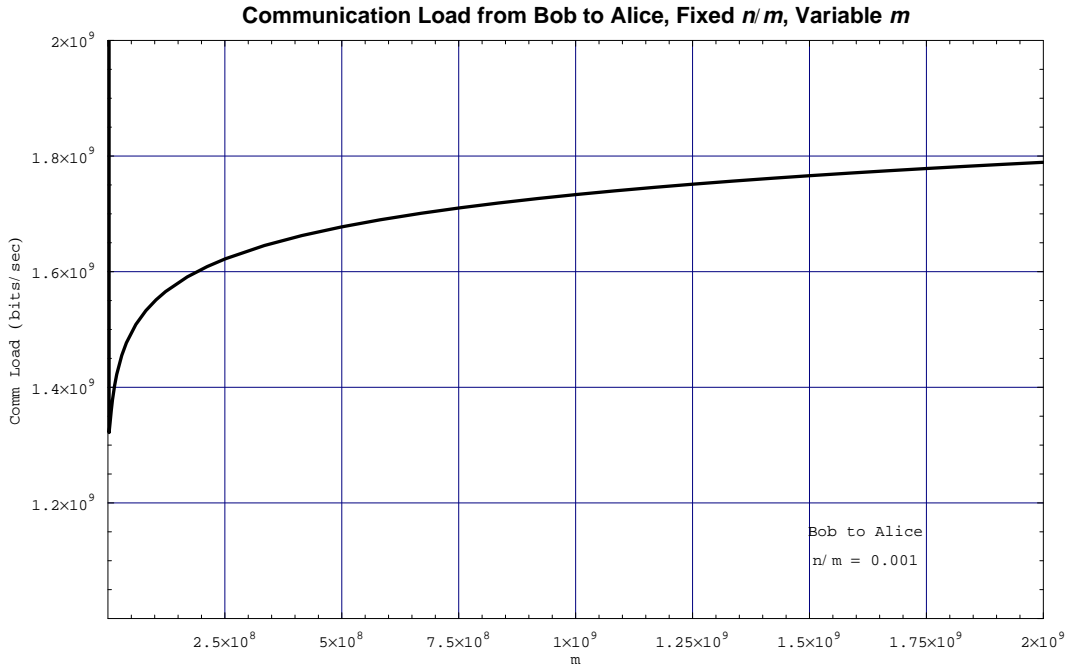


Figure 21: Communication Load from Bob to Alice, Fixed n/m , Variable m

Compute equivalence checking tag

(n bits in, g_{EC} bits out)

Get privacy amplification key

($2n$ bits)

Compute privacy amplification tag

(n bits in, $L \approx n$ bits out)

Bob's computational load represents an approximate upper bound for Alice's computational load, since Alice does not need to compute an equivalence checking tag, but otherwise has to perform computations of comparable complexity. We may thus restrict our discussion to Bob's computations without loss of generality.

We obtain a rough estimate of the total computational load by addressing the computational loads associated with each of the above steps. First, we assume that the operations of packing, unpacking, sifting, block extraction, bisective search, and parity computation require 25 assembly language statements (or operations) per bit processed on each iteration. Sections of assembly code developed to implement a subset of these operations indicate that this should consistently overestimate the required computations. For example, the code segment for computing parity included in the appendix requires only 5 operations per iteration. The intent of this analysis is to use these conservative estimates for most of the steps in the computation, but to analyze more carefully those parts of the computation whose contribution to the rates is more sensitive to the block size. (Note that computations with loads that are

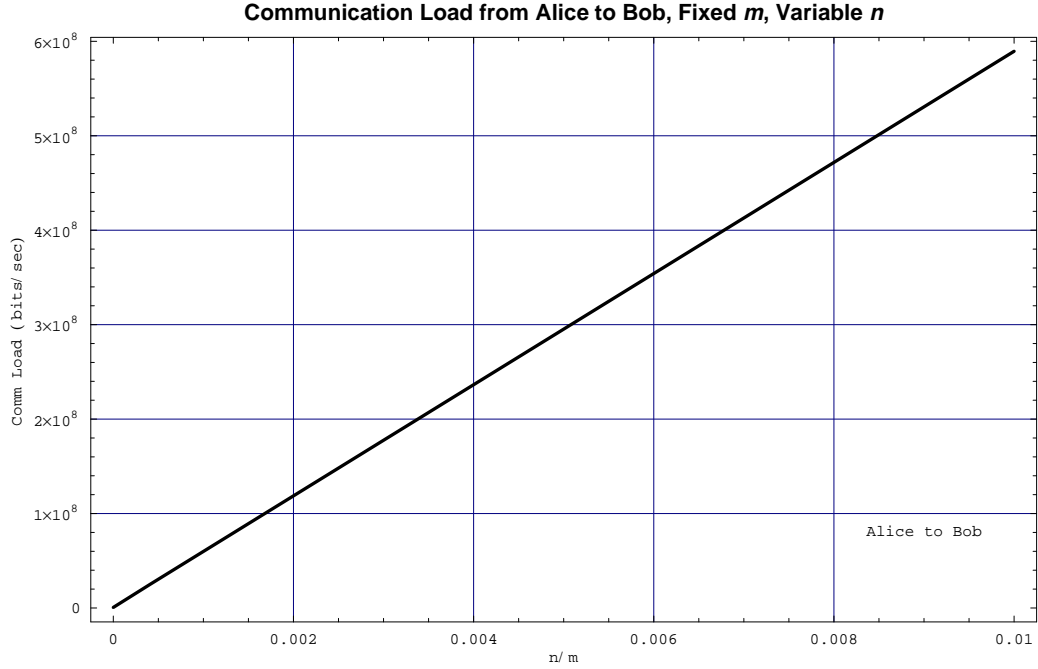


Figure 22: Communication Load from Alice to Bob, Fixed m , Variable n

strictly linear in the block size lead to rates that are independent of the blocksize, since the amount of time available for computation for each block is proportional to the block size.)

In applying this assumption to the above steps, we note that the initial block parity calculations for the error detection and correction step process every bit in the string. The bisective searches process every bit in the substring under examination, except for 1 bit. (For the purposes of this analysis, we simply include the extra bit.) The initial block parity calculations for the validation step process half of the bits in the string.

The estimate of the load for the bisective search in the error detection and correction step involves a summation over the iterations internal to the step:

$$\mathcal{L}_B^{(EDC,BS)} = 25 \cdot \sum_{i=1}^{N_1} e_f^{(i)} k^{(i)} . \quad (274)$$

This may be expressed in terms of fundamental parameters by using results from the appendix “Statistical Results for Error Correction.” We obtain:

$$\begin{aligned} \mathcal{L}_B^{(EDC,BS)} &= 25 \cdot \sum_{i=1}^{N_1} (1 - \beta) \beta^{i-1} e_T^{(0)} \frac{\varrho n}{\beta^{i-1} e_T^{(0)}} \\ &= 25 \cdot \varrho n (1 - \beta) N_1 \end{aligned}$$

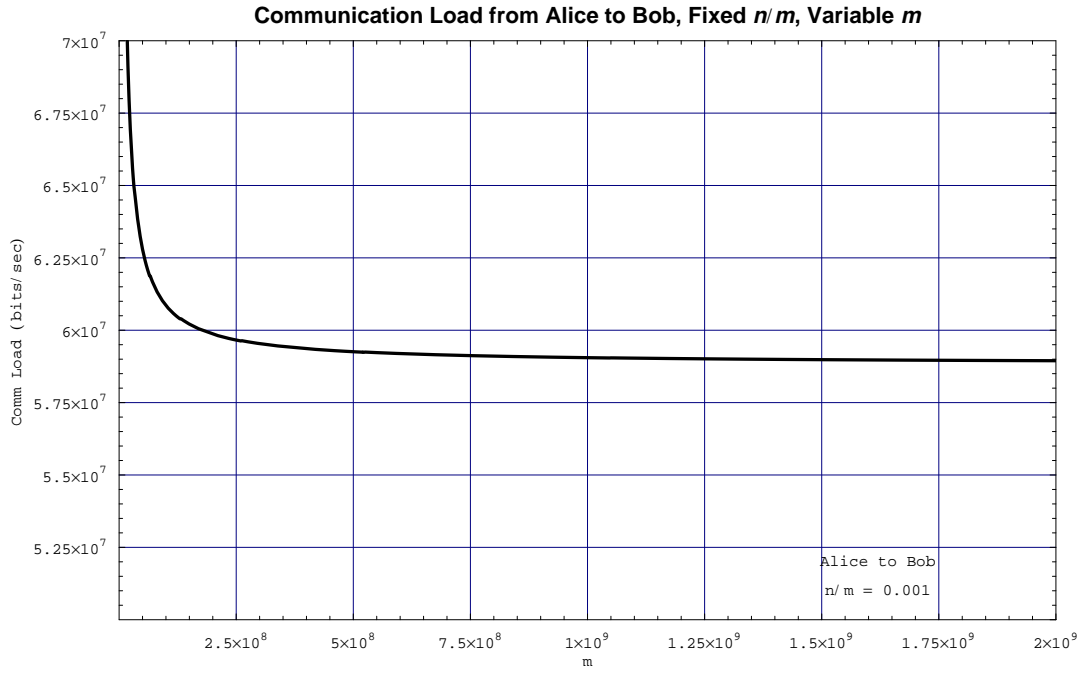


Figure 23: Communication Load from Alice to Bob, Fixed n/m , Variable m

$$\begin{aligned}
 &= 25 \cdot \varrho \left(1 - \frac{2\varrho - 1 + e^{-2\varrho}}{2\varrho} \right) \frac{\log_2 \frac{2\varrho}{e_T^{(0)}}}{\log_2 \beta} n \\
 &= 12.5 \left(1 - e^{-2\varrho} \right) \frac{\log_2 \frac{2\varrho}{e_T^{(0)}}}{\log_2 \beta} n \\
 &= 12.5 \left(1 - e^{-2\varrho} \right) N_1 n . \tag{275}
 \end{aligned}$$

The computations for the authentication and error correction tags are relatively complex, and require more detailed attention. As described by Wegman and Carter, [36], the algorithm proceeds by partitioning the input string into substrings of length $2s$, where

$$s = g_{auth} + \log_2 \log_2 c , \tag{276}$$

and c is the length of the input string. An auxiliary hash function is applied to each of the substrings resulting in a set of strings of length s . The results are concatenated and repartitioned into substrings of length $2s$. The process is repeated until the concatenated string is of length s . The final tag is taken from the lower order bits of this string. The hash function is applied $\lceil \frac{c}{2s} \rceil$ times in the first iteration. The length of the input string is reduced by one half in each successive iteration, so that the hash function is applied $\lceil \frac{c}{2^i s} \rceil$ times during the i th iteration. The process continues until

$$\frac{c}{2^{i_{max}} s} \leq 1 , \quad (277)$$

or, equivalently,

$$i_{max} \geq \log_2 \frac{c}{s} . \quad (278)$$

The total number of times the hash function is applied is then

$$n_{hash} \simeq \sum_{i=1}^{\log_2 \frac{c}{s}} \frac{c}{2^i s} . \quad (279)$$

We obtain a rough upper bound by extending the summation to infinity, yielding the simple estimate

$$n_{hash} \simeq \frac{c}{s} . \quad (280)$$

The hash function itself involves the multiplication and an addition of integers encoded as bit strings of length $2s$. For $g \sim 30$ and $c \sim 10^{12}$ bits, we have, using eq. (276),

$$2s = 2g + 2 \log_2 \log_2 c \sim 70 . \quad (281)$$

This is slightly longer than 64 bits, so we will assume that the integer operations operate on double words. Each application of the hash function requires three operations: a substring of length $2s$ is extracted from the string, the hash operation is applied to the substring, and the substring is inserted into the output string. Assembly code segments for extracting the substring and applying the hash operation are presented in the appendix. These segments contain 26 and 43 instructions respectively. The code for inserting the result in the output string should be roughly as complex as the extraction and will thus require an additional 26 operations. If we add 15 instructions to handle the loop control, we obtain a total of 110 operations for each application of the hash operation. The resulting estimate of the computational load for the authentication and equivalence checking steps is then

$$\mathcal{L}_B^{auth} = \mathcal{L}_B^{EC} \simeq 110 \cdot \frac{c}{s} . \quad (282)$$

Potentially the largest contribution to the computational load is the privacy amplification hash function. This is due largely to the presence of nested loops in the code that result in a

quadratic dependence on the size of the sifted string, n . The assembly code for this function is given in the appendix. The resulting load is given by⁶⁶

$$\mathcal{L}_B^{PA} \approx 43 \left(\frac{n}{w} \right) + 46 \left(\frac{n}{w} \right)^2 . \quad (283)$$

This represents the number of instructions required to perform the hash computation for a single block of sifted, error corrected bits of length n . The parameter w is the wordsize of the processor in bits.

We find the total load by summing the contributions from each of the individual steps:

$$\begin{aligned} \mathcal{L}_B &\leq \mathcal{L}_B^{(0)} \\ &+ 25 \cdot (2n(1 + \log_2 m)) \\ &+ 110 \cdot \frac{2n(1 + \log_2 m)}{g_{auth} + \log_2 \log_2 [2n(1 + \log_2 m)]} \\ &+ 25 \cdot 2n \\ &+ 110 \cdot \frac{2n}{g_{auth} + \log_2 \log_2 (2n)} \\ &+ 25 \cdot 2n \\ &+ 25 \cdot n \\ &+ N_1 \cdot 25 \cdot n \\ &+ 12.5 \left(1 - e^{-2\varrho}\right) N_1 n \\ &+ \left(N_2^{(n)} + N_2^{(f)}\right) \cdot 25 \cdot n \\ &+ \left(N_2^{(n)} + N_2^{(f)}\right) \cdot 25 \cdot \frac{n}{2} \\ &+ e_T^{(r)} \cdot 25 \cdot \frac{n}{2} \\ &+ 25 \cdot n \\ &+ 110 \cdot \frac{n}{g_{EC} + \log_2 \log_2 n} \\ &+ 25 \cdot (2n) \\ &+ 43 \cdot \left(\frac{n}{w} \right) + 46 \cdot \left(\frac{n}{w} \right)^2 . \end{aligned} \quad (284)$$

Each term corresponds to one of the steps in the processing. $\mathcal{L}_B^{(0)}$ is the “non-iterative”

⁶⁶ The authors of [60] introduce an alternative class of hash functions the computational complexity of which is linear in the key size. Use of this class of hash function in privacy amplification could result in a moderate reduction in the computational load (as computed in eq.(289) below), and/or allow for a significant increase in the allowed processing block size [61]. In this case the block size is limited by memory requirements and the $n(1 + \log_2 m)$ term in eq.(284).

portion of the load, representing code that executes once for each block of data processed. (Note that there may be iterative loops in this code as well. The point is that these loops do not represent processing that iterates bit-by-bit through the string.) We simplify the result by collecting terms, noting from eq.(368) that the residual error count after error correction and detection is given approximately by

$$e_T^{(r)} \simeq 2\varrho . \quad (285)$$

We also drop the double log terms in the denominators, thus replacing those terms by larger quantities. The resulting expression is

$$\begin{aligned} \mathcal{L}_B \leq & \mathcal{L}_B^{(0)} \\ & + \left(50 + \frac{220}{g_{auth}} \right) n (1 + \log_2 m) \\ & + \left[200 + 25N_1 + 12.5 \left(1 - e^{-2\varrho} \right) N_1 + 25\varrho + 37.5 \left(N_2^{(n)} + N_2^{(f)} \right) \right. \\ & \quad \left. + \frac{43}{w} + \frac{220}{g_{auth}} + \frac{110}{g_{EC}} \right] n \\ & + \frac{46}{w^2} n^2 . \end{aligned} \quad (286)$$

It is instructive to evaluate this expression for the same example used in finding the communications load. We take the non-iterative contribution to the load to be substantial:

$$\mathcal{L}_B^{(0)} = 10^6 \text{ operations per block} . \quad (287)$$

We take the wordsize of the processor to be 64 bits. The other parameters are as before ($m = 2 \times 10^8$ bits, $n = 2 \times 10^5$ bits, $e_T^{(0)} = 2 \times 10^3$ bits, $\tau = 10^{-10}$ sec, $\varrho = 0.5$, $g_{EC} = g_{auth} = N_2 = 30$). The resulting estimate of the load is 1.1 billion operations per block. The quadratic term contributes 450 million operations to the total. Of the other terms, the dominant contributions are the term in $N_2^{(n)} + N_2^{(f)}$, which is due to parity checks and random block extractions during the validation step of error correction, and the term in $(1 + \log_2 m)$, which is due to sifting. Note that the non-iterative overhead load is negligible in comparison with the other contributions. This indicates that a substantial amount of “bookkeeping” code can be included along with the core software that is essential to arriving at the final secret key without significantly affecting the processing requirements. One of the uses of eq.(286) is to establish a load budget for such code during software design and implementation to ensure that the bulk of the processing resources are available for the core software functions.

The computation rate \mathcal{R}_B^{comp} required to support key distribution is found by dividing the load per block by $m\tau$, the time required to transmit one block over the quantum channel:

$$\mathcal{R}_B^{comp} = \frac{\mathcal{L}_B}{m\tau} . \quad (288)$$

Applying this to our preceding example yields an estimated processing rate requirement of

$$\mathcal{R}_B^{comp} = 56 \text{ billion operations/sec} . \quad (289)$$

This is rather high for a single general purpose processor, but should be achievable in a parallel architecture in which each block of the input data is allocated to a single processor as it becomes available. Recall also that general purpose computers are far from optimal for this type of operation. Most of the processing steps involving the packing and unpacking of the bits would not be necessary in a special purpose device, and many of the other processing steps, notably block parity computations and random selection of substrings, could be accomplished much more efficiently using special purpose hardware.

5 High-Speed Quantum Cryptography

In this section of the paper we analyze the possibility of achieving very high data throughput rates for a QKD system. We first discuss essential elements that such a system requires, and then make use of the analysis in the preceding sections of effective secrecy capacity, system losses and loads to deduce universal maximal rates achievable in QKD.

5.1 Methods to Achieve High-Speed Quantum Cryptography

There are three different techniques that may be applied to achieve high data throughput values:

- Reducing the value of the bit cell period, τ , in the effective secrecy capacity
or
- Combining some number of quantum bit transmitting setups together, *i.e.*, combining some number of Alice systems together, by multiplexing the outputs into a common bit stream
or
- Applying both of the above techniques together.⁶⁷

The optimal effective secrecy rate \mathcal{R}_{opt} is inversely proportional to the bit cell period τ . For the first technique identified above, in decreasing the size of the bit cell period to increase the effective rate we need to ensure that Bob's detector apparatus can count incoming photons at a correspondingly higher speed as well. A decrease in the bit cell period means that the source laser must operate at a higher pulse repetition frequency (PRF) than before, so we must also make use of pulsed lasers with the necessary stability to operate at the required PRF values. Furthermore, we must ensure that the various opto-electronic components and switches can likewise operate at the required high frequencies. The collection of various components, all operating at very high repetition frequencies, must be properly synchronized together for the protocol to be properly executed. In addition, real-time data recording of all necessary quantities must be taken at the required high rate. We discuss in the sections below various practical approaches to each of these critical requirements on a high speed quantum cryptography system. All of them are requirements that must be satisfied if we are to increase the rate by making the bit cell period smaller.

⁶⁷ The throughput rate could also in principle be increased by employing a quantum bit generating device at the Alice end that, through whatever means, does not generate any multiple particle states. In this idealized case the multi-photon privacy amplification function ν employed by Alice and Bob could be set to $\nu = 0$, which would result in a significant increase in the throughput rate. If the qubit source produced multiple states, but with a smaller likelihood per bit cell than for the Poisson distribution considered in detail in Section 3 of this paper, the resulting required value for ν would lie between 0 and the values of the expressions found in eqs.(141) through (151), resulting in an improved throughput rate.

The second technique identified above, the multiplexing together of a number of output streams into a common transmission, leads us to different concerns. As deduced in Section 4.4.3 above, the execution of the QKD protocol imposes calculable requirements on the necessary computing resources, and for a system operating at a high speed, this is already a significant burden for a single Alice device. The required computing resources will be even larger for several Alices operating in tandem. As discussed briefly in Section 3.1.7 above, for the multiplexing of several data streams to succeed we must ensure that we are not exceeding the computing capacity available to the system. In Section 5.2.6 below we work out how the system throughput can be increased while taking into account these computing requirements constraints.

5.2 System Components and Constraints

In this section we address the practical capabilities of a proposed realistic high-speed quantum cryptography system, taking into account engineering constraints on the various system components. Our purpose here is to illustrate with specific examples that such high-speed systems are in principle *feasible*. These examples of specific components are chosen to support the argument that it is possible to design and build such a system entirely out of currently available, commercially produced equipment, with the exception of the required high-speed photon detectors. For these, we have identified and analyzed the possibilities inherent in a promising new approach to high-speed photon detection, as described in Section 5.2.1 below.⁶⁸ The overall design of the Alice and Bob systems, respectively, are illustrated in Figures 24 and 25. The general structure of both systems is based on previously proposed design concepts [62, 32, 3]. The primary innovation here is the proposed very high speed of operation of the system, which we briefly sketch now. The basic source of the quantum bits is a high-speed pulsed laser producing pulses at a PRF of 10 GHz, along with a second synchronized laser producing a bright timing pulse. In the Alice system the random choices of both polarization bases and states are implemented with two suitable high speed random number generators, which operate on a set of three high-speed Mach-Zender interferometers, the first intended to select the polarization basis, and the second and third to select the specific polarization states. The outputs are balanced by being fed through variable attenuators, after which they are passed through appropriate filters and put into states of definite polarization. These polarized streams are then combined into a common output stream to be transmitted through the quantum channel to the Bob system. The necessary real-time records of all the random selections for bases and states are obtained *via* suitable high-speed data recording and processing devices, for which appropriate de-multiplexing techniques are required, constrained by the speed of available computer data bus rates. The Bob system is purely passive, so that all basis and state selection is accomplished, purely randomly, solely *via* optical components. After being passed through a solar filter, the received stream of pulses is separated into the data and timing parts by a dichroic beamsplitter, after which

⁶⁸ We do not specifically advocate the use of the *particular* components described herein as necessarily comprising the “best” approach to the problem of building a high-speed quantum cryptography system.

High-Speed Alice

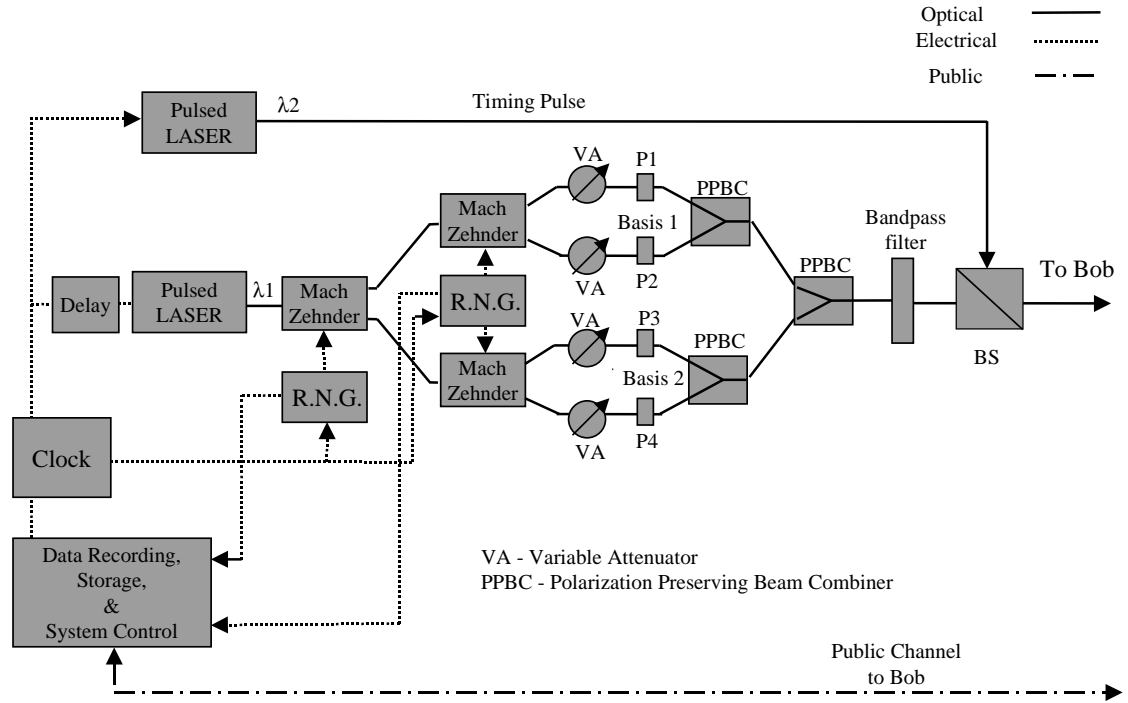


Figure 24: Block Diagram for Alice System

the cipher stream is passed through a passive beamsplitter. The “basis stream” outputs are sent through two additional polarizing beamsplitters, after which the four separated streams are then focussed onto four high-speed photon detectors. As with the Alice system, accurate real-time, high-speed recording of the random choices of basis and state are obtained *via* a suitable de-multiplexing scheme.

The Significance of the 10 GHz System Clock Speed

What is the significance of the 10 GHz system clock speed we have discussed above? We are interested in exploring conditions and constraints that will allow quantum cryptography to be implemented at high data throughput rates. The overriding requirement for the success of

High-Speed Bob

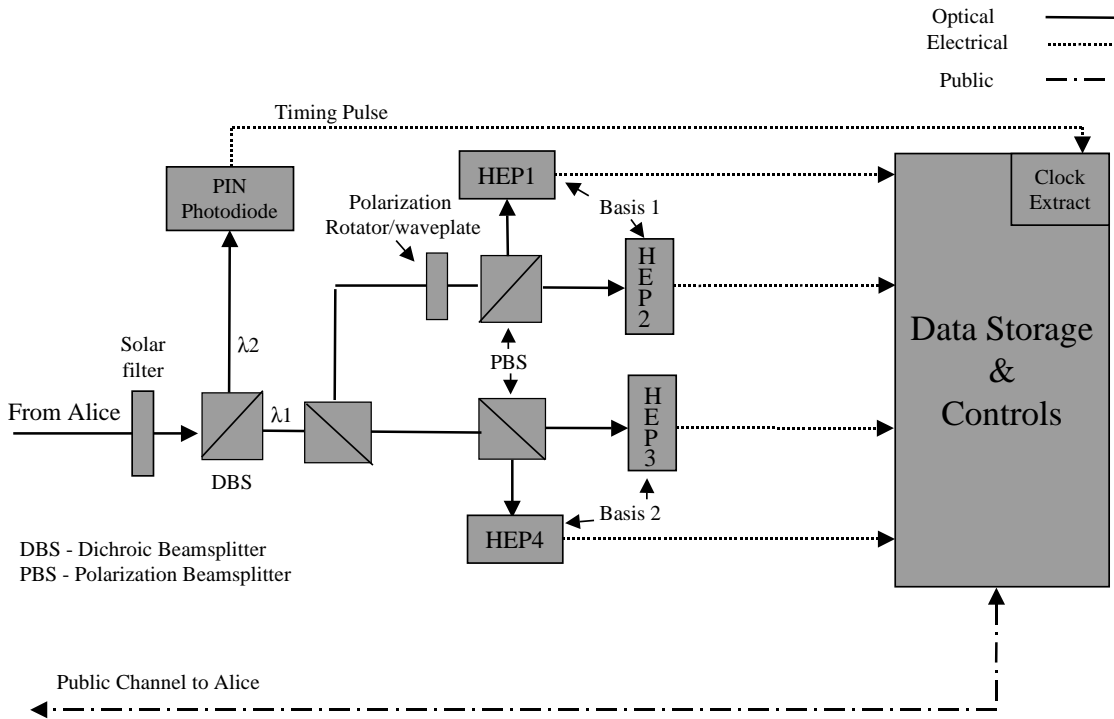


Figure 25: Block Diagram for Bob System

such a scheme is to employ robust, stable equipment built from high-speed components. As outlined above, this can be achieved by exploiting recent developments in high-speed optical communications technology, along with the proposed use of a novel experimental technique for high-speed single photon counting that employs cooled thin-film devices. There are a variety of commercially available high-speed components for optical classical communications (*i.e.*, conveying information in pulses containing very many photons) with 10 GHz throughput. This motivates the possibility of carrying out quantum cryptography at the same basic clock rate. We have chosen the clock speed of 10 GHz as representative of what can be achieved in classical optical communications systems solely with commercially available equipment. However, in classical optical communications it is not necessary to count individual photons, and in particular not at a rate of 10 GHz. Thus the only additional

component required for quantum cryptography at such a clock speed beyond that which is commercially available is a suitable means of achieving high-speed single photon detection. (Higher system clock speeds would require additional components that are not yet commercially available.) Of course, the actual *throughput* rate that can be achieved will be considerably lower than the basic system clock rate, as expected based on the analysis in Sections 3 and 4 and as discussed with specific examples in Section 5.3 below.

In the sections below we describe in more detail the various high-speed components that should allow such a system to be implemented in practice.

5.2.1 Fast Photon Detectors: Hot-Electron Photo-Effect

It is an essential requirement in achieving high-speed quantum cryptography that we make use of a fast data source for the quantum bits transmitted by Alice to Bob. It is necessary that the qubit detector apparatus keep strict pace with the rate of qubit generation. There are a number of different approaches to the detection of single photons, including the use of single photon avalanche diodes, photomultiplier tubes, single-electron transistors and superconducting tunnel junctions. Unfortunately none of these approaches to photon detection are ideally suited for the high-speed quantum cryptography system that we propose. We require a method to detect individual photons at a wavelength of 1550 nanometers and at a sustained rate of 10 GHz, with a suitably high quantum efficiency of detection and a very low intrinsic dark count rate. With respect to these requirements various drawbacks characterize the existing approaches listed above. These include insufficient sensitivity in the required wavelength window, low photon counting rates, requirements for cooling to millikelvin temperatures, *etc.* However, recent advances [63] in work on picosecond response time single photon detectors based on the use of superconducting thin films of Niobium Nitride (NbN) to exploit the so-called “hot electron photo-effect” suggest that a new approach, well suited to the requirements for high-speed quantum cryptography, can be developed.

Here we will sketch the main features of the proposed approach.⁶⁹ Hot-electron photodetectors (HEPs) based on ultrathin niobium nitride films can operate as single-photon counters in the wavelength range from below 0.5 micrometers to at least 2 micrometers. The NbN single-photon counter is characterized by a high (40%) intrinsic quantum efficiency and practically negligible dark counts [64].⁷⁰ The counting rate is intrinsically limited by the electron-phonon interaction time, measured to be 10 picosecond. The response of practical devices is further limited by the phonon escape time from the film to the substrate and is equal to approximately 30 picosecond [66]. The primary detector element consists of an

⁶⁹ All other elements of our proposed approach to high speed quantum cryptography are based on existing, mature technology. High-speed (10 GHz) detection of photons at 1550 nanometers wavelength, however, is not an existing, mature technology. We have identified and here discuss an approach to high-speed photon counting for quantum communications at telecommunications wavelengths that is very promising, based on initial experimental results.

⁷⁰ The dark count probability can be estimated to be no greater than approximately $e^{-40} \approx 4.25 \times 10^{-18}$ based on an experimentally measured signal-to-noise ratio of 40 in a given HEP cycle period [65].

ultrathin (5 nanometers), very narrow (0.2 micrometers) NbN strip, maintained at a temperature of 4.2 K. Although this low temperature requirement may be problematic for standard “long-haul” telecommunications applications, its proposed use here is for the specialized area of secure quantum communications for which it is entirely acceptable. In this connection we emphasize that the systems we propose, in the case of free space implementations of quantum cryptography, involve placing the Alice system on the orbiting satellite, so that the Bob system, which is where the necessary cryogenic apparatus will have to be situated, is either on the ground or on an airplane. In either case it is much easier to arrange for the operation of the cryogenic system than would be the case if we envisaged placing the Bob system on the satellite. In early experiments such detectors have already been demonstrated to be able to count individual photons, characterized thus far by a *measured* response time of 100 picoseconds, which although lower than the theoretically predicted maximum of 30 picoseconds is already fast enough to allow photon counting at 10 GHz. The actual PRF of the source laser in completed experiments was much slower, pulsing in different experimental setups at a 76 MHz PRF producing 790 nanometers wavelength light, or at 1 KHz PRF producing pulses at wavelengths of 500 nanometers, 1500 nanometers and 2100 nanometers.⁷¹ In early experimental results the initial estimated quantum efficiency was determined to be 20%, which is not yet as high as the theoretically achievable value. An advantage of the HEP approach to single photon counting, apart from the ability to achieve extremely high detection rates, is the lack of the so-called “afterpulsing” problem that plagues other approaches.

The extremely narrow width of the NbN strip in the detecting element necessitates the manufacturing and use of long-microbridge and meander structures to increase the active area so as to mitigate the “behind-the-telescope” loss discussed in Section 4.1.4 above. The overall design would require the side-by-side placement of a small number of detector “chips,” on each of which would be affixed a single meander structure of NbN thin film. Each such meander structure would incorporate a single input lead and single output lead, so that capacitance constraints on the set of chips can be expected to be minimal.

A fuller discussion of this emerging technology and its application to high speed quantum communication will be presented elsewhere [68].

5.2.2 High Pulse-Repetition-Frequency Lasers

The state-of-the-art in experimental research in high-speed pulsed lasers (*e.g.*, [69]) makes the use of 10 GHz PRF sources a completely realistic possibility, assuming that we can also count single photons at the same rate. Commercial fiber mode-locked lasers operating at this PRF value are available, making this a very practical instrument to incorporate into an actual QC system implementation.

Recent “heroic” experiments [70] in which pulsed lasers operating at a PRF of over 450 GHz have been carried out, demonstrating the possibility that at some point in the future

⁷¹ Work is in progress [67] to obtain results at higher PRFs, specifically at 1550 nanometers wavelength.

it *might* be possible to implement a practical QC system operating at a bit cell period of 2.2 picoseconds if it should prove possible to detect individual photons at the same rate. Of course, as we discuss below, the critical difficulty here is to maintain real-time date recording at this rate.

5.2.3 High Speed Opto-electronics Components

The use of Mach-Zender interferometers that operate at switching speeds of 10 GHz has been common in the laboratory for many years. Much recent work has been done on achieving substantially higher switching speeds for Mach-Zender interferometers [73, 74, 75, 76], leading to the current situation in which it is should be feasible as such to incorporate 40 GHz devices in practical quantum cryptography systems, if photon detection and suitable real-time data recording can also be accomplished at the same rate.

5.2.4 Synchronization Constraints

As has been proposed and demonstrated elsewhere (*e.g.*, [3]), a bright timing pulse generated by a suitable pulsed laser operating at the same PRF as the source laser can be used to provide necessary system synchronization across the various components. In the system that we envisage for high speed quantum cryptography, the bright timing pulse laser will be connected to the 10 GHz system master clock. In addition to this, the stringent synchronization requirements that are dictated by a high-speed system also require that the master clock must be connected *via* 4- and 10-way splitters to the data recording de-multiplexing system, as illustrated in Figures 24, 25 and 26, which serves to synchronize the “internal” oscillators of the data recording computers to the “external” pulse rate of the Alice laser system.

5.2.5 Data Recording De-multiplexing Constraints

In considering a practical design for a quantum cryptography system intended to achieve high-speed throughput, an important requirement is to isolate the potential “clogging points” of the overall scheme. The crucial question is: What is the limiting engineering design issue that slows down the system operation? It is clear from all the preceding analysis in this paper that, having properly accounted for the many system losses and loads, and assuming that very fast photon detection at a suitably high value of quantum efficiency is possible, the main “engineering” issue to address is that of keeping proper, error-free, *real-time* records, at both the Alice *and* Bob ends of the system, of the continuous stream of information, such as polarization basis and state information, that must be carried out in order to perform the processing required in the protocol. Here we are limited mainly by the current state of the art in achieving *sufficiently high data bus speeds*. The speeds, as such, of the central

processing units in the various control computers do *not* furnish the limiting constraint here: it is essential to keep a running tally of the polarization state of each and every bit cell transmitted from Alice to Bob, and to do so without errors.

In our analysis we will consider a situation in which we are constrained to make use of practical data bus devices which can accomodate incoming data at a rate of 250 Megabits per second, which is many times slower than the 10 GHz PRF of our proposed laser source.⁷² The solution to this problem is to design a suitable de-multiplexing system that can connect these very different rates, making sure to include appropriate error correction capability. One possible (although expensive) approach to this problem is to employ existing OC-192 telecommunications equipment intended to operate at a 10 GHz repetition rate. As illustrated in Figure 26, one may envisage employing commercially available OC-192 4:1 DEMUX chips in a practical quantum cryptography implementation. These typically include a framer to support channelized OC-192 “synchronous optical network” (SONET) and “synchronous digital hierarchy” (SDH) traffic and 10 GHz bit error rate testing in various telecommunications applications.⁷³ In the same system one may also employ commercially available 10:1 DEMUX chips that operate at a repetition frequency of 2.5 GHz. A parallelized set of four of these can be linked in sequence to the OC-192 DEMUX unit to achieve a net demultiplexing ratio of 40:1, which then produces an integrated output suitable for routing through a 250 Megabit per second data bus. The data stream would be fed *via* Gigabit per second ethernet link to the data storage components of the system for real-time processing according to the QKD protocol.

The principal objective here is to be able to carry out *real-time* quantum cryptography, where at any given moment during the transmission of qubits a previously transmitted batch are being processed. The data recording de-multiplexing solution described above, and other approaches to the problem of real-time data recording furnish practical solutions that can be implemented entirely with currently existing technology. A more thorough analysis [77] of the actual requirements and system details, including a comparison with related real-time data recording solutions from both telecommunications and experimental particle physics applications can be carried out to demonstrate that this problem can be completely (at some cost) solved for practical quantum cryptography systems.

⁷² Although this rate is also somewhat faster than the bus *speeds* currently found in typical, commercially available personal computers, this apparent incompatibility in fact does not pose a problem. The *effective* data recording rate is dictated by both the intrinsic bus rate *and* the width of the bus. Taking both these factors into account it is clear that the requirement of 250 Megabits per second is well within the capabilities of commercially available high-end personal computers today.

⁷³ The standard commerical OC-192 bit error rate test units are typically designed to be compatible with the SONET family of protocols, which would require that appropriate SONET pattern framing be encoded in suitable segments of the bright timing pulse in order to use such equipment “as is” for high speed quantum cryptography. Other framing schemes are obviously possible as well.

High-Speed DEMUX and Data Storage

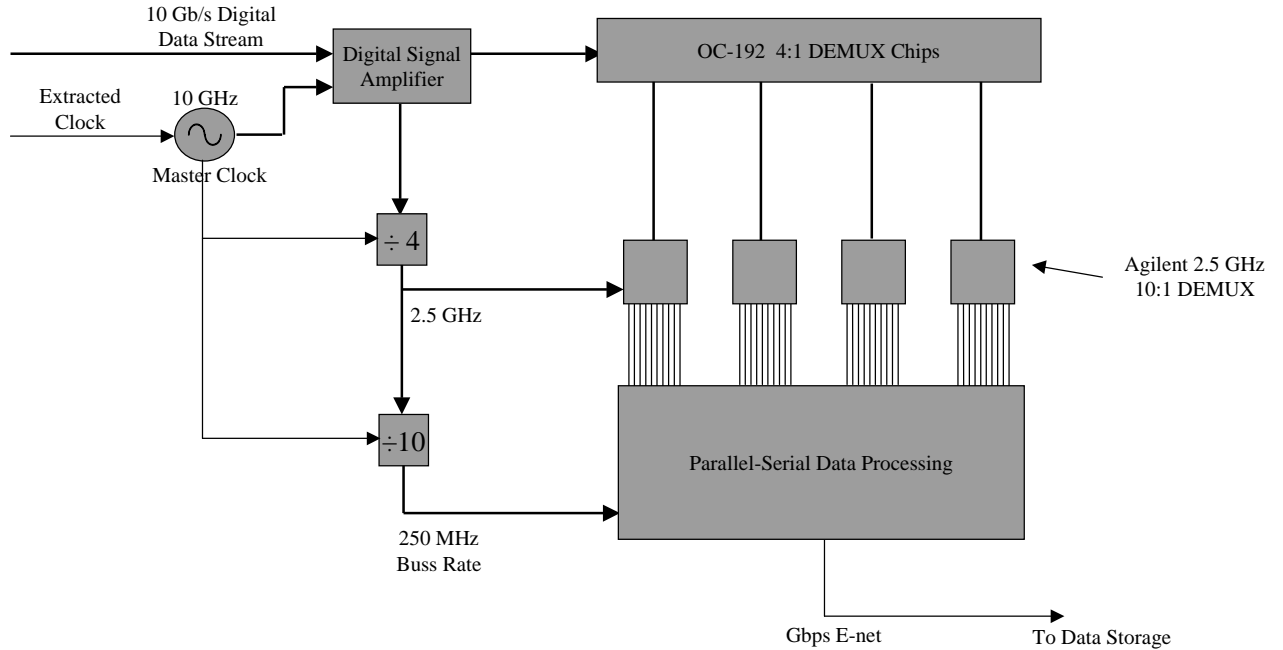


Figure 26: Block Diagram for Data Recording System

5.2.6 Multiple Transmitter-Receiver Multiplexing Analysis

Here we outline the methods whereby the throughput of a quantum cryptography system can be increased by multiplexing together the outputs of some number of transmitters into a common data stream.⁷⁴ The notion of multibeam transmission has been previously proposed for deep space, classical lasercomm applications [79]. Here we extend that concept to the area of quantum communications.

⁷⁴ Note that the “multiplexing” referred to in this section is different than the “(de)multiplexing” referred to in the previous section. In the previous section “(de)multiplexing” pertained to data *recording* associated with a *single* Alice-and-Bob system, while in the present section “multiplexing” refers to data *transmission* associated with *several* Alice-and-Bob systems.

To determine what are the throughput possibilities and constraints for any scheme involving the pooling together of the output streams of more than one Alice device we need two mathematical relationships: (1) the explicit function that provides a relationship between processing block size and the associated computing resource requirements, and (2) the explicit relationship between processing block size and throughput rate. We have derived both of these in this paper. Together, these two pieces of information allow us to determine the relationship between fiducial block size and throughput rate for any individual Alice-and-Bob system, as well as for any combination of Alice-and-Bob systems multiplexed together with different chosen block sizes.

The general approach to this problem is as follows:

- First we establish, for a given single Alice-and-Bob system operating at a specified inverse bit cell period τ^{-1} , what is the largest allowable processing block size based on the maximum computing machine power available using the known relationship between block size and computing resources (*cf* eq.(286)). We denote the maximum available computing resources (measured in terms of basic computer instructions per second)⁷⁵ by $C_{ceiling}$, and we denote the associated processing block size, referred to as the “ceiling” block size, by the symbol $B_{ceiling}$. Thus $B_{ceiling}$ is the largest possible processing block size on which a single Alice-and-Bob system can operate as constrained by the available computing resources. The block size $B_{ceiling}$ is then used in the known relationship between block size and rate, *i.e.*, the equation for the optimal effective secrecy rate (*cf* eq.(173)), to determine what the highest rate is, constrained by the available computing resources, for a single Alice and Bob setup.⁷⁶
- Second, we examine the consequences of reducing the ceiling block size to some proposed smaller size $B_{smaller}$. Using again the known relationship between the block size and computing resources, we determine how many *copies* of Alice-and-Bob systems can be operated at the smaller processing block size without exceeding the overall computing resource constraint dictated by the value $C_{ceiling}$.
- Third, we again employ the known relationship between the system throughput and processing block size to determine the rate that can be achieved by a single Alice-and-Bob system operating on processing blocks of the smaller size $B_{smaller}$. By comparing this with the previously determined rate that applies for a single Alice-and-Bob system operating on the larger block size $B_{ceiling}$, we may obtain the decrease in rate that arises upon replacement of $B_{ceiling}$ with $B_{smaller}$.

⁷⁵ The “maximum available computing resources” will be determined on a case-by-case basis for the particular application that is envisaged. In the case of a free space implementation for which Alice is placed on an orbiting satellite, for example, there may be more stringent constraints (dictated at least in part by how much computing machinery can be physically fitted on board the satellite) than those that apply when both Alice and Bob are on the ground.

⁷⁶ We now see explicitly why it is impossible to analyze any such multiplexing scheme by using expressions for the effective secrecy capacity and effective secrecy rate that are only valid in the abstract limit of an infinitely long cipher. In the infinitely long cipher limit, the transmit block size, which is simply some specified number of raw bits m_0 , *completely drops out* of the expressions for \mathcal{S} and \mathcal{R} .

- Fourth, we combine the above results to obtain the final change in total throughput rate that occurs when some number of copies of single Alice-and-Bob systems, each operating on processing blocks of size $B_{smaller}$, are multiplexed together.

Going through the above steps in detail, we write the expression that relates the general block size B to the associated required computing resources C as

$$\begin{aligned} C &= C(B) \\ &= a_1 B^2 + \dots \\ &\simeq a_1 B^2, \end{aligned} \tag{290}$$

where the detailed form of this relation, including the explicit value of the leading coefficient a_1 , was derived in Section 4.4.3 above and is given in eq.(286). It is sufficient for the present discussion to note that the computing resources scale quadratically with the processing block size.

We now take as given some fixed amount of computing power that for whatever reason may not be exceeded for *any* implementation, and call this amount $C_{ceiling}$. Using the above equation we find the associated block size, $B_{ceiling}$, determined by:

$$\begin{aligned} C_{ceiling} &\equiv C(B_{ceiling}) \\ &\simeq a_1 B_{ceiling}^2, \end{aligned} \tag{291}$$

associated to which we find the largest possible rate for a single Alice-and-Bob system, $\mathcal{R}_{max}^{(single)}$, as

$$\mathcal{R}_{max}^{(single)} \equiv \mathcal{R}_{opt}(B_{ceiling}), \tag{292}$$

where we have displayed only the processing block size dependence in the argument of \mathcal{R}_{opt} and suppressed all other dependences (*cf* eq.(168)).

We now propose a new, smaller processing block size $B_{smaller}$, that is related to the ceiling block size by the reduction factor $b < 1$:

$$B_{smaller} = b B_{ceiling}. \tag{293}$$

The computing resources consumed for a single Alice-and-Bob system that employs the smaller block size $B_{smaller}$ are calculated to be

$$\begin{aligned} C_{smaller} &\equiv C(B_{smaller}) \\ &= C(b B_{ceiling}) \\ &= a_1 b^2 B_{ceiling}^2 + \dots \\ &\simeq a_1 b^2 B_{ceiling}^2 \\ &\simeq b^2 C_{ceiling}, \end{aligned} \tag{294}$$

and thus we find

$$C_{ceiling} \simeq b^{-2} \times C_{smaller}. \tag{295}$$

Thus, we may simultaneously run altogether as many as b^{-2} parallel implementations of *single* Alice-and-Bob systems, each employing a processing block of size $B_{smaller}$ (and thus each consuming an amount $C_{smaller}$ of computing resources), and *still* satisfy the overall computing resource constraint dictated by the value $C_{ceiling}$. This can be done simultaneously by interleaving the output streams of the individual Alice-and-Bob systems into a common stream using any one of several multiplexing schemes, including for instance simple time division multiplexing, space division mutiplexing, *etc.* (*e.g.*, [80]).⁷⁷

To determine the total throughput rate that would be achieved in such a multiplexed system, we first determine the rate that applies for a single Alice-and-Bob system operating on the smaller processing block

$$\mathcal{R}_{smaller}^{(single)} \equiv \mathcal{R}_{opt}(B_{smaller}) , \quad (296)$$

from which we deduce the relative rate decrease, r , that characterizes the replacement of $B_{ceiling}$ with $B_{smaller}$:

$$r \equiv \frac{\mathcal{R}_{smaller}^{(single)}}{\mathcal{R}_{max}^{(single)}} . \quad (297)$$

The main point is that the total throughput rate that can be achieved in the multiplexed system will be better than that which can be achieved with a single system operating on the ceiling processing block size by a factor of as much as $b^{-2} \times r$, if as many as b^{-2} Alice-and-Bob systems operating on blocks of size $B_{smaller}$ are multiplexed together. Depending on the competing values of b and r , this can be a quite significant increase in rate, and as long as the rate decrease r is larger than $O(b^2)$, there will at least be some increase in the rate.⁷⁸ We may now obtain the final throughput rate that will be achieved in the multiplexed system, $\mathcal{R}_{max}^{(multiplexed)}$, as

$$\mathcal{R}_{max}^{(multiplexed)} = (b^{-2} \times r) \times \mathcal{R}_{max}^{(single)} , \quad (298)$$

where this maximal result specifically applies to the case that a total of b^{-2} Alice-and-Bob systems are multiplexed together.

5.2.7 High Speed Random Number Generation

Although for the purely passive Bob setup that we advocate there is no need to actively generate random numbers with which to associate the successive choices of polarization basis, such an active choice may be required at the Alice end of the system. This topic, which is of crucial importance to the successful execution of quantum cryptography, cannot be discussed in an unrestricted publication and will be treated elsewhere.

⁷⁷ Of course, there is a computing resource cost associated to the actual multiplexing implementation, *per sé*, but this is very small for the simple time division multiplexing which would be adequate to achieve the objective under discussion here.

⁷⁸ One may of course choose to multiplex fewer than b^{-2} Alice-and-Bob systems together, and still achieve a (smaller) increase in rate, depending on the actual value of r .

5.3 Universal Maximal Rate Predictions

In this section we make use of the different results obtained in this paper to deduce universal bounds on the maximal throughput rates that can be achieved with various quantum cryptography systems and scenarios. We consider examples of ground-ground, ground-satellite, air-satellite and satellite-satellite links.

5.3.1 Necessary Condition for Unconditional Secrecy

Although the full derivation of the complete effective secrecy capacity is rather complicated, the necessary condition that must be satisfied in order to ensure that Alice and Bob share at least *some* unconditionally secret bits (in the sense of privacy amplification) is extremely simple. There will be at least some number of secret bits shared between Alice and Bob if the optimal effective secrecy capacity is positive:

$$\mathcal{S}_{\text{opt}} > 0 . \quad (299)$$

If this simple necessary condition is satisfied then we are guaranteed that there will be some secret bits, as we have constructed \mathcal{S}_{opt} to account for *all* system effects, so that there are by definition and construction no losses suffered by the system other than those which are already incorporated in \mathcal{S}_{opt} .

Given that the condition in eq.(299) is satisfied, *any* quantum cryptography system will produce some number of secret bits shared between Alice and Bob. The particular *rate* at which these secret bits are generated will then be entirely determined by the value of the bit cell period and by the number of multiple beams, if any, that are multiplexed together.

5.3.2 Systems with Single Transmitter-Receiver Arrangement

In this section we consider a number of representative examples of quantum cryptography systems to illustrate the throughput rates that can be achieved for the exchange of unconditionally secret Vernam cipher material between Alice and Bob. For all of the examples below we assume for definiteness that the laser at the Alice end of the system produces pulses of light at a wavelength of 1550 nanometers. Although they are not available today, we also *assume* for all but the last of these examples that high-speed HEP photon detectors, of the kind described in Section 5.2.1 above, will in the near future be available to count photons at a rate of 10 GHz corresponding to a bit cell period $\tau = 100$ picoseconds, with a dark count per bit cell of 4.25×10^{-18} (as discussed in footnote 70 above). In the last example below we will calculate rates based on the use of generic, currently available commercial photon detectors capable of detecting photons at a rate of 1 MHz with an assumed dark count per bit cell rating of 1×10^{-6} .

(i) *Free Space Quantum Channel: Aircraft-to-Satellite (LEO) Link*

For this example we consider a quantum cryptography setup in which Alice is located on a LEO satellite at an altitude of 300 kilometers above MSL and Bob is located on a platform at an altitude that is substantially above the bulk of the atmospheric turbulence, which we take to be an aircraft flying at 35000 feet or higher (*e.g.*, such as a suitably modified Joint Surveillance Target Attack Radar System (Joint STARS) aircraft). As with the various examples given in Section 4.1.3 above, we take the diameter of the aperture of Alice's transmitting instrument to be $D_A = 30$ cm. Inspection of Figure 15 reveals that in this situation the line attenuation will be given by $\alpha = -10$ dB if we take a value of $D_B = 58$ cm for the diameter of the aperture of Bob's receiving instrument.⁷⁹ ⁸⁰

In Figure 27 we plot the optimal effective secrecy rate, \mathcal{R}_{opt} , for the above QC system

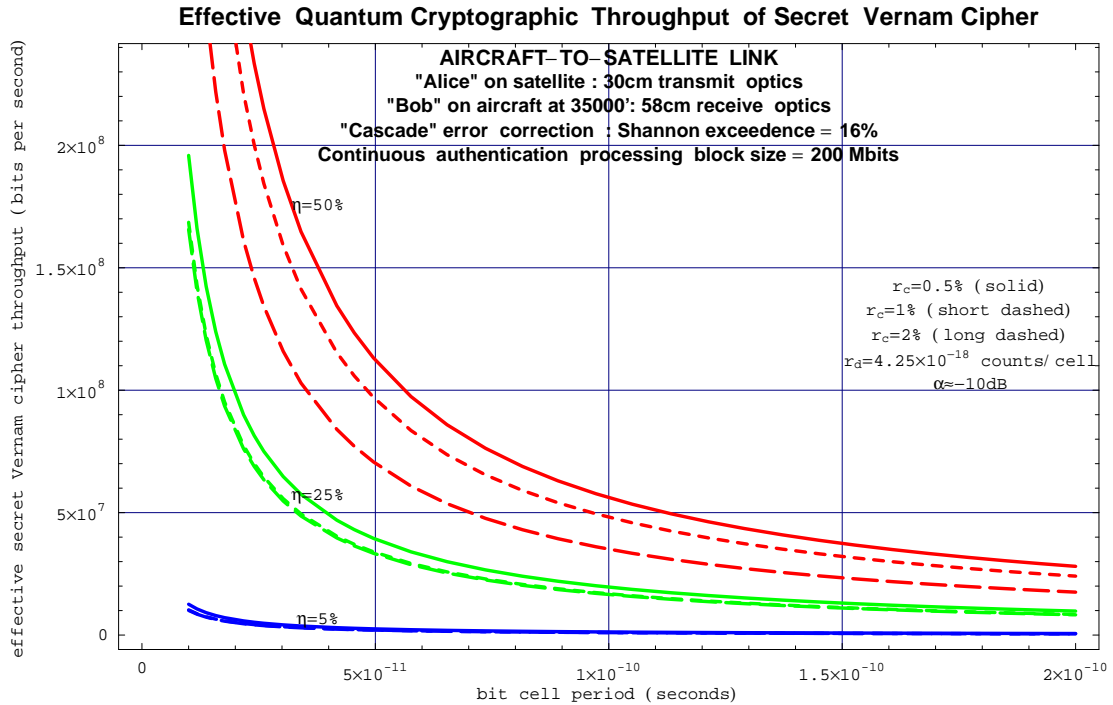


Figure 27: Effective Rate Graph for Aircraft-to-Satellite (LEO) Link: $\alpha = -10$ dB ("Bob" - 58 cm telescope at 35000'; "Alice" - 30 cm telescope on LEO satellite)

as a function of the bit cell period. Inspection of the graph reveals that for a bit cell period of 100 picoseconds, corresponding to a laser with a PRF of 10 GHz, and a photon detector device efficiency η of 50%, the maximum rate for the generation of Vernam cipher

⁷⁹ This is a realistic value for the size of airborne optics. For example, it is publicly known [81] that the U.S. Department of Defense U-2 and U-2R aircraft have in the past been equipped with the 30-inch (76.2 cm) Optical Bar Camera, in addition to other sensors.

⁸⁰ We emphasize again, as discussed at the beginning of Section 4.1 above, that the line attenuation α is not the "total" attenuation suffered by the signal.

material is about 57 Megabits per second,⁸¹ based on a calculated value for the optimal mean photon number per pulse of $\mu_{\text{opt}} = 0.455$, which is obtained by numerically solving eq.(170). This is illustrated in Figure 28, where the (real) solution to eq.(170) is plotted. For this example we have taken an assumed fractional intrinsic channel error rate value of

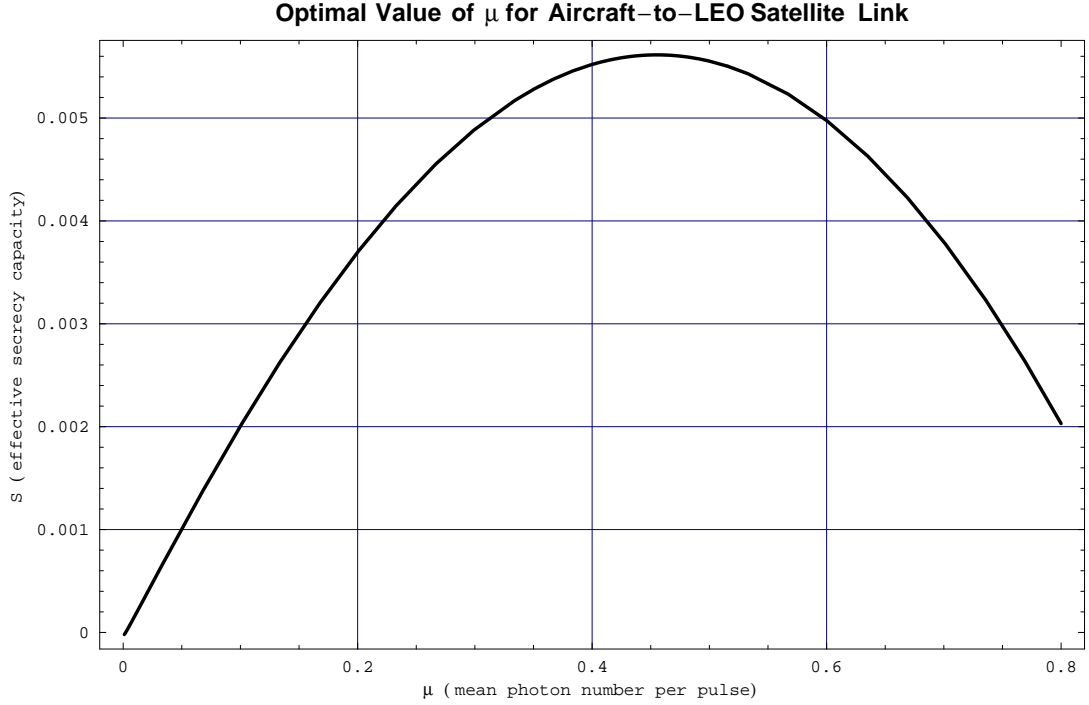


Figure 28: Effective Secrecy Capacity Graph for Aircraft-to-LEO Link: $\eta = 50\%$; $r_c = 0.005$ $\alpha = -10$ dB (58 cm telescope at 35000' - LEO satellite)

$r_c = 0.005$. From eq.(206) we see that this value of r_c requires active control of the relative angular misalignment between the satellite and the airborne platform so as to restrict overall relative motion within a cone of solid angle

$$\begin{aligned}
 2\delta &\lesssim 2 \arcsin(\sqrt{0.005}) \\
 &= 0.142 \text{ radian} \\
 &= 8.11 \text{ degrees} .
 \end{aligned} \tag{300}$$

This throughput rate is higher than that provided by a standard T3 telecommunications link, and in particular is faster than the 45 Megabits per second data rate of the TACLANE encryptor system [82].

We see that for $r_c = 0.01$, which (as described in the text below eq.(206)) requires attitude control within a cone of solid angle 11.5 degrees, the optimal effective secrecy rate decreases

⁸¹ Due to the assumption in this example that Bob is above most of the atmospheric turbulence we note that the rates for this scenario are independent of the slant angle between Bob and Alice.

to $\mathcal{R}_{\text{opt}} = 49$ Megabits per second, in this case for a lower optimal mean photon number per pulse value of $\mu_{\text{opt}} = 0.426$. If we allow instead for a value of $r_c = 0.02$, which only requires attitude control within a cone of solid angle of 16.3 degrees, we find an optimal throughput rate of $\mathcal{R}_{\text{opt}} = 36$ Megabits per second, for $\mu_{\text{opt}} = 0.37$.

If we consider now a photon detector apparatus with a lower intrinsic device efficiency of $\eta = 25\%$, we find that for a value of $r_c = 0.005$ the optimal throughput rate drops to about 21 Megabits per second (for a value of $\mu_{\text{opt}} = 0.131$), with rate values of about 18 Megabits per second for quantum channels characterized by fractional intrinsic error values of either 1% or 2% (for $\mu_{\text{opt}} = 0.125$ and $\mu_{\text{opt}} = 0.122$, respectively). Finally, we note that when the device efficiency of the photon detector apparatus drops below about $\eta \approx 5\%$, there can be no unconditionally secret Vernam cipher material exchanged *at all* between Alice and Bob.

For all of the above scenarios we have taken a value for the Shannon deficit parameter x of $x = 1.16$ (*cf* eq.(43)), which means that we are assuming that an efficient method of error correction has been employed that approaches the Shannon limit to within 16%, and we use a raw bit processing block size of $m = 200$ Megabits. In addition, we have also set all of the continuous authentication security parameter values, g_i , (*cf* eq.(152)), as well as the privacy amplification security parameter g_{pa} , equal to 30, and we have employed a value of $\epsilon = 10^{-9}$ for the selectable infinitesimal quantity that determines the success likelihood for attacks on single-photon pulses (*cf* eq.(49) and the discussion in the text above eq.(45)).

(ii) Free Space Quantum Channel: Earth-to-Satellite (LEO) Link; clear weather

For this example we consider a quantum cryptography setup in which Alice is on a LEO satellite at an altitude of 300 kilometers and Bob is on the ground at MSL. Unlike the previous example, in this scenario the full effects of atmospheric turbulence are important. As before we take the diameter of the aperture of the transmit optics to be $D_A = 30$ cm, and we see from Figure 15 that in order to achieve a value for the line attenuation of $\alpha = -20$ dB we must take a value of $D_B = 50$ cm for the diameter of the aperture of Bob's receiving instrument. As before, we assume a value for the Shannon deficit parameter of $x = 1.16$ and employ a raw bit processing block size of $m = 200$ Megabits.

In Figure 29 we plot the optimal effective secrecy rate for this QC system as a function of the bit cell period. Inspection of the graph reveals that, for a pulsed laser source with a PRF of 10 GHz and a photon detector with an intrinsic device efficiency of $\eta = 50\%$, the maximum rate for the generation of Vernam cipher material is now about 1.3 Megabits per second, for a calculated value of the optimal mean photon number per pulse of $\mu_{\text{opt}} = 0.131$, where we have assumed that $r_c = 0.005$. If we instead consider values of $r_c = 0.01$ and $r_c = 0.02$, we find corresponding throughput rates of 1.05 Megabits per second and 665 Kilobits per second for values of $\mu_{\text{opt}} = 0.125$ and $\mu_{\text{opt}} = 0.111$, respectively.

We note that the effective throughput rates drop precipitously if we consider photon detector apparatuses with a smaller intrinsic device efficiency of $\eta = 25\%$. In this case we find that, for a value of $r_c = 0.005$ there is a maximum throughput rate of unconditionally secret

Vernam cipher material of about 165 Kilobits per second (for a value of $\mu_{\text{opt}} = 0.0898$), and for a value of $r_c = 0.01$ the maximum rate is about 105 Kilobits per second (for a value of $\mu_{\text{opt}} = 0.0848$). Poorer values for *either* the detector efficiency η or the fractional intrinsic quantum channel error r_c produce essentially no viable throughput of Vernam cipher material at all.

For the above examples we have assumed “clear” weather conditions for the input to the FASCODE runs (as described in Section 4.1.2 above, this is defined as yielding 23 kilometers visibility), and we have taken the LEO satellite to be located at *zenith* above Bob. We have also taken values of $g_i = g_{pa} = 30$ and $\epsilon = 10^{-9}$.

In contrast to the previous example in which maximal rates in excess of those characterized by T3 telecommunications lines are possible, we see that the effects of atmospheric turbulence reduce the maximal possible rate for a ground-to-LEO satellite link in clear weather conditions to slightly less than that provided by a standard T1 telecommunications line, if we make use of a small (50 cm) receiving telescope.⁸²

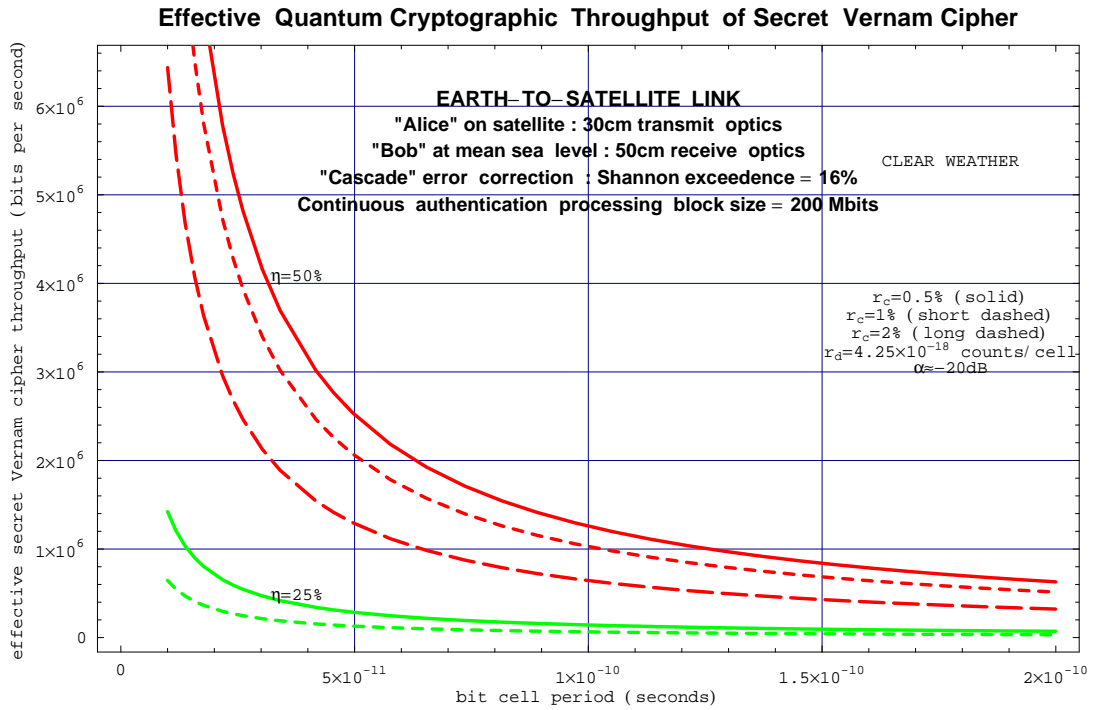


Figure 29: Effective Rate Graph for Earth-to-Satellite (LEO) Link: $\alpha = -20$ dB (“Bob” - 50 cm telescope at mean sea level ; “Alice” - 30 cm telescope on LEO satellite; clear weather)

However, further inspection of Figure 15 reveals that we may achieve the much better line attenuation value of $\alpha = -10$ dB by employing instead a receiving telescope with an optical

⁸² Note that the publicly acknowledged data rate for the radiation-hardened U.S. Department of Defense MILSTAR satellite is that of a T1 link [83].

aperture of $D_B = 1.6$ m. (Since the Bob apparatus is on the ground in this example, the larger size of the receiving telescope optics is acceptable compared to the previously considered scenario in which Bob is located on an airborne platform.) In this case, the effective throughput rates will be identical to those obtained for the aircraft-to-satellite link example considered above, as we illustrate in Figure 30.⁸³ Thus it should be possible to establish

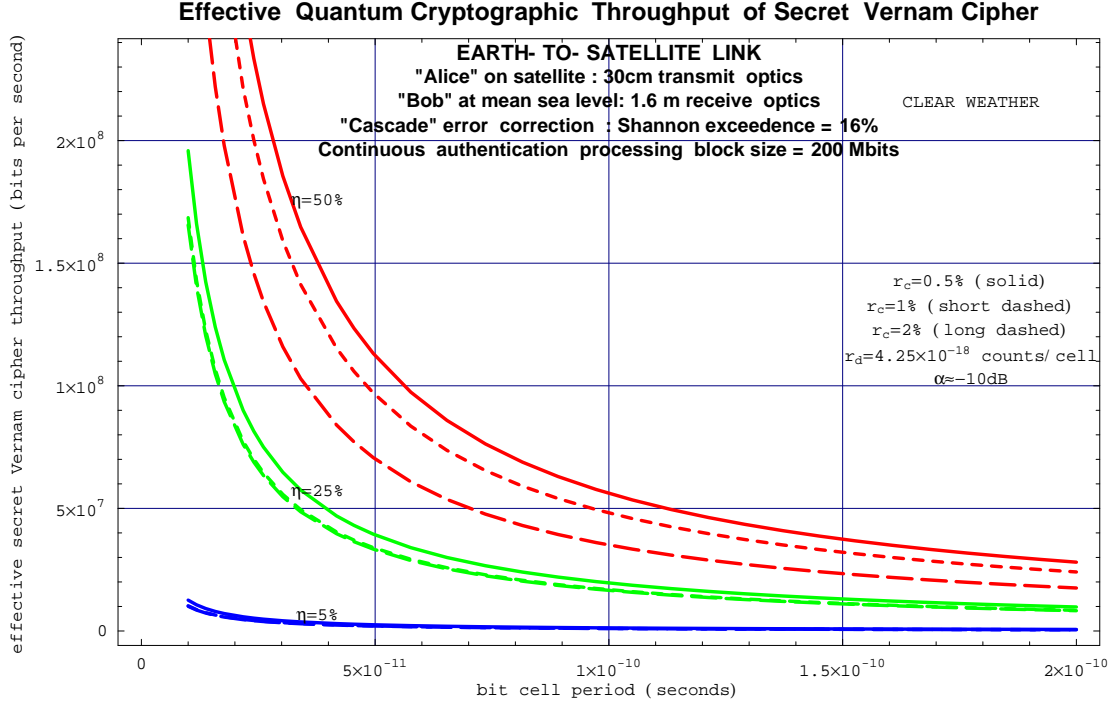


Figure 30: Effective Rate Graph for Earth-to-Satellite (LEO) Link: $\alpha = -10$ dB (“Bob” - 1.6 m telescope at mean sea level ; “Alice” - 30 cm telescope on LEO satellite; clear weather)

between a ground station and a LEO satellite a clear weather quantum cryptography link that operates at a rate somewhat faster than that provided by a T3 line when the satellite is at the zenith location. (When the satellite drops to the 45 degree declination position the value of the line attenuation will change to about $\alpha = -11.8$ dB, causing a drop in the throughput rate.)

(iii) Free Space Quantum Channel: Earth-to-Satellite (LEO) Link; light rain

To illustrate the severe link degradation that can spoil a quantum cryptography system in the presence of adverse weather conditions, we again consider an example in which, as before, Alice and Bob are located, respectively, on a LEO satellite and at a ground station at MSL. In this case, we replace the assumption of clear weather conditions with the assumption

⁸³ In this example we keep all parameters at the same values used for the calculation of the ground-to-LEO satellite link rate with the 50 cm receive optics, except that we use the values for μ_{opt} that we found in Scenario (i) above for the aircraft-to-LEO satellite case (because the line attenuation has the same value).

of “light rain” conditions. This is quantitatively incorporated in the problem by running the FASCODE computer program with the appropriate corresponding input parameters, for which “light rain” is defined (as in standard meteorological analysis) as comprising 5 mm per hour of precipitation. Numerical results analogous to those displayed in the graph in Figure 15 indicate that if we take the diameter of the aperture of the transmit optics to be $D_A = 30$

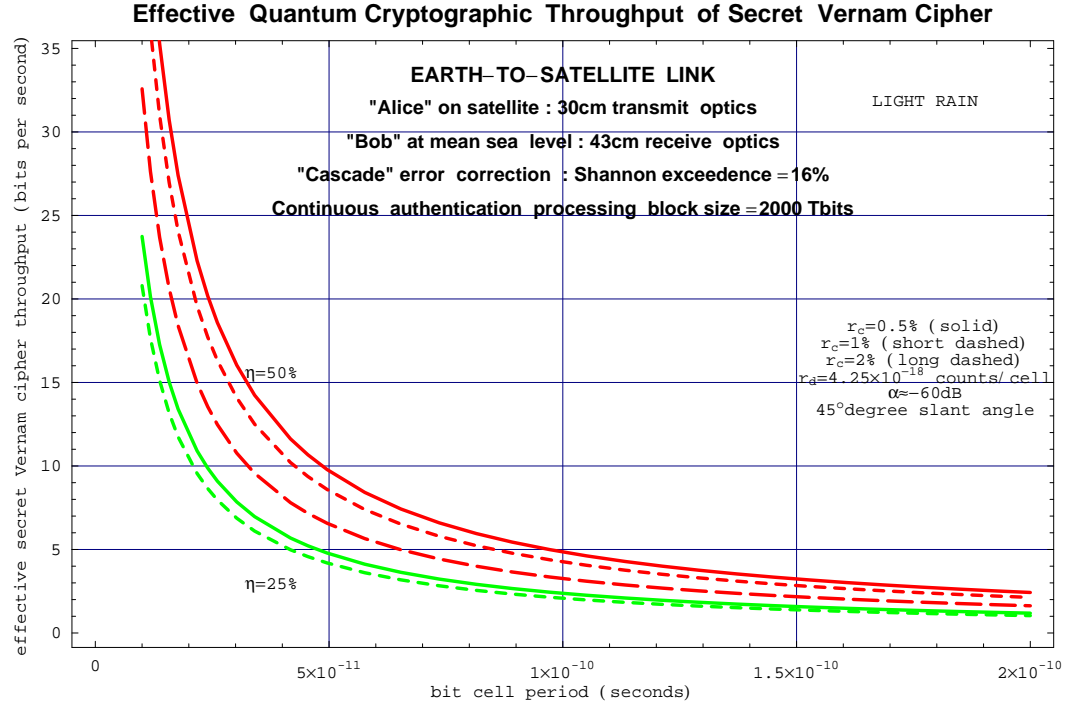


Figure 31: Effective Rate Graph for Earth-to-Satellite (LEO) Link: $\alpha = -60$ dB (“Bob” - 43 cm telescope at mean sea level ; “Alice” - 30 cm telescope on LEO satellite; light rain)

cm and the diameter of the aperture of the receive optics to be $D_B = 43$ cm (slightly smaller than, but roughly comparable to, the smaller of the two receive apertures used in Scenario (ii) above in the clear weather example), the line attenuation will be given by $\alpha = -60$ dB for a slant angle of 45 degrees. For this scenario we observe a very severe decrease in the throughput rate of the system, as can be seen from the results plotted in Figure 31. With the parameters g_i , g_{pa} , ϵ and x set identically to the values taken in the clear weather example above, we find that the maximum throughput rate for a ground-to-LEO satellite link in the presence of light rain is given by about 5 bits per second for a bit cell period of 100 picoseconds and a detector efficiency of 50%, assuming a quantum channel fractional intrinsic error of $r_c = 0.005$ and employing a calculated optimal value of $\mu_{opt} = 0.00328$. This drops to a rate of about 2.25 bits per second for a system with a photon detector efficiency of 25% and a quantum channel fractional error of $r_c = 0.02$, corresponding to a value of $\mu_{opt} = 0.0029$. Note that, in order to achieve even these low throughput rates it is necessary to take a value for the raw bit processing block of $m = 2000$ Terabits (as opposed to the value of $m = 200$ Megabits employed in the previous examples). Smaller values for the raw

bit processing block do not yield any shared secret Vernam cipher material at all, due to the very severe degradation to the quantum channel caused by the rain. Although the use of such a large processing block can in principle be arranged so as *not* to introduce a larger classical communications bandwidth requirement between Alice and Bob,⁸⁴ a processing block of this large size is nevertheless not realistic for satcom quantum cryptography applications. This is because the *physical size* requirements on the memory that Alice must utilize to accept such a large raw bit processing block are incompatible with typical satellite space (and power and cooling) constraints.⁸⁵ Furthermore, without monitoring of click statistics by Bob it is impossible to achieve any viable throughput in this scenario, so that we have made use of the appropriately modified form of the privacy amplification function in computing these rates (*cf* eq.(81)), wherein the the leading term is down by a factor of η compared to the version without monitoring of click statistics. In addition to the preceding, we have *also* had to employ a slightly modified value of $\hat{z}_E(\mu)$ (*cf* eq.(57)) to achieve even these rates: following the discussion in the text between eqs.(57) and (58), we have (in this example only) assumed that the enemy is unable to achieve the full strength direct attack implied by eq.(57), which varies as $\hat{z}_E(\mu) = \frac{1}{12}\mu^3 + O(\mu^4)$, and instead taken a value of one-third of this, so that in the corresponding privacy amplification function we have $\hat{z}_E(\mu) = \frac{1}{36}\mu^3 + O(\mu^4)$. Of course, it would be possible to achieve higher throughput in the presence of adverse weather conditions by employing a larger aperture for the receive optics at the Bob site (modulo the above-mentioned concerns regarding physical constraints on memory that can be placed on a realistic satellite). If we instead use a receiving telescope with an optical aperture of $D_B = 1.4$ m we obtain the better line attenuation value of $\alpha = -50$ dB. The results for this case are illustrated in Figure 32, inspection of which reveals a maximum throughput rate of 164 bits per second for a detector efficiency of $\eta = 50\%$, a bit cell period of 100 picoseconds, a quantum channel fractional error of $r_c = 0.005$ and at a calculated optimal value of $\mu_{\text{opt}} = 0.0106$ with a slant angle of 45 degrees.

(iv) *Free Space Quantum Channel: Earth-to-Satellite (LEO) Link; moderate rain*

In the presence of “moderate rain,” which is defined for FASCODE runs as comprising 12.5 mm per hour of precipitation, the line attenuation α becomes much worse, never any better than -76 dB even for a LEO satellite located at zenith above the ground station with a receiving optics aperture of $D_B = 1.6$ m diameter. In this case the only means of producing *any* shared, unconditionally secret Vernam cipher at all is to increase the processing block size to a value which is not practical for currently available computing machinery that can

⁸⁴ The communications load in bits per second is actually smaller for a larger raw block size, m_0 , provided the sifted block size, n_0 , does not change. This may be understood on the basis of two observations: the number of transmitted bits per block is roughly linear in the size of the sifted block and depends only weakly on the size of the raw block, and the amount of time available to carry out the transmission increases linearly with the raw block size. The communications load then varies roughly as n_0/m_0 , which decreases with increasing m_0 at constant n_0 .

⁸⁵ A rough estimate based on the characteristics of currently available memory modules indicates that such a processing block would require enough space on the satellite - for the memory alone - to accomodate a large vehicle such as a truck.

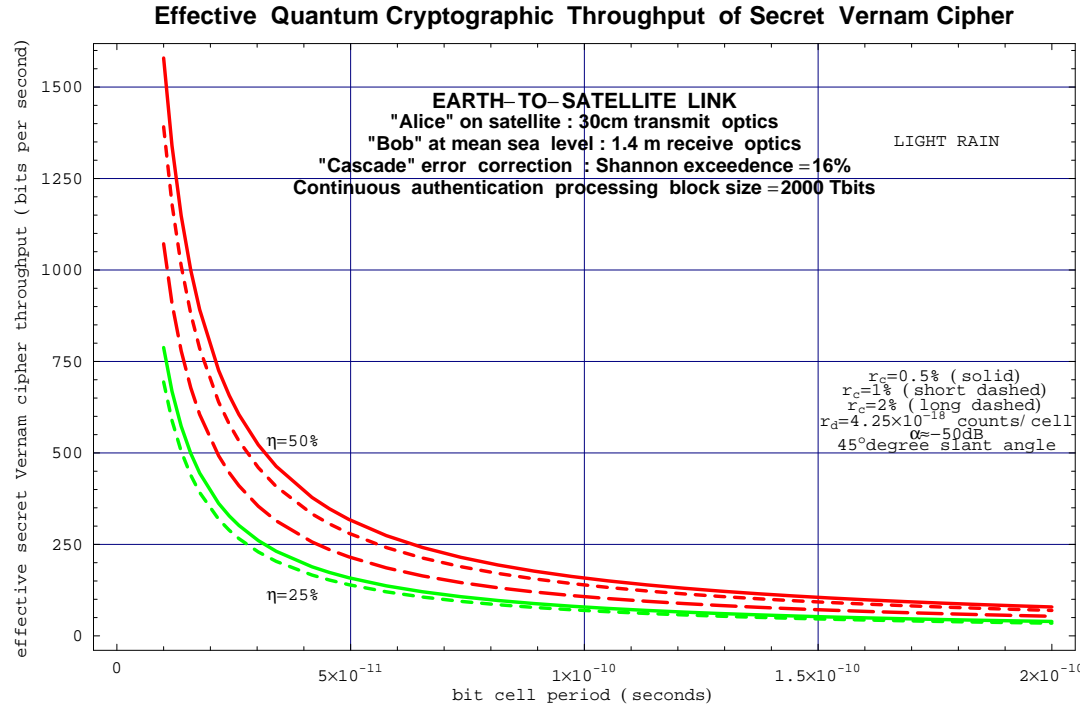


Figure 32: Effective Rate Graph for Earth-to-Satellite (LEO) Link: $\alpha = -50$ dB (“Bob” - 1.4 m telescope at mean sea level ; “Alice” - 30 cm telescope on LEO satellite; light rain)

be fitted on a satellite.

(v) *Free Space Quantum Channel: Earth-to-Satellite (GEO) Link; clear weather*

We now consider the example of a ground-to-GEO satellite link. Thus, we assume that Alice is located on a geosynchronous satellite above the Earth at an altitude of 35783 kilometers (22236 miles) above mean sea level. In order to achieve a viable effective throughput rate of Vernam cipher material we envisage for this scenario that Bob is located at a sufficiently high altitude so as to mitigate somewhat the effects of atmospheric turbulence. Unlike the example of the aircraft-to-satellite link considered above, we here want to describe a situation in which there would be a more-or-less permanent link between the Bob and Alice, so that Bob should be located at a ground receiving station. An important point here is that the GEO link should be available for a much more extended period of time that is the case for the LEO link, which would provide access for a roughly nine minute period before the satellite drops below the horizon visible to Bob. Thus, we may hope to achieve effective, *integrated* throughput values that are higher in the GEO link case than in the LEO link case.

For this computation we have taken the parameters g_i , g_{pa} , ϵ and x as in the previous examples, but we now choose a value of $m = 2$ Gigabits for the raw bit processing block size. Unlike the example of the Earth-to-LEO satellite link in the presence of light rain, for

which it was necessary to take a much larger value for the raw bit processing block size, *this* value imposes no practical difficulties regarding either communications bandwidth or physical space requirements for memory size on the satellite. We do adopt, however, as in the example above of the Earth-to-LEO satellite scenario, the assumption that Bob actively monitors click statistics, and we use the corresponding privacy amplification function for the direct attack as a result. Without the use of the form of the privacy amplification function associated to active click statistics monitoring by Bob, no viable throughput can be established for the Earth-to-GEO satellite link.⁸⁶ An important requirement to achieve viable throughput is to employ a sufficiently large receiving telescope aperture, since the line attenuation due to the spreading of the beam is otherwise completely prohibitive.

For this example we envisage a receiving telescope with an effective optical aperture of 10 meters. Although this is a very large optical instrument, this size of receive aperture is characteristic of what has been proposed in the literature [79] for use in optical communications for deep space missions (coincidentally, such proposals for classical optical deep space lasercomm have also incorporated 30 cm transmit optics), and this is also available at the Keck Telescope Facility on Mauna Kea mountain in Hawaii at an altitude of 13500 feet. For the purposes of this example we will imagine that Bob is located at such a site and has access to such an instrument. In this case the line attenuation α can be calculated using eq.(204) and is found to be given by $\alpha = -26.4$ dB, and we use this value in the numerical evaluation of \mathcal{R}_{opt} . In Figure 33 we plot the optimal effective secrecy rate that characterizes such a ground-to-GEO satellite quantum cryptography system. Inspection of the curves in the graph reveals that, with a laser PRF of 100 picoseconds, a photon detector device efficiency of $\eta = 50\%$ and a value for the quantum channel intrinsic error of $r_c = 0.005$, such a system should achieve a throughput rate of about 240 Kilobits per second, for a value of $\mu_{\text{opt}} = 0.0891$. This throughput rate, which should be essentially continuously available since Alice is on a GEO satellite, is roughly one-sixth the rate of a standard T1 telecommunications link.⁸⁷ The important point is that, as mentioned above, such a link would be available for more than the approximately nine-minute period provided by a LEO link prior to the disappearance of the latter type of satellite below the horizon, thus potentially providing a comparable (or higher) effective integrated throughput value compared to the latter. If we now consider a photon detector with a lower device efficiency given by $\eta = 30\%$, we find (again for an intrinsic channel error value of $r_c = 0.005$) an effective throughput rate of about 118 Kilobits per second (for a value of $\mu_{\text{opt}} = 0.0884$).

(vi) Free Space Quantum Channel: Satellite-to-Satellite (GEO-to-GEO) Link

It is interesting to consider the possible use of quantum cryptography for satellite-to-satellite communications. There are a wide range of scenarios that might be considered: to illustrate

⁸⁶ We do assume that the enemy can mount the strongest possible direct attack, as measured by $\hat{z}_E(\mu)$ given in eq.(57).

⁸⁷ Note that this rate is approximately equal to the throughput rates currently available for the “Mobile Subscriber Equipment” (MSE) and “Tri-Service Tactical Communications” (TRITAC) systems, employed by the U.S. Army and U.S. Air Force/U.S. Marine Corps, respectively.

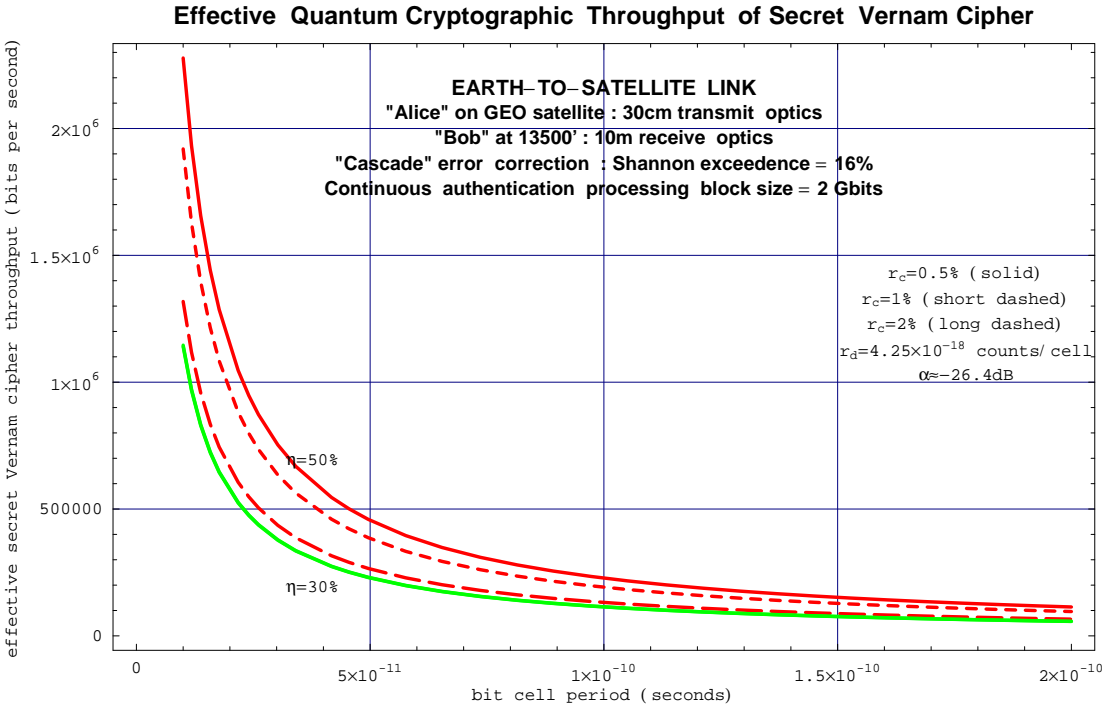


Figure 33: Effective Rate Graph for Earth-to-Satellite (GEO) Link: $\alpha = -26.4$ dB (“Bob” - 10 m telescope at 13500’ ; “Alice” - 30 cm telescope on GEO satellite)

the general problem we will only briefly discuss a GEO-to-GEO satellite link. We will take a very simple model of a three-satellite constellation set up to provide a combined footprint covering most of the Earth (with the exception of the polar regions), here for simplicity assumed to be situated at 120 degree angles with respect to each other. Assuming a GEO altitude of 35783 kilometers and noting that the radius of the Earth is 6378 kilometers, we consider a satellite-to-satellite crosslink distance of about 48683 kilometers (30250 miles). It is clear from the previous example that the line attenuation due to beam spreading will be even larger here than for the Earth-to-GEO scenario. In order to achieve useful throughput values this large amount of line attenuation would presumably require that the Bob satellite be equipped with a receiving instrument that has an effective optical aperture of at least 10 meters in size, which is considerably larger than the 2.6 meter aperture of the Hubble Space Telescope. It might be possible in the future to obtain such an effective aperture for a spaceborne light-collecting instrument. In this connection the U.S. National Aeronautics and Space Administration (NASA) has recently announced the “Gossamer Spacecraft Initiative” [84, 85] which is intended to result in a spaceborne telescope with an effective aperture of 50 meters or more in size. Although this initiative is still in the earliest planning stages, such an instrument could be used for quantum cryptography as well as astronomical research activities.

(vii) Fiber Optic Quantum Channel

In this example we consider a fiber-optic cable implementation of quantum cryptography. We envisage for this example the use of high-quality, polarization-preserving fiber characterized by an intrinsic attenuation characteristic of 0.2 dB per kilometer, and for purposes of illustration compare the associated throughput values with results for lower quality fiber with an attenuation characteristic of 0.3 dB per kilometer. We take the photon detector device efficiency to be $\eta = 50\%$, and we assume that appropriate splicing and insertion of suitable dispersion-compensating fiber segments, as discussed in Section 4.2 above, has been carried out so as to mitigate the dispersion losses described and analyzed there. To account for the associated splicing loss and other system imperfections we assume that the quantum channel is characterized by a total bulk loss of -5 dB, in addition to the losses associated with the attenuation per unit length.

In Figure 34 we plot several effective secrecy rate curves for this system. In this example, we compute throughput rates in the case that the cable remains untouched by the enemy. We see that, for a good quality cable with an attenuation characteristic of 0.2 dB per kilometer and an intrinsic channel error value of $r_c = 0.01$, the rate to a distance of 10 kilometers along the cable should be at least as high as about 115 Megabits per second, whereas for a cable with an attenuation characteristic of 0.3 dB per kilometer (and the same value for r_c) the corresponding rate should be at least as high as about 88 Megabits per second (in each case using a value of $\mu_{\text{opt}} = 0.4$). We note that, for *any* of the illustrated parameter values,⁸⁸ for the cable with the attenuation characteristic of 0.3 dB per kilometer *any* exchange of unconditionally secret Vernam cipher material beyond about 33 kilometers is impossible. For the higher-quality cable with a loss characteristic of 0.2 dB per kilometer, throughput of at least *some* number of secret key bits is just barely possible to the 50 kilometer point in the case of a low error value of $r_c = 0.01$.

We now consider the case that the enemy has somehow been able to surreptitiously replace the cable with one which is effectively lossless. In Figure 35 we plot several effective secrecy rate curves for this system. We see that, for a good quality cable as above with an attenuation characteristic of 0.2 dB per kilometer and an intrinsic channel error value of $r_c = 0.01$, the rate to a distance of 10 kilometers along the cable should drop to a value at least as high as about 29 Megabits per second, whereas for a cable with an attenuation characteristic of 0.3 dB per kilometer (and the same value for r_c) the corresponding rate should drop to a value at least as high as about 20 Megabits per second (in each case in this example we use a value of $\mu_{\text{opt}} = 0.1$). We note that, for any of the illustrated parameter values, for the cable with the attenuation characteristic of 0.3 dB per kilometer any exchange of unconditionally secret Vernam cipher material beyond about 24 kilometers is impossible. For the higher-quality cable with a loss characteristic of 0.2 dB per kilometer, throughput of at least *some* number of secret key bits is just barely possible to the 36 kilometer point in the case of a low error value of $r_c = 0.01$.

⁸⁸ We display curves with values of $r_c = \{0.01, 0.02, 0.03, 0.04, 0.05\}$.

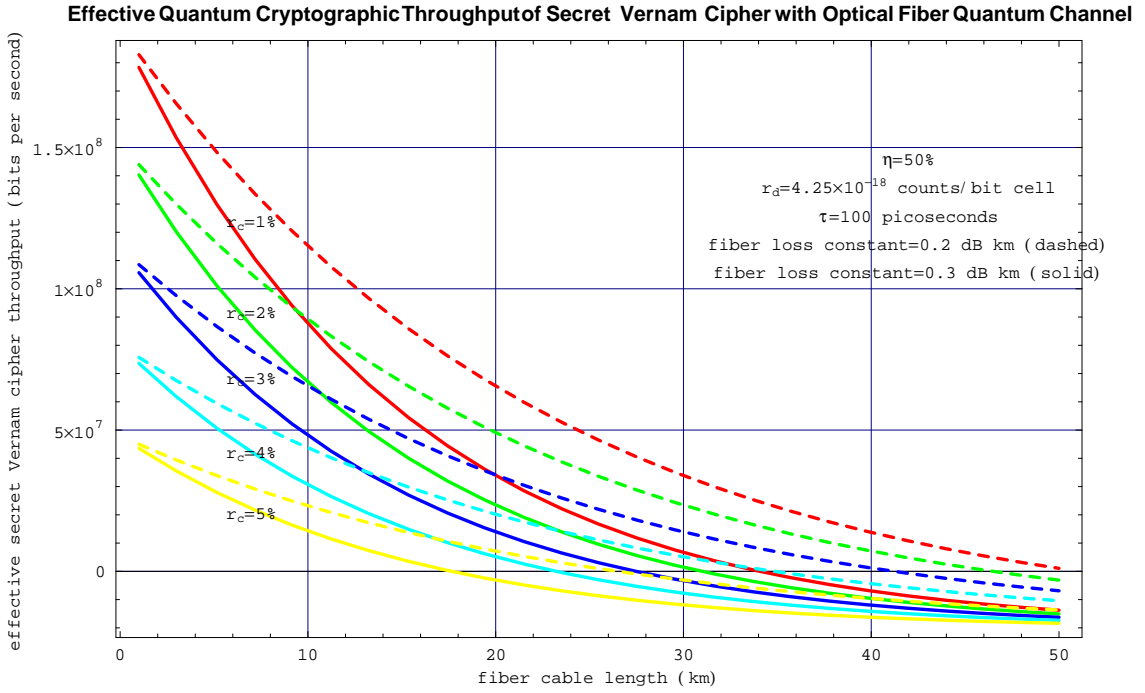


Figure 34: Effective Rate Graph for Fiber-Optic Cable Link without Surreptitious Cable Replacement

(viii) *Free Space Quantum Channel: Aircraft-to-Satellite (LEO) Link; 1 MHz Photon Detector*

In the above examples we analyzed the throughput rates that will be available with the potential development in the future of high-speed photon detectors capable of counting photons at a rate of 10 GHz. Here, we compare the rates predicted for the aircraft-to-LEO satellite link considered in Figure 27 with the effective throughput rates of unconditionally secret Vernam cipher that are possible with the use of a “generic” commercially available photon detector capable of counting at a rate of 1 MHz, with an assumed value of $r_d = 1 \times 10^{-6}$.

In Figure 36 we plot curves corresponding to those shown in Figure 27. The various environmental conditions are taken to be identical here as for the previous case, so that the various values for μ_{opt} are identical for each curve (the replacement of $r_d = 4.25 \times 10^{-18}$ with $r_d = 1 \times 10^{-6}$ makes a negligible change in the solution to the optimization equation, eq.(170)). We find that the new rates reflect the simple, inverse dependence of \mathcal{R}_{opt} on the bit cell period τ : the highest rate possible in this scenario is about 5700 bits per second for a good photon detector with a quantum efficiency of 50% and a high quality quantum channel with $r_c = 0.005$, with various lower rates for the other combinations, as expected. The case of $\eta = 25\%$ and $r_c = 0.01$, which is more realistic, yields a highest possible rate of about 1760 bits per second.

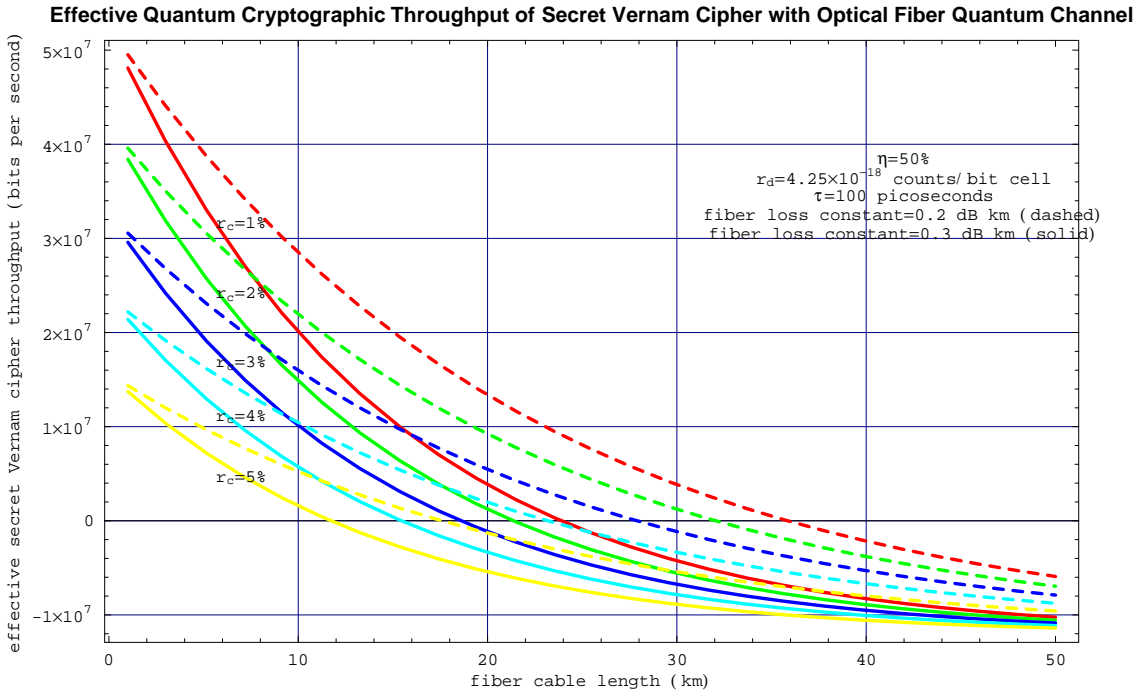


Figure 35: Effective Rate Graph for Fiber-Optic Cable Link with Surreptitious Cable Replacement

5.3.3 Systems with Multiple Transmitter-Receiver Arrangement

The rates presented in the preceding section were calculated based on the assumption that the Alice-and-Bob systems comprise a single transmitter and receiver combination. In considering how the data throughput rate may be increased by multiplexing together a number of Alice-and-Bob systems, we may make use of the analysis presented in Section 5.2.6. It is possible to show that in various situations the effective system throughput rate can be increased by making use of a suitably multiplexed multi-beam transmission, just as is done in classical lasercomm systems [71, 72]. An analysis of the various rate improvements that are possible through the use of the multiplexing technique described in Section 5.2.6 above will be presented in a future paper [77].

5.3.4 Rate Improvement with Additional Emerging and Possible Future Technology

A number of other emerging commercial technology developments, as well as research efforts that are currently underway, may provide additional means to achieve and improve the overall performance characteristics of high speed quantum cryptography systems in the future.

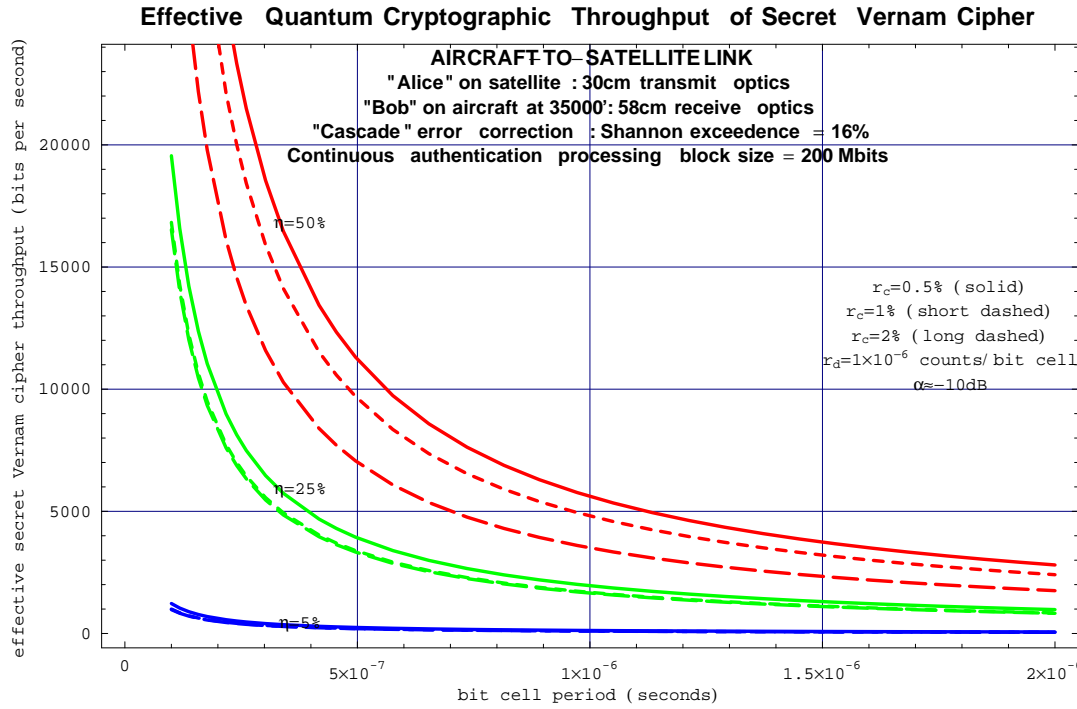


Figure 36: Effective Rate Graph for Aircraft-to-Satellite (LEO) Link: $\alpha = -10$ dB (“Bob” - 58 cm telescope at 35000’ ; “Alice” - 30 cm telescope on LEO satellite; commercial (1 MHz) photon detector)

An emerging commercial technology area that may find useful application in high speed quantum cryptography systems in the future would be the incorporation of tiny, fast mirror switches, such as the mirror components in the recently introduced Lucent WaveStar LambdaRouterTM [86]. The incorporation of these small optical components in networked systems, extending the application of quantum cryptography to allow for integration into existing, multi-node communications architectures, is an area that has not been thoroughly studied.

A promising research activity currently supported by the U.S. Defense Advanced Research Projects Agency (DARPA) is a project called “Steered Agile Beams” (STAB) conducted by the U.S. Air Force Research Laboratory, which is intended to develop chip-scale laser beam control components for a number of applications [87]. If successful, this work should in particular benefit applications that depend on adaptive optics to correct for the types of atmospheric-induced losses that were considered and calculated in detail in Section 4.1 above.

6 Discussion

We have carried out a detailed analysis of the various processes and constraints that determine the operating characteristics of a practical quantum key distribution system. This analysis applies generally to quantum cryptography systems built entirely from currently available commercial technology. Our results also allow us to establish the requirements that need to be satisfied in order to execute practical, unconditionally secret high-speed quantum cryptography in actual physical environments. An important objective has been to determine the extent to which it is possible to increase system throughput rates to high values for actual quantum cryptography systems. Insofar as is possible, we have been guided by the desire to achieve this solely with mature, currently available commercial technology. Based on the results of our analysis, we have proposed a general quantum cryptography design that meets this criterion, with the only system element that is not available today as mature technology identified as the necessary fast photon detection apparatus. We have mathematically shown that it should be possible to achieve high-speed transmission of secret Vernam cipher throughput in various scenarios with sufficiently fast photon detectors that can operate at a speed of 10 Gigabits-per-second, and we have identified HEP photon detection as a promising approach to solving this technological problem. Although our calculations show that, due to the extremely large losses and loads that characterize and constrain any practical QC system even this very high speed of photon detection will not suffice to achieve Gigabit-per-second throughput values for a single beam arrangement, a properly multiplexed multiple beam architecture should be able to achieve rates approaching this.

7 Acknowledgements

The members of the MITRE Quantum Information Processing Group, including A. Donadio, M. Drake, R. Ewing, J. Guttman, P. Henry and J. Thayer are thanked for many useful discussions and comments, with special thanks to A. Donadio for carrying out the FASCODE computer simulations and to R. Ewing and J. Guttman for specific helpful contributions to the research reported in this paper. J. Babcock, T. Elkins and R. Fante are thanked for reading the draft version of this document and for providing various helpful suggestions. M. Visser (Washington University in St. Louis) is thanked for several discussions and for carrying out the calculation in Appendix A. The authors wish to thank R. Sobolewski (University of Rochester) and I. Duling, III (U.S. Naval Research Laboratory) for useful discussions and comments. The authors also wish to thank particular employees of the U.S. National Security Agency for helpful comments and questions. GG in addition wishes to thank Ja. F. Providakes and Ji. F. Providakes for encouragement, and especially D. Lehman and the MITRE Technology Program for supporting this work and helping him to establish the MITRE Quantum Information Processing Group.

8 Appendices

A Derivation of the Relation between Intrinsic Channel Error and Polarizer Misalignment

In this section we shall develop for the case of a free-space implementation of quantum cryptography an explicit estimate for r_c , the intrinsic channel error rate. The most obvious of the problems that could lead to intrinsic channel error are due to the misalignment of the polarizers: if they are not quite at 45 degrees or 90 degrees the analysis of the protocol must be altered; we now proceed to perform such an analysis in terms of the angular mismatch of the polarizers.

Suppose we have two polarizers, one at the emitting end and one at the receiving end, that are rotated with respect to each other by an angle $\Delta\theta$. Then the probability that a photon will get through the second, given that it gets through the first (and so be detected if it is emitted in the first place) is given by Malus's law:

$$\text{Prob}(\Delta\theta) = \cos^2(\Delta\theta). \quad (301)$$

In the situation we are interested in, the photon is emitted in one of four polarization states, conventionally at roughly 0, 45, 90, or 135 degrees, ($\theta \in \{0, \pi/4, \pi/2, 3\pi/4\}$): we shall denote these nominal states by $\leftrightarrow, \nearrow, \uparrow, \nwarrow$ respectively) with roughly equal (classical) probabilities of $\approx 1/4$. Call the actual probabilities p_e^i (here e stands for emission; i stands for one of the four orientations), and call the actual angles the emission polarizers are set at θ_e^i .

Now call the actual angles the reception polarizers are set at θ_r^i ; and the actual probability that the reception polarizer is set to this position p_r^i .

The probability that the detector actually sees a photon if it is at a particular setting θ_r^i is

$$\text{Prob}(\text{detect at } i) = \sum_j p_e^j \cos^2(\theta_e^j - \theta_r^i). \quad (302)$$

(We note that, if all values are nominal so that $p_e \rightarrow 1/4$, $\Delta\theta \in \{0, \pi/4, \pi/2, 3\pi/4\}$, this reduces to $\text{Prob}(\text{detect at } i) \rightarrow \frac{1}{2}$, independent of i , as it should.)

If we now average over all detector settings, the probability of detecting a photon is

$$\text{Prob}(\text{detect}) = \sum_i \sum_j p_e^j p_r^i \cos^2(\theta_e^j - \theta_r^i). \quad (303)$$

This is rather complicated in general. We now consider a useful special case by assuming that the probabilities are nominal, so that $p_e^i = p_r^i = 1/4$, and that the reception and emission

polarizers are each perfectly aligned internally, with at most a relative mismatch of δ . That is:

$$\theta_r^i \in \{0, \pi/4, \pi/2, 3\pi/4\} \quad (304)$$

and

$$\theta_e^i \in \{0 + \delta, \pi/4 + \delta, \pi/2 + \delta, 3\pi/4 + \delta\} . \quad (305)$$

Then we find

$$\begin{aligned} \text{Prob(detect)} &= (1/4) \cdot (1/4) \cdot 4 \cdot \\ &\quad \left[\cos^2(\delta) + \cos^2(\pi/4 + \delta) \right. \\ &\quad \left. + \cos^2(\pi/2 + \delta) + \cos^2(3\pi/4 + \delta) \right] , \end{aligned} \quad (306)$$

so that

$$\begin{aligned} \text{Prob(detect)} &= (1/4) \left[\cos^2(\delta) + \cos^2(\pi/4 + \delta) + \sin^2(\delta) + \sin^2(\pi/4 + \delta) \right] \\ &= \frac{1}{2} . \end{aligned} \quad (307)$$

This is exactly the same as if there were no angular mismatch, so we do not lose here, but this is only the “raw” rate before any processing. The next step proceeds as follows. If Bob detects a photon and knows that the receiving polarizer is at angle θ_r^i , he may query Alice as to whether her polarizer was nominally set at $P_+ = \{0, \pi/2\} = \{\leftrightarrow, \uparrow\}$ or $P_\times = \{\pi/4, 3\pi/4\} = \{\swarrow, \nwarrow\}$. When θ_r^i as used by Bob is in the same nominal polarization class as (P_+ or P_\times) as the bit sent by Alice, Bob keeps it, and otherwise discards it, attributing it to a case of crossed polarizers. Doing so nominally throws away half the received bits.

If we allow p_e^i to deviate from 1/4, the probability that Bob keeps the received bit (received at θ_r^i) is then given by summing the probabilities that this bit was sent when Alice had her polarizers at one of the nominally compatible positions:

$$\text{Prob}(\text{keep at } i \mid \text{detect at } i) = \sum_j p_e^j \Theta(j \text{ compatible with } i) . \quad (308)$$

(Here Θ is 1 or 0 depending on whether the polarizer orientations are compatible or incompatible.)

To be more explicit, we may write

$$\Theta(\uparrow, \uparrow) = \Theta(\uparrow, \leftrightarrow) = \Theta(\leftrightarrow, \uparrow) = \Theta(\leftrightarrow, \leftrightarrow) = 1 , \quad (309)$$

$$\Theta(\swarrow, \swarrow) = \Theta(\swarrow, \nwarrow) = \Theta(\nwarrow, \swarrow) = \Theta(\nwarrow, \nwarrow) = 1 , \quad (310)$$

$$\Theta(\uparrow, \nwarrow) = \Theta(\uparrow, \swarrow) = \Theta(\leftrightarrow, \nwarrow) = \Theta(\leftrightarrow, \swarrow) = 0 \quad (311)$$

and

$$\Theta(\nwarrow, \uparrow) = \Theta(\nwarrow, \leftrightarrow) = \Theta(\swarrow, \uparrow) = \Theta(\swarrow, \leftrightarrow) = 0 . \quad (312)$$

This can be made more compact by defining the simple function:

$$\wp : \{\leftrightarrow, \nearrow, \uparrow, \nwarrow\} \rightarrow \{+, \times\} \quad (313)$$

so that in terms of the ordinary Kronecker delta one has

$$\Theta(i \text{ compatible with } j) = \delta_{\wp(i)\wp(j)} , \quad (314)$$

and thus

$$\text{Prob}(\text{keep at } i \mid \text{detect at } i) = \sum_j p_e^j \delta_{\wp(i)\wp(j)} . \quad (315)$$

Note that this is independent of the actual mismatch angles, and depends only on *a priori* conventional decisions of what constitutes a nominal match or mismatch of the polarization orientations. (We note that if all $p_e^j = 1/4$ we have $\text{Prob}(\text{keep at } i \mid \text{detect at } i) \rightarrow (1/4) \cdot (1 + 0 + 1 + 0) = (1/4) \cdot 2 = \frac{1}{2}$, which is independent of i as it should be.)

Now, the key step addresses the question: What is the probability that an error is made in this last negotiation?

An error occurs if, despite the fact that Bob and Alice agree on the nominal polarization class (P_+ or P_\times) they disagree on the value of the bit that was transmitted. This happens if $\theta_e \neq \theta_r$ but θ_e and θ_r are in the same polarization class. (That is, $\theta_e \approx \theta_r \pm \pi/2$; we will write this as $\theta_e = \text{Crossover}(\theta_r)$, meaning pick the other supposedly orthogonal element of the polarization basis.) This is explicitly given by:

$$\text{Crossover}(\theta_r[\leftrightarrow]) = \theta_e[\uparrow] , \quad (316)$$

$$\text{Crossover}(\theta_r[\nearrow]) = \theta_e[\nwarrow] , \quad (317)$$

$$\text{Crossover}(\theta_r[\uparrow]) = \theta_e[\leftrightarrow] \quad (318)$$

and

$$\text{Crossover}(\theta_r[\nwarrow]) = \theta_e[\nearrow] . \quad (319)$$

The probability of such an error occurring is then:

$$\text{Prob}(\text{error at } i \mid \text{keep at } i) = \cos^2(\theta_r^i - \text{Crossover}(\theta_r^i)) . \quad (320)$$

The easiest case to deal with is when the emitting and receiving polarizers are each internally properly aligned, and the only mismatch is due to an overall rotation between the two. (We have already seen that in this case $\text{Prob}(\text{detect}) = \frac{1}{2}$ and $\text{Prob}(\text{keep}) = \frac{1}{2}$ are unaffected.) Recall that now we have as *exact* statements that:

$$\theta_r \in \{0, \pi/4, \pi/2, 3\pi/4\} \quad (321)$$

and

$$\theta_e \in \{0 + \delta, \pi/4 + \delta, \pi/2 + \delta, 3\pi/4 + \delta\} . \quad (322)$$

In this situation

$$\text{Crossover}(\theta_r) = \theta_r + \pi/2 + \delta , \quad (323)$$

and the probability of error is independent of i and equals

$$\text{Prob}(\text{error} \mid \text{keep}) = \cos^2(\pi/2 + \delta) = \sin^2(\delta) . \quad (324)$$

In particular, even if δ is as big as $1/10$ radian (5.7 degrees), the probability of error is less than 1%, which is a very useful result, as this amount of airborne platform attitude control is easily achievable in practice.

We now consider the completely general case with arbitrary values for the system angles. We already have

$$\text{Prob}(\text{detect}) = \sum_i \sum_j p_e^j p_r^i \cos^2(\theta_e^j - \theta_r^i) . \quad (325)$$

In the same way we find

$$\text{Prob}(\text{keep}) = \sum_i p_r^i \text{Prob}(\text{keep at } i) \quad (326)$$

$$= \sum_i p_r^i \text{Prob}(\text{keep at } i \mid \text{detect at } i) \text{Prob}(\text{detect at } i) \quad (327)$$

$$= \sum_i p_r^i \left(\sum_j p_e^j \delta_{\varphi(i)\varphi(j)} \right) \left(\sum_j p_e^j \cos^2(\theta_e^j - \theta_r^i) \right) . \quad (328)$$

We also have

$$\text{Prob}(\text{error}) = \sum_i p_r^i \text{Prob}(\text{error at } i) \quad (329)$$

$$= \sum_i p_r^i \text{Prob}(\text{error at } i \mid \text{keep at } i) \times \text{Prob}(\text{keep at } i \mid \text{detect at } i) \text{Prob}(\text{detect at } i) \quad (330)$$

$$= \sum_i p_r^i \left(\cos^2(\theta_r^i - \text{Crossover}(\theta_r^i)) \right) \left(\sum_j p_e^j \delta_{\varphi(i)\varphi(j)} \right) \times \left(\sum_j p_e^j \cos^2(\theta_e^j - \theta_r^i) \right) . \quad (331)$$

Although these expressions are rather complicated and too cumbersome to be analytically useful, they do have all the correct limits. The important point is that with the application of suitably high quality design control the possibility of intrinsic mismatch should not constitute a high priority issue.

Thus, the final, practical result for actual systems is given by eq.(324): The fractional error rate due to net polarizer misalignment is given by

$$r_c = \sin^2(\delta) \quad (332)$$

as presented in the text in eq.(206).

B Packetization Approximation

Consider a message of length M bits. Applying an error correction code to the message results in a string of length χ_{EC} bits. If the communications protocol supports data frames of length m_p , then the number of packets transmitted is

$$\mathcal{N} = \left\lceil \frac{\chi_{EC}M}{m_p} \right\rceil. \quad (333)$$

All packets but the last are of length $m_p + f_o$, where f_o is the frame overhead of the communications protocol. The last packet is shorter, due to the fact that its data frame is not full, but contains only $(\chi_{EC}M) \bmod m_p$ bits. The total number of bits in the transmission is then

$$\mathcal{C} = (m_p + f_o) \left\lfloor \frac{\chi_{EC}M}{m_p} \right\rfloor + (\chi_{EC}M) \bmod m_p + f_o \mathcal{D}(\chi_{EC}M, m_p), \quad (334)$$

where

$$\mathcal{D}(a, b) \equiv \begin{cases} 1 & \text{if } a \bmod b \neq 0 \\ 0 & \text{if } a \bmod b = 0 \end{cases}. \quad (335)$$

The idea of the packetization approximation is to simplify this expression for large numbers of packets so as to avoid the mathematical complication introduced by treating the last packet as a special case. We begin by writing the identity

$$\chi_{EC}M = \left\lfloor \frac{\chi_{EC}M}{m_p} \right\rfloor m_p + (\chi_{EC}M) \bmod m_p, \quad (336)$$

from which it follows that

$$\left\lfloor \frac{\chi_{EC}M}{m_p} \right\rfloor = \frac{\chi_{EC}M}{m_p} - \frac{(\chi_{EC}M) \bmod m_p}{m_p}. \quad (337)$$

Substituting this in eq.(334) gives

$$\begin{aligned} \mathcal{C} &= (m_p + f_o) \frac{\chi_{EC}M}{m_p} - (m_p + f_o) \frac{(\chi_{EC}M) \bmod m_p}{m_p} \\ &\quad + (\chi_{EC}M) \bmod m_p + f_o \mathcal{D}(\chi_{EC}M, m_p) \end{aligned}$$

$$= \left(1 + \frac{f_o}{m_p}\right) \chi_{EC} M + f_o \left[\mathcal{D}(\chi_{EC} M, m_p) - \frac{(\chi_{EC} M) \bmod m_p}{m_p} \right] . \quad (338)$$

The quantity in square brackets is always in the range $[0, 1)$, so that

$$f_o \left[\mathcal{D}(\chi_{EC} M, m_p) - \frac{(\chi_{EC} M) \bmod m_p}{m_p} \right] < f_o . \quad (339)$$

If the message is long enough to require several packets, that is, if

$$\frac{\chi_{EC} M}{m_p} \gg 1 , \quad (340)$$

then

$$f_o \ll f_o \frac{\chi_{EC} M}{m_p} < \left(1 + \frac{f_o}{m_p}\right) \chi_{EC} M , \quad (341)$$

which, with eq.(339), gives

$$f_o \left[\mathcal{D}(\chi_{EC} M, m_p) - \frac{(\chi_{EC} M) \bmod m_p}{m_p} \right] \ll \left(1 + \frac{f_o}{m_p}\right) \chi_{EC} M . \quad (342)$$

We may therefore neglect the term in square brackets in eq.(338) to obtain

$$\mathcal{C} \simeq \left(1 + \frac{f_o}{m_p}\right) \chi_{EC} M , \quad (343)$$

which is valid as long as eq.(340) is satisfied.

C Statistical Results for Error Correction

The length of the entire sifted string is n . The number of errors in the string after the i th iteration of the error detection and correction step is denoted by $e_T^{(i)}$, and the number of errors before error correction begins is

$$e_T^{(0)} \equiv e_T . \quad (344)$$

Each iteration of the error detection and correction step begins by breaking the string into blocks such that the expected number of errors in each block is less than or equal to the parameter ϱ . The number of blocks in the string is then

$$J^{(i)} = \left\lceil \frac{e_T^{(i-1)}}{\varrho} \right\rceil. \quad (345)$$

and the average number of bits per block is

$$k^{(i)} = \frac{n}{J^{(i)}}. \quad (346)$$

We wish to find an expression for the number of errors remaining after each iteration, from which the other parameters of interest can be obtained. At the beginning of the i th iteration, there are $e_T^{(i-1)}$ errors distributed among $J^{(i)}$ blocks, so that the probability of a given error being in a particular block is

$$\mathcal{P}(\text{one specific error in a given block}) = \frac{1}{J^{(i)}} \simeq \frac{\varrho}{e_T^{(i-1)}}. \quad (347)$$

The probability of l errors occurring in a given block is given by a binomial distribution:

$$\mathcal{P}(l \text{ errors in a given block}) \simeq \binom{e_T^{(i-1)}}{l} \left(\frac{\varrho}{e_T^{(i-1)}} \right)^l \left[1 - \left(\frac{\varrho}{e_T^{(i-1)}} \right) \right]^{e_T^{(i-1)} - l}. \quad (348)$$

If the number of errors, and thus the number of blocks, is large, this can be approximated by a Poisson distribution [88] as follows:

$$\mathcal{P}(l \text{ errors in a given block}) \simeq e^{-\varrho} \frac{\varrho^l}{l!}. \quad (349)$$

The parity check will reveal an error in the block if and only if there is an odd number of errors in the block. The probability of detecting an error is thus

$$\mathcal{P}(\text{finding an error in the block}) \simeq e^{-\varrho} \sum_{l \text{ odd}}^{\infty} \frac{\varrho^l}{l!}. \quad (350)$$

To find the sum over odd l , note first that

$$e^{\varrho} = \sum_{l=0}^{\infty} \frac{\varrho^l}{l!}, \quad (351)$$

and

$$e^{-\varrho} = \sum_{l=0}^{\infty} (-1)^l \frac{\varrho^l}{l!}, \quad (352)$$

so that

$$e^{\varrho} - e^{-\varrho} = 2 \sum_{l \text{ odd}}^{\infty} \frac{\varrho^l}{l!}, \quad (353)$$

or

$$\sum_{l \text{ odd}}^{\infty} \frac{\varrho^l}{l!} = \frac{1}{2} (e^{\varrho} - e^{-\varrho}), \quad (354)$$

and eq.(350) becomes

$$\mathcal{P}(\text{finding an error in the block}) \simeq \frac{1 - e^{-2\varrho}}{2}. \quad (355)$$

The expected number of errors found in the i th iteration is then

$$\begin{aligned} e_f^{(i)} &\simeq J^{(i)} \frac{1 - e^{-2\varrho}}{2} \\ &\simeq e_T^{(i-1)} \frac{1 - e^{-2\varrho}}{2\varrho}. \end{aligned} \quad (356)$$

The number of errors remaining after the i th iteration is

$$\begin{aligned} e_T^{(i)} &\equiv e_T^{(i-1)} - e_f^{(i)} \\ &\simeq e_T^{(i)} \left[1 - \frac{1 - e^{-2\varrho}}{2\varrho} \right] \\ &\simeq e_T^{(i)} \left(\frac{2\varrho - 1 + e^{-2\varrho}}{2\varrho} \right). \end{aligned} \quad (357)$$

The quantity in parentheses is a function of ϱ only. We introduce the notation

$$\beta \equiv \frac{2\varrho - 1 + e^{-2\varrho}}{2\varrho} , \quad (358)$$

in terms of which eq.(357) becomes

$$e_T^{(i)} \simeq \beta e_T^{(i-1)} . \quad (359)$$

We proceed by induction to obtain the number of errors remaining after the i th iteration in terms of the initial number of errors and β , which is a function of the parameter ϱ introduced to establish the block size for error detection:

$$e_T^{(i)} \simeq \beta^i e_T^{(0)} . \quad (360)$$

The number of errors found during the i th iteration is then

$$\begin{aligned} e_f^{(i)} &\simeq e_T^{(i-1)} - e_T^{(i)} \\ &\simeq (1 - \beta) \beta^{i-1} e_T^{(0)} . \end{aligned} \quad (361)$$

The number of blocks for the i th pass is approximately

$$\begin{aligned} J^{(i)} &\simeq \frac{e_T^{(i-1)}}{\varrho} \\ &\simeq \beta^{i-1} \frac{e_T^{(0)}}{\varrho} , \end{aligned} \quad (362)$$

and the number of bits in a block is

$$\begin{aligned} k^{(i)} &= \frac{n}{J^{(i)}} \\ &\simeq \frac{\varrho n}{\beta^{i-1} e_T^{(0)}} . \end{aligned} \quad (363)$$

The error detection and correction step ends when there would be two or fewer blocks for the subsequent iteration. The number of iterations completed, N_1 , thus satisfies

$$J^{(N_1+1)} \leq 2 , \quad (364)$$

or

$$\beta^{N_1} \frac{e_T^{(0)}}{\varrho} \leq 2 , \quad (365)$$

so that

$$\beta^{N_1} \leq \frac{2\varrho}{e_T^{(0)}} , \quad (366)$$

and, since $\beta < 1$,

$$N_1 \simeq \left\lceil \frac{\log_2 \frac{2\varrho}{e_T^{(0)}}}{\log_2 \beta} \right\rceil . \quad (367)$$

The expected number of errors remaining after this step is then

$$\begin{aligned} e_T^{(r)} &\simeq \beta^{N_1} e_T^{(0)} \\ &\simeq 2\varrho . \end{aligned} \quad (368)$$

We next estimate the number of iterations in the validation step. Each iteration detects either a single error or no errors. Let $N_2^{(n)}$ denote the number of iterations in which no error is detected, and let $N_2^{(f)}$ denote the number of iterations in which an error is detected. The iterations continue until there are N_2 successive iterations in which no error is detected.

First we find $N_2^{(n)}$, which can be written

$$N_2^{(n)} \equiv \sum_{l=0}^{\infty} \hat{N}^{(n)}(l) \mathcal{P}(l \text{ residual errors}) , \quad (369)$$

where $\hat{N}^{(n)}(l)$ is the expected number of error-free iterations when there are initially l errors. We find this by induction. If there are no errors, no iterations will detect an error, and the process will end after N_2 iterations:

$$\hat{N}^{(n)}(0) = N_2 . \quad (370)$$

If there are $l + 1$ errors, then one of two things can occur. There may be N_2 successive iterations without errors, or an error may be detected on the iteration following N error-free

iterations, where $0 \leq N \leq N_2 - 1$. If an error is found, the process repeats from a starting point of l residual errors. This gives the following recurrence relation:

$$\begin{aligned}\hat{N}^{(n)}(l+1) &= N_2 \mathcal{P} \left(N_2 \text{ successive error-free iterations} \mid l+1 \text{ residual errors} \right) \\ &+ \sum_{N=0}^{N_2-1} \left[N + \hat{N}^{(n)}(l) \right] \mathcal{P} \left(N \text{ successive error-free iterations} \mid l+1 \text{ residual errors} \right) \\ &\cdot \mathcal{P} \left(1 \text{ error-detection iteration} \mid l+1 \text{ residual errors} \right) .\end{aligned}\quad (371)$$

We need to find several probabilities to make use of this formula. We begin by investigating the probability of an error-detected iteration given l residual errors. The error detection algorithm first builds a block of bits by selecting bits from the original string at random. The parity of the block is computed, and an error will be detected if there is an odd number of errors in the randomly selected block. This gives the following expression for the desired probability:

$$\mathcal{P} \left(1 \text{ error-detection iteration} \mid l \text{ residual errors} \right) = \sum_{l' \text{ odd}}^l \binom{l}{l'} \left(\frac{1}{2} \right)^{l'} \left(\frac{1}{2} \right)^{l-l'} \quad (372)$$

We use the identities

$$\sum_{l'=0}^l \binom{l}{l'} \left(\frac{1}{2} \right)^{l'} \left(\frac{1}{2} \right)^{l-l'} - \sum_{l'=0}^l \binom{l}{l'} \left(\frac{1}{2} \right)^{l'} \left(-\frac{1}{2} \right)^{l-l'} = 2 \sum_{l' \text{ odd}}^l \binom{l}{l'} \left(\frac{1}{2} \right)^{l'} \left(\frac{1}{2} \right)^{l-l'} , \quad (373)$$

and

$$\begin{aligned}\sum_{l'=0}^l \binom{l}{l'} \left(\frac{1}{2} \right)^{l'} \left(\frac{1}{2} \right)^{l-l'} - \sum_{l'=0}^l \binom{l}{l'} \left(\frac{1}{2} \right)^{l'} \left(-\frac{1}{2} \right)^{l-l'} &= \left(\frac{1}{2} + \frac{1}{2} \right)^l - \left[\frac{1}{2} + \left(-\frac{1}{2} \right) \right]^l \\ &= 1 ,\end{aligned}\quad (374)$$

which holds for $l \geq 1$. This gives

$$\sum_{l' \text{ odd}}^l \binom{l}{l'} \left(\frac{1}{2} \right)^{l'} \left(\frac{1}{2} \right)^{l-l'} = \frac{1}{2} , \quad (375)$$

from which we obtain the result

$$\mathcal{P} (1 \text{ error} - \text{detected iteration} \mid l \text{ residual errors}) = \frac{1}{2} , \quad (376)$$

provided $l \neq 0$. If $l = 0$, there is no error to detect, and the probability is 0, so that our final result is

$$\mathcal{P} (1 \text{ error} - \text{detected iteration} \mid l \text{ residual errors}) = \frac{1}{2} (1 - \delta_{l,0}) . \quad (377)$$

This is a sensible result. Since the block of bits is selected at random, there should be no bias towards an even or an odd number of errors in the block, unless there are no errors to start with.

The probability of an error-free iteration is found by subtracting this result from 1:

$$\mathcal{P} (1 \text{ error} - \text{free iteration} \mid l \text{ residual errors}) = \frac{1}{2} (1 + \delta_{l,0}) . \quad (378)$$

The probability of N successive error-free iterations is thus

$$\mathcal{P} (N \text{ successive error-free iterations} \mid l \text{ residual errors}) = \delta_{l,0} + (1 - \delta_{l,0}) \left(\frac{1}{2} \right)^N . \quad (379)$$

With these results, eq.(371) becomes

$$\begin{aligned} \hat{N}^{(n)} (l+1) &= N_2 \left(\frac{1}{2} \right)^{N_2} \\ &\quad + \sum_{N=0}^{N_2-1} [N + \hat{N}^{(n)} (l)] \left(\frac{1}{2} \right)^N \cdot \left(\frac{1}{2} \right) \\ &= \left(\frac{1}{2} \right)^{N_2} N_2 \\ &\quad + \sum_{N=0}^{N_2-1} \left(\frac{1}{2} \right)^{N+1} [N + \hat{N}^{(n)} (l)] \\ &= \left[1 - \left(\frac{1}{2} \right)^{N_2} \right] + \left[1 - \left(\frac{1}{2} \right)^{N_2} \right] \hat{N}^{(n)} (l) . \end{aligned} \quad (380)$$

Introducing

$$A \equiv \left[1 - \left(\frac{1}{2} \right)^{N_2} \right] , \quad (381)$$

this becomes

$$\begin{aligned} \hat{N}^{(n)}(l+1) &= A + A\hat{N}^{(n)}(l) \\ &= A^{l+1}\hat{N}^{(0)}(l) + \sum_{s=1}^l A^s \\ &= A^{l+1}N_2 + \frac{A - A^{l+2}}{1 - A} \end{aligned} \quad (382)$$

Renaming the argument of the function to l gives, for $l > 0$,

$$\begin{aligned} \hat{N}^{(n)}(l) &= A^l N_2 + \frac{A - A^{l+1}}{1 - A} \\ &= A^l N_2 + \frac{1 - A^l}{1 - A} A \\ &= \left[1 - \left(\frac{1}{2} \right)^{N_2} \right]^l N_2 + 2^{N_2} \left\{ 1 - \left[1 - \left(\frac{1}{2} \right)^{N_2} \right]^l \right\} \\ &= \left[1 - \left(\frac{1}{2} \right)^{N_2} \right]^l (N_2 - 2^{N_2} + 1) + (2^{N_2} - 1) \end{aligned} \quad (383)$$

Practical values of $N_2 \sim 30$ imply that

$$\left(\frac{1}{2} \right)^{N_2} \ll 1 . \quad (384)$$

In this limit, eq.(383) becomes

$$\begin{aligned} \hat{N}^{(n)}(l) &\simeq \left[1 - l \left(\frac{1}{2} \right)^{N_2} \right] (N_2 - 2^{N_2} + 1) + (2^{N_2} - 1) \\ &\simeq N_2 \left[1 - l \left(\frac{1}{2} \right)^{N_2} \right] + l \left(\frac{1}{2} \right)^{N_2} (2^{N_2} - 1) \\ &\simeq N_2 + l . \end{aligned} \quad (385)$$

Substituting this in eq.(369) yields

$$\begin{aligned}
N_2^{(n)} &\simeq N_2 + \langle l \rangle \\
&\simeq N_2 + e_T^{(r)} \\
&\simeq N_2 + 2\varrho ,
\end{aligned} \tag{386}$$

where we have used eq.(368) to estimate the number of errors at the beginning of the process.

The recurrence relation for $\hat{N}_2^{(f)}$, the number of iterations during which an error is detected is

$$\begin{aligned}
\hat{N}_2^{(f)}(l+1) &= 0 \cdot \mathcal{P}(N_2 \text{ successive error-free iterations} \mid l+1 \text{ residual errors}) \\
&\quad + \sum_{N=0}^{N_2-1} [1 + \hat{N}_2^{(f)}(l)] \mathcal{P}(N \text{ successive error-free iterations} \mid l+1 \text{ residual errors}) \\
&\quad \cdot \mathcal{P}(1 \text{ error-detected iteration} \mid l+1 \text{ residual errors}) .
\end{aligned} \tag{387}$$

The value at $l = 0$ is

$$\hat{N}_2^{(f)}(0) = 0 , \tag{388}$$

since there are no errors to be detected in this case. Use of eq.(377) and eq.(379) yields the result

$$\begin{aligned}
\hat{N}_2^{(f)}(l) &\simeq (2^{N_2} - 1) \left\{ 1 - \left[1 - \left(\frac{1}{2} \right)^{N_2} \right]^l \right\} \\
&\simeq l ,
\end{aligned} \tag{389}$$

from which we find

$$\begin{aligned}
N_2^{(f)} &\simeq \langle l \rangle \\
&\simeq e_T^{(r)} \\
&\simeq 2\varrho .
\end{aligned} \tag{390}$$

Finally, we estimate an upper bound for the probability that an error remains after the validation step. The probability of one or more residual errors is

$$\begin{aligned}
p_{\text{resid}} &= \mathcal{P}(\text{residual errors} \mid N_2 \text{ error free iterations}) \\
&= \frac{\mathcal{P}(\text{residual errors and } N_2 \text{ error free iterations})}{\mathcal{P}(N_2 \text{ error free iterations})} \\
&= \frac{\sum_{l=1}^{\infty} \mathcal{P}(N_2 \text{ error free iterations} \mid l \text{ residual errors}) \mathcal{P}(l \text{ residual errors})}{\sum_{l=0}^{\infty} \mathcal{P}(N_2 \text{ error free iterations} \mid l \text{ residual errors}) \mathcal{P}(l \text{ residual errors})} \\
&\leq \frac{\sum_{l=1}^{\infty} \mathcal{P}(N_2 \text{ error free iterations} \mid l \text{ residual errors}) \mathcal{P}(l \text{ residual errors})}{\mathcal{P}(N_2 \text{ error free iterations} \mid 0 \text{ residual errors}) \mathcal{P}(0 \text{ residual errors})}.
\end{aligned} \tag{391}$$

By the argument that led to eq.(379), if there are residual errors in the string, the probability of N_2 successive error-free iterations is

$$\mathcal{P}(N_2 \text{ error free iterations} \mid l \text{ residual errors}) = \left(\frac{1}{2}\right)^{N_2}, \tag{392}$$

and the probability of any number of error free iterations in the absence of residual errors is 1, so that eq.(391) becomes

$$\begin{aligned}
p_{\text{resid}} &\leq \frac{\sum_{l=1}^{\infty} \left(\frac{1}{2}\right)^{N_2} \mathcal{P}(l \text{ residual errors})}{\mathcal{P}(0 \text{ residual errors})} \\
&\leq \frac{\left(\frac{1}{2}\right)^{N_2} \mathcal{P}(\text{residual errors})}{\mathcal{P}(0 \text{ residual errors})} \\
&\leq \frac{\left(\frac{1}{2}\right)^{N_2}}{\mathcal{P}(0 \text{ residual errors})}.
\end{aligned} \tag{393}$$

The probability of 0 residual errors after the validation step is no less than the probability of 0 residual errors after the error detection and correction step, since the validation step introduces no errors. We expect the errors remaining after the error detection step to be Poisson distributed with mean $\sim 2\varrho$, so that

$$\mathcal{P}(0 \text{ residual errors}) \geq e^{-2\varrho} \tag{394}$$

and

$$\begin{aligned}
p_{resid} &\leq \frac{\left(\frac{1}{2}\right)^{N_2}}{e^{-2\rho}} \\
&\leq e^{2\rho} \left(\frac{1}{2}\right)^{N_2}.
\end{aligned} \tag{395}$$

For a reasonable choice of $\rho \sim 0.5$, the exponential factor is less than an order of magnitude, so that we may write

$$p_{resid} \leq O(10) \cdot \left(\frac{1}{2}\right)^{N_2} \tag{396}$$

for an upper bound on the probability that residual errors remain in the string after the validation step. This is a crucial result, since even a single error in the string will render the entire key useless after the privacy amplification hash function is applied.

D Assembly Code Segments

These segments of assembly code were developed to support an estimate of the number of operations required to carry out the computations in sifting, error correction, and privacy amplification. The emphasis is on the code that executes within loops that iterate through the bits of the key material being processed. In each case, a description of the context required for the code segment precedes the code itself.

The assembly language used is a variant of the IBM 370 assembly language. The principal extension is the use of register increment and decrement instructions. We have also ignored the distinction between incrementing a counter by one and incrementing an index register by the size of an array element, since either operation requires exactly one instruction. Note also the use of unsigned arithmetic operations when operating on multi-word integers.

D.1 Code to compute block parity

The bits have been unpacked so that each bit occupies one word

Register B contains the address of the beginning of the block

Register END contains the address of the first word beyond the end of the block

When done, register PARITY will contain the parity of the block

STARTLOOP	SR	PARITY, PARITY	Clear parity register Check if end of block is reached
	CR	B, END	
	BGE	DONE	
DONE	XOR	PARITY, 0(B)	Update parity register Increment to get address of next bit
	INC	B	
DONE	B	STARTLOOP	Exit from loop
	EQU	*	

Instruction count: 5 instructions in loop

Iteration count: 1 iteration per input bit

D.2 Code to extract substring for hash function

BUF contains the full bit string packed into memory

I0 contains the word index for the start of the substring

I1 contains the bit offset for the start of the substring

J0 contains the word index for the start of the next substring

J1 contains the bit offset for the start of the next substring

MASKA and MASKB are arrays containing bit masks for right and left justified substrings within a word

SHIFTA = $W - \log_2 W$ and SHIFTB = $\log_2 W$ are shift counts used to update the start of string indices, I0, I1, J0, and J1, for the next iteration, where W is the wordsize of the machine

LEN = $2s$ is the size of the substring to which the hash function is applied

Register names of form R0, R1 indicate linked even-odd register pairs

When done, register pair A0, A1 will contain the substring, right justified

L	A1,BUF(I0)	First part of substring, right justified in A0+A1
N	A1,MASKA(I1)	
SR	A0, A0	
LR	DELTA, J0	

SR	DELTA, I0	
C	DELTA, ONE	Substring spans 2 words or 3?
BLE	TWOWORDS	
C	J1, ZERO	
BE	TWOWORDS	
LR	A0, A1	Move first part of substring into higher register
LR	K, I0	
INC	K	
L	A1, BUF(K)	Move second part of substring into lower register
TWOWORDS	L	B1, BUF(J0)
	N	B1, MASKB(J1)
	SR	B0, B0
	SLDLR	B0, J1
		Final part of substring, right justified in B0
	SLDLR	A0, J1
	OR	A1, B0
	LR	I0, J0
		Substring right justified in A0+A1
		Increment substring indices for next iteration
	LR	I1, J1
	SLL	J1, SHIFTA
	SLDL	J0, SHIFTB
	A	J0, LEN
	SRDL	J0, SHIFTB
	SRL	J1, SHIFTA

Instruction count: 26 instructions

D.3 Code to compute Carter-Wegman affine hash function for double-word integers

Input in linked pair of registers A0, A1

Multiplier in M0, M1

Additive parameter in P0, P1

When done, result is in registers E0, E1, E2, and E3

LR B1, A0 Upper word

	LR	C1, A1	Lower word
	LR	D1, A0	Upper word
	SR	A0, A0	Clear upper words for multiplication
	SR	B0, B0	
	SR	C0, C0	
	SR	D0, D0	
	MU	A0, M1	Multiply pairwise
	MU	B0, M1	
	MU	C0, M0	
	MU	D0, M0	
	SR	CARRY, CARRY	Clear carry for additions
	LR	E3, A1	Lowest order word
	AUR	E3, P1	
	BCZ	NOCARRY1	Branch if carry is zero
	INC	CARRY	
NOCARRY1	LR	E2, CARRY	Next higher order word
	SR	CARRY, CARRY	
	AUR	E2, A0	
	BCZ	NOCARRY2	
	INC	CARRY	
NOCARRY2	AUR	E2, B1	
	BCZ	NOCARRY3	
	INC	CARRY	
NOCARRY3	AUR	E2, C1	
	BCZ	NOCARRY4	
	INC	CARRY	
NOCARRY4	AUR	E2, P0	
	BCZ	NOCARRY5	
	INC	CARRY	
NOCARRY5	LR	E1, CARRY	Next higher order word
	SR	CARRY, CARRY	
	AUR	E1, B0	
	BCZ	NOCARRY6	
	INC	CARRY	
NOCARRY6	AUR	E1, C0	
	BCZ	NOCARRY7	
	INC	CARRY	
NOCARRY7	AUR	E1, D1	
	BCZ	NOCARRY8	
	INC	CARRY	
NOCARRY8	LR	E0, CARRY	Highest order word
	AUR	E0, D0	

Instruction count: 43 instructions

D.4 Code to compute multi-word hash function for privacy amplification

Input string is the multiplicand (N words)

Multiplier is first parameter of hash function (N words)

Output array initially contains the second, additive parameter of hash function in the lower order N words, the higher order $N + 1$ words are clear ($2N + 1$ words)

ASTART and AEND are addresses of highest and lowest order words of multiplier

BSTART and BEND are addresses of highest and lowest order words of multiplicand

CSTART is address of array of partial products

CROW is the size of a row of partial products ($2N + 1$ words)

CSIZE is the full size of the array of partial products ($N(2N + 1)$ words)

CEND is address of first word beyond partial products array

DSTART and DEND are addresses of the highest and lowest order words in output array

When done, the output array contains the full result of the affine transformation. The selection of the hashed substring is accomplished by saving only the portions of the output array that constitute the hashed substring.

	SR	Z, Z	Zero
	L	I, CSTART	Start of output array
	LR	J, I	
	A	J, CSIZE	One word beyond end of array
CLEAR	CR	I, J	
	BGE	MULTIPLY	
	ST	Z, 0(I)	Clear output array entry
	INC	I	
	B	CLEAR	
MULTIPLY	L	I, AEND	Multiplier index
	L	K, CSTART	
	A	K, CROW	
	DEC	K	Partial products end of row index

MPLIER	C	I, ASTART	
	BL	ADD	Branch when done multiplication
	L	MP, 0(I)	Get multiplier word
	L	J, BEND	Multiplicand index
	LR	L, K	Partial products entry index
	LR	LP, L	
	DEC	LP	Next higher order entry index
	LR	LPP, LP	
	DEC	LPP	Next higher order entry index
	C	J, BSTART	
MCAND	BL	MCANDEND	Branch when this row done
	L	MC1,0(J)	Get multiplicand word
	SR	HCARRY, HCARRY	Clear high order carry
	SR	MC0, MC0	
	MUR	MC0, MP	Multiply unsigned
	AU	MC1, 0(L)	Add carry from previous multiply
	BCZ	NOCARRY1	Carry?
	INC	MC0	Add in the carry
	BCZ	NOCARRY1	Carry?
	INC	HCARRY	Increment high order carry
NOCARRY1	A	MC0, 0(LP)	Add previous high order carry
	BCZ	NOCARRY2	Carry?
	INC	HCARRY	Increment high order carry
	ST	MC1, 0(L)	Store results
NOCARRY2	ST	MC0, 0(LP)	
	ST	HCARRY, 0(LPP)	
	DEC	J	Decrement indices for next word of multiplicand
	DEC	L	
MCANDEND	DEC	LP	
	DEC	LPP	
	B	MCAND	
	DEC	I	Update indices for next word of multiplier
ADD	A	K, CROW	
	DEC	K	
	B	MPLIER	
	L	L, CSTART	
	A	L, CROW	
	DEC	L	Low order word in row
	LR	M, DEND	Result index
OUTER	SR	CARRY, CARRY	Clear carry
	C	M, DSTART	
	BL	OUTEREND	

	LR	SUM, CARRY	Start with carry from previous sum
	SR	CARRY, CARRY	Clear carry
	LR	K, L	Entry index
INNER	C	K, CEND	
	BGE	INNEREND	
	AU	SUM, 0(K)	Add unsigned
	BCZ	NOCARRY3	
	INC	CARRY	
NOCARRY3	A	K, CROW	Next word to add
	B	INNER	
INNEREND	ST	SUM, 0(M)	Store result in output array
	DEC	L	Start for next column
	DEC	M	Index for next entry in output array
	B	OUTER	
OUTEREND	EQU	*	DONE

We introduce the notation

$$N_w \equiv \frac{n}{w} \quad (397)$$

for the number of words in the string to be hashed, where n is the number of bits in the string and w is the wordsize.

Instruction and iteration counts:

CLEAR loop - 5 instructions, $(2N_w + 1)N_w$ iterations

MPLIER loop - 13 instructions, N_w iterations

MCAND loop - 22 instructions, N_w^2 iterations

OUTER loop - 9 instructions, $(2N_w + 1)$ iterations

INNER loop - 7 instructions, $(2N_w + 1)N_w$ iterations

Total: $9 + 43N_w + 46N_w^2$ instructions

References

- [1] C.E. Shannon, "Communication Theory of Secrecy Systems," *Bell Syst. Tech. J.* **28**, 656 (1949).
- [2] G.S. Vernam, "Cipher Printing Telegraph Systems for Secret Wire and Radio Telegraphic Communications," *J. Amer. Inst. Elect. Eng.* **XLV**, 109-115 (1926).
- [3] W.T. Buttler, R.J. Hughes, S.K. Lamoreaux, G.L. Morgan, J.E. Nordholt and C.G. Peterson, "Daylight quantum key distribution over 1.6 km," *arXive e-print quant-ph/0001088* (2000).
- [4] R.J. Hughes, G.L. Morgan and C.G. Peterson, "Practical quantum key distribution over a 48-km optical fiber network," *arXive e-print quant-ph/9904038* (1999).
- [5] W.T. Buttler, R.J. Hughes, P.G. Kwiat, S.K. Lamoreaux, G.G. Luther, G.L. Morgan, J.E. Nordholt, C.G. Peterson and C.M. Simmons, "Practical free-space quantum key distribution over 1 km," *Phys. Rev. Lett.* **81**, 3283-3286 (1998).
- [6] R.J. Hughes, D.M. Alde, P. Dyer, G.G. Luther, G.L. Morgan and M. Schauer, "Quantum Cryptography," *arXive e-print quant-ph/9504002* (1995).
- [7] G. Ribordy, J.-D. Gautier, N. Gisin, O. Guinnard and H. Zbinden, "Fast and User-friendly Quantum Key Distribution," *arXive e-print quant-ph/9905056* (1999).
- [8] P.D. Townsend, "Experimental investigation of the performance limits for first telecommunications-window quantum cryptography systems," *IEEE Phot. Tech. Lett.* **10**, 7, 1048 (July 1, 1998).
- [9] P.D. Townsend, "Quantum cryptography on multi-user optical fibre networks," *Nature* **385**, 6611, 47 (January 2, 1997).
- [10] J.D. Franson, "Quantum cryptography," *Opt. Phot. News* **6**, 3, 30 (March 1, 1995).
- [11] J.D. Franson and H. Ilves, "Quantum cryptography using optical fibers," *App. Opt.* **33**, 14, 2949 (May 10, 1994).
- [12] A.J. Menezes, P.C. van Oorschot and S.A. Vanstone, *Handbook of Applied Cryptography*, CRC Press (1996).
- [13] B. Schneier, *Applied Cryptography: Protocols, Algorithms and Source Code in C*, John Wiley & Sons (1994).
- [14] C.H. Bennett and G. Brassard, in *Proc. IEEE Int. Conference on Computers, Systems and Signal Processing*, IEEE Press, New York (1984).

- [15] Federal Telecommunications Standards Committee, *Federal Standard 1037C: Glossary of Telecommunications Terms (FED-STD-1037C)*, National Communications System Technology Program Office, Arlington, Virginia (1996).
- [16] National Security Telecommunications and Information Systems Security Committee, *National Information Systems Security (INFOSEC) Glossary* (NSTISSI No. 4009), U.S. National Security Agency, Ft. Meade, Maryland (June 5, 1992).
- [17] B. Schneier, Crypto-Gram Newsletter, Counterpane Internet Security, Inc. (May 15, 2000).
- [18] A.K. Ekert, Phys. Rev. Lett. **67**, 661 (1991).
- [19] G. Ribordy, J. Brendel, J.-D. Gautier, N. Gisin and H. Zbinden, “Long distance entanglement based quantum key distribution,” *arXive e-print* quant-ph/0008039 (2000).
- [20] G. Gilbert, J. Guttman, M. Hamrick, J. Shapiro, J. Thayer, In preparation.
- [21] B. Slutsky, P.-C. Sun, Y. Mazurenko, R. Rao and Y. Fainman, “Effect of channel imperfection on the secrecy capacity of a quantum cryptographic system,” J. Mod. Opt. **44**, 5, 953-961 (1997).
- [22] M. Dusek, M. Jahma and N. Lütkenhaus, “Unambiguous state discrimination in quantum cryptography with weak coherent states,” Phys. Rev. **A62**, 022306 (2000).
- [23] G. Brassard, N. Lütkenhaus, T. Mor and B.C. Sanders, “Security Aspects of Practical Quantum Cryptography,” *arXive e-print* quant-ph/9911054 (1999).
- [24] C. H. Bennett, G. Brassard, C. Crépeau, and U. Maurer, “Generalized Privacy Amplification,” IEEE Trans. Inf. Th. **41**, 1915 (1995).
- [25] P. Shor and J. Preskill, “Simple Proof of Security of the BB84 Quantum Key Distribution Protocol,” Phys. Rev. Lett. **85**, 441-444 (2000).
- [26] E. Biham, M. Boyer, P.O. Boykin, T. Mor and V. Roychowdhury, “A Proof of the security of quantum key distribution,” *arXive e-print* quant-ph/9912053 (1999).
- [27] D. Mayers, “Unconditional security in quantum cryptography,” *arXive e-print* quant-ph/9802025 (1998).
- [28] H.-K. Lo, “A simple proof of the unconditional security of quantum key distribution,” *arXive e-print* quant-ph/9904091 (1999).
- [29] N. Gisin and S. Wolf, “Quantum cryptography on noisy channels: quantum versus classical key-agreement protocols,” Phys. Rev. Lett. **83**, 20, 4200 (November 15, 1999).
- [30] B. Slutsky, R. Rao, P.-C. Sun, L. Tancevski and S. Fainman, “Defense frontier analysis of quantum cryptographic systems,” App. Opt. **37**, 14, 2869-2878 (1998).

- [31] N. Lütkenhaus, Ph.D. thesis, University of Strathclyde, Glasgow, Scotland (1996).
- [32] N. Lütkenhaus, “Estimates for practical quantum cryptography,” Phys. Rev. **A59**, 3301-3319 (1999).
- [33] A. Chefles and S. Barnett, “Quantum State Separation, Unambiguous Discrimination and Exact Cloning,” J. Phys. **A31**, 10097-10103 (1998).
- [34] C. H. Bennett, F. Bessette, G. Brassard, L. Salvail, and J. Smolin, “Experimental quantum cryptography,” J. Cryptology **5**, 3 (1992).
- [35] H.P. Yuen, “Quantum amplifiers, quantum duplicators and quantum cryptography,” Quantum Semiclass. Opt. **8**, 939-949 (1996).
- [36] M. N. Wegman and J.L. Carter, “New hash functions and their use in authentication and set equality,” J. Comp. Syst. Sciences **22**, 265 (1981).
- [37] H.J.P. Smith, D.J. Dube, M.E. Gardner, S.A. Clough, F.X. Kneizys and L.S. Rothman, “FASCODE- Fast Atmospheric Signature Code (Spectral Transmittance and Radiance),” U.S. Air Force Geophysics Laboratory Technical Report AFGL-TR-78-0081, Hanscom AFB, MA (1978).
- [38] J. Wang and G.P. Anderson, “Validation of FASCOD3 and MODTRAN3: Comparison of Model Calculations with Interferometer Observations from SPECTRE and ITRA, in Passive Infrared Remote Sensing of Clouds and the Atmosphere II,” David K. Lynch (ed.), Proc. SPIE **2309**, 170-183 (1994); also, Appl. Opt. **35**, 6028-6040 (1996).
- [39] L. Rothman, HITRAN (High Resolution Transmission Molecular Absorption) 1996 Database, Hanscom Air Force Base, Massachusetts (1996).
- [40] PLEXUS (Phillips Laboratory EXpert-assisted User Software) Version 2.1a, Air Force Research Lab, Hanscom Air Force Base, Massachusetts (August, 1996).
- [41] R.E. Hufnagel, “Propagation through atmospheric turbulence,” in *The Infrared Handbook*, Chap. 6, U.S. Government Printing Office, Washington, D.C. (1974).
- [42] P.B. Ulrich, “Hufnagel-Valley profiles for specified values of the coherence length and isoplanatic angle,” MA-TN-88-013, W.J. Schaffer Associates (1988).
- [43] G.C. Valley, “Isoplanatic degradation of tilt correction and short-term imaging systems,” Appl. Opt. **19**, 574 (1980).
- [44] R.R. Beland and J.H. Brown, “A deterministic temperature model for stratospheric turbulence,” Physica Scripta **37**, 419 (1988).
- [45] F.P. Battles, E.A. Murphy and J.P. Noonan, “The contribution of atmospheric density to the drop-off rate of C_n^2 ,” Physica Scripta **37**, 151 (1988).

[46] J.H. Brown and R.R. Beland, “A site comparison of optical turbulence in the lower stratosphere at night using thermosonde data,” *Physica Scripta* **37**, 424 (1988).

[47] R.L. Fante, “Electromagnetic beam propagation in turbulent media,” *Proc. IEEE* **63**, 1669 (1975).

[48] F.G. Smith (ed.), *The Infrared & Electro-Optical Systems Handbook*, Volume 2: Atmospheric Propagation of Radiation, SPIE Optical Engineering Press, Bellingham, Washington USA (1993); see Chapter 2: Propagation through Atmospheric Optical Turbulence.

[49] D.M. Boroson, *GeoLITE Lasercom Terminal Overview*, MIT Lincoln Laboratory GeoLITE Program Briefing, (8 April 1999); Presented at the: Communications and Information Systems Technology, Joint Advisory Committee Technical Seminar, MIT/Lincoln Laboratory, Air Force Contract No. F19628-95-C-0002.

[50] M. Born and E. Wolf, *Principles of Optics*, 6th ed., Cambridge University Press, Cambridge (1980).

[51] M. Jeganathan, M. Toyoshima, K. Wilson, J. James, G. Xu and J. Lesh, “Data Analysis Results from the GOLD Experiments,” *SPIE* **2990**, 70-81 (1997).

[52] M. Katzmann (ed.), *Laser Satellite Communications*, Prentice-Hall Inc. (1987).

[53] Space Telescope Science Institute, “About Hubble Space Telescope,” <http://www.stsci.edu/hst/CP7overview.html> (June 23, 1998).

[54] A. Muller, T. Herzog, B. Huttner, W. Tittel, H. Zbinden and N. Gisin “Plug and play’ systems for quantum cryptography,” *arXive e-print quant-ph/9611042* (1996).

[55] G. Ribordy, J.-D. Gautier, N. Gisin, O. Guinnard and H. Zbinden, “Automated ‘plug & play’ quantum key distribution,” *Elect. Lett.* **34**, 22, 2116-2117 (29th October 1998).

[56] N. Gisin, J.P. Von der Weid, J.-P. Pellaux, *J. Lightwave Technol.* **9**, 821-827 (1991).

[57] A.J. Viterbi and J.K. Omura, *Principles of Digital Communication and Coding*, McGraw-Hill, New York (1979).

[58] G. Brassard and L. Salvail, “Secret key reconciliation by public discussion,” *Lect. Notes in Computer Science* **765**, 410 (1994).

[59] D.E. Knuth, *Seminumerical Algorithms*, Addison-Wesley, Reading (1969).

[60] J. L. Carter and M. N. Wegman, “Universal classes of hash functions,” *J. Comp. Syst. Sciences* **18**, 143 (1979).

[61] G. Gilbert, J. Guttman, M. Hamrick and J. Thayer, “Analysis of Computational Loads in Quantum Cryptography,” In progress.

- [62] P.D. Townsend, S.J.D. Phoenix and S.M. Barnett, "Design of quantum cryptography systems for passive optical networks," *Elect. Lett.* **30**, 22, 1875 (October 27, 1994).
- [63] K.S. Il'in, I.I. Milostnaya, A.A. Verevkin, G.N. Gol'tsman, E.M. Gershenson and R. Sobolewski, "Ultimate quantum efficiency of a superconducting hot-electron photodetector," *Appl. Phys. Lett.* **73**, 3938-3940 (1998).
- [64] G. N. Gol'tsman, G. Chulkova, A. Dzardanov, A. Lipatov, O. Okunev, A. D. Semenov, K. Smirnov, B. Voronov, C. Williams, and R. Sobolewski, "Picosecond superconducting single-photon optical detector," *Nature*, submitted for publication.
- [65] R. Sobolewski, "Ultrafast Superconducting Hot-Electron Photodetectors," seminar at MITRE (March 16, 2000).
- [66] K. S. Il'in, M. Lindgren, M. Currie A. D. Semenov, G. N. Gol'tsman, R. Sobolewski, S. I. Cherednichenko, and E. M. Gershenson, "Picosecond hot-electron energy relaxation in NbN superconducting photodetectors," *Appl. Phys. Lett.* **76**, 2752 (2000).
- [67] R. Sobolewski, private communication (August 2000).
- [68] G. Gilbert and R. Sobolewski, "Application of Hot Electron Photon Detectors to Quantum Communications," In progress.
- [69] K. Sato, I. Kotaka, Y. Kondo and M. Yamamoto, "High-Repetition Frequency Pulse Generation at over 40 GHz Using Mode-Locked Lasers Integrated with Electroabsorption Modulators," *IEICE Trans.* **E-81**, 2, 146-150 (February 2, 1998).
- [70] M.C. Lu and Y.-K. Chen, "Monolithic colliding pulse modelocked diode lasers," in *Compact Sources of Ultrashort Pulses*, I.N. Duling, III (ed.), Cambridge University Press, Cambridge (1995).
- [71] G. Nykolak, P.F. Szajowski, A. Cashion, H.M. Presby, G.E. Tourgee and J. Auborn, "40-Gb/s DWDM free-space optical transmission link over 4.4 km," *Proc. SPIE* **3932**, *Free-Space Laser Communication Technologies XII*, 16-20 (May 2000).
- [72] P.F. Szajowski, G. Nykolak, J. Auborn, H.M. Presby, G.E. Tourgee, D.M. Romain, "High-power optical amplifiers enable 1550-nm terrestrial free-space optical data links operating at WDM 2.5-Gb/s data rates," *Proc. SPIE* **3850**, *Optical Wireless Communications II*, 2-10 (December 1999).
- [73] G. Thomas, D. Ackemrman, P. Prucnal and S.L. Cooper, "Physics in the whirlwind of optical communications," *Physics Today*, 30-36 (September 2000).
- [74] K. Noguchi, H. Miyazawa and O. Mitomi, "40-Gbit/s Ti:LiNbO₃ Optical Modulator with a Two-Stage Electrode," *IEICE Trans. Electron.*, **E81-C**, 8, 1316-1320 (August 8, 1998).

- [75] Lucent Technologies, Microelectronics Group, “40 Gbits/s Lithium Niobate Electro-Optic Modulator - Product Definition Sheet,” DS99-365LWP, (August 1999).
- [76] S. Nakamura, Y. Ueno and K. Tajima, “Femtosecond operation of a polarization-discriminating symmetric mach-zender all-optical switch and improvement in its high-repetition operation,” IEICE Trans. Commun., **E82-B**, 2, 379-386 (February 2, 1999).
- [77] R. Ewing and G. Gilbert, “Multiple beam quantum cryptography,” in preparation.
- [78] D. Begley, “Laser cross-link systems and technology,” IEEE Comm. Mag. **38**, 8, 126-132 (August, 2000).
- [79] K. Wilson and M. Enoch, “Optical communications for deep space missions,” IEEE Comm. Mag. **38**, 8, 134-139 (August, 2000).
- [80] M. Tsukuda and A. Keating, “Broadcast-and-select switching system based on optical time-division multiplexing (OTDM) technology,” IEICE Trans. Commun. **E82-B**, 2, 335-343 (February 2, 1998).
- [81] See, *e.g.*, “SENIOR YEAR Electro-Optical Reconnaissance System [SYERS],” <http://www.fas.org/irp/program/collect/syers.htm> (1998).
- [82] “TACLANE Encryptor (KG-175),” <http://www.gd-cs.com/Products/taclane.html> (2000).
- [83] “MILSTAR Fact Sheet,” United States Air Force Space Command, <http://www.spacecom.af.mil/hqafspc/library/facts/milstar.htm> (1997).
- [84] G. Clark, “NASA Plans Gargantuan Featherweight Telescope for Next Century,” <http://www.space.com/news/gossamer.html> (September 3, 1999).
- [85] National Aeronautics and Space Administration, “Gossamer Spacecraft Exploratory Research and Technology Draft,” <http://spacescience.nasa.gov/nradraft/00-oss-xx/> (1999).
- [86] Lucent Technologies, “Lambda WaveStar Router,” <http://www.lucent-optical.com/solutions/products/lambdarouter/> (1999).
- [87] J. Keller, “DARPA, Air Force search for a better way to steer military lasers,” Mil. and Aero. Elect., 19 (August 2000).
- [88] A. Papoulis, *Probability, Random Variables, and Stochastic Processes*, McGraw-Hill, New York (1965).